Analysing the Reactivity and Mechanisms of Artificial Substrates for Biological Catalysts

The University of Sheffield

Department of Chemistry

Adel Omar Ahmad Al Hussain

April 2017

Submitted to The University of Sheffield in part- fulfilment of the requirements for the degree of Doctor of Philosophy.

Declaration

The work described herein was undertaken at the Chemistry Department, University of Sheffield between April 2013 and April 2017 under the supervision of Professor N. H. Williams. This thesis and the data presented within it was completed solely by the author and has not previously been submitted for any degree at this or any other institution.

Adel Omar Ahmad Al Hussain

April 2017

Acknowledgements

This thesis dedicated to my Mum who although is no longer with us,

would be very proud of this achievement.

Abstract

It has recently been noted that enzymes can be promiscuous in their activity, and catalyse the reactions of a range of functional groups, including those not found in natural systems. Defining the fundamental details of these reactions will assist in understanding the chemical basis for this observation. This thesis describes phosphoryl and sulfuryl transfer reactions, using Free Energy Relationship (FER) to investigate their transition states.

The hydrolysis of sulfonate esters has been proposed to involve an intermediate, based on non-linear FER data. By using a series of 3-hydroxy pyridyl leaving groups, it is shown that a Hammett analysis is a more appropriate analysis, leading to a linear relationship and removing the requirement to invoke an intermediate.

The 3-hydroxy pyridyl leaving groups provide a novel series of compounds that have low pK_as, but without strong mesomeric contributions. This is used to investigate the FER of phosphate and sulfate diesters, to explore the relative contributions of inductive/field and mesomeric effects on reactivity. Brønsted analysis gives the best correlation for these compounds, in contrast with Hammett analysis for sulfonate esters.

The FER for a series of related triesters are described. Similarly to previous reports in the literature, triesters that contain a six membered ring with simple structural variations show a weak dependence on the pK_a of aryloxy leaving group (β_{lg} = -0.33 $\pm$ 0.06) when they react with hydroxide. However, when a carbonyl is present in the ring, the reaction is remarkably sensitive to the leaving group (β_{lg} = -1.8 $\pm$ 0.08) and shows much higher reactivity (10^8 fold greater when 4-nitrophenyl is the leaving group). As the aryloxy leaving group becomes poorer, a second order dependence on hydroxide is observed. However, extending the series to include alkoxy leaving groups revealed quite different behaviour: expulsion of the leaving group becomes a minor pathway, and ring opening becomes the dominant reaction. This latter reaction leads to the formation of a phosphate monoester as the ultimate product, and might provide a basis for a new prodrug strategy to deliver phosphorylated drugs.

Abbreviations

LFER	Linear free energy relationship	ATP	Adenosine triphosphate
lg	Leaving group	DNA	Deoxyribonucleic acid
nuc	Nucleophile	RNA	Ribonucleic acid
NLG	Non leaving group	A_N+D_N	Associative
equ	Equilibrium	A_ND_N	Concerted
β	Brønsted coefficient	D_N+A_N	Dissociative
ρ	Hammett constant	NMR	Nuclear magnetic resonance
KIE	Kinetic isotopic effect	MS	Mass spectrometry
ΔS	Entropy changes	μM	Micromolar
ΔH	Enthalpy changes	DMSO	Dimethyl sulfoxide
PMH	Phosphate monoester hydrolase	MES	4-Morpholineethanesulfonic acid
AS	Aryl sulfatases	MOPS	4-Morpholinepropanesulfonic acid
NPP	Nucleotide pyrophosphatase	HEPES	4-(2-Hydroxyethyl)piperazine-1-ethanesulfonic acid
AP	Alkaline phosphatase	CHES	2-(Cyclohexylamino)ethanesulfonic acid
σ	Hammett substituent constant	CAPS	3-(Cyclohexylamino)-1-propanesulfonic acid

I	Ionic strength
R	Correlation coefficient
EPPS	4-(2-Hydroxyethyl)piperazine-1-propanesulfonic acid
Abs	Absorbance
pTsOH	Para toluenesulfonic acid
DMAP	4-(dimethyl amine) pyridine
TFA	Trifluoroacetic acid
HPLC	High performance liquid chromatography
THF	Tetrahydrofuran
TEA	Triethylamine
Et$_2$O	Diethyl ether
EtOAc	Ethyl acetate
MCPBA	Meta chloroperoxybenzoic acid
(Boc)$_2$O	Di-*tert*-butyl dicarbonate
TLC	Thin layer chromatography
R.t.	Retention time

Contents

Chapter one: General introduction

1.1 Introduction

During the two past decades, large efforts have been made to understand the mechanism and transition state of phosphoryl and sulfonyl transfer reactions.[1,2] Understanding the mechanism of any reaction is beneficial to improve the synthetic routes in organic chemistry.[3] However, understanding the mechanism of sulfonyl and phosphoryl transfer is crucial since these species are involved in many biological activities, such as biosynthesis, energy production, signaling, cellular communication, hormone regulation and others.[4-6] The main molecules that have interested researchers are phosphate mono-, di-, and triesters which are related to the phosphoryl transfer reaction. On the other hand, sulfate and sulfonate ester were related to the sulfonyl transfer reactions as shown in **Figure 1**.
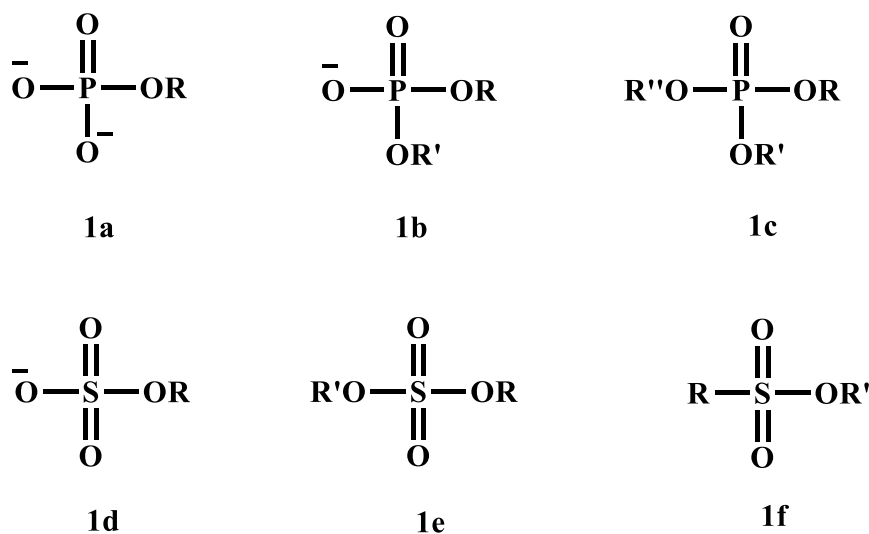
Figure 1: Structure of phosphate, sulfate, and sulfonate esters; **1a** = phosphate monoester, **1b** = phosphate diester, **1c** = phosphate triester, **1d** = sulfate monoester, **1e** = sulfate diester, **1f** = sulfonate ester.

The reactivity of these species is slow under mild conditions and without enzyme catalysis. The nonenzymatic reaction would help to understand the enzymatic catalytic reaction.

To investigate the mechanism and transition states of these reactions a set of tools need to be used. The common tools that have been used are the linear free energy relationship[7], kinetic isotope effect[8,9], activation parameter measurements[10-12], and computational and theory calculations.[13]

1.2 Types of potential reaction mechanism

Before explaining the tools that have been used to study the reaction mechanism of phosphoryl and sulfuryl reactions, it is worth explaining the types of mechanism they might follow. In general, there are three main mechanisms for these species (**Scheme 1**):

1. Dissociative mechanism
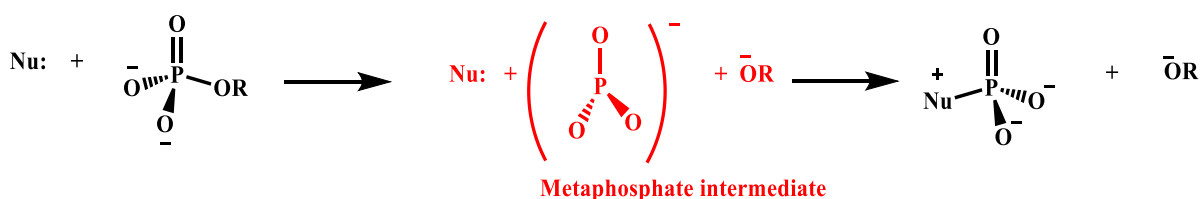
2. Associative mechanism
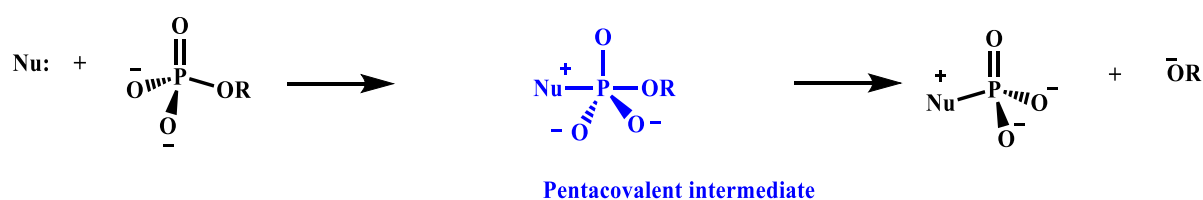
3. Concerted mechanism
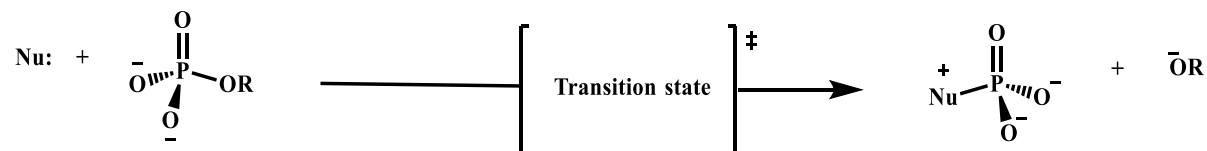
Scheme 1: Possible mechanisms of phosphate ester cleavage.[2,14]

A dissociative mechanism is when the reaction occurs in two steps: the first step is the departure

3

of the leaving group and the second is the addition of the nucleophile. This mechanism proceeds with a stable intermediate, like the metaphosphate intermediate. A concerted mechanism is a one-step mechanism with a single transition state.[4] The associative mechanism also occurs in two steps like the dissociative mechanism. However, the first step is the addition of the nucleophile and the second step is the elimination step of the leaving group. This mechanism proceeds through a stable pentacovalent intermediate.

The concerted mechanism could exist in three possible of transition states (**Scheme 2**). The first is a tight transition state when the phosphorus atom, for example, has more net bonding to the nucleophile and the leaving group than in the ground state. The opposite to this is the loose transition state, when the net bonding of phosphorus atom to the nucleophile and to the leaving group is less than in the ground state.[15] The last is the synchronous transition state which is intermediate between the loose and tight transition states. In this type, the net bonding of the phosphorus atom to the nucleophile and the leaving group is comparable to that in the ground state.
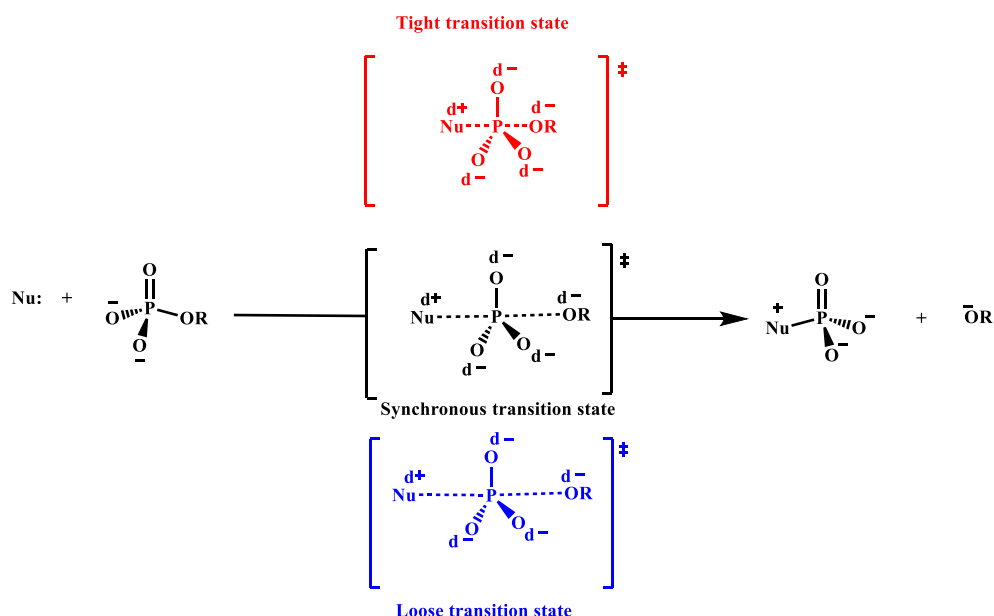
Scheme 2: Possible transition states for phosphate esters.

1.3 Linear free energy relationship

Polar substituents in organic chemistry can have a very large effect on the course of a reaction. The free energy relationship is a method of quantifying these polar effects. The dissociation of benzoic acid **2** in water was the first quantitative measurement of polar substituent effects (**Scheme 3**).[16,17]

2
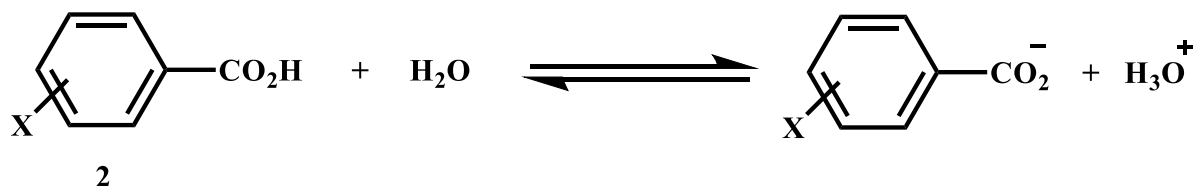
Scheme 3: Ionisation of benzoic acid.

The stability of the benzoate anion can be assessed by the pK_a of benzoic acid, which in turn depends on whether the substituent is electron withdrawing or donating.[18] The position of the equilibrium is, therefore, dependent upon the electronic effects of the substituent group, which affects the charge stabilization of the anion.[19,20] In the early twentieth century, Brønsted[21] and Hammett[22] defined the first free energy relationships which play important roles in understanding and determining mechanisms.

1.3.1 Classes of free energy relationship

In general, there are two main classes of free energy relationship. The first involves correlating the rate constant and the equilibrium constant for the same process and was studied by Brønsted and Leffler. The second class involves correlating two processes that are not directly related and is more widely used than the first one. The Hammett equation is the most well-known of the second class.

5

1.3.2 Brønsted equation

The Brønsted equation is used to study proton transfer reactions, or nucleophilicity.[23] Brønsted

derived two equations, one for acids (1) and one for bases (2).[21]

$$\log k_{HA} = -\alpha\, pK_a^{HA} + c \qquad \textbf{Equation 1}$$

$$\log k_B = -\beta\, pK_a^{HB} + c \qquad \textbf{Equation 2}$$

α and β are characteristic slopes for an acid and base catalysed reaction respectively.

In general, a linear free energy relationship studies the effect of the substituent on the reaction

rate or equilibrium state and gives a picture about the transition state. The notion is simple; the

electron density and charge will be changed in the transition state if a bond is broken or formed.

The effect of the substituent will vary depending on whether it is a donating or withdrawing

group. For example, an electron withdrawing group will withdraw the electron density and

stabilize the developed negative charge, while a donating group will destabilize the developed

negative charge and stabilize the developed positive charge.[23] As a consequence, this effect

will impact on the pK_a of the compound, for example the pK_a of phenol drops from 9.95 to 7.14

by adding a nitro group which stabilizes the negative charge on the phenolate and withdraws

the electron density as explained in **Scheme 4**.
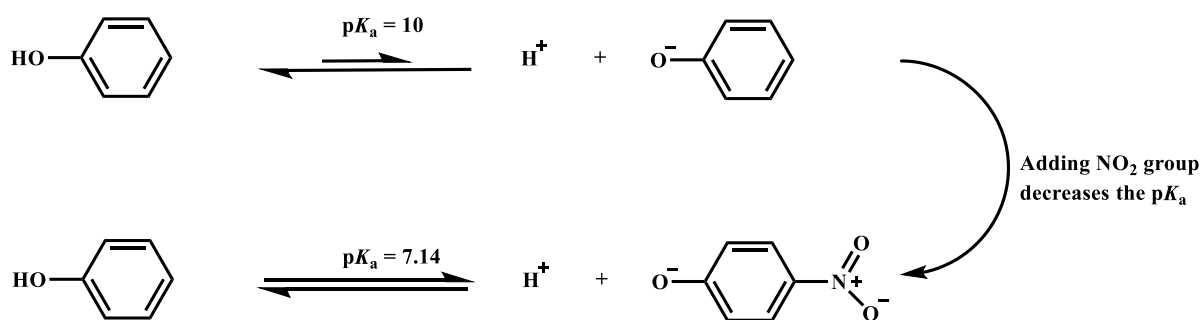
Scheme 4: Stabilisation of the negative charge on phenolate by a nitro group.[2]

6

To evaluate the charge build up in the transition state, electron donating and electron withdrawing groups are usually added to the structure. For example, adding a nitro group to the phenyl phosphate monoester will increase the rate of reaction since it stabilizes the developing negative charge and withdraws the electron density. How much negative charge is developed in the transition state will be determined by how much the rate constant increases with the withdrawing group, such as a nitro group.
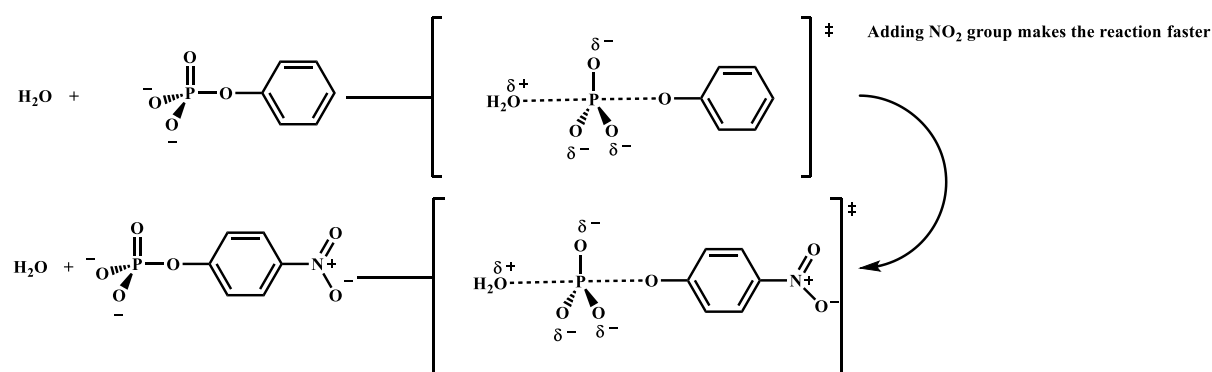
Scheme 5: Electron withdrawing groups stabilize the developing negative charge on the oxygen atom of leaving the group.[2]

In a tight transition state when there is little bond cleavage, electron withdrawing groups have little or no impact on the rate of reaction. However, in the loose transition state where there is large bond cleavage, and as a result there is a largely developed charge, the electron withdrawing group can increase the rate of reaction significantly. The extended LFER could assist to give an explanation about the transition state and reaction mechanism. The extended Brønsted plot is a correlation between the logarithm of rate of reaction or equilibrium and the pK_a of the leaving group or the nucleophile[24], as explained in equations 3 and 4.

$\log k \ or \ \log K = \beta_{lg} \, pK_a + c$ **Equation 3**

$\log k \ or \ \log K = \beta_{nuc} \, pK_a + c$ **Equation 4**

These equations will yield β_{lg} for equation 3 and β_{nuc} for equation 4. The Brønsted slope gives an indication of how much charge builds up on the transition state and explains the sensitivity of the reaction to the change of pK_a of the leaving group or the nucleophile.[15]

The β_{lg} is always negative while β_{nuc} is positive. The values of these Brønsted coefficients could be affected by several factors: The first is the system structure, for instance, phosphate mono esters have large values of β_{lg} = -1.1[25] which correspond to a loose transition state. Phosphate diesters have smaller β_{lg} = -0.64[26] to -0.97[27] compared with phosphate monoester. These values are believed to correspond to the synchronous transition state. Phosphate triesters often give β_{lg} between -0.35 to to -0.45[10] and are thought to proceed via a tight transition state. The second factor depends on whether the leaving group is an oxygen leaving group or nitrogen, and the same with the nucleophile. However, sometimes there is a challenge to interpret the Brønsted coefficients and in this case, β equilibrium might play a role in the interpretation. The way to do that is to divided the β_{lg} or β_{nuc} by β_{eq} which is known as a Leffler parameter but the main difficultly is that the equilibrium constants are not straight forward to measure.

1.3.3 Hammett equation

Hammett found a linear correlation between the rate constants for *meta* and *para* substituted benzoate derivatives and the pK_as of similarly substituted of benzoic acids.[28]

The Hammett equation is:

$$\log k_X/k_H \text{ or } \log K_X/K_H = \rho\,\sigma \qquad \textbf{Equation 5}$$

Where σ is the Hammett substituent constant which is obtained from $\sigma = pK_a^H - pK_a^X$, ρ is the Hammett reaction constant, k_X is the rate constant, and K_X is the equilibrium constant. The ortho position was not studied because of steric effects between the reacting carbonyl group and the substituent. Aliphatic compounds were not studied by Hammett for the same reason.[29]

The Hammett reaction constant (ρ) describes how the reaction responds to electronic variation. A negative ρ value means the electron density in the transition state, near the aromatic ring, is lower than in the starting material, whereas a positive ρ value means that the transition state has a higher electron density than in the starting material. A large magnitude ρ value indicates that there is a large charge change close to the aromatic ring, whereas a small value indicates a small charge change near the aromatic ring, but does not rule out larger changes further from this part of the molecule.[30]

1.3.4 The Yukawa- Tsuno equation

Resonance structures can occur between the substituents and the reaction centre in the transition state structure for some reactions. Yukawa and Tsuno created the parameter 'r' as a measurement of the extent of resonance with the reaction centre.[31,32] They described two equations: the first where positive charge is built up on the reaction centre[23] (equation 6), and the second where the reaction centre carries a negative charge (equation 7).

$\log (k/k_H) = \rho[\sigma + r\,(\sigma^+ - \sigma)]$ **Equation 6**

$\log (k/k_H) = \rho[\sigma + r\,(\sigma^- - \sigma)]$ **Equation 7**

'r' is a measure of how extensively π delocalisation has occurred and perhaps how far bond cleavage has proceeded in the transition structure. In addition to that, it was found that adding a new parameter can help to obtain a conclusive answer. Nakata *et al.*[33] have studied theoretically the effects of the substituent on the gas phase stabilization of the phenoxide anion using a proton transfer reaction.
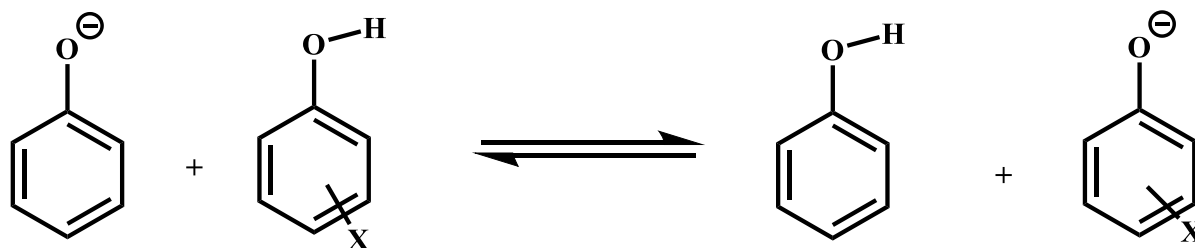
Scheme 6: Proton transfer reaction of phenoxide anion.

25 types of ring substitution have been studied using the proton transfer reaction and it was deduced that there are three terms affecting the gas phase stability; resonance, saturation, and inductive effects. In addition, they have found by the using the extended Yukawa-Tsuno (equation 8) they can obtain a description about the effects of substituents on the stability of phenoxide anions.

$$-\Delta E_X = \rho \, (\sigma^{\circ} + r^{-} \, \Delta\sigma^{-}_R + s\Delta\sigma^{-}_S) \qquad \textbf{Equation 8}$$

1.4 Kinetic isotope effect

The kinetic isotope effect (KIE) investigates the changes in bonding that take place in the transition state by comparing the reaction rate measurement between two isotopes of the atom of interest in the molecule, normally by replacing with a heavier atom. Based on the quantum mechanics of the system, each bond has zero-point energy. At this point, the bond is in its minimum vibrational energy state. The zero-point energy depends on the masses of the atoms that participate in the bond and the bond strength. For example, increasing the mass of the atom will decrease the zero-point energy. If the bond is completely broken, this will affect the vibrational energy of the bond and it will lost. In other words, there will be no variance in vibrational energy between light and heavy isotopes. As a result, the energy barrier of bond cleavage for a heavy atom will be larger and will lead to slower reaction rate and in this case yields a normal KIE when the ratio of (k_{light}/ k_{heavy}) is greater than 1.[9] For the partially broken bond in the transition state, the vibrational energy of the zero point between light and heavy

10

isotopes will decrease compared to that in the ground state and can lead to (k_{light}/k_{heavy}) smaller than 1. There are two types of kinetic isotope effect[34]: the first one called primary isotope effect which yields from the substitution of isotopes at the position of bond formation or cleavage. The other is the secondary isotope effect which results from isotopic substitution that is indirectly participating in bond formation or cleavage. The vibration state in the primary isotope effect results from gain or loss stretching mode including the groups in the bond formation or cleavage. Whereas in the secondary isotope effect, the vibrational contribution comes from alteration in the geometry. Although the kinetic isotope effect can give good information about the transition state, sometimes the interpretation is a challenge since it is sensitive to the bond length and geometry, and any change could affect the vibrational energy.

1.5 Activation parameters measurements

The activation parameters also have been used by researchers to get information about the transition state, and often the activation parameter measurements were consistent with KIE and LFER and have suggested a loose transition state for substitution in diester and triesters. The activation parameters measurement encompass the difference of entropy in the ground state and the transition state. Activation entropy is determined by measuring the rate of reaction at a different temperature[35] as shown in equation 9:

$\ln k/T = -\Delta H/RT + \Delta S/R + \ln k_B K/h.$ **Equation 9**

Where k_B is the Boltzmann constant, K represents the transmission coefficients (usually to be assumed 1), and h is the Planck's constant. Plotting $\ln (k/T)$ against (1/T) will yield the slope $\Delta H/R$ and the intercept $\ln (k_B/h) + \Delta S/R$. The entropy could give information about the transition state. For example, the loose transition state has a larger activation entropy than the tight transition state. Also, the values of ΔS will be increased with increasing substituents from monoester to triester. Therefore, phosphate diesters[27] and triesters[10] have reduced values of

11

activation entropy compared to the phosphate monesters.

1.6 Enzyme promiscuity

Enzymes are known to be specialist catalysts, in the other words, one enzyme for one substrate. However, this notion has been challenged by the flexibility of some enzymes to catalyse more than one substrate and give considerable rate acceleration.[36,37] This is called enzyme promiscuity, which was originally introduced by Jensen[38] in 1976, and can be defined as the phenomenon that an enzyme can catalyse more than one substrate by stabilizing their transition state.[39,40] For example, PMH (Phosphate monoester hydrolase) which originally catalyses phosphonate monoesters can also catalyse another five different classes of substrate.[41] These classes encompasses phosphate mono-, di-, and triesters, sulfate monoesters and sulfonate triesters. **Table 1** shows the PMH reactivity with rate acceleration with different substrates.

Enzyme	Activity	k_{cat}/K_M (M^{-1}s^{-1})
PMH	Phosphate diester	9.2×10^3
	Phosphonate monoester	1.5×10^4
	Sulfonate monoester	4.9×10^1
	Phosphate monoester	2.2×10^1
	Sulfate	5.6×10^{-1}
	Phosphate triester	1.6×10^{-2}

Table 1: Rate acceleration and promiscuity of PMH on six classes of substrates.[41]

In addition to PMH, there are common promiscuity enzymes such as AP (Alkaline phosphatase), AS (Aryl sulfatase) and NPP (Nucleotide pyrophosphatase) which can catalyse more than one substrate, as shown in **Figure 2**.
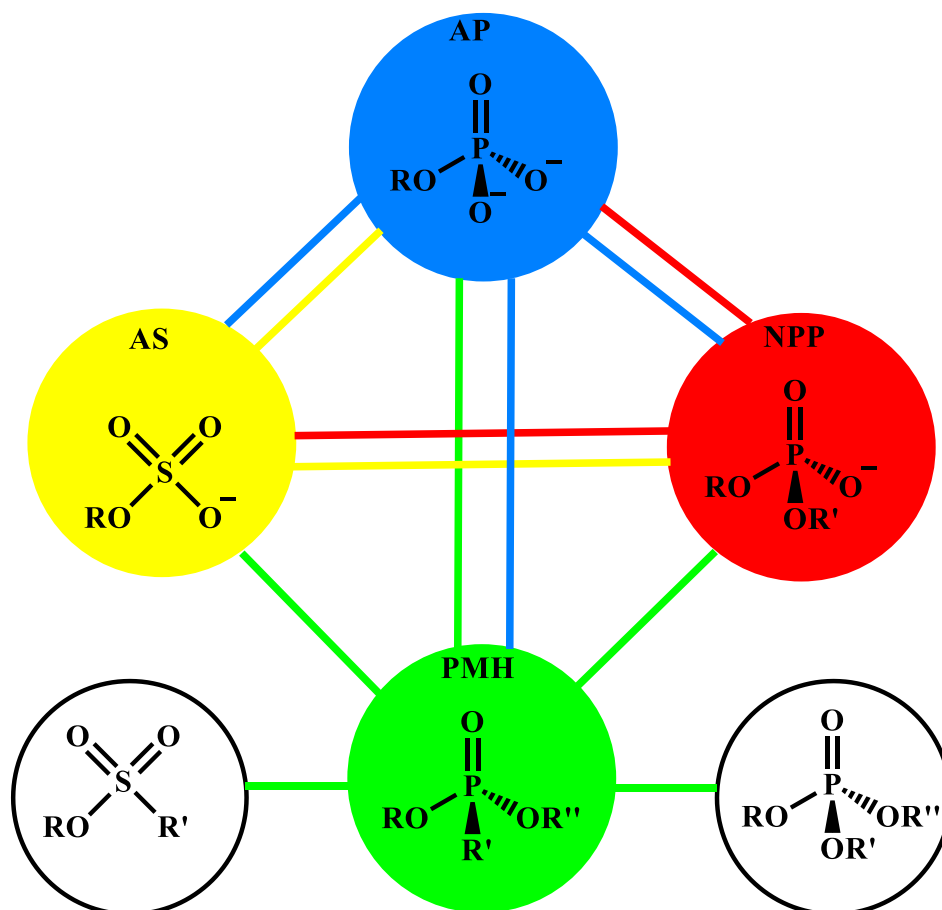
Figure 2: The cross promiscuity of the AP superfamily. The substrates inside the coloured circle represent the native (original) substrate that the enzyme catalyses, whereas the coloured lines illustrate the promiscuity of the enzyme. The figure adopted from Pabis[42] paper and originally published by reference (42)[43] and (43).[44]

The question exists of what determines enzyme promiscuity. As it is known enzymes contain metal ions and these metal ions can play roles in the high reactivity of these enzyme on the non-native substrate. The metal ions could contribute to activate the phosphate by polarisation,

13

and can lower the pK_a which activates the nucleophile. Moreover the metal ion could activate the leaving group via stabilizing the negative charge on the atom.[45] The diameter of the active site could be another factor to cause the promiscuity of enzyme. However, more research is needed to investigate how to understand the mechanism and transition state for these enzymes with different substrates. The implication of enzyme promiscuity was discovered to play a role in the enzyme artificial revolution via the mechanism of gene duplication.[38,46-48]

1.7 General aims

It is important to know the transition state of the reaction, which will assist in understanding how the enzyme catalyses the reaction.[49] The phosphoryl and the sulfuryl transfer reactions are especially important as they have been involved in biology[1] and the common promiscuous enzymes found to catalyse these species.[42] Therefore, the overall aim is to study the reactivity of the sulfonate, sulfate diesters and phosphate diesters with pyridyl leaving group and its derivatives. This is because they are good leaving groups due to inductive and field effects, which will be compared with the classic leaving groups such as 4-nitro as they are good leaving groups due to resonance effects. Moreover, the effects of varying the functional groups such as a carbonyl group on cyclic phosphate triesters will be studied. Further, varying the leaving group for these species to produce a linear free energy relationship (LFER) to investigate the transition state of the reaction.

Chapter two: Sulfonate esters

2.1 Introduction: Sulfonate esters

Sulfonate and sulfate ester hydrolysis has had less attention than phosphate ester hydrolysis.[50,51] However, recently several studies have shown a revival of interest in sulfate[52,53] and other similar transfer reactions.[54,55] Sulfate hydrolysis has some biological roles: for example; detoxification and cellular signalling.[56] Sulfonate esters can be used by aerobic bacteria when the concentration of sulfur is low.[57,58] Sulfonate compounds could be used as drugs in medicine[59] and as intermediates in organic synthesis.[60,61]

Moreover, there has been an increased awareness in the occurrence of catalytic promiscuity in an enzyme that catalyses sulfuryl and phosphoryl transfer reactions.[43,62] This phenomenon was found to play a central role in artificial enzyme design[63] and protein evolution.[48] Recently, van Loo *et al*[41] found PMH (phosphonate monoester hydrolase) can catalyse five classes of hydrolytic reactions in addition to its native phosphonate monoesterase activity.[41] They have investigated the promiscuity of PMH enzyme on sulfonate monesters and k_{cat}/K_M values were determined to be 1.4 and 49 $M^{-1}s^{-1}$ for compound **3a** and **3b** respectively. The data revealed, in addition to the ability of PMH to catalyse phosphate mono, di, triester and sulfate monoester, it can catalyse sulfonate monoester hydrolysis.
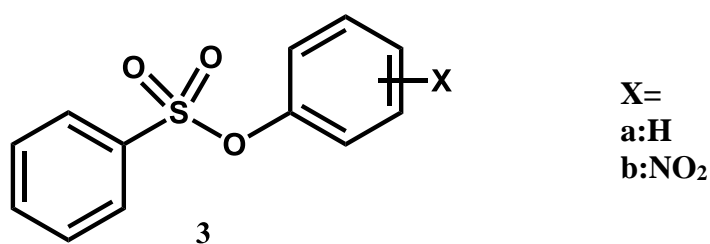
Figure 3: Substituted phenyl benzene sulfonate monester that studied by van Loo *et al*.[41]

2.2 Mechanism of sulfonate esters

Recently the mechanism of sulfonate ester hydrolysis has been under debate, whether it occurs by a stepwise mechanism via an intermediate[55,64-66] (**Figure 4A**) or proceeds through a concerted mechanism.[67,68](**Figure 4B**).
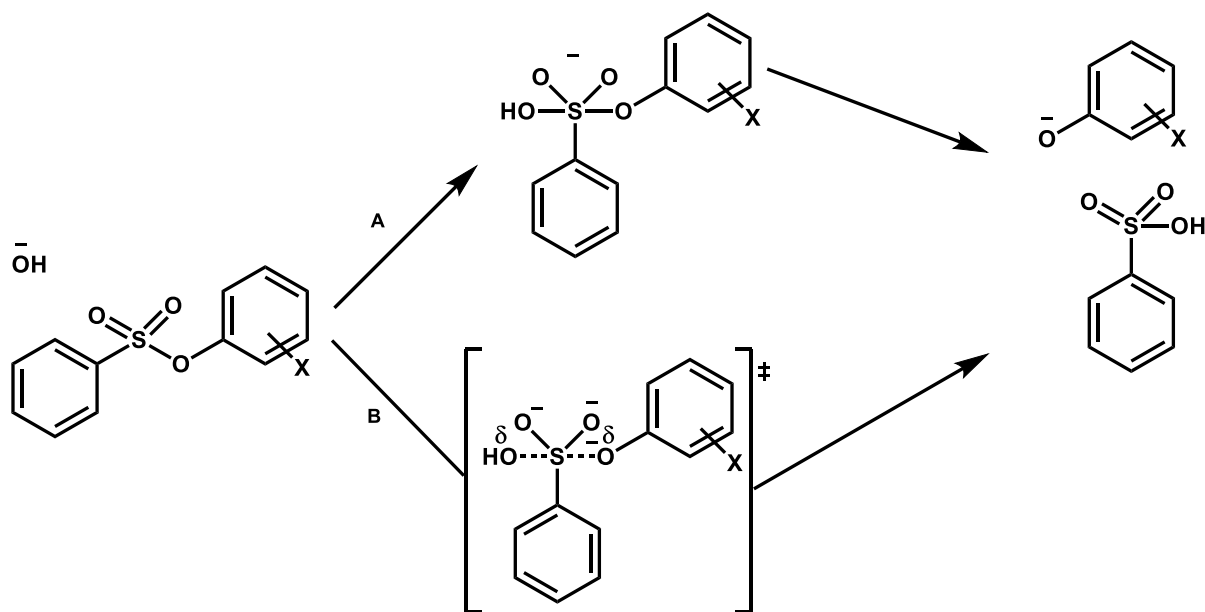
Figure 4: Potential mechanisms of alkaline hydrolysis of aryl benzenesulfonate ester: **A** stepwise mechanism and **B** concerted mechanism.

In particular, a study by Babtie *et. al*[55]. proposed that the alkaline hydrolysis of a series of benzene sulfonates occurs by a stepwise mechanism when the pK_a of the leaving group is greater than ~ 8.5 ($\beta = -0.97$) while the concerted mechanism is prevalent when the pK_a is less than ~ 8.5 ($\beta = -0.27$) as shown in **Figure 6**.

The correlation of the Brønsted plot gives an indication about the mechanism of the reaction. For instance, downward curvature usually indicates a change in the rate limiting step which means a stepwise mechanism,[69] while a smooth correlation indicates that the reaction proceeds through a single transition state.

17

2.3 Previous studies

Babtie *et al.*[55] studied the alkaline hydrolysis of sulfonate esters with different substituents (compounds **4a-h**) and found a break point in the Brønsted correlation, with β_{lg} (leaving group) of -0.27 for pK_as less than 8.5 and -0.97 for pK_as greater than 8.5 (**Figure 6**).

X=
a: 3-F-4-NO$_2$
b: 4-NO$_2$
c: 4-CN
d: 3-NO$_2$
e: 3-CN
f: 4-Cl
g: 3,4-dimethyl
h: H
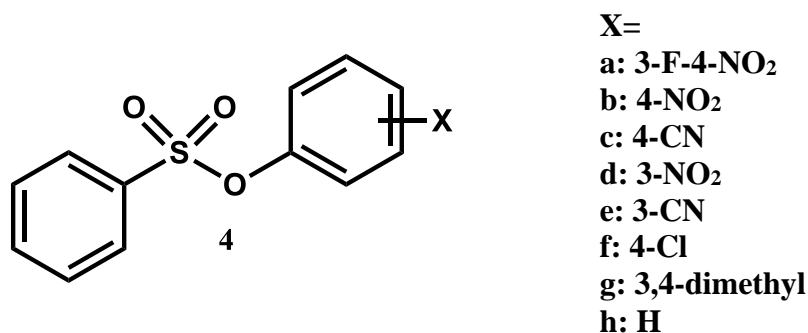
Figure 5: Aryl benzene sulfonates that have been studied by Babtie *et al.*[55]
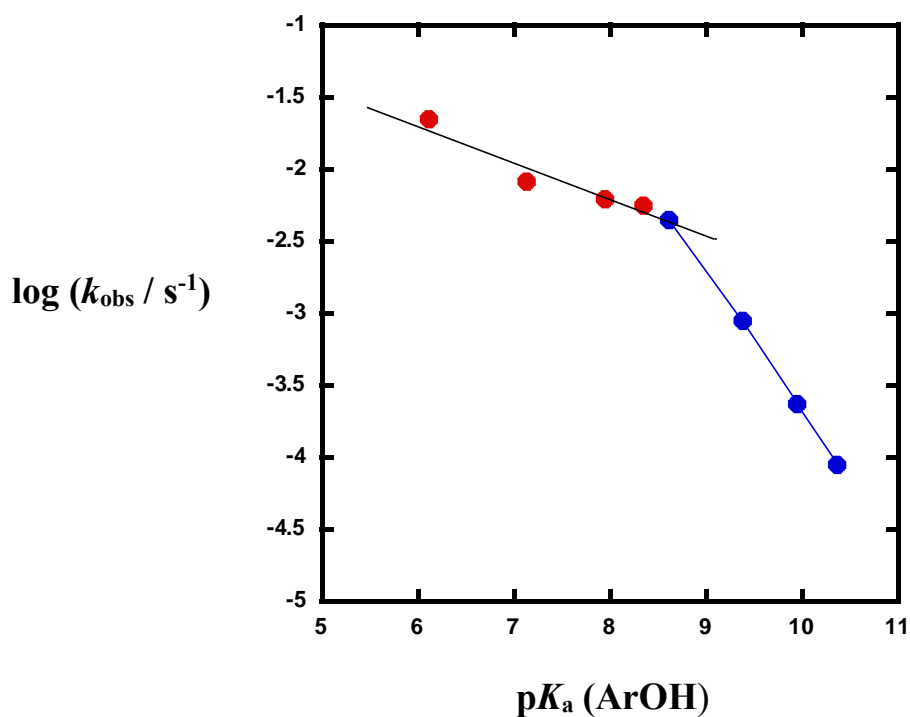
Figure 6: Brønsted correlation for the alkaline hydrolysis of aryl benzene sulfonates as reported by Babtie *et al.*[55]

They concluded that the alkaline hydrolysis of these sulfonates occurs by a stepwise mechanism with poor leaving groups and by a concerted mechanism with good leaving groups.[55] Usually, this form of curvature would indicate a change in the rate limiting step rather than a change in mechanism.

Williams and co-workers[67] examined the reaction of 4-nitrophenyl 4-nitrobenzene sulfonate **5g** with different oxyanions that have a range of basicities spanning over 8 pK_a unit, and the reaction of substituted phenyl benzene sulfonic acid **5a-i** with phenoxide. In both reactions, the Brønsted plot gave a linear correlation with β_{lg} of -0.91 and β_{nuc} of 0.64 which indicate the reaction could proceed via a single transition state.

X=
a: 4-Cl-2,6-$(NO_2)_2$
b: 2,6-$(NO_2)_2$
c: 2,4-$(NO_2)_2$
d: 2,4-$(Cl)2$-6-NO_2
e: 2,5-$(NO_2)_2$
f: 4-Cl-2 $(NO_2)_2$
g: 4-NO_2
h: 2-NO_2
i: 3-NO_2
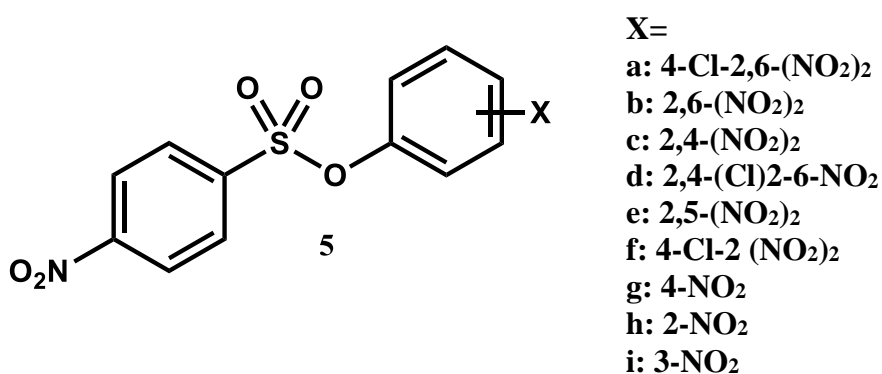
Figure 7: A series of substituted phenyl 4-nitrobenzene sulfonate reported by Williams and co-workers.[67]

Zaborsky and Kaiser[70] studied the substituent effect in the alkaline hydrolysis of aromatic five-membered cyclic sulfonates. They followed the hydrolysis of 2-hydroxy-α-toluensulfonic acid sultones with different substitutions at position 5 at 25 °C. From the Hammett plot, the ρ of +1.23 indicates that electron withdrawing group acts as an accelerating factor in that position on the aromatic ring (**Figure 9**).
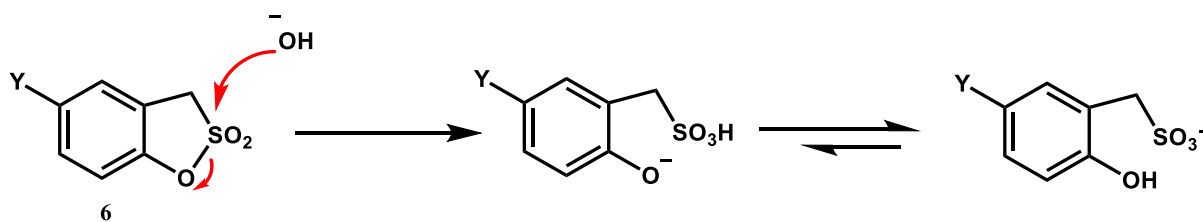
Figure 8: Mechanism of hydrolysis of aromatic five-membered sultones.[70]
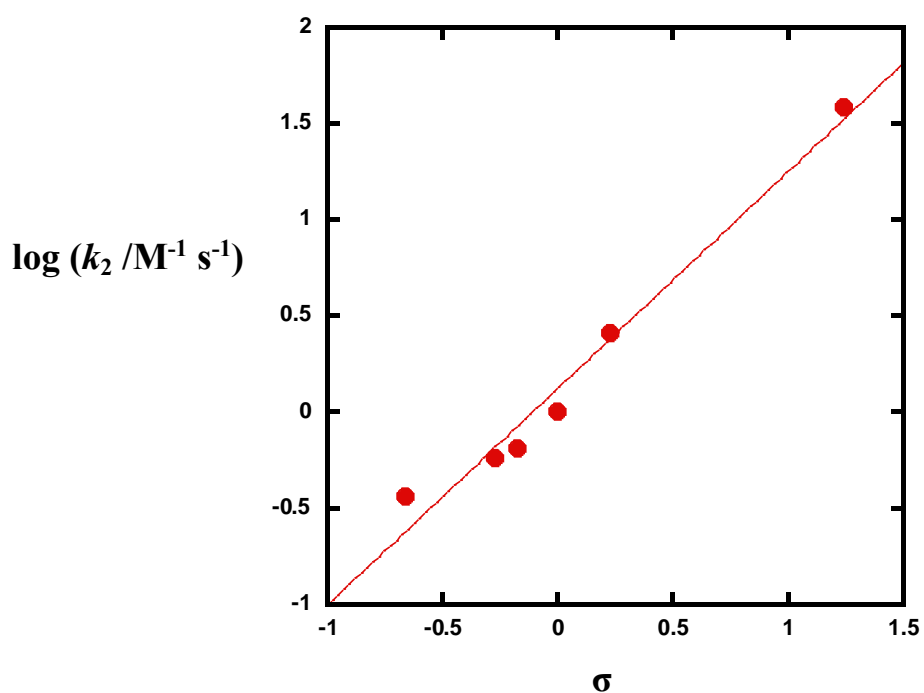
Figure 9: Hammett plot for the hydrolysis of aromatic five-membered cyclic sulfonates.[70]

The hydrolysis of 2-hydroxyl 4-nitro benzene phenyl sulfonate **7** was studied by Farrar and Williams.[71] The pH profile shows a sigmoid shape with pK_a value close to phenolic hydroxyl. The data of positive entropy activation, absence of buffer effect and solvent deuterium oxide demonstrated that the intramolecular nucleophile catalysis plays an essential role in the mechanism of the reaction.

7
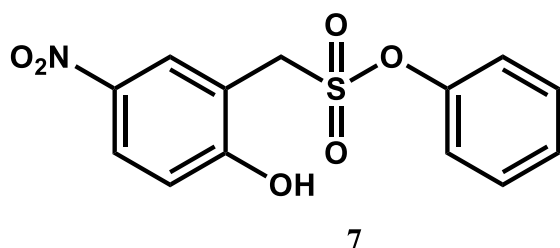
Im *et al.* [68] have studied the mechanism of the alkaline hydrolysis of substituted phenyl benzene sulfonates **8** with OH in water containing 20% DMSO at 25 °C.
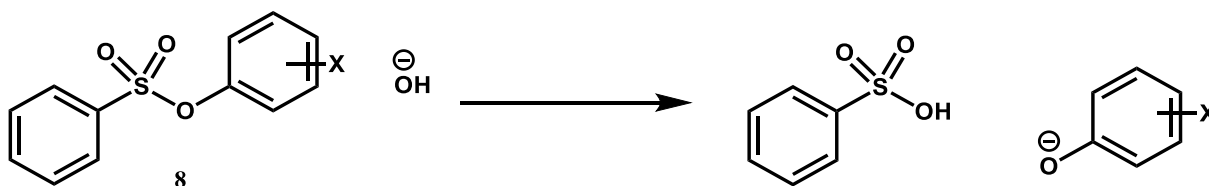
Figure 10: Alkaline hydrolysis of substituted phenyl benzene sulfonates.

The alkaline hydrolysis of substituted phenyl benzene sulfonates has been deduced to occur by a concerted mechanism using Brønsted, Hammett, and Yukawa-Tsuno equations. The Brønsted plot showed a linear correlation with β_{lg} of -0.55 which indicate the reaction could occur by a concerted mechanism because of the reasonable large negative value of β_{lg} that has a good correlation (**Figure 11**).
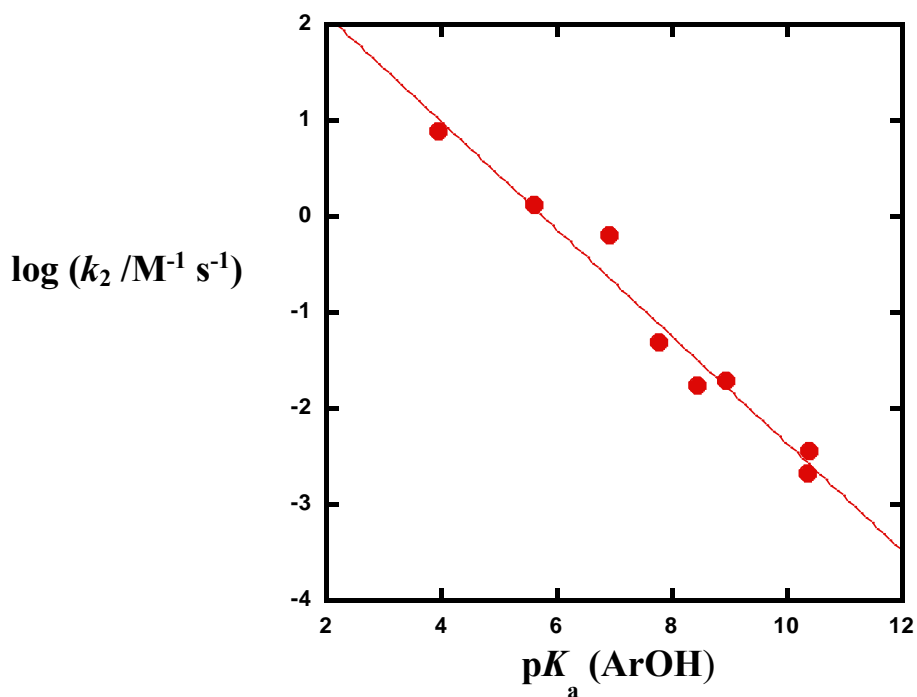
Figure 11: Brønsted plot for for alkaline hydrolysis substituted phenyl benzenesulfonates at 25 °C, in 80:20 H_2O to DMSO.[68]

The Hammett plot did not give a good linear correlation compared to Brønsted and exhibited slightly scattered points (**Figure 12**).
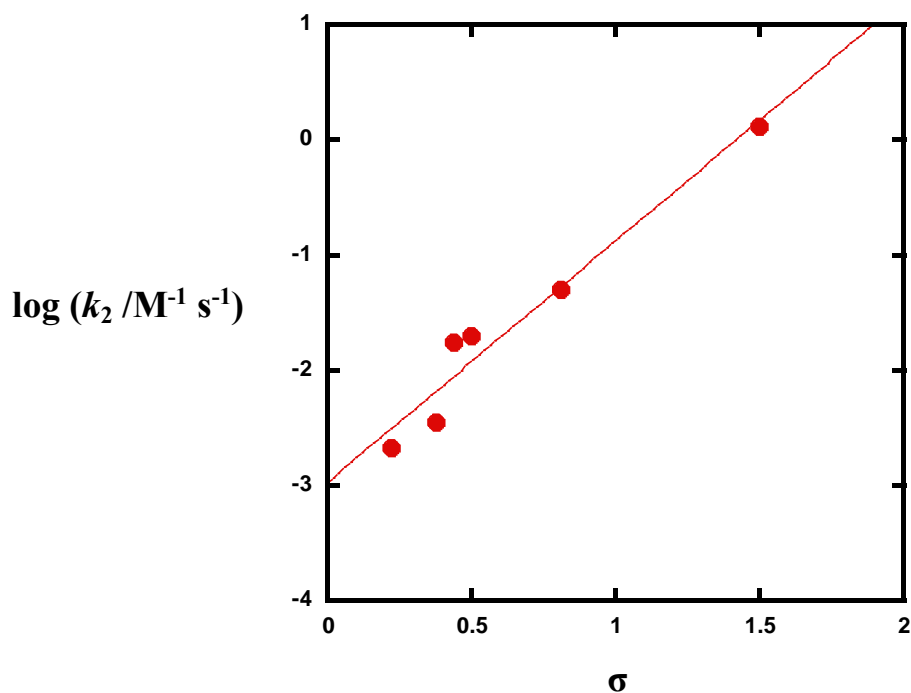
Figure 12: Hammett plot correlated with σ constants for alkaline hydrolysis substituted phenyl benzenesulfonates at 25 °C, in 80:20 H_2O to DMSO.[68]

Yukawa-Tsuno plot exhibited an excellent correlation with r of 0.52 (**Figure 13**) which indicates that the hydrolysis of phenyl benzyl sulfonates might occur by either concerted mechanism or stepwise mechanism. The stepwise mechanism was discounted on the basis that hydroxide ion is much more basic than aryloxide. Thus, the reaction is more likely to happen by a concerted mechanism.
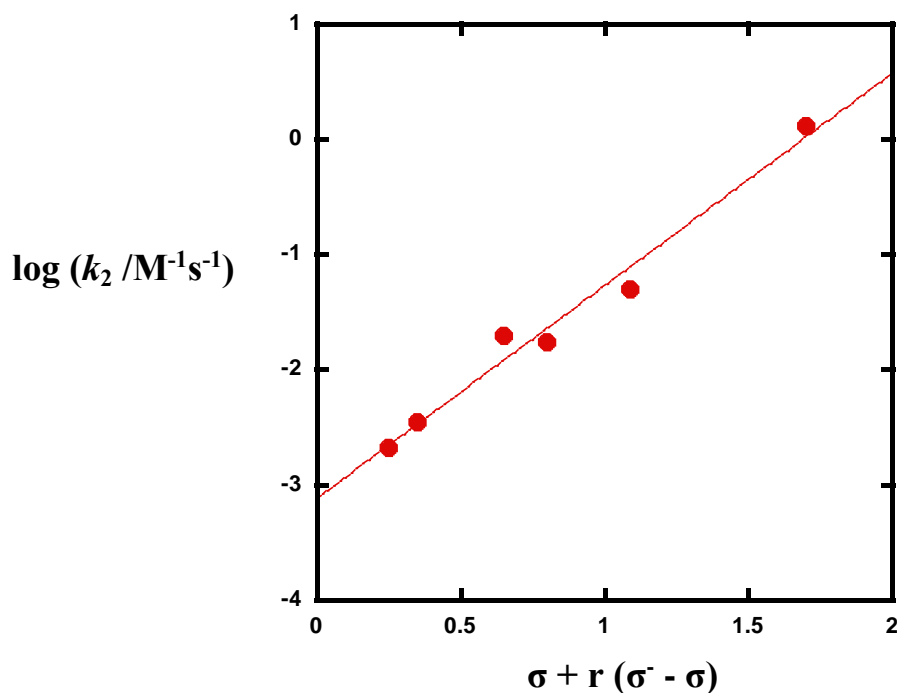
Figure 13: Yukawa-Tsuno plot for reactions benzenesulfonates at 25 °C, 80:20 H_2O to DMSO.[68]

It can be noticed from these examples care is needed when plotting the data with single parameter (e.g. Brønsted plot) and it is important to test the reliability of the plot by adding an extra parameter (like Hammett or Yukawa-Tsuno) which might help to a more reliable analysis.

2.4 Aims

The scenario has been conducted in the previous study[55] about the mechanism of a series aryl benzene sulfonate ester. They concluded that the reaction proceeded via a stepwise mechanism when the pK_a of leaving group was more than 8 while a concerted mechanism could occur when the pK_a of the leaving group was less than 8. The aim of this chapter is to study the reactivity and mechanism of aryl benzene sulfonates with pyridyl leaving groups and their derivatives (**10-12**). These leaving groups are good leaving groups due to the field and inductive effect rather than mesomeric effects.
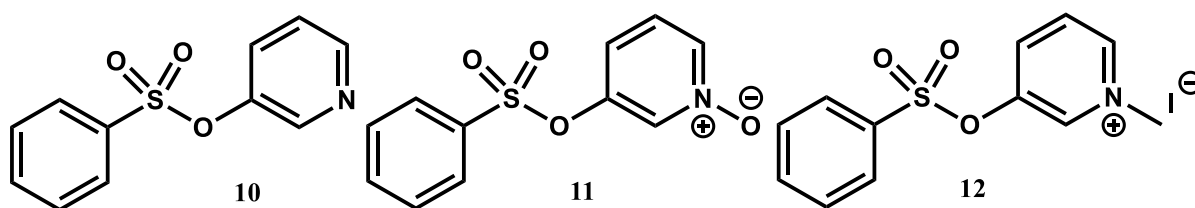
Figure 14: Proposed pyridyl benzene sulfonate and its derivatives **10-12** in this study.

The leaving groups where chosen as we believe that the substituted phenyls with a low pK_a have strong resonance stabilization of the oxyanion product. So, the pyridyl substituted are good leaving groups due to the field and inductive effect rather than a resonance effect. In addition, if the Brønsted plot relies on the behaviour of leaving group ability then these compounds would appear near to the previous data. If not, and the data demonstrate a linear Hammett correlation, then the experimental evidence for the break would no longer appear.

To explain more about the properties of these leaving groups, the pK_a was plotted against the sigma value of the leaving groups studied by Babtie.[55] From **Figure 15**, we can see that clearly pyridyl leaving group **13-15** (blue) fall on a line while the good leaving groups **5a-5c** deviate from the line (red points).
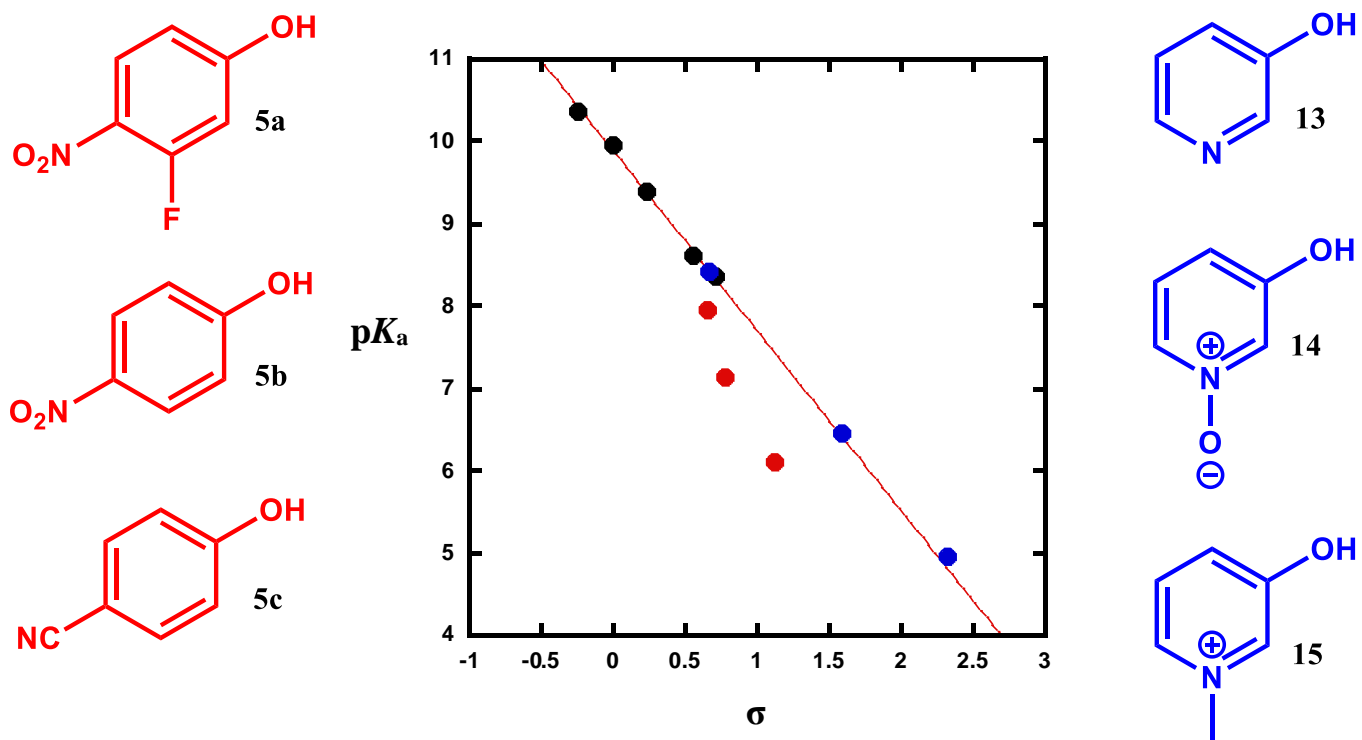
Figure 15: pK_a against sigma values of phenols; red points are **5a-5c** and blue points are pyridyl leaving groups **13-15**, black points are **5d-5h** (poor leaving groups).

2.5 Results and discussion

To investigate the mechanism of aryl benzene sulfonate ester, first the same data reported by Babtie *et al*[55]. can be plotted by a Hammett relationship (**Figure 16B**). The Hammett plot shows a good correlation as σ ignores the resonance effect.
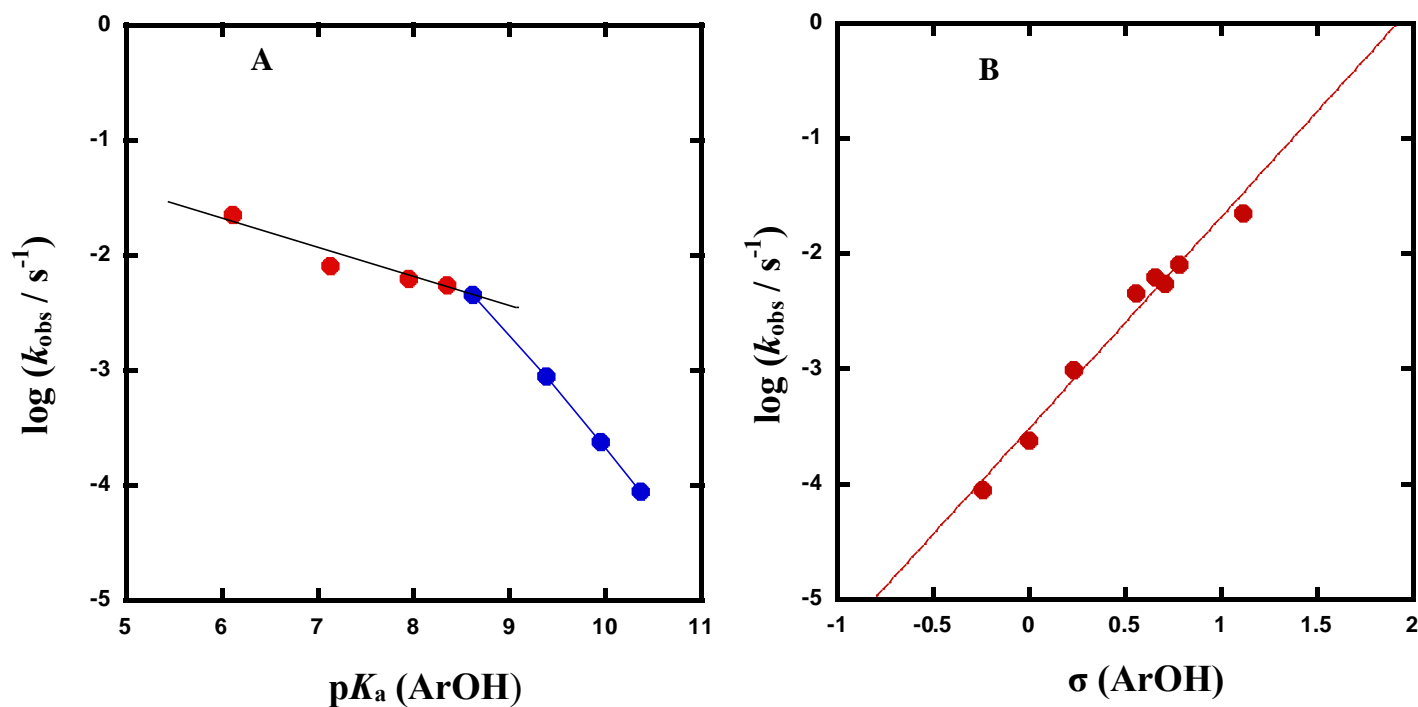
Figure 16 : A: Brønsted correlation for the alkaline hydrolysis of aryl benzene sulfonates, **B**: Hammett correlation ρ of 1.83 ± 0.07 for the same data.

The good correlation shown by the Hammett plot raises the question whether the pK_a is a suitable parameter for such reactions. Buncel *et al*[65]. found that to study the sulfonate ester promoted by ethoxide in ethanol solution, σ is more appropriate than σ⁻ (which is analogous to pK_a).

2.5.1 Synthesis of pyridyl sulfonate ester

The pyridyl compound **10** was synthesised as shown in (**Scheme 7**). **10** was used to prepare *N*-oxide and *N*-methyl derivatives. The *N*-oxide **11** was prepared by reacting **10** in CHCl$_3$ with 3-chloroperbenzoic acid. Moreover, the *N*-methyl compound **12** was synthesised by refluxing **10** in acetone with methyl iodide to produce a yellow solid. This was not purified via column since the product is too polar. The compound was then recrystallized by dissolving in a small amount of methanol and was precipitated with an excess amount of diethyl ether.
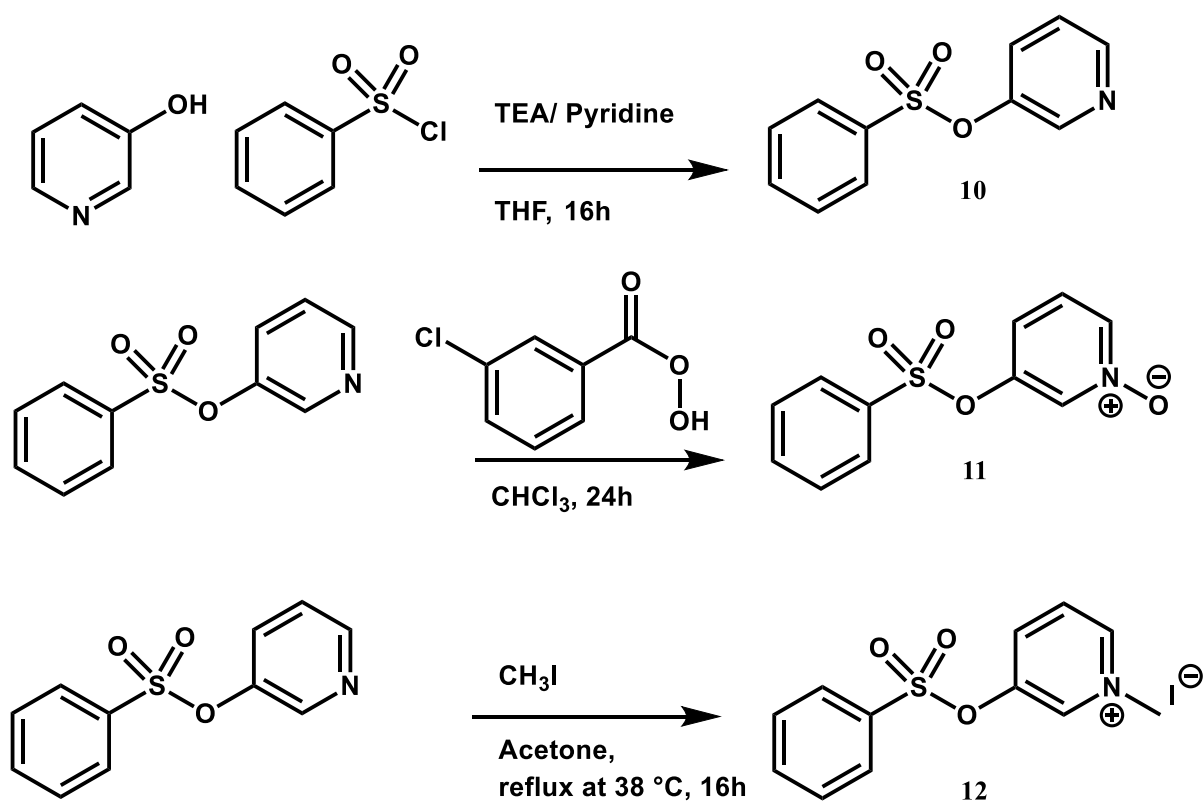
Scheme 7: Synthesis of pyridyl benzene sulfonate and its derivatives.

2.5.2 Hydrolysis of sulfonate esters

Compounds (**10-12**) have been studied at 50 ± 0.1 °C, and 0.5 M KCl which are the same conditions that were used in the previous study.[55] The alkaline hydrolysis reactions of compounds **10-12** were cleanly first order and the second order rate constants (**Table 2**) were obtained for compounds **10-12** by plotting k_{obs} values against the concentration of KOH as can been seen in **Figure 17**.

Substrate	pK$_a$ of the leaving group	k_2 / M^{-1}S^{-1}
10 (Pyridyl)	8.42	0.066 ± 0.002
11 (N-oxide)	6.45	1.54 ± 0.014
12 (N-methyl)	4.96	12.2 ± 0.4

Table 2: Second order rate constants of the alkaline hydrolysis of **10-12**.
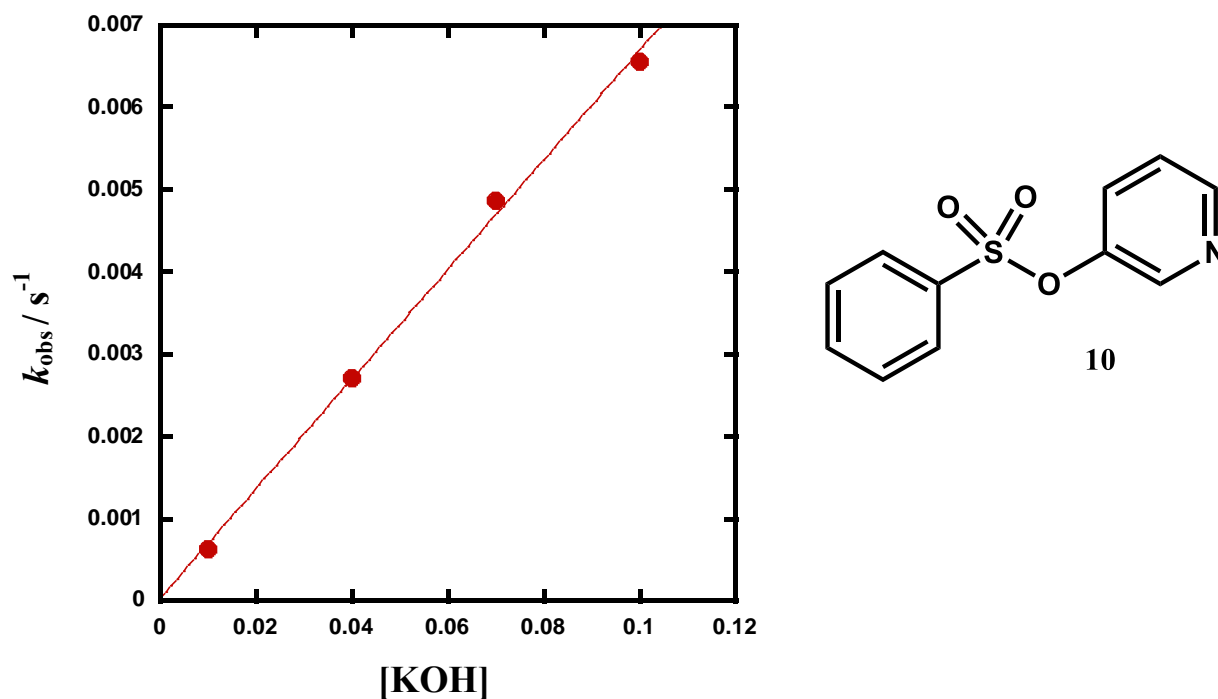
Figure 17: Hydrolysis of compound **10**, 0.5 M KCl, 50 ± 0.1 °C, $k_2 = 0.066 \pm 0.002$ M^{-1}s^{-1}, R^2 = 0.997.
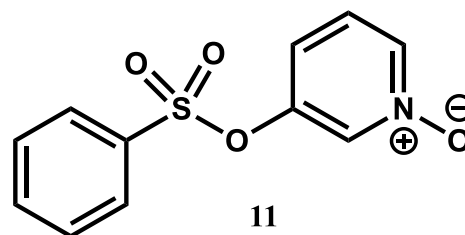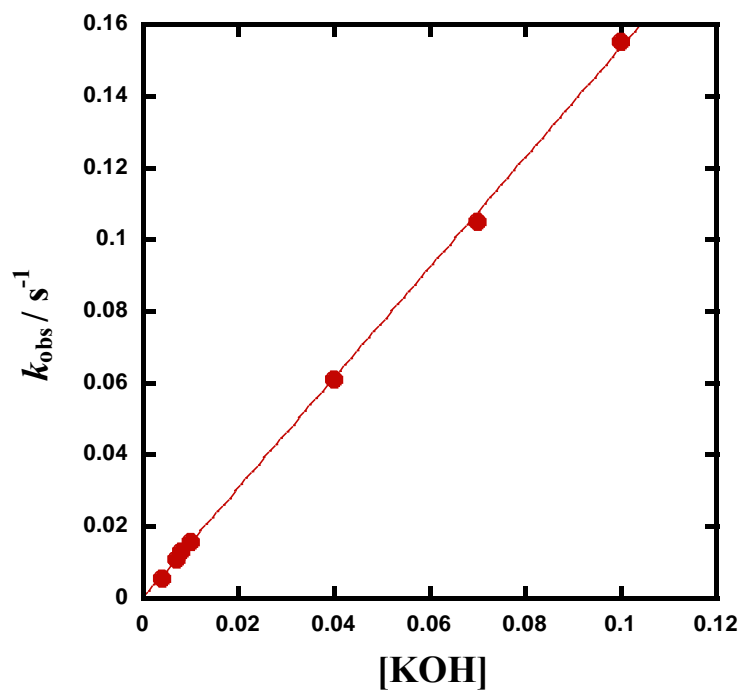
Figure 18: Hydrolysis of compound **11**, 0.5 M KCl, 50 ± 0.1 °C, k_2=1.54 ± 0.014 $M^{-1}s^{-1}$, R^2 = 0.999.
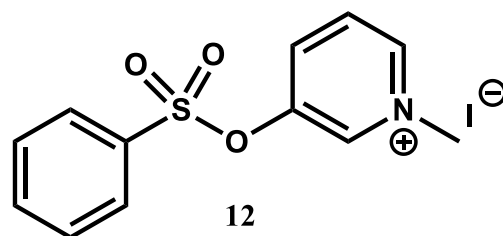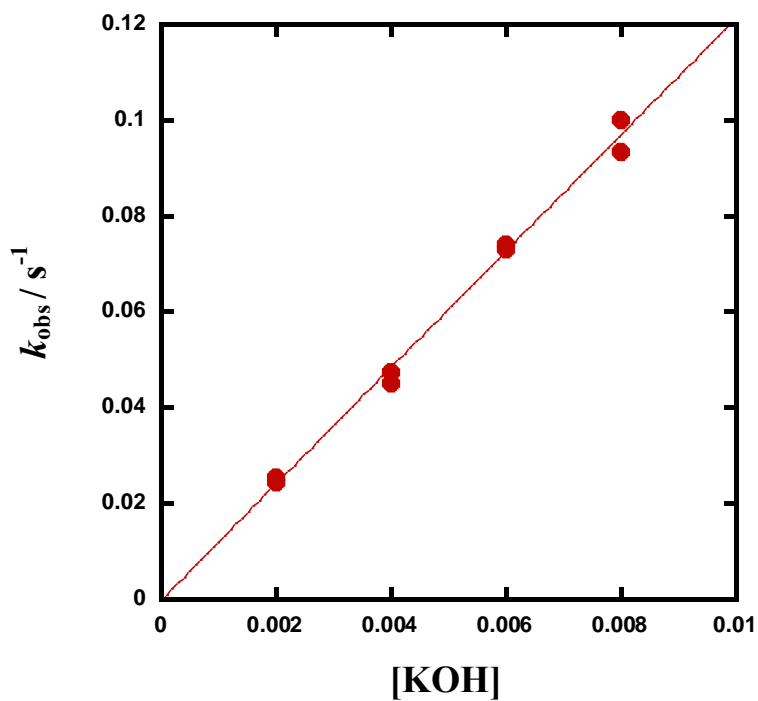
Figure 19: Hydrolysis of compound **12**, 0.5 M KCl, 50 ± 0.1 °C, k_2=12.2 ± 0.4 $M^{-1}s^{-1}$, R^2 = 0.999.

2.5.3 Linear free energy relationship of aryl benzene sulfonate esters

These compounds (**10-12**) demonstrated excellent correlation with both classes of linear free energy relationship as shown in (**Figure 20**).
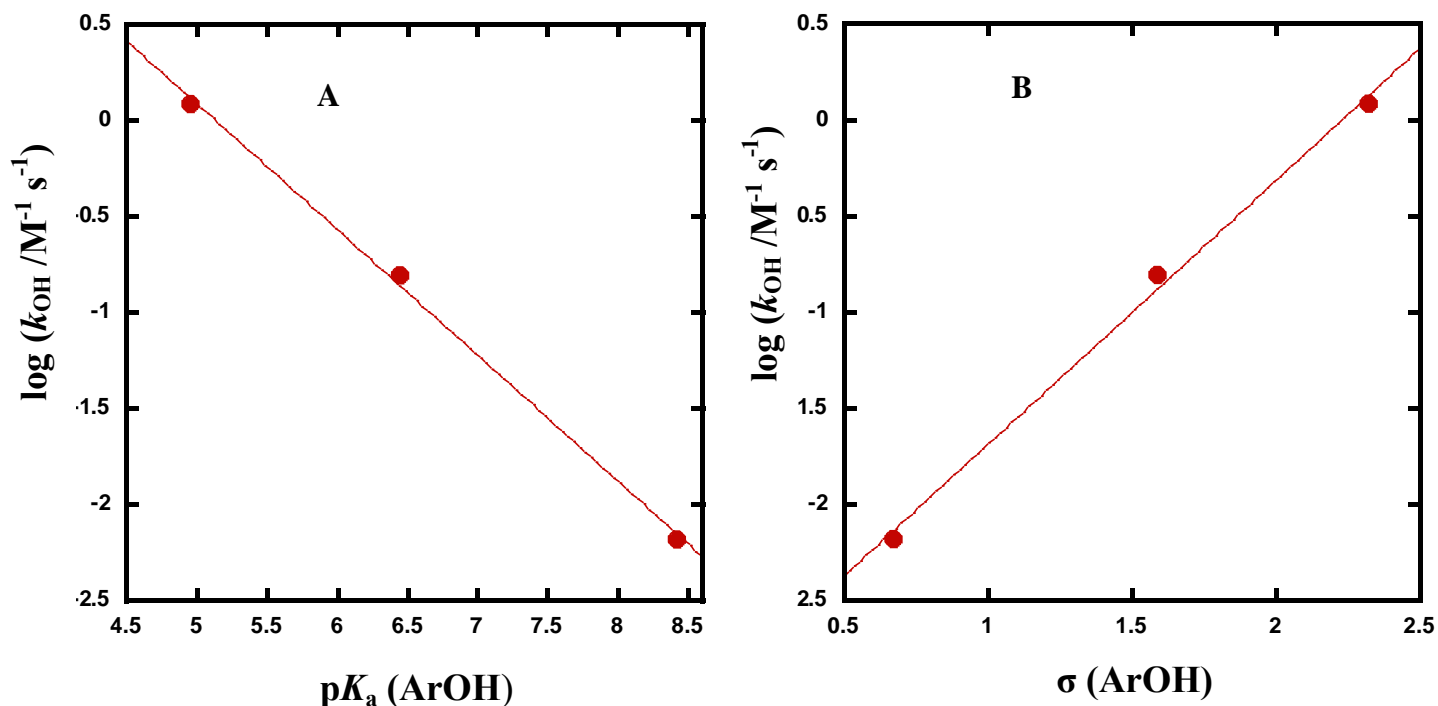
Figure 20: **A**: Brønsted plot for the alkaline hydrolysis of the pyridyl compounds (**10-12**), β = -0.66 ± 0.02, R^2 = 0.998, **B**: Hammett plot for the same data, ρ = 1.37 ± 0.07, R^2 = 0.997.

The rate constants of compounds (**10-12**) under the same conditions as the data shown in **Figure 6** are added to the previously reported data[55] in **Figure 21A**. This shows the apparent smooth curvature of the Brønsted plot has disappeared to become a linear, somewhat scattered correlation. **Figure 21B** shows that the new data contributes to a Hammett plot that retains a much better correlation. The much better correlation with σ rather than pK_a suggests that the leaving group has not broken its bond to the sulfur to any significant degree in the transition state and so mesomeric interactions do not have a large impact. The data suggested little

bond cleavage to the leaving group in the transition state and small amounts of structural variation with leaving group ability.
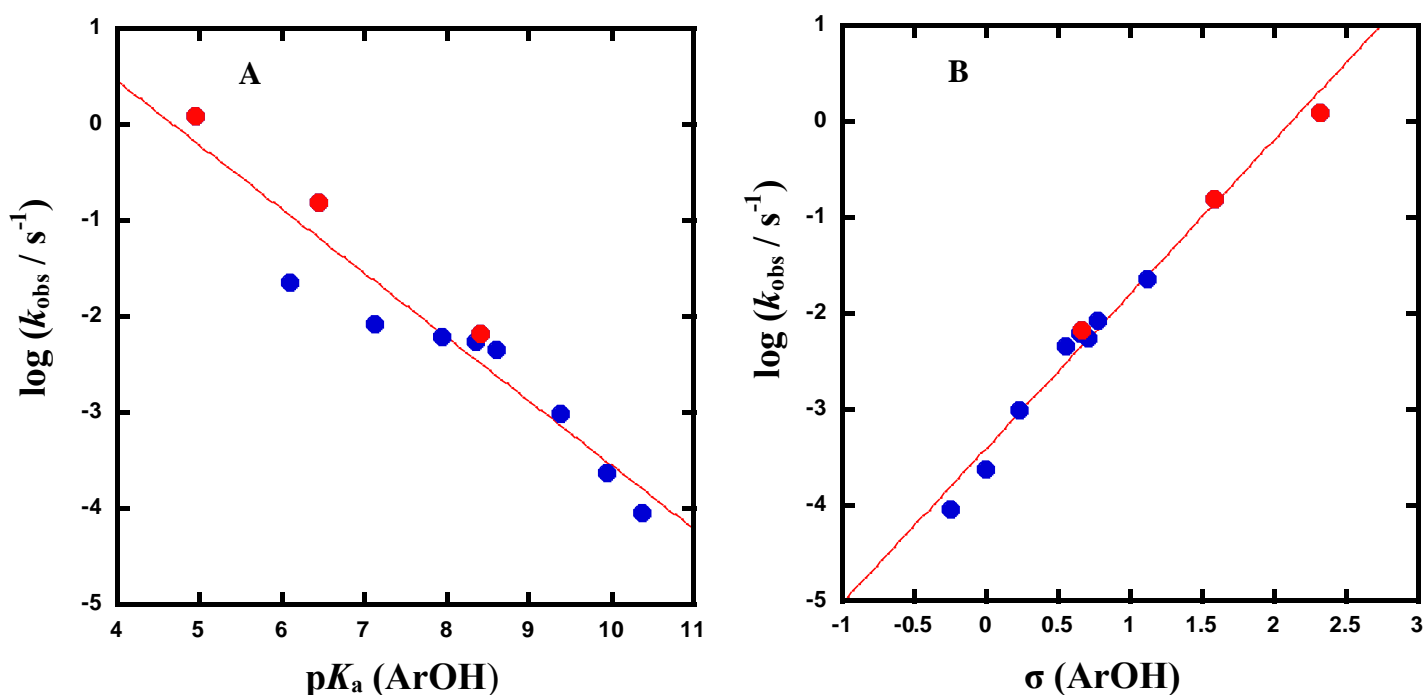
Figure 21: A: Brønsted correlation for the alkaline hydrolysis of aryl benzene sulfonates (black points reported in ref[55]; red points correspond to compounds (**10-12**). The red line is the linear least-squares fit to all the data, giving $\beta = -0.67 \pm 0.07$, $R^2 = 0.912$. **B**: Hammett correlation for the same data. The red line is the linear least-squares fit to all the data giving $\rho = 1.61 \pm 0.07$ and $R^2 = 0.983$.

Furthermore, a computational study on the same compounds **4a-h** was reported by Duarte *et al*[72] (**Figure 5**). The theoretical study[72] explored the effect of including an increasing number of discrete water molecules (2, 8 and 10) in the calculations on the nature of the transition state using the Hartree-Fock (HF) method, for direct comparison with the previous work.[55]

The experimental data are also consistent with the theoretical picture.[72] According to the calculations, the main changes that occur lie in the interaction of the nucleophile with a sulfur atom. This will be affected by the electronic character of the leaving group oxygen which will

perturb the electrophilicity of the sulfur atom and so affect the reaction rate. The minimal variation in leaving group bond lengths suggests that bond cleavage is not extensive; a slight lengthening is to be expected as the nature of the sulfur atom in the bond is altered. The better the leaving group the longer the bond to the nucleophile in the transition state, suggesting that the nature of the electrophilic sulfur has changed less, and a correspondingly smaller variation with σ is observed in this region of the plot; i.e., there is slightly concave downward curvature of the Hammett plot.

The ρ value is 1.61; this can be compared with the ρ value for the overall equilibrium process to provide some insight into the reaction progress as described by the effective charge on the leaving group. Williams has measured the β for the equilibrium as 1.81 which leads to the assignment of an effective charge of 0.8[73] on the leaving oxygen atom in the starting substrate. The β value can be converted to an equilibrium value for ρ by using the ρ for the ionization of phenols (2.1), and so the equilibrium $\rho = 2.1 \times 1.8 = 3.8$. This is, in turn, leads to an estimate of the Leffler index for this reaction as $1.61/3.8 = 0.42$, which further reinforces the early nature of the transition state, and this corresponds to a change of the effective charge on the leaving oxygen atom from +0.8 to 0 in the transition state $(0.8 - 0.42 \times 1.8 = 0.04)$.[74] Williams has thoroughly described this method of analysis[74], showing that the principle assumptions linking the analysis of type (2) LFER apply to both Hammett and Brønsted correlations. In molecular terms, as the hydroxide ion attacks the sulfur, the leaving group is converted from a strong electron withdrawing group to an essentially neutral substituent. The ρ value reflects this change in character, rather than any significant cleavage of the sulfur-oxygen bond.

The conclusions from this analysis are broadly consistent with the earlier analysis of Buncel, concerning the reactions of sulfonate esters with ethoxide in ethanol.[64,65] These authors showed improved correlations with σ rather than σ⁻ and concluded that this could be interrupted in

either the rate limiting formation of an intermediate or a transition state that closely resembles this. The large ρ values measured for these reactions led Buncel to suggest that the reaction closely resembles the formation of a pentavalent species in the rate limiting step, or a transition state that closely resembles a putative pentavalent intermediate. Likewise, the recent work of Um and Buncel suggests a small resonance demand from the leaving group in the transition state in anhydrous ethanol is consistent with this description of the reaction character.[75]

2.6 Conclusions

Three novel sulfonate esters with pyridyl leaving groups and their derivatives were synthesised successfully. These compounds gave excellent correlations with both classes of free energy relationship. On the basis of the experimental and computational evidence presented in this work, the data are best analysed in terms of a concerted pathway, where bond cleavage to the leaving group is not greatly advanced in the transition state.
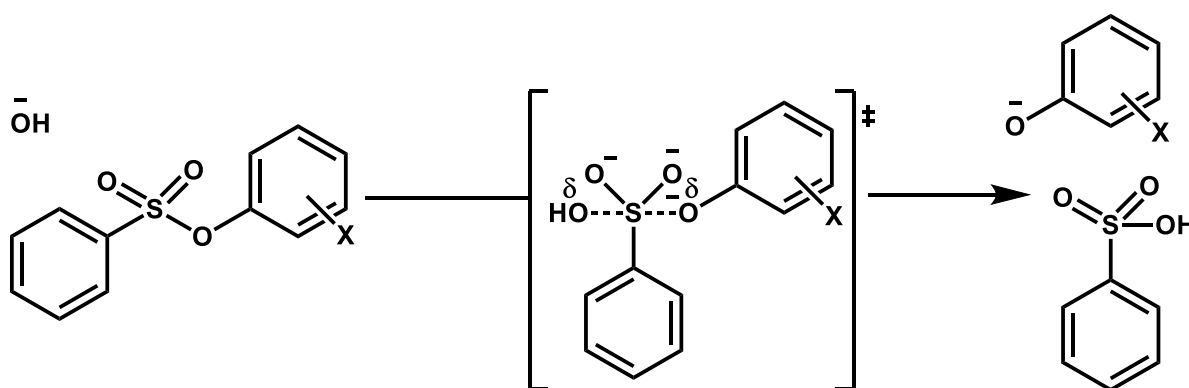
Figure 22: proposed mechanism of aryl benzene sulfonate ester.

Lastly, in considering how to correlate reactivity data with the electronic properties of a leaving group. We suggest that the substituted pyridyl leaving groups provide a useful series that extend the range of leaving groups only affected by inductive and field effects down to low pK_a. These may be better than, and certainly a complement, to the widely utilized 4-nitrophenyl substituent.

33

Chapter three: Phosphate diesters

3.1 Introduction: Phosphate diesters

Phosphoryl transfer plays a significant role in many biological processes. For instance, it is involved in signaling, biosynthesis, ATP production and energy regulation and genetic replication.[1,4,5,76,77] Phosphate diesters are of particular importance as many biological molecules, including DNA and RNA, contain this moiety.[1] The inclusion of the phosphate diester group in DNA helps to preserve the genetic code.[4] Synthesis, hydrolysis and repair of DNA is performed by DNA polymerase enzymes[78] at these phosphate diester sites. Therefore, understanding the mechanism of the enzyme-catalysed phosphate diester cleavage is extremely important in understanding phosphoryl transfer in such molecules as DNA.

Phosphoryl transfer is extremely slow in solution under mild conditions especially, for phosphate mono- and di-esters. For instance, the hydrolysis of the phosphate dianion **17** in neutral water[11] has a half life time of one trillion years (first order rate constant $2 \times 10^{-20}\,\text{s}^{-1}$).
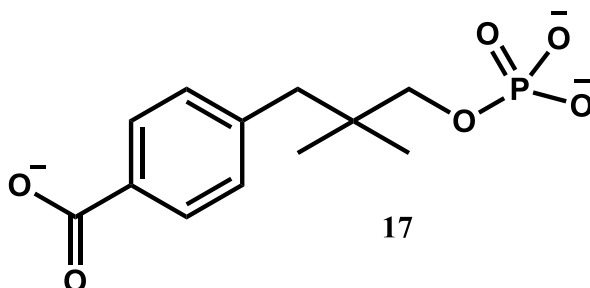
Figure 23: Model compound for phosphate monoester reported by Lad *et al.*[11]

The spontaneous hydrolysis of Np2*P, compound **18,** was studied by Schroder *et al.*[79] The γ branching in the alcohol leaving group prevents the cleavage of C-O. This forces the cleavage to occur at the P-O bond. The rate constant for this reaction was determined to be $7 \times 10^{-16}\,\text{s}^{-1}$ with a half-life of 31 million years at 25 °C.

35

18
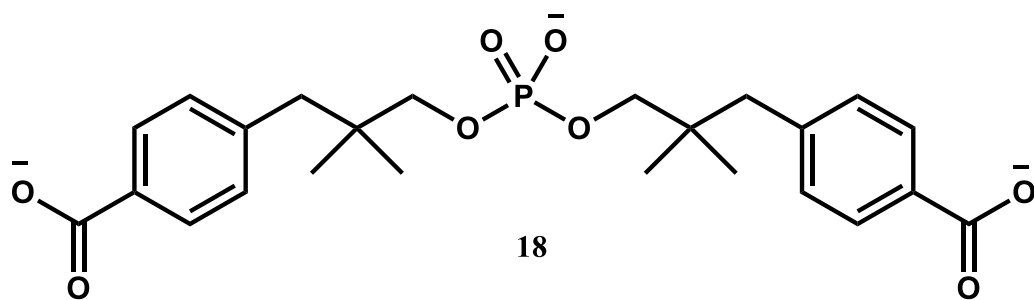
Figure 24: model compound of phosphate diester reported by Schroder *et al.*[79]

The kinetic stability of these phosphate species makes them suitable for biological roles.[1] Studying the non-enzymatic cleavage of these compounds could aid understanding as to how these enzymes enhance the rate of reaction magnificently compared to the uncatalysed reaction in solution. Furthermore, studying the transition state of the non-enzymatic reaction could give insight into the catalytic mechanism.[2]

3.2 Previous work

Kirby and Younas[27] studied the reactivity of a series of substituted bis-phenyl phosphate diesters at 100 °C, 1 M ionic strength and they found that, generally, these species were unreactive at 100 °C. However, their susceptibility to hydrolysis relies on the basicity of the leaving group.

X=
a: 2,4-$(NO_2)_2$
b: 4-acetyl-2-NO_2
c: 4-Cl, 2-NO_2
d: 4-NO_2
e: 2-NO_2
f: 3-NO_2
g: H

19
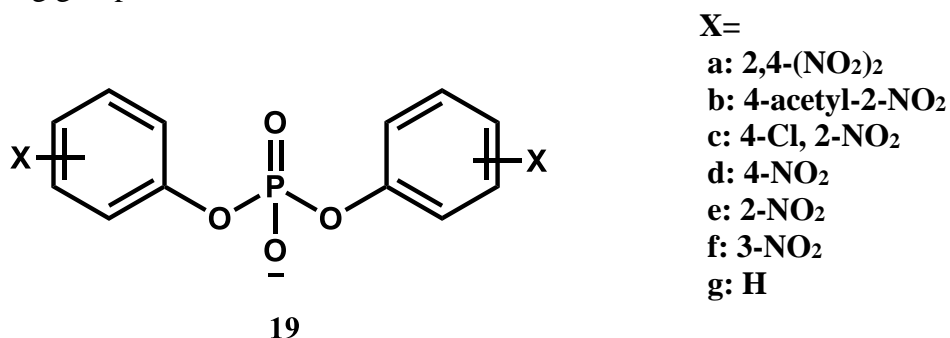
Figure 25: Series of phosphate diesters studied by Kirby and Younas.[27]

A Brønsted plot showed that the β_{lg} value was -0.97 which indicates that the reactivity of phosphate diester is very sensitive to the variation of pK_a of the leaving group (**Figure 26**).
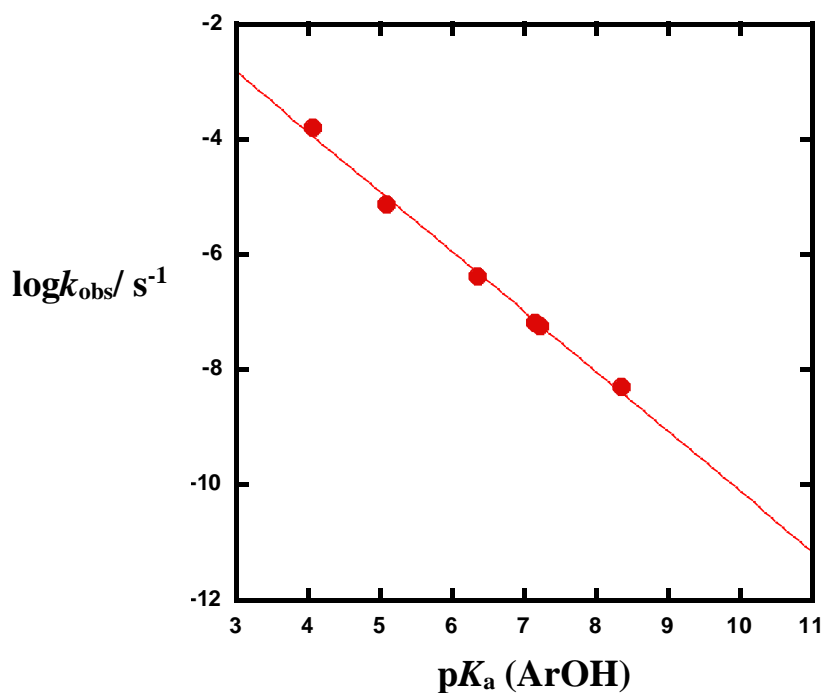
Figure 26: Brønsted plot of spontaneous hydrolysis of substituted diaryl phosphate diester; β_{lg} = -0.97 ± 0.03, I = 1 M KCl, 100 °C.

Further, they measured the entropy of activation of compound **19a** to be -25.5 J K^{-1} mol^{-1} and the kinetic isotope effect of the solvolysis reaction was found to be $k_H/k_D = 1.45$. Based on the solvent isotope effect and entropy of activation measurements, they proposed an S$_N$2 mechanism to explain the spontaneous hydrolysis of the phosphate diester via a single step.

Subsequently, the alkaline hydrolysis of substituted diaryl phosphate diesters with the same leaving groups **19a-g** were studied by Younas *et al*[80] at 39 °C and 1 M ionic strength. The Brønsted coefficient β_{lg} was determined to be -0.68 (**Figure 27**) which indicates that the alkaline hydrolysis is a rather less sensitive to the basicity of the leaving group compared with spontaneous hydrolysis[27] of the same series that were examined at 100 °C.
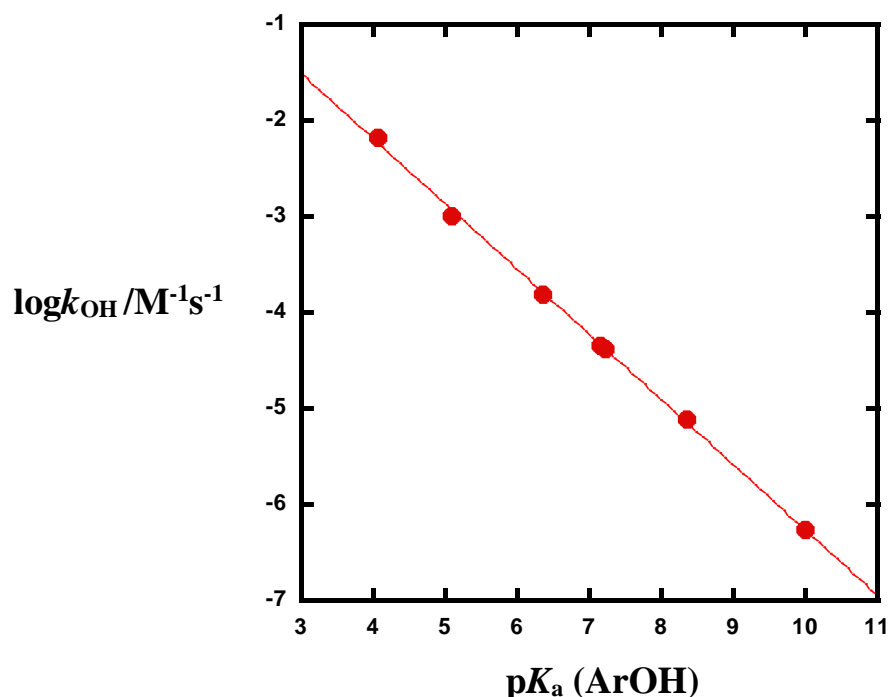
Figure 27: Brønsted plot of alkaline hydrolysis of substituted diaryl phosphate diester; $\beta_{lg} = -0.68 \pm 0.01$, $I = 1$ M KCl, 39 °C.[80]

The β_{lg} value -0.97 at 100 °C is estimated to be equivalent to -1.16 at 39 °C since temperature

has an effect on the β_{lg} values. Increasing the temperature [10] lowers the β_{lg} value according to the following equation which was originally applied to ρ values from Hammett type plots[81]:

$$\beta_2 = \beta_1 \times T_1/T_2 \qquad \textbf{Equation 10}$$

where T is the temperature in Kelvin.

Zalatan and Herschlag[15] have investigated the enzymatic and non-enzymatic alkaline hydrolysis reactions at 25 °C and 42 °C respectively for a series of substituted phenyl methyl phosphate diesters (**Figure 28**). LFERs were applied to examine the transition state structure. They suggested that compounds **20a** and **20c** (4-NO$_2$ and 4-CN) deviate from the correlations due to resonance effects. The β_{lg} values were -0.94 ± 0.05 and -0.95 ± 0.08 for non-enzymatic and enzymatic reactions respectively. The data that were represented in their work suggest that the reaction could be described by a synchronous transition state which means the transition state is in the middle, between tight and loose transition states.

X=
a: 4-NO$_2$
b: 4-Cl-3-NO$_2$
c: 4-CN
d: 3,4-(Cl$_2$)$_2$
e: 3-Cl
f: 3-F
g: 4-Cl
h: 4-F
i: H
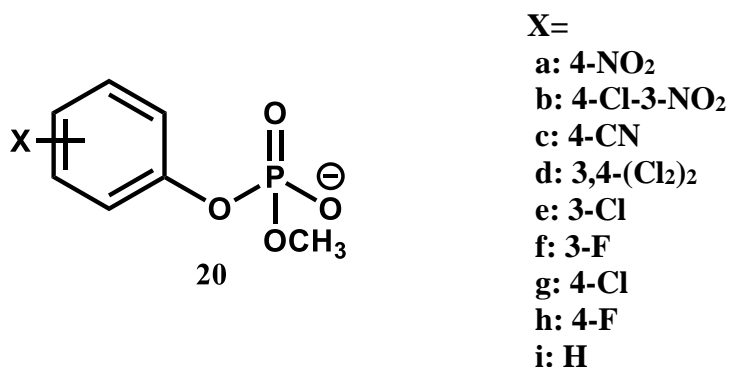
Figure 28: Series of substituted phenyl methyl phosphate diester reported by Zalatan and Herschlag.[15]
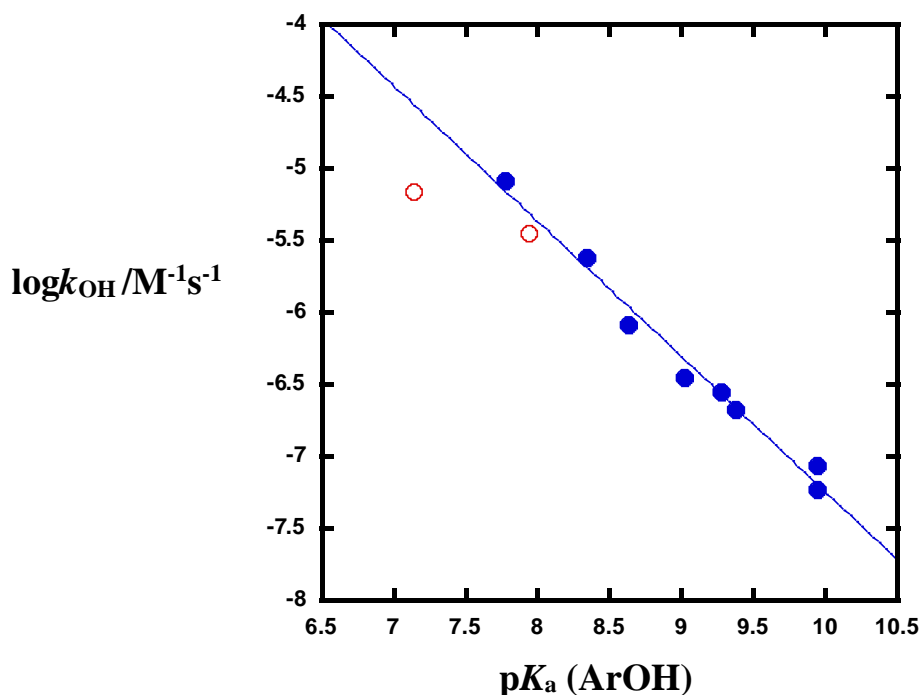
Figure 29: Brønsted plot of alkaline hydrolysis of substituted aryl phosphate diester; open circles are 4-nitro **20a** and 4-cyano **20c** (their rate constants were omitted from the fitting line) $\beta_{lg} = -0.94 \pm 0.05$, $I = 1$ M NaCl, 42 °C.[15]

In order to obtain a conclusive answer about the mechanism of aryl methyl phosphate diester hydrolysis. Rosta *et al.*[4] examined theoretically the same compounds **20a-i**. Computational tools such as *ab-intio* potential energy surfaces were used to explore the nature of the transition state and reaction coordinate. Based on the calculation of the free energy surface, the distance between the phosphorus atom and the oxygen atom were 1.9 A° and 2.4 A° for leaving group and nucleophile respectively. The calculated surface shows only a single transition state for a concerted mechanism. The computational results were identical to the results observed experimentally. However, an associative, concerted mechanism was concluded depending on the values of the P-O bond length for the leaving group and nucleophile.

Metal ion complexes have been used to catalyse phosphate diester hydrolysis. Some examples of metal ion catalysed phosphate diester hydrolysis and their effects on the reaction transition

state are described here. In these examples, we will see how the reaction can be catalysed and the effects of catalyst on $\beta_{lg.}$

Padovani *et al*[82]. examined the hydrolysis of a series of methyl aryl phosphate diester compounds **21a-g** using a cobalt (III) complex **22** (TrpCo (III) (OH)(OH$_2$) at 37°C and ionic strength adjusted to 0.1 M NaClO$_4$. From their results, the pH rate profile illustrated only the aqua hydroxyl part of the complex shows significant activity.

X=
a: 3-Cl
b: 3-NO$_2$
c: 4-NO$_2$
d: 3,5-(NO$_2$)$_2$
e: 3-F,4-NO$_2$
f: 3,4-(NO$_2$)$_2$
g: 2,4-(NO$_2$)$_2$
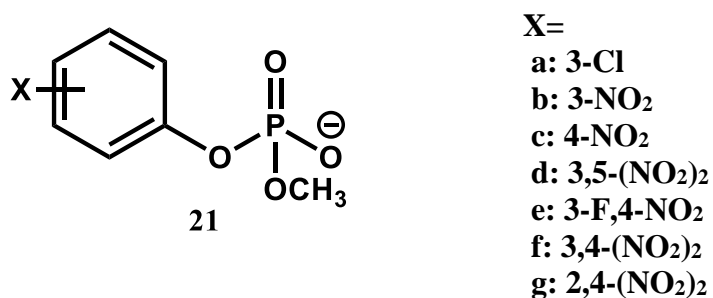
Figure 30: Series of substituted phenyl methyl phosphate diester reported by Padovani *et al.*[82]

The LFER was studied and it was found to be nonlinear with β_{lg} of -0.15 to -1.05 when the leaving group varied to poorer leaving group. The bend in the Brønsted plot suggests presence of a change in the rate limiting step. Thus, the following mechanism was proposed in which phosphate diester hydrolysis was promoted by the Co (III) complex as shown in **Scheme 8**.
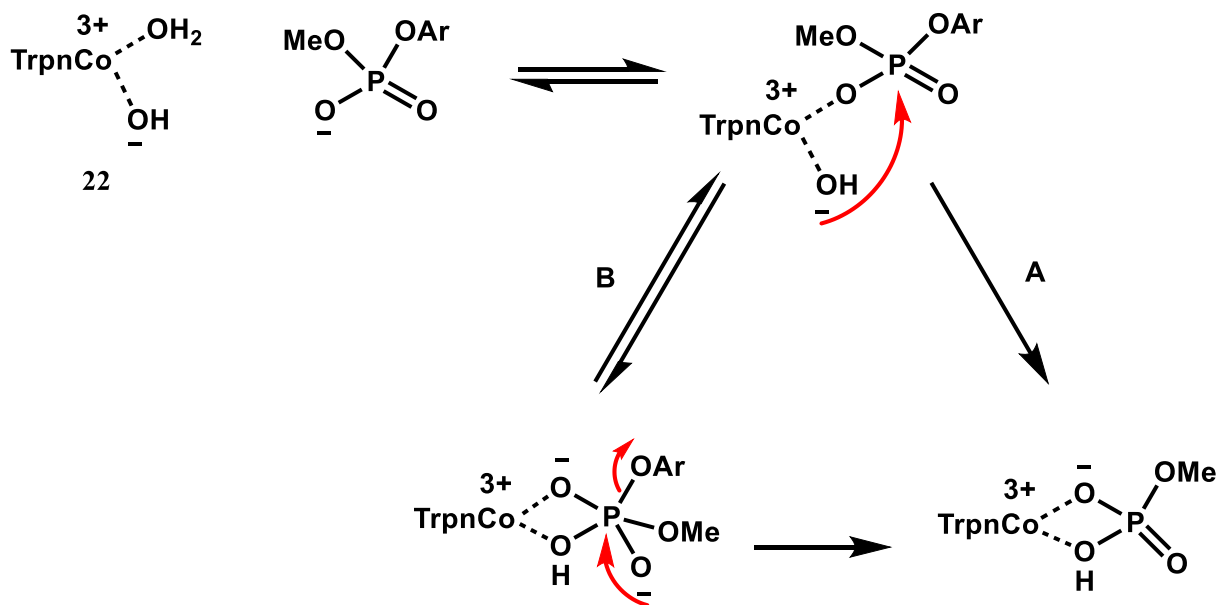
Scheme 8: Possible mechanism of phosphate diester hydrolysis promoted by Co (Ⅲ) complex.[82]

Comparison between the reactivities of aryl methyl phosphate diesters coordinated with dinuclear Co (III) complex **23**, and uncoupled aryl methyl diesters were investigated at 25 °C by Williams *et al.*[26]

X=
a: 3-F,4-NO$_2$
b: 4-NO$_2$
c: 3-NO$_2$
d:H
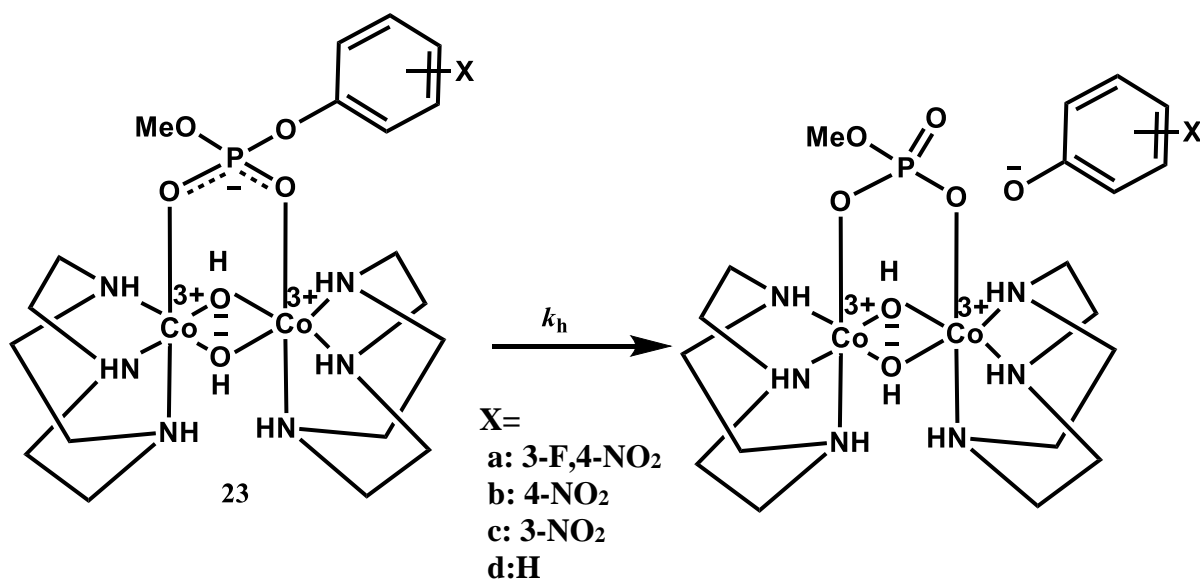
Scheme 9: The hydrolysis of Co (Ⅲ) complex coordinated to aryl methyl phosphate diesters.[26]

LFER were utilized to assess the reaction mechanism and transition state structure. Thus, β_{lg} were determined to be -1.38 ± 0.01 and -0.64 ± 0.03 with respect to the bound and unbound aryl methyl phosphate diesters respectively (**Figure 31**). The high value of β_{lg} = -1.38 corresponding to the bound complex indicates a mechanism in which there was significant charge development on the oxygen atom of the leaving group whilst the unbound complex showed less charge development with β_{lg} = -0.64. The β_{lg} value for the un-bound species of -0.64 is very close to the β_{lg} value of -0.69 ± 0.03 determined in a study[34] examining analogous compounds of methyl substituted phosphonate esters under the same conditions. This study found that the reaction can proceed via a concerted mechanism.
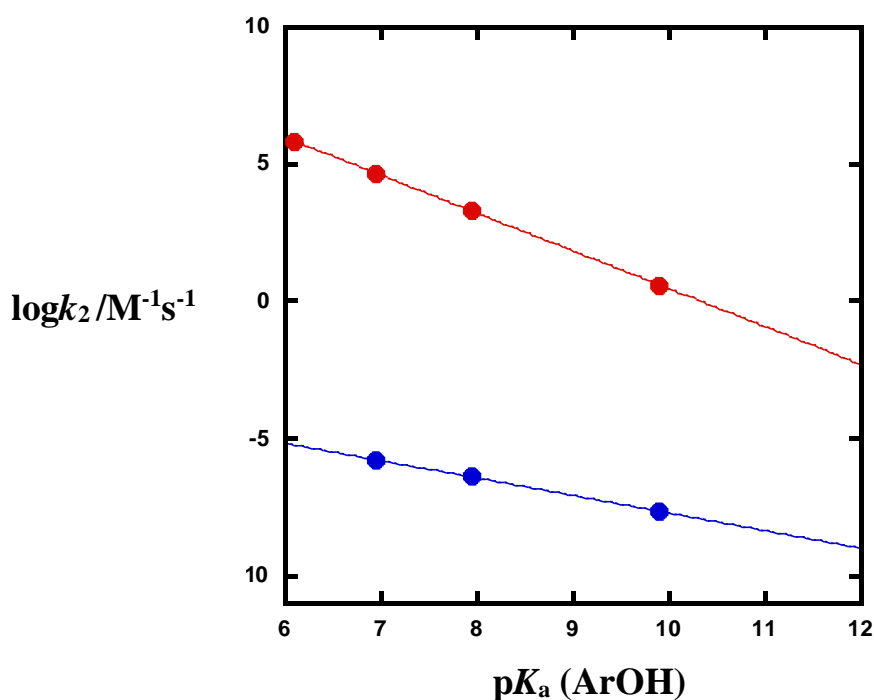
Figure 31 : Brønsted plot of hydrolysis of aryl methyl phosphate diester (red points, β_{lg} = -1.38 ± 0.01) coordinated with Co (Ⅲ) complex and (blue points, β_{lg} = -0.64 ± -0.03) corresponding to unbound aryl methyl phosphonates, I = 0.1M NaClO$_4$, 25 °C.[26]

43

In a recent study[83], the reactivity of Zn (II) complexes **24-26** was examined with bis 4-nitrophenyl phosphate (BNPP) at 25 °C in aqeous solution. The reactivity was increased by 350 fold compared to the alcohol analogue. Complex **26** was the most reactive species due to not allowing the nucleophile to form a bond with a metal ion. In order to investigate the transition state, the reactivity of complex **26** was studied towards substituted aryl methyl phosphate diester varying the pK_a of the leaving group from 7.14 to 9.95.
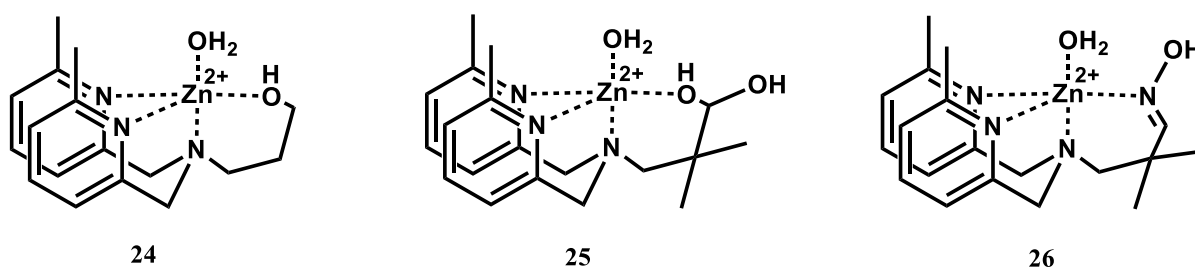
Figure 32: Zn (II) complexes **24-26** reported by Tirel and Williams.[83]
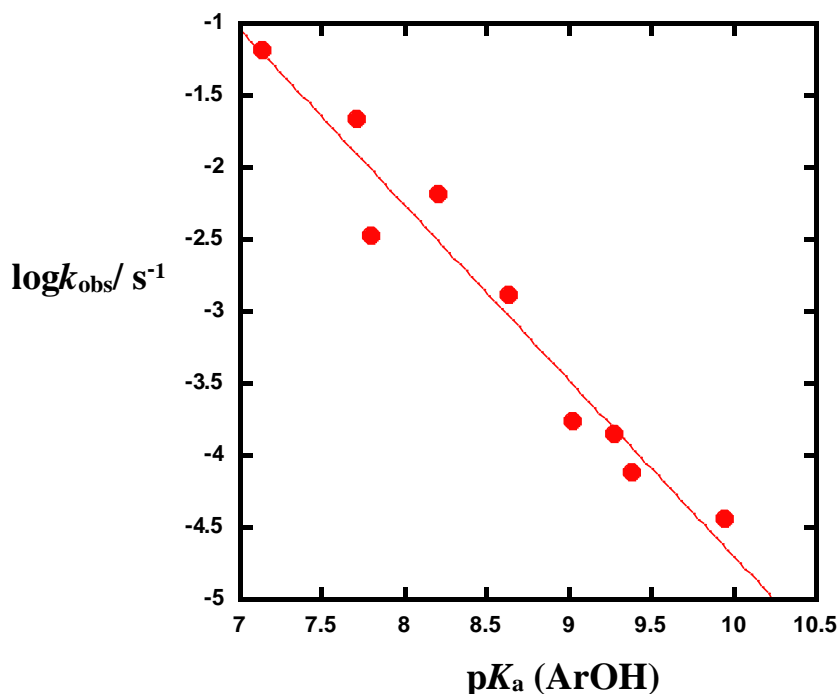
Figure 33: Brønsted plot of aryl methyl phosphate diester catalysed by complex **26**; $\beta_{lg} = -1.2 \pm 0.1$, 25 °C, 0.1 M NaNO$_3$, 2 mM complex **26**, pH 8.1.[83]

44

The Brønsted plot (**Figure 33**) showed a scattered correlation with β_{lg} of -1.2 ± 0.1 which is higher than the β_{lg} of -0.94 ± 0.05 for hydroxyl promted reaction of the analogue compounds.[15] The high value of β_{lg} -1.2 suggested that the transition state is more sensitive to the varying bascitity of the leaving group.

3.3 Aims

It has been shown from the study of sulfonate esters (chapter two) that the pyridyl leaving groups could give complementary data to the 4-nitro substituent in terms of the reactivity and mechanism of the reaction. Specially 4-nitro and 4-cyano substituents (**Figure 29**) were often outliers on the linear free energy relationship correlations for phosphate diesters due to resonance effects.[15] Therefore, the pyridyl leaving groups (**Figure 34**) were chosen to study the mechanism of phosphate diesters and to investigate whether they are better leaving groups to use than 4-nitro phenol.
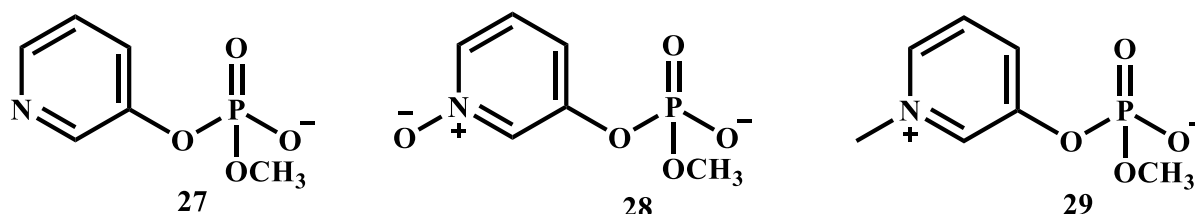
Figure 34: Pyridyl phosphate diesters **27-29** in this study.

45

3.4 Results and discussions

3.4.1 Synthesis phosphate diester

The proposed reaction to synthesise aryl methyl phosphate diester is explained in **Scheme 10**. The reaction involved two steps[84,85], the first was reacting the desired phenol with methyl dichloro phosphate in DCM in the presence of triethylamine to yield a phosphate triester. The second step was to convert the phosphate triester to the phosphate diester by adding sodium hydroxide, followed by cation exchange to form sodium methyl phosphate diester.
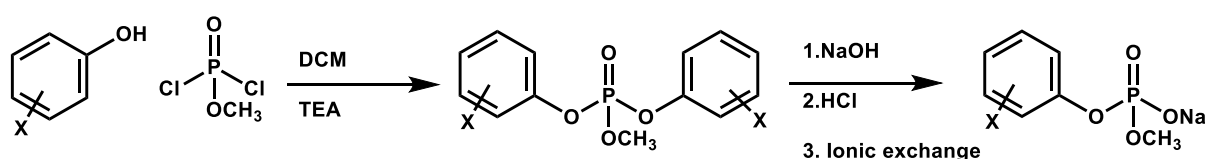
Scheme 10: First attempt to synthesis aryl methyl phosphate diester.[84,85]

However, the first step was not successful and changes to the base, solvent or leaving group did not facilitate the reaction. For example, pyridine was used instead of TEA as a base and THF used instead of DCM as a solvent. It was concluded that this proposed procedure is sensitive to the structure since it was originally proposed for phenols and we tried it for 3-hydroxy pyridine and its derivatives.

Therefore, a different route was used as shown in **Scheme 11**. The new route[82] included using a different reagent and base which were dimethyl chlorophosphate and imidazole respectively. The reaction was started by adding 3-hydroxy pyridine and imidazole to the dimethyl chlorophosphate to form phosphate triester **30**. Then the phosphate diester was obtained by refluxing the phosphate triester in acetone with lithium chloride. Surprisingly, the pyridyl methyl phosphate diester **27** was not formed and *N*-methyl phosphate diester **29** was formed instead, due to the nucleophilicity of the nitrogen in the 3-hydoxy pyridine ring.

Moreover, the reaction happened even better without adding lithium chloride, just by refluxing in acetone. Therefore, the reaction was achieved without lithium chloride. The attempt to synthesise dimethyl *N*-oxide pyridyl phosphate **31** by oxidising dimethyl pyridyl phosphate triester **30** using 3-chloroperbenzoic acid was not successful. As a result, the reaction was achieved with the same methodology as dimethyl 3-hydroxy pyridine phosphate triester. The *N*-oxide pyridyl phosphate triester **31** was synthesised by using *N*-oxide pyridyl as leaving group and CH₃CN was used as solvent because the *N*-oxide has poor solubility in DCM. Then **31** was converted to **28** using lithium chloride in acetone with reflux.
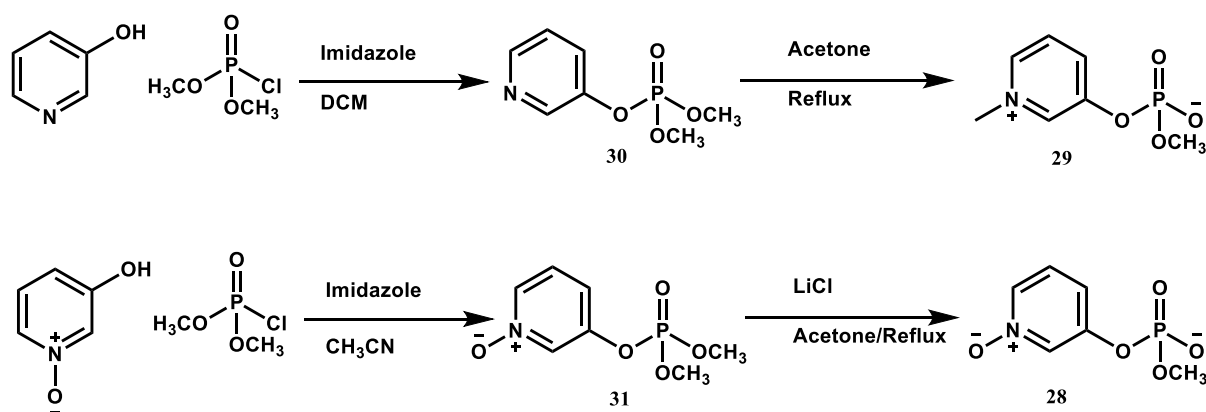
Scheme 11: Second attempt to synthesise aryl methyl phosphate diester.

3.4.2 Alkaline hydrolysis of pyridyl phosphate diester

The hydrolysis of compounds **28** and **29** were studied using uv-vis spectrometry at 42 ± 0.04 °C, 1 M (NaCl) ionic strength and different concentrations of NaOH to allow for direct comparison with the literature.[15] Excess NaOH was used and its concentration varied at least 10 fold with more than eight different values. For slow reactions, when the concentration of NaOH was low, initial rate measurements were used to follow between 1-5 % of the reaction using 10 times higher substrate concentration. All the reactions of compounds **28** and **29** obeyed pseudo first-order or linear initial rate reaction. The second order rate constants for compound **28** ($k_2 = 4.11 \pm 0.03 \times 10^{-5}\,\mathrm{M^{-1}s^{-1}}$) and **29** ($k_2 = 3.6 \pm 0.05 \times 10^{-4}\,\mathrm{M^{-1}s^{-1}}$) were obtained by plotting the k_{obs} values of each reaction against the concentration of NaOH as shown in

Figure 35.
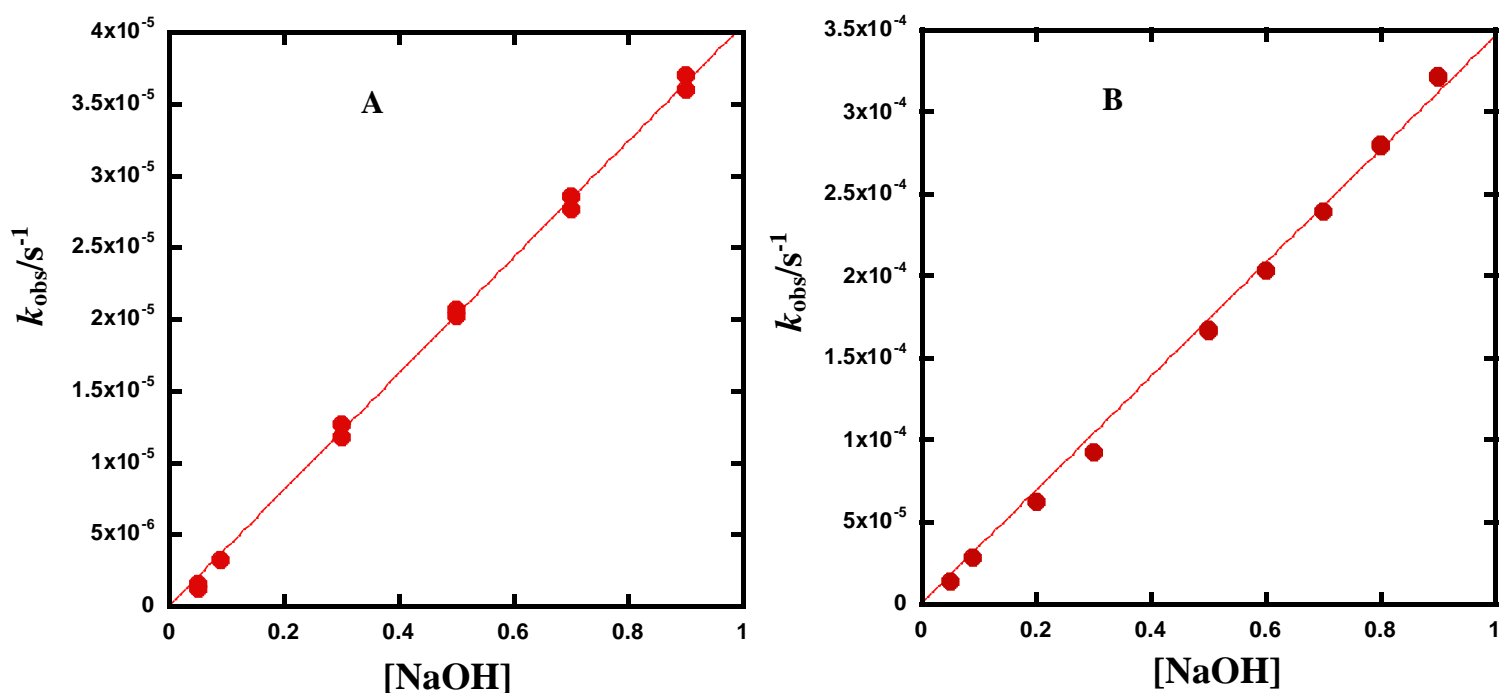
Figure 35: Alkaline hydrolysis of phosphate diester at 42 °C $\pm$ 0.04 and 1 M NaCl; A: *N*-oxide compound **28**, $k_2 = 4.11 \pm 0.03 \times 10^{-5}\,\mathrm{M^{-1}s^{-1}}$; $R^2 = 0.999$; B: *N*-methyl compound **29**, $k_2 = 3.6 \pm 0.05 \times 10^{-4}\,\mathrm{M^{-1}s^{-1}}$; $R^2 = 0.999$.

3.4.3 Product analysis

The product after hydrolysis was investigated by following the hydrolysis of *N*-methyl pyridyl methyl phosphate diester **29** by ^{1}H NMR and ^{31}P NMR spectroscopies and using 0.1 M NaOD in D$_2$O. The ^{1}H NMR and ^{31}P NMR spectra confirm the products were the leaving group and methyl phosphate as shown in **Figure 36** and **Figure 37**.
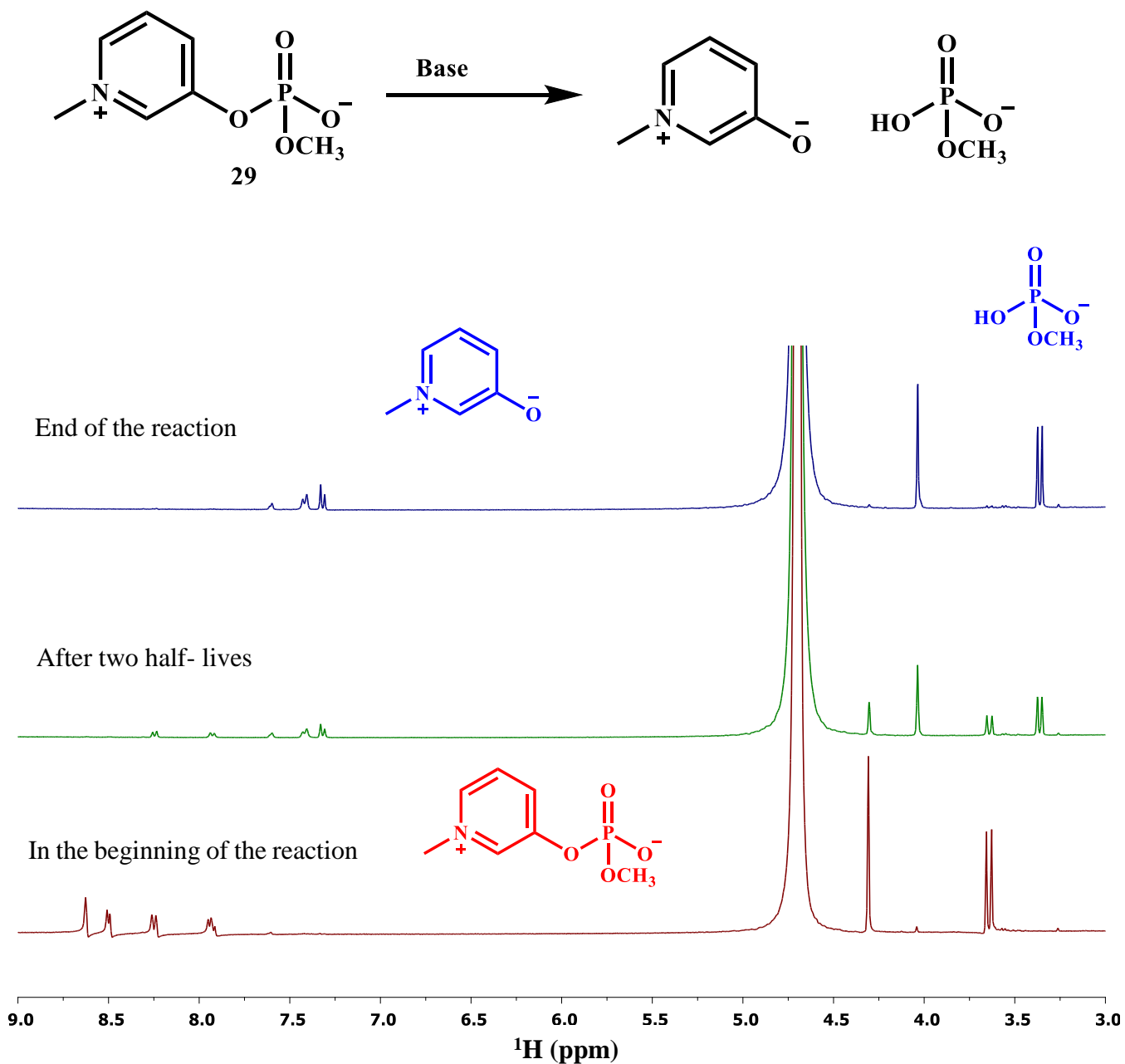
Figure 36: Following the hydrolysis of *N*-methyl pyridyl methyl phosphate diester **29** by ^{1}H NMR, 0.1 NaOD in D$_2$O.
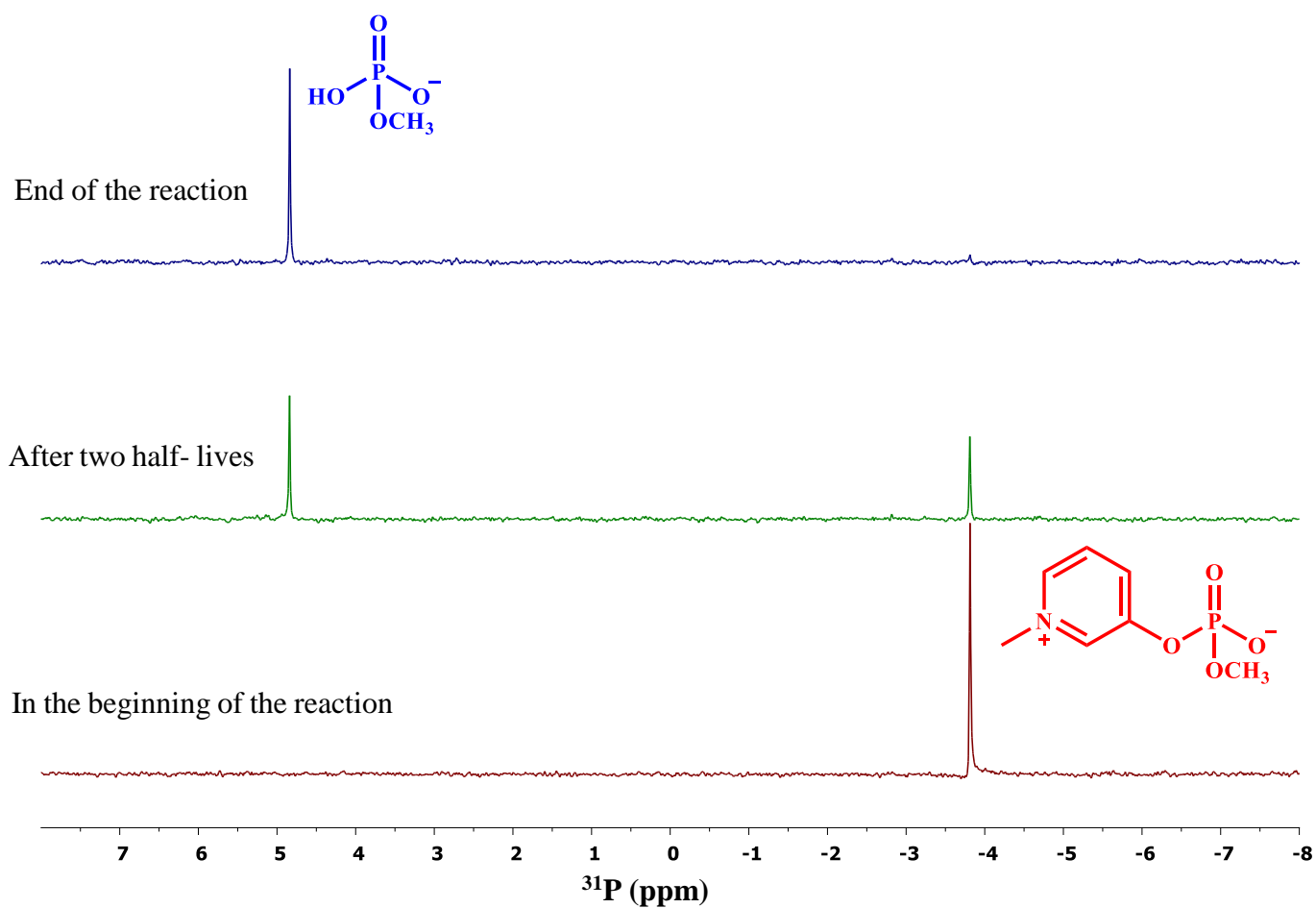
Figure 37: Following the hydrolysis of *N*-methyl pyridyl methyl phosphate diester **29** by ^{31}P NMR, 0.1 NaOD in D₂O.

3.4.4 pK_a measurements of substituted pyridyl leaving group

Brønsted correlations require the pK_a values of the leaving group. Thus, it is important to obtain these values accurately. In most cases, the pK_a values from the literature were measured at 25 °C and did not take account of the effect of ionic strength. Therefore, the pK_a values of pyridyl leaving group **14** and **15** have been measured under the same conditions of the kinetic experiment 42 ± 0.2 °C and 1 M NaCl (**Figure 38** and **Figure 39**). Additionally, the pK_a values of phenols were measured by Alkherraz *et al*[86] at the same mentioned conditions. 4-Cyano phenol (**Figure 40**) was also measured under the same experimental condition since it was not measured by Alkherraz *et al.*[86] As can be seen from **Table 3** there is difference between literature values and measured values. This is maybe because of the effect of temperature and ionic strength.

Substituted of phenols	pK_a (literature)[86]	pK_a (measured)
20a (4-NO$_2$)	7.14	6.75
20b (4-Cl-3-NO$_2$)	7.78	7.45
20c (4-CN)	7.95	7.63
20d (3-NO$_2$)	8.35	7.97
20e (3,4-Cl$_2$)	8.63	8.36
20f (3-Cl)	9.02	8.85
20g (3-F)	9.28	9.0
20h (4-Cl)	9.38	9.22
20i (4-F)	9.95	9.67
20k (phenol)	9.95	10.0
14 (*N*-oxide pyridyl)	6.45	5.91
15 (*N*-methyl pyridyl)	4.96	4.84

Table 3: pK_a values of substituted phenols and pyridyl leaving groups from the literature at 25 °C and experimentally measured at 42 °C and 1 M NaCl.
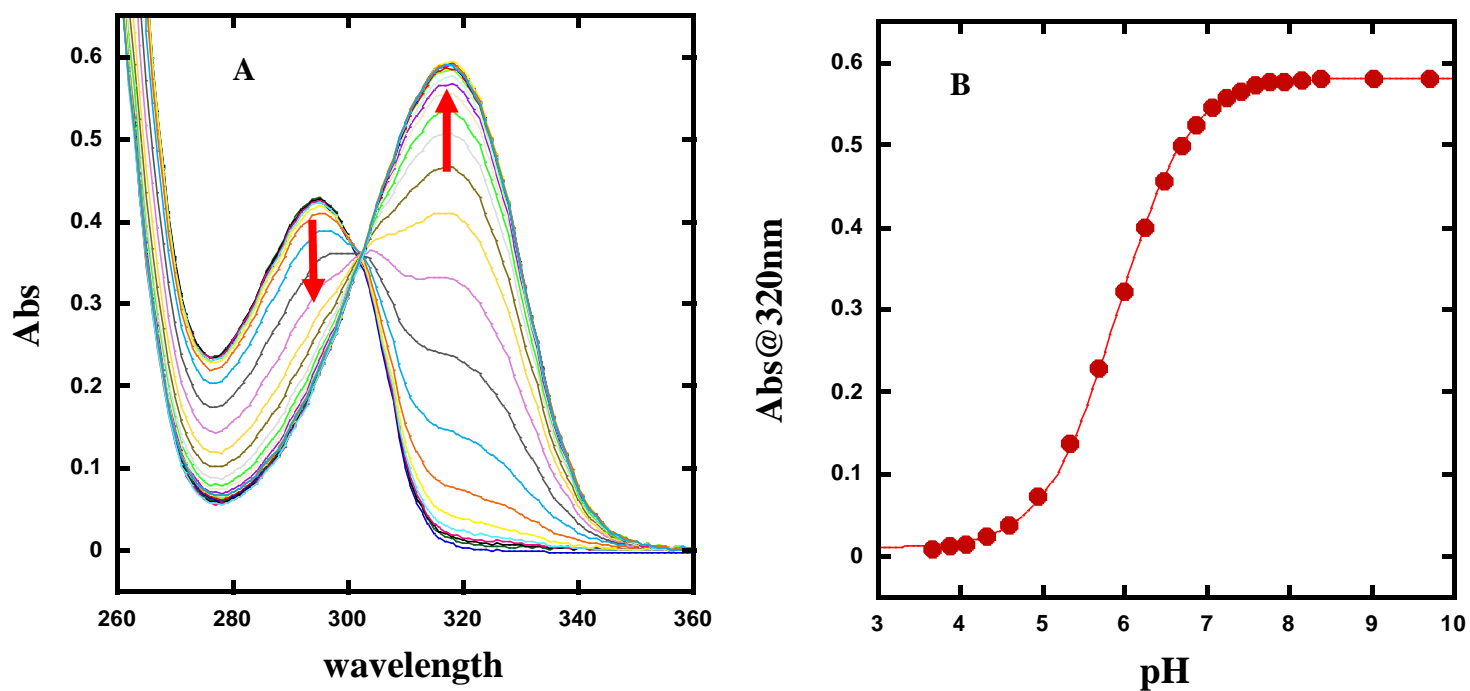
Figure 38: **A**: UV titration of *N*-oxide pyridyl **14** at 42 ± 0.2 °C, 1 M NaCl; **B**: dependence of absorbance on pH measurement; $pK_a = 5.91 \pm 0.01$; $R^2 = 0.999$.
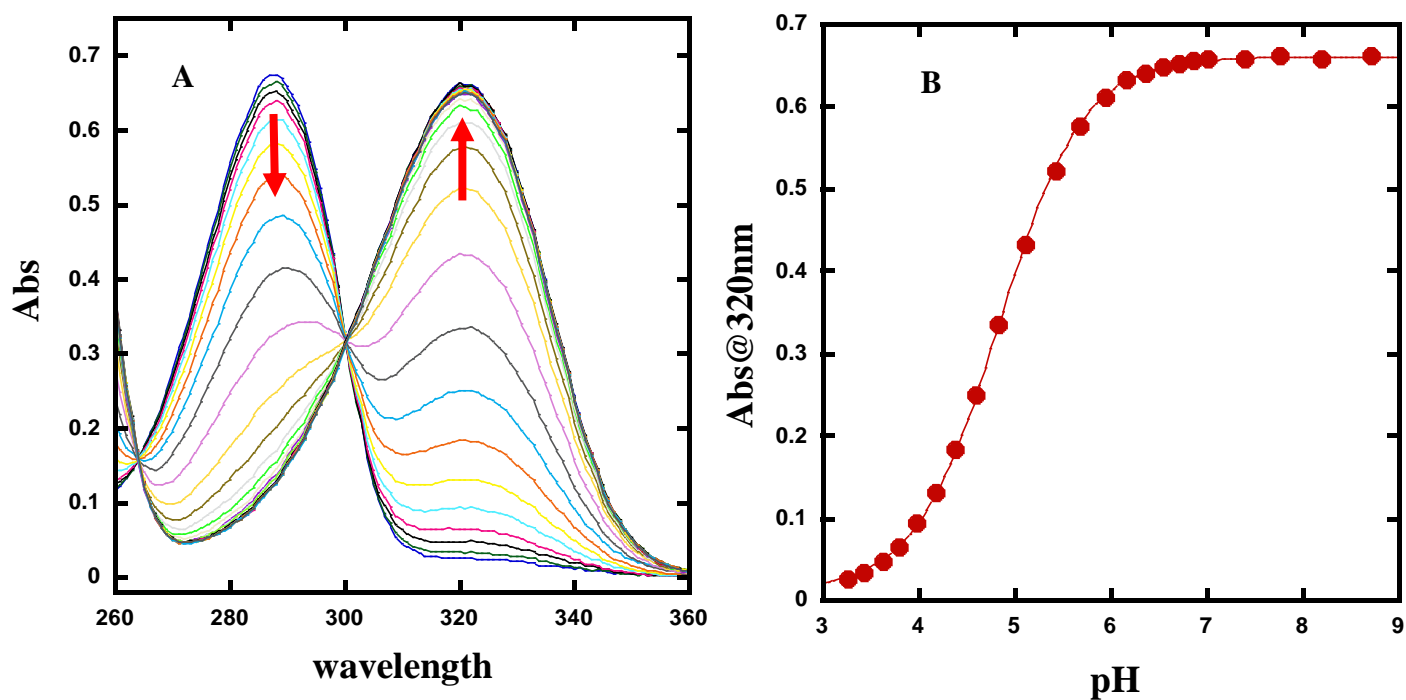
Figure 39: A: UV titration of *N*-methyl pyridyl **15** at 42 ± 0.2 °C, 1 M NaCl; **B**: dependence of absorbance on pH measurement; $pK_a = 4.84 \pm 0.01$; $R^2 = 0.999$.
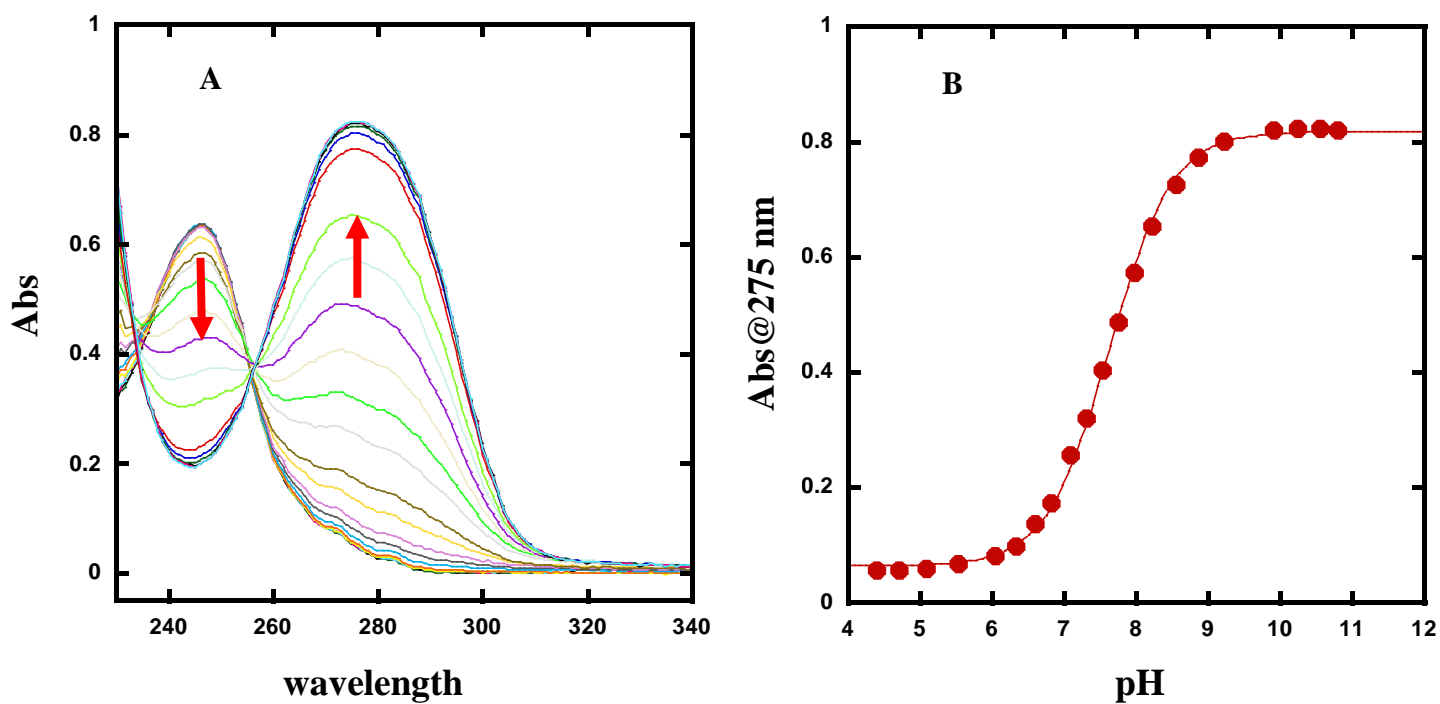
Figure 40: A: UV titration of 4-cyanophenol **20c** at 42 ± 0.2 °C, 1 M NaCl; **B**: dependence of absorbance on pH measurement; pK_a= 7.63 ± 0.01; $R^2 = 0.999$.

3.4.5 Linear free energy relationship

The synthesis of pyridyl methyl phosphate diester **27** was not successful due to the nucleophilicity of the nitrogen atom, therefore, just two compounds have been synthesised. Plotting the second order rate constants of reactions of compounds **28** and **29** alongside the substituted phenyls that have been studied in the literature by Zalatan and Herschlag[15] against the pK_a values of the leaving group in order to yield the Brønsted correlation coefficient β_{lg}.

As shown in **Figure 41** the new data of compounds **28** and **29** show the logarithmic dependence of the second order rate constants on the pK_a value of the leaving group. The correlation of these data was in good agreement with the literature data[15] with no deviation and gave $\beta_{lg} = -0.74 \pm 0.03$, which is smaller than to the original value of -0.94 ± 0.05. However, the correlation here is much better and it improved after including the two new compounds.
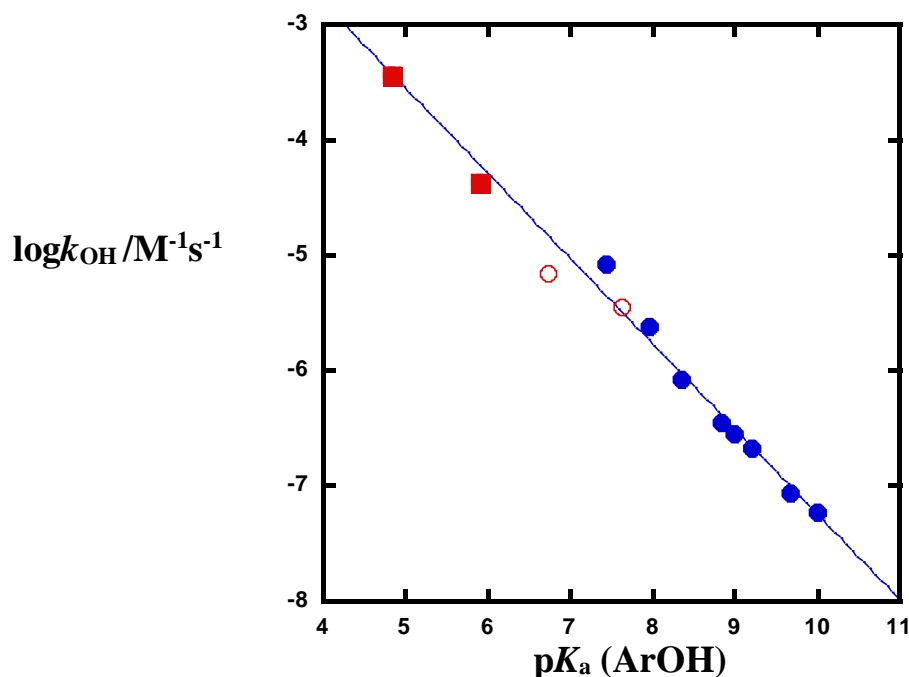
Figure 41: Brønsted plot of alkaline hydrolysis of substituted phenyl methyl phosphate diester at 42°C ± 0.04, 1 M NaCl. Red squares are compounds **28** and **29**, empty circles are 4-nitro and 4-cyano, blue points represent data reported in the literature[15]; $\beta_{lg} = -0.74 \pm 0.03$; $R^2 = 0.98$, the pK_a values of pyridyl leaving group measured under experimental condition; the pK_a of phenols measured by Alkherraz *et al.*[86] under the same experimental condition.

In addition, the measured pK_a of 4-cyano phenol improved the correlation and did not deviate from the line compared with original data in **Figure 29**. Furthermore, the β_{lg}= -0.94 that was obtained in ref[15] ruled out the 4-nitro and 4-cyano leaving groups as they were described as outliers from the line of correlation due to resonance effects. Including or not including these points does not affect β_{lg} much, the difference is $\pm$ 0.015. The β_{lg} = -0.74 obtained by including the points for **28** and **29** was close to β_{lg} = -0.68 that was obtained for the alkaline hydrolysis of phosphate diester **19a-f** by Younas *et al*[80] at 39 °C. The determined β_{lg} = -0.74 suggested that the mechanism of methyl phosphate diesters proceeds via a synchronous transition state when the breaking of leaving group and formation of the new bond with nucleophile occur at the same time. In general, there is agreement with the previously reported studies[26,27,87-89] where the value of Brønsted coefficients β_{lg} ranged from -0.64 to -0.97 supporting roughly synchronous transition states where the bond cleavage of the leaving group and bond formation of nucleophile occur at the same time.

Further, when the data were plotted with the Hammett relationship with both σ and σ⁻ values, as can be seen from **Figure 42**, the correlation with σ⁻ is slightly better than σ. We can observed the correlation with σ⁻ to be comparable with Brønsted plot (**Figure 41**) since phenol pK_a values are used to define σ⁻. Hong *et al*[90]. found that the correlation of the Hammett plot with σ⁻ is better than σ for the alkaline hydrolysis of a series of phenyl diphenyl phosphinates. The Hammett plot yielded ρ = 1.66 and 1.64 which indicated there is a developing negative charge on the oxygen atom and this value is in a good agreement with the value of ρ = 1.61 for the experimental and theoretical study[72] of alkaline hydrolysis of the sulfonate esters which was concluded to occur by a concerted mechanism.
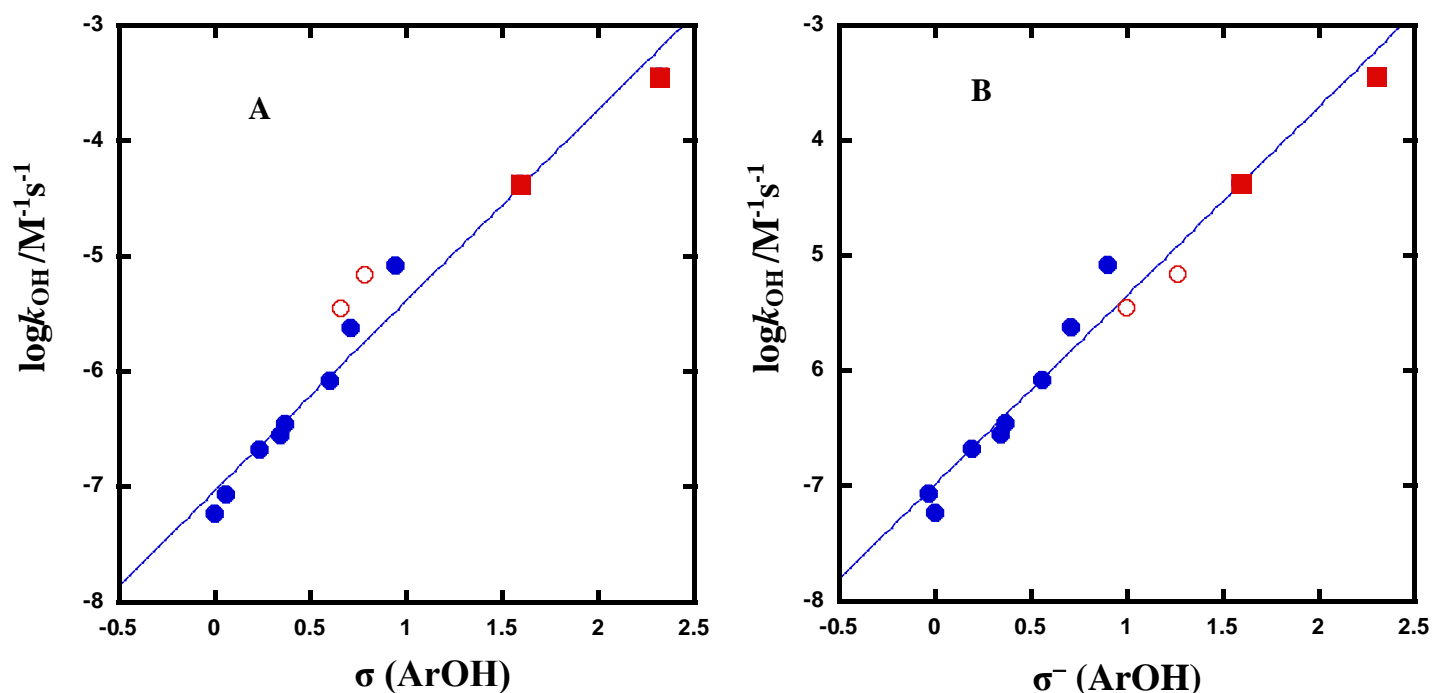
Figure 42: Hammett plots of the alkaline hydrolysis of substituted phenyl methyl phosphate diesters at 42 ± 0.04 °C, 1 M NaCl, red squares are compounds **28** and **29**, empty circles are 4-nitro and 4-cyano, blue points data reported in the literature[15]; **A**: $\rho = 1.66 \pm 0.09$; $R^2 = 0.975$, **B**: $\rho = 1.64 \pm 0.09$; $R^2 = 0.974$.

The effective charge of the transition state is the fraction of β_{lg}/β_{eq} where β_{eq} represents the Brønsted coefficient equilibrium, and can be calculated from the slope of $\log(K_{eq})$ plotted against the pK_a values of the leaving group.[73,91] The estimated β_{eq} for substituted phenyl phosphate diesters is -1.73[92] therefore, the effective charge would be -0.43 when β_{lg} and β_{eq} are -0.74 and -1.73 respectively. The loose transition state was ruled out since usually it has a large value, for instance, the effective charge in the hydrolysis of phosphate monoester is -0.9 by estimating -1.23 for β_{lg} and -1.35 for β_{eq} which indicates leaving group bond is mostly broken in the transition state.[92,93]

3.5 Conclusions

Two novel pyridyl methyl phosphate diesters have been successfully synthesised and the inclusion of these two points in the Brønsted plot gave good agreement with the data that was reported by Zalatan and Herschlag.[15] The Brønsted plot shows a very good correlation after including the data for **28** and **29**, indicating the importance of this type of leaving groups to improve such plots and give a complete picture about the hydrolysis of phosphate diesters and other species. In addition, inclusion of these data in the Hammett plot gave a linear correlation, but the correlation with σ^- is better than σ and the correlation with σ^- was similar to the Brønsted plot. The synthesis and analysis of these two new pyridyl compounds **28** and **29** have expanded the range of pK_as of the leaving groups which can be used to construct LFER correlations. Based on Brønsted and Hammett correlations, there is one single mechanism for the reaction and the reaction could occur through the synchronous concerted mechanism.
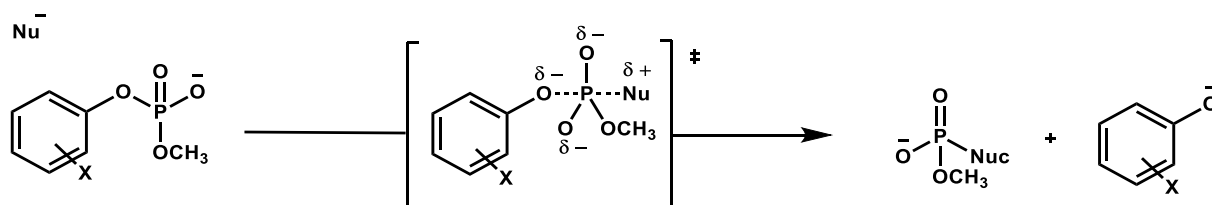
Figure 43: Proposed mechanism of aryl methyl phosphate diesters.

Chapter four: Sulfate diesters

4.1 Introduction: Sulfate diesters

Sulfate diesters have not been studied to the same extent as sulfate monoesters, which have more biological importance.[1,94,95] Sulfate monoesters play a crucial role in many biological processes, for example, hormone regulation, cell signaling, and detoxification. Sulfate diesters act as powerful alkylation reagents in organic synthetic reactions.[6] The mechanism reaction of the sulfate diesters (via S-O cleavage or C-O cleavage) depends on the structure of the diester and the leaving group. Buncel and co-workers[96,97] studied the alkaline hydrolysis of a series of alkyl aryl sulfate diesters **32a-e** with different nucleophiles (methanol, methoxide, and phenoxide) in methanol (**Figure 44**).

X=
a: 4-NO$_2$
b: 3-NO$_2$
c: 4-Br
d: 4-Me
e: H
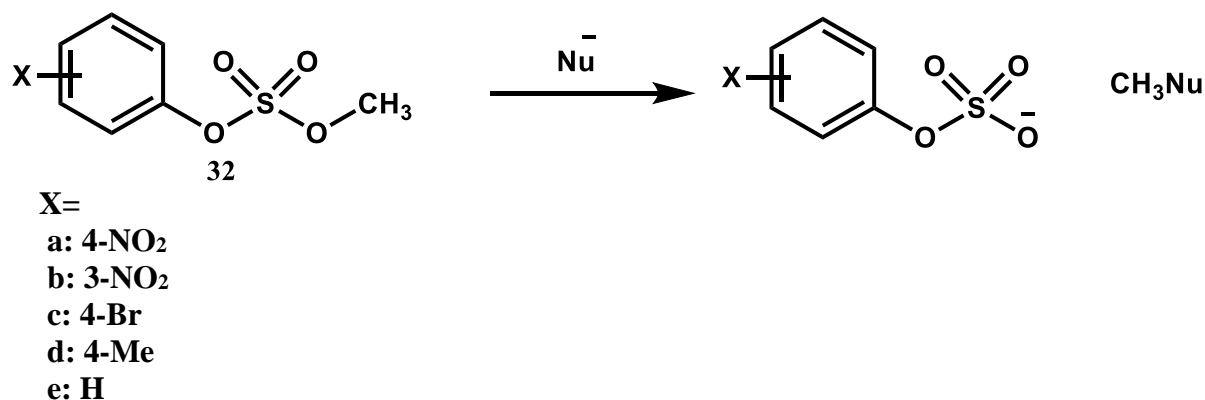
Figure 44: Alkaline hydrolysis of alkyl aryl sulfate diesters in methanol

They found that the alkaline hydrolysis of this type of sulfate diester yields aryl sulfonate monesters as the products i.e the reaction occurs by attack of the nucleophile on aliphatic carbon and cleavage of the alkyl oxygen bond rather than the sulfate oxygen bond.

The first study of a diaryl sulfate diester was in 1965 by Kaiser *et al*[98] who concluded that the products for the alkaline hydrolysis of diphenyl sulfate diester **33** were mainly phenyl sulfate monoester and phenol. However, the position of the cleavage and mechanism of the reaction were not highlighted in the study.
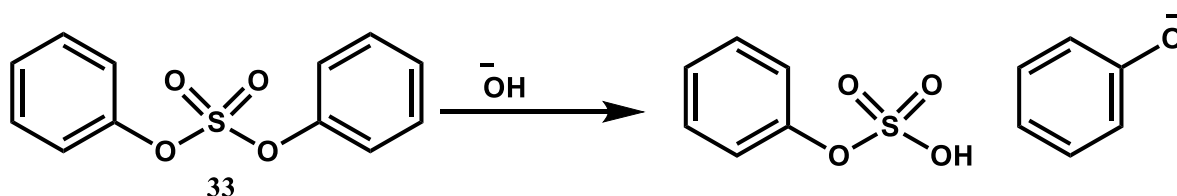
Figure 45: Alkaline hydrolysis of diphenyl sulfate diester.

The only detailed study was by Younker and Hengge.[99] In their study, they investigated the mechanism of aryl phenyl sulfate diester hydrolysis by varying the pK_a of the leaving group from 5.3 to 7.7. A combination of KIE, activation parameters and LFER were measured.

X=
a: 3-F-4-NO$_2$
b: 2,3,4,5,6-F$_5$
c: 2-F,4-NO$_2$
d: 2,6-F$_2$
e: 4-NO$_2$
f: 4-Cl,3-NO$_2$
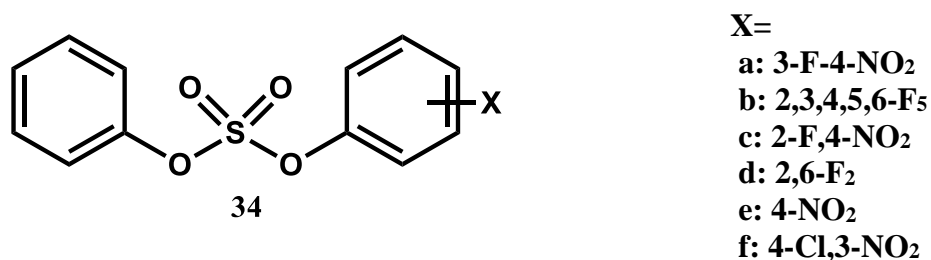
Figure 46: Series of sulfate diesters reported by Younker and Hengge.[99]

The Brønsted correlation gave a β_{lg} of - 0.7 which indicates that the transition state develops a reasonably large negative charge and shows sensitivity to the varying of the pK_a of the leaving group. However, the correlation of the second order rate constant against pK_a of leaving the group was slightly scattered (**Figure 47**). This may be due to the choice of leaving groups that have a substitution in position 2, for instance, **34b-d** which are not favorable because of steric effects with other classic leaving groups (4-NO$_2$, 3-F-4-NO$_2$) which also have resonance effects.
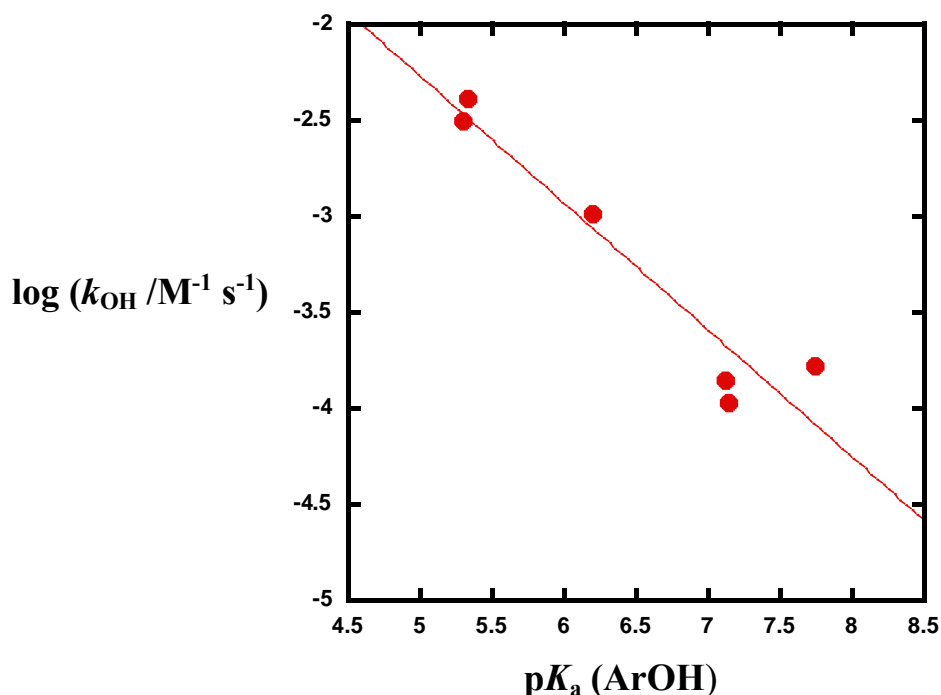
Figure 47: Brønsted plot for alkaline hydrolysis of aryl phenyl sulfate diesters.[99]

Further, activation parameters of **34e** and **34f** were measured to be ΔH = +88 and 84.83 kJ mol^{-1} and ΔS = -37 and -50.2 J.K^{-1} mole^{-1} respectively. The KIE of **34e** for the oxygen atom and nitrogen atom of the leaving group gave values of ^{15}k = 1.000 ± 0.0005 and $^{18}k_{1g}$ = 1.003 ± 0.0002 as explained in **Figure 48**.
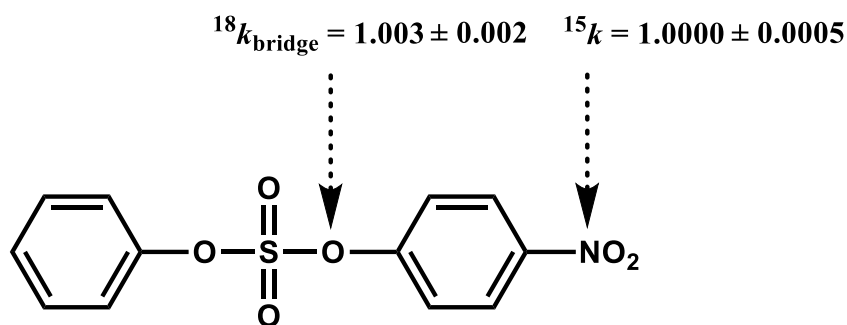
Figure 48: Compound **34e** with the positions and values of KEI measurements.

Based on a combination of KIE, activation measurements, and LFER, they conclude that the mechanism of the reaction occurs through the cleavage of S-O bond and the attack of nucleophile and cleavage of leaving group occur at the same step.

4.2 Mechanism of sulfate diesters

There are three possible mechanisms for the hydroxide promoted hydrolysis of aryl phenyl sulfate[99,100] (**Figure 49**). The concerted mechanism (A_ND_N) [101], when the attack of nucleophile and departure the leaving group occur in the single transition state. A dissociative mechanism (D_N+A_N), when the reaction occurs in two steps, the first step is the departure of the leaving group to form an intermediate, and the second step is the attack of the nucleophile. Finally, an associative mechanism (A_N+D_N), when the nucleophile attacks first and forms an intermediate and the second step is the cleavage bond of the leaving group.
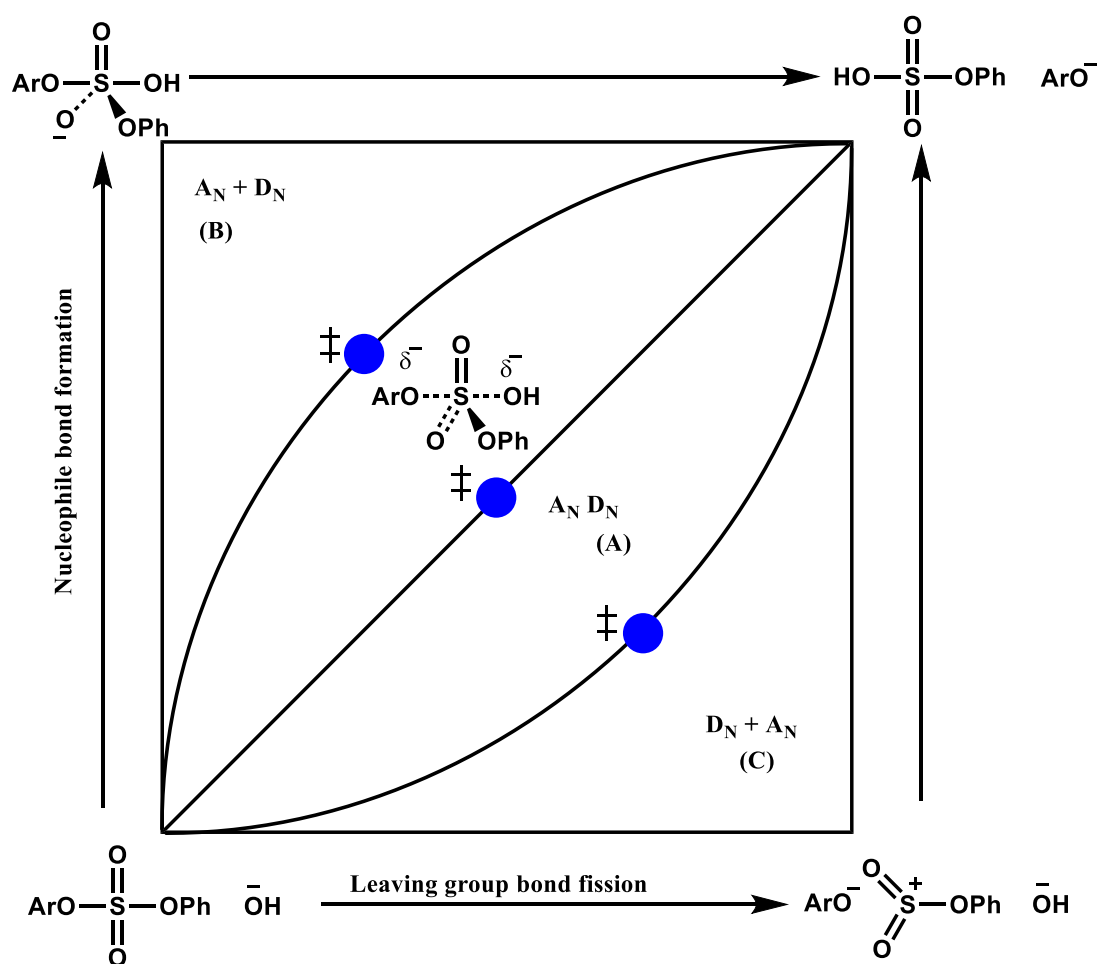
Figure 49: More O'Ferrall-Jencks diagram explaining the possible mechanisms for the hydrolysis of sulfate diester; reactants on the bottom left and products are on the top right, A = concerted, B = associative and C = dissociative mechanism.

4.3 Aims

Diaryl sulfate diesters have had less attention compared with sulfate monoesters and the aim of this chapter is to describe the reactivity and mechanism of substituted pyridyl phenyl sulfate diesters **35-37** as shown in **Figure 50**. LFER will be studied to investigate the transition state by varying the leaving group from pK_a 4.9 to 8.06.
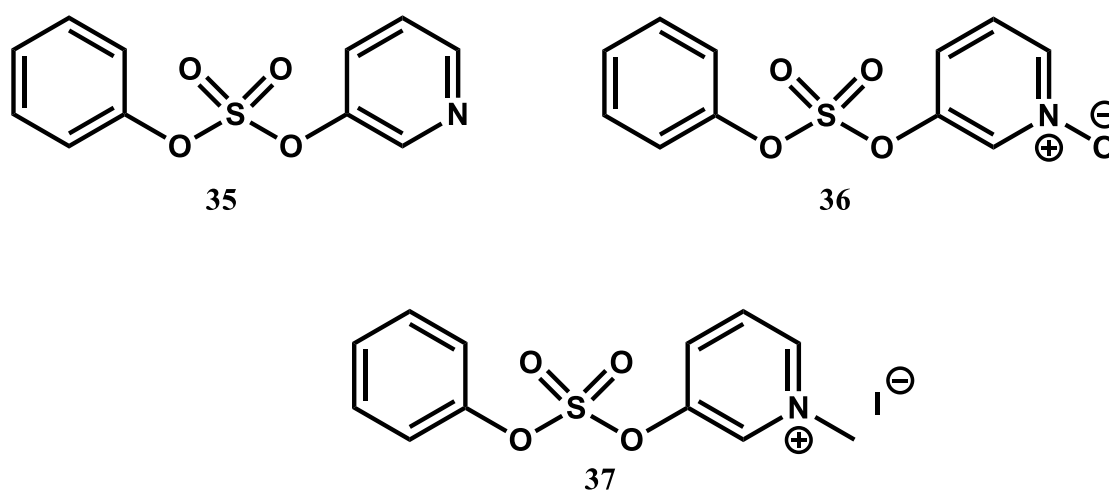
Figure 50: Phenyl pyridyl sulfate diesters used in this study.

4.4 Results and discussion

4.4.1 Synthesis of substituted pyridyl phenyl sulfate diesters

The substituted pyridyl phenyl sulfate diesters were synthesised as in **Scheme 12**.
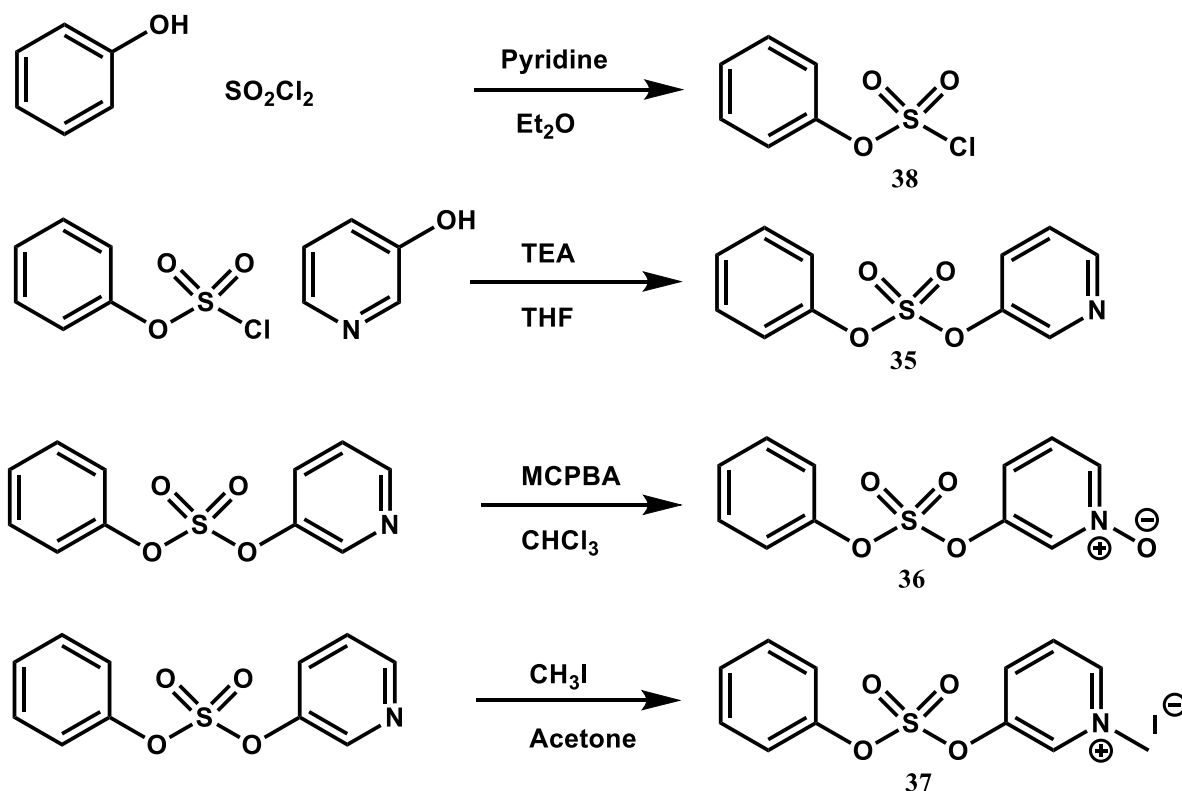
Scheme 12: Synthesis of substituted pyridyl phenyl sulfate diester and its derivatives.

Phenyl chloro sulfonate **38** was synthesised under anhydrous conditions. Therefore, distilled sulfuryl chloride was added to a mixture of phenol and dry pyridine in dry diethyl ether which was stirred under nitrogen at -78 °C. The slow addition and low temperature were required at beginning of the reaction to avoid forming diaryl sulfate. The pyridyl phenyl sulfate diester **35** was prepared by adding phenyl chloro sulfonate **38** slowly to a mixture of 3-hydroxy pyridine with triethylamine in dry THF to yield a yellow oil which was used to prepare compounds **36** and **37**. The *N*-oxide pyridyl phenyl sulfate **36** was synthesised by oxidation of pyridyl phenyl sulfate diester using 3-chloroperbenzoic acid in chloroform. The *N*-methyl pyridyl phenyl

sulfate **37** was prepared by methylation of **35** with iodomethane in acetone.

4.4.2 Alkaline hydrolysis of substituted pyridyl sulfate diester

The alkaline hydrolysis of substituted pyridyl phenyl sulfate diesters **35-37** was studied spectrophotometrically at 40 ± 0.04 °C, in 10% dioxane. The ionic strength was maintained with 1 M NaCl in order to allow for direct comparison with the literature.[99] The concentration of NaOH was varied more than 10 fold and all the reactions were first order in sodium hydroxide. The k_{obs} values were determined for each reaction by following the appearance of the leaving group. The second order rate constants are **35** $k_{OH} = (4.8 \pm 0.04) \times 10^{-5}$ M^{-1} s^{-1}, **36** $k_{OH} = (1.57 \pm 0.02) \times 10^{-3}$ M^{-1} s^{-1} and **37** $k_{OH} = (1.56 \pm 0.01) \times 10^{-2}$ M^{-1} s^{-1} from plotting the k_{obs} values against the concentration of sodium hydroxide (**Figure 51**).
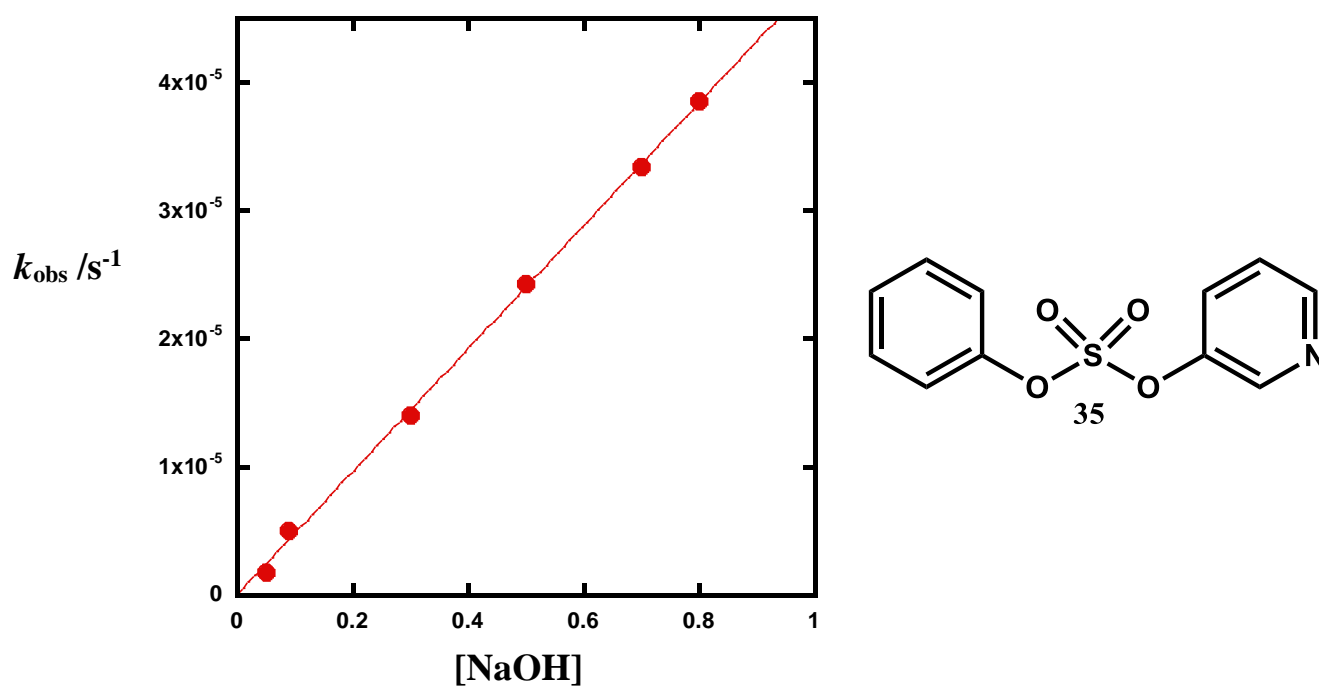
Figure 51: Alkaline hydrolysis of compound **35**; 1 M NaCl; 40 ± 0.04 °C; $k_{OH} = (4.8 \pm 0.04) \times 10^{-5}$ M^{-1} s^{-1}, R$^2 = 0.999$.
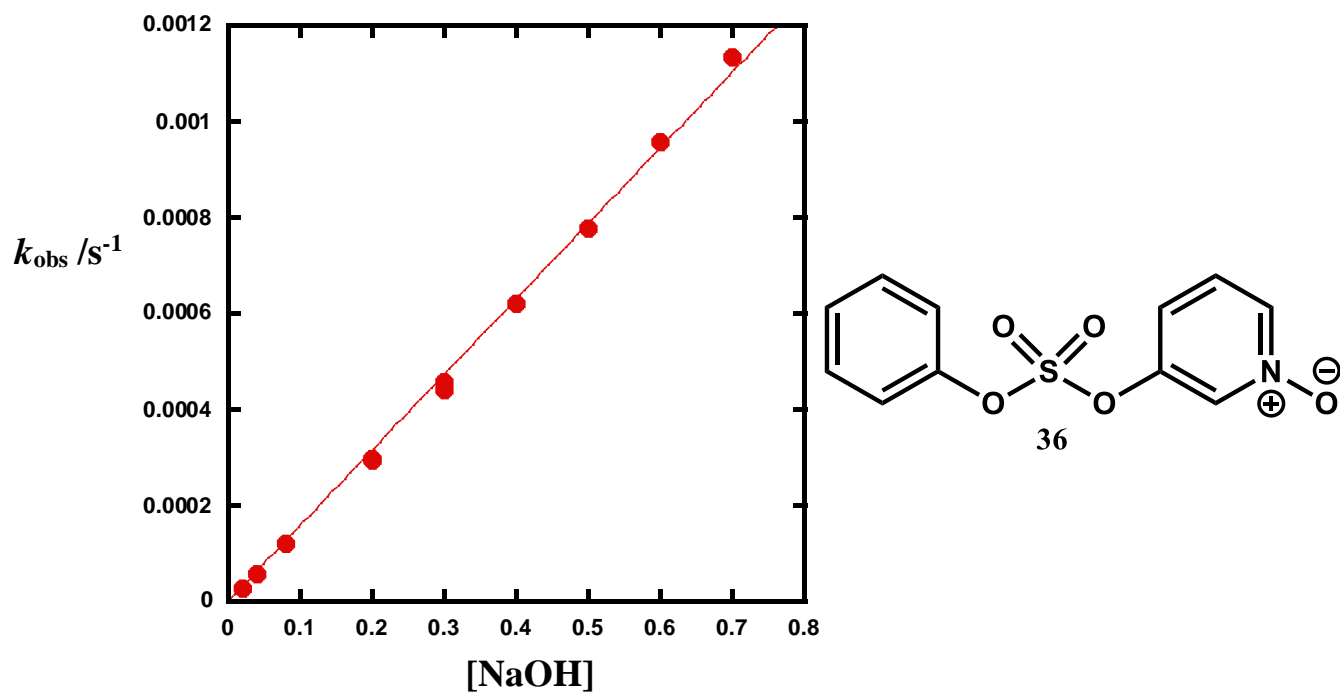
Figure 52: Alkaline hydrolysis of compound **36**; 1 M NaCl; 40 ± 0.04 °C; $k_{OH} = (1.57 \pm 0.02) \times 10^{-3}$ M^{-1} s^{-1}, R^2 = 0.997.
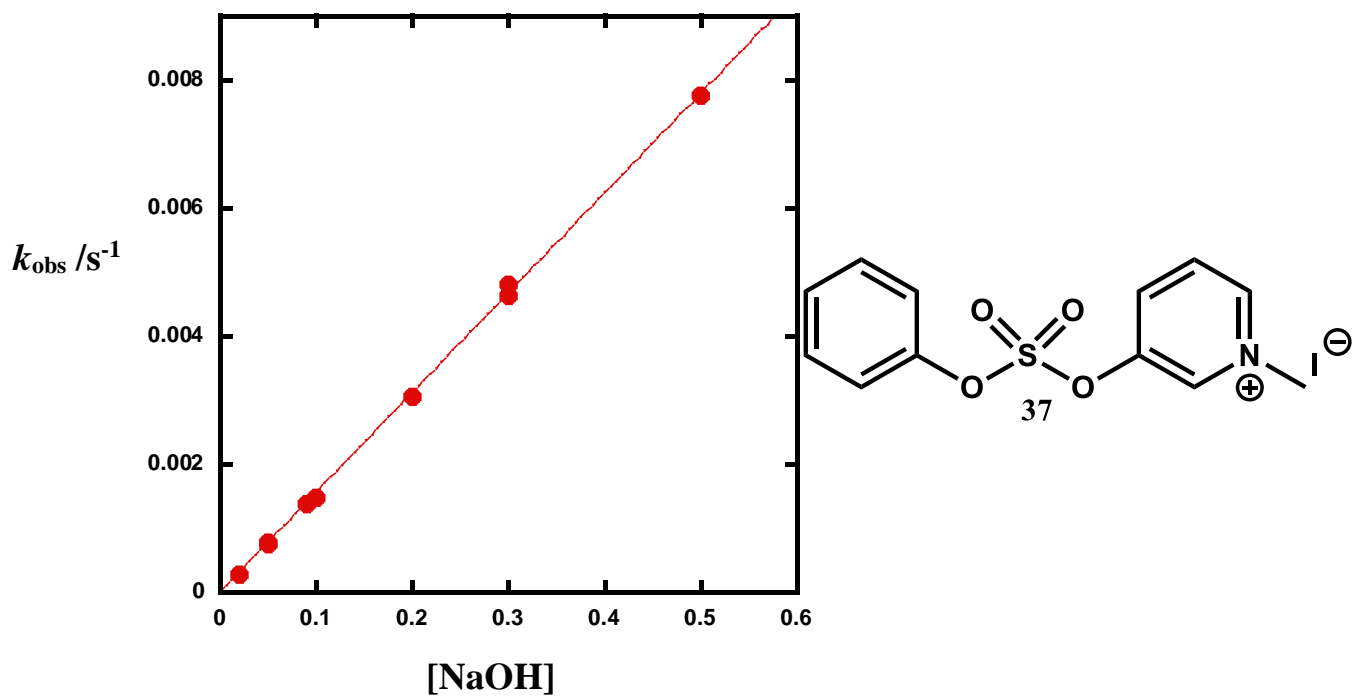
Figure 53: Alkaline hydrolysis of compound **37**; 1 M NaCl; 40 ± 0.04 °C; $k_{OH} = (1.56 \pm 0.01) \times 10^{-2}$ M^{-1} s^{-1}; R^2 = 0.999.

4.4.3 Product analysis

The products of reaction were analysed by UV- visible spectrophotometry and HPLC. The UV spectra were taken of the reactions mixture of **35-37** after hydrolysis and showed maximum absorbance at wavelength of 300, 320 and 320 nm which correspond to the leaving groups **13, 14** and **15** respectively.
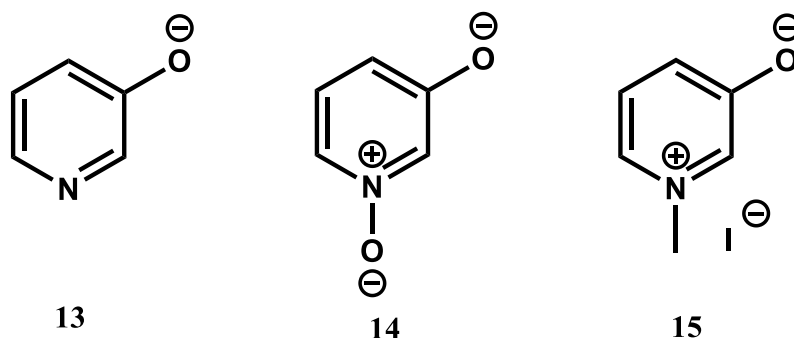
Figure 54: 3-hydroxy pyridine and its derivatives.

HPLC analysis confirms the presence of phenyl mono sulfate and the leaving group. **Table 10** (in appendix) contains a summary of the solvent system, retention time and structure of the products of hydrolysis. This analysis is in good agreement with Younker and Hengge[99] who analysed the products of sulfate diester hydrolysis by following the reaction of **34e** by HPLC for three half-lives.

4.4.4 pK_a measurements of 3-hydroxy pyridine and its derivatives 13-15

The pK_a values of the leaving groups for 3-hydroxy pyridine and its derivatives **13-15** were measured at 40 ± 0.2 °C, 1 M NaCl, and 10% dioxane. The measured pK_a values were determined to be 8.06, 5.95 and 4.87. The obtained pK_a values are somewhat lower than those reported in the literature (8.42, 6.45 and 4.96) probably because of the effect of salt and temperature. In addition, the pK_a values of *N*-oxide **14** and *N*-methyl pyridyl **15** that were measured here (10% dioxane and 40 °C) are very close to those which were measured in water

at 42 °C (chapter 3). For 3-hydroxy pyridine **13**, it has two pK_a values which depend whether

its structure is the zwitterion or the neutral form (**Scheme 13**). For instance, **13A+** is the first

pK_a which is different to the second pK_a of **13A-** and the second pK_a is needed in the calculation

to fit Brønsted plot. The measured pK_as for **13A+** and **13A-** were 4.93 and 8.36, however, these

values may be lower or higher depending on the equilibrium (K_T) between **13A** and **13A ±**.

This is called a microscopic pK_a. From the calculation (see appendix) the microscopic pK_a

should be higher than the first pK_a by 0.3 and lower than the second pK_a by 0.3 as $K_T = 1$.

Therefore, the first and second pK_a will be 5.23 and 8.06 respectively.
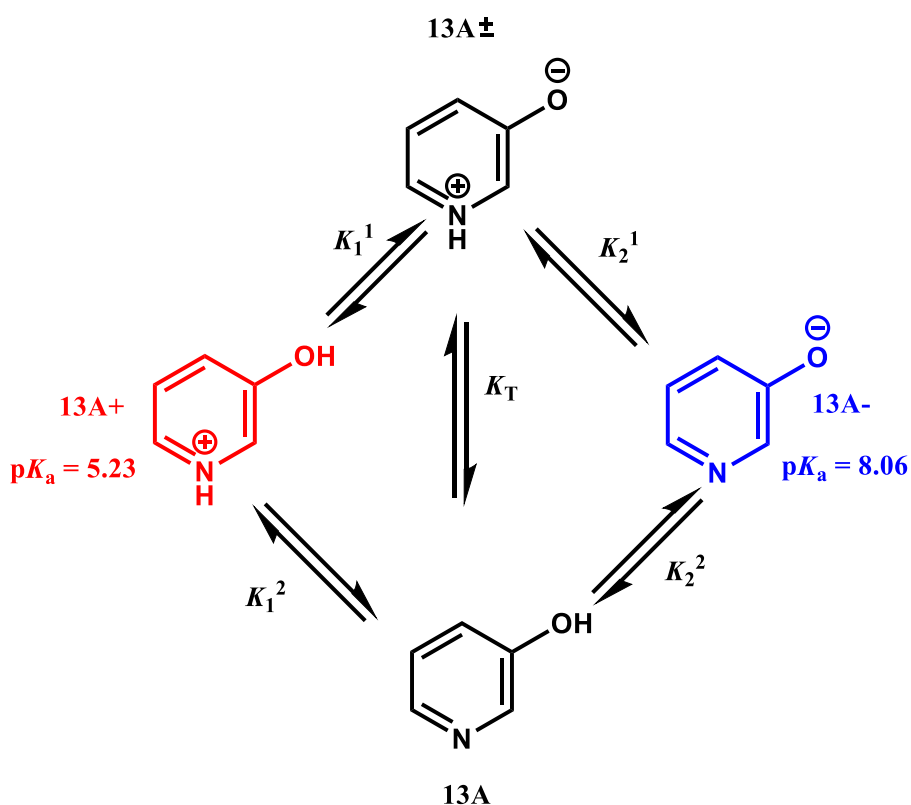
Scheme 13: The possible forms of 3-hydroxyl pyridine **13** in acidic, neutral and basic conditions.
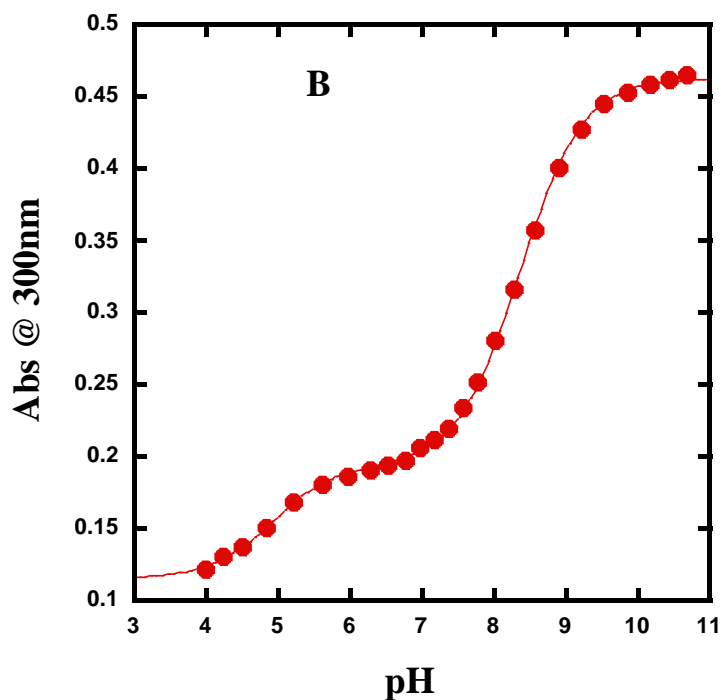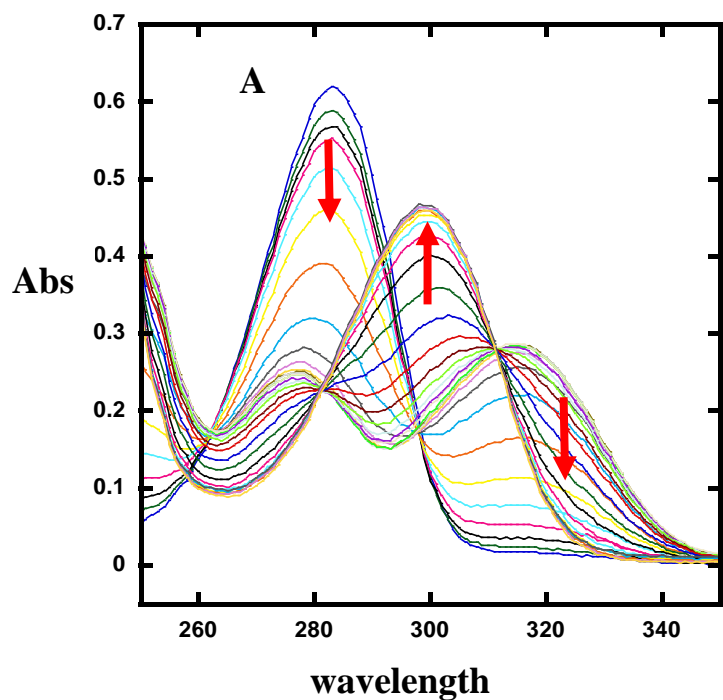
Figure 55: A: UV titration of **13**; **B**: dependence of absorbance on pH 1 M NaCl; 40 ± 0.2 °C; $pK_a = 8.06 \pm 0.009$; $R^2 = 0.999$.
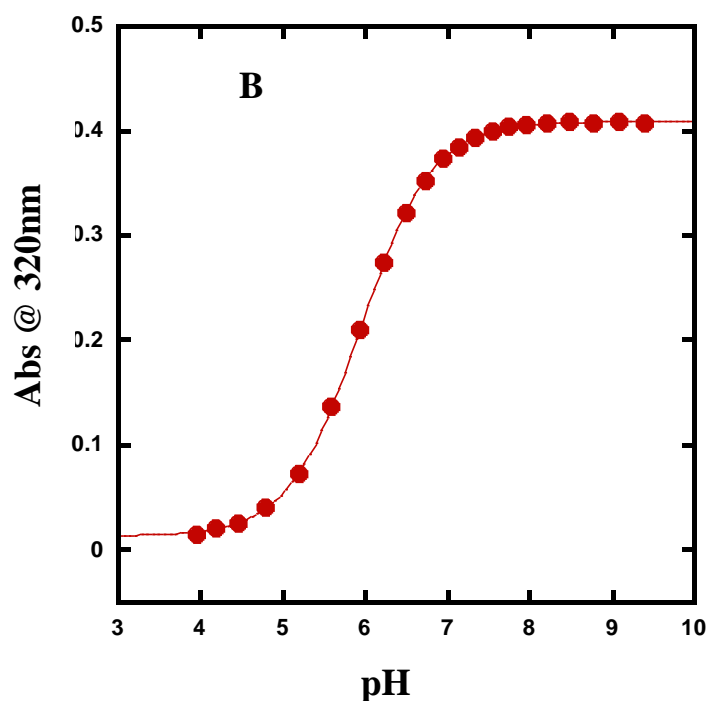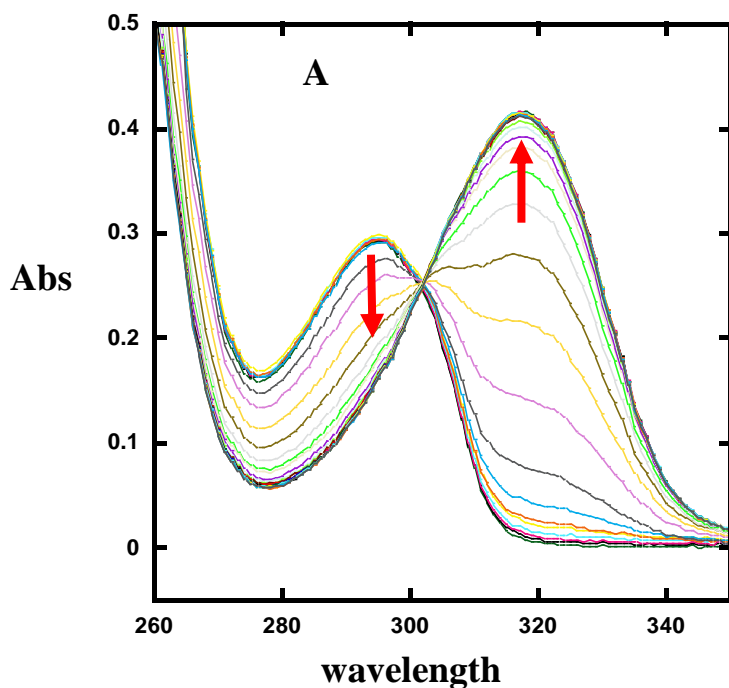
Figure 56: A: UV titration of **14**; **B**: dependence of absorbance on pH 1 M NaCl; 40 ± 0.2 °C; $pK_a = 5.94 \pm 0.004$; $R^2 = 0.999$.

69
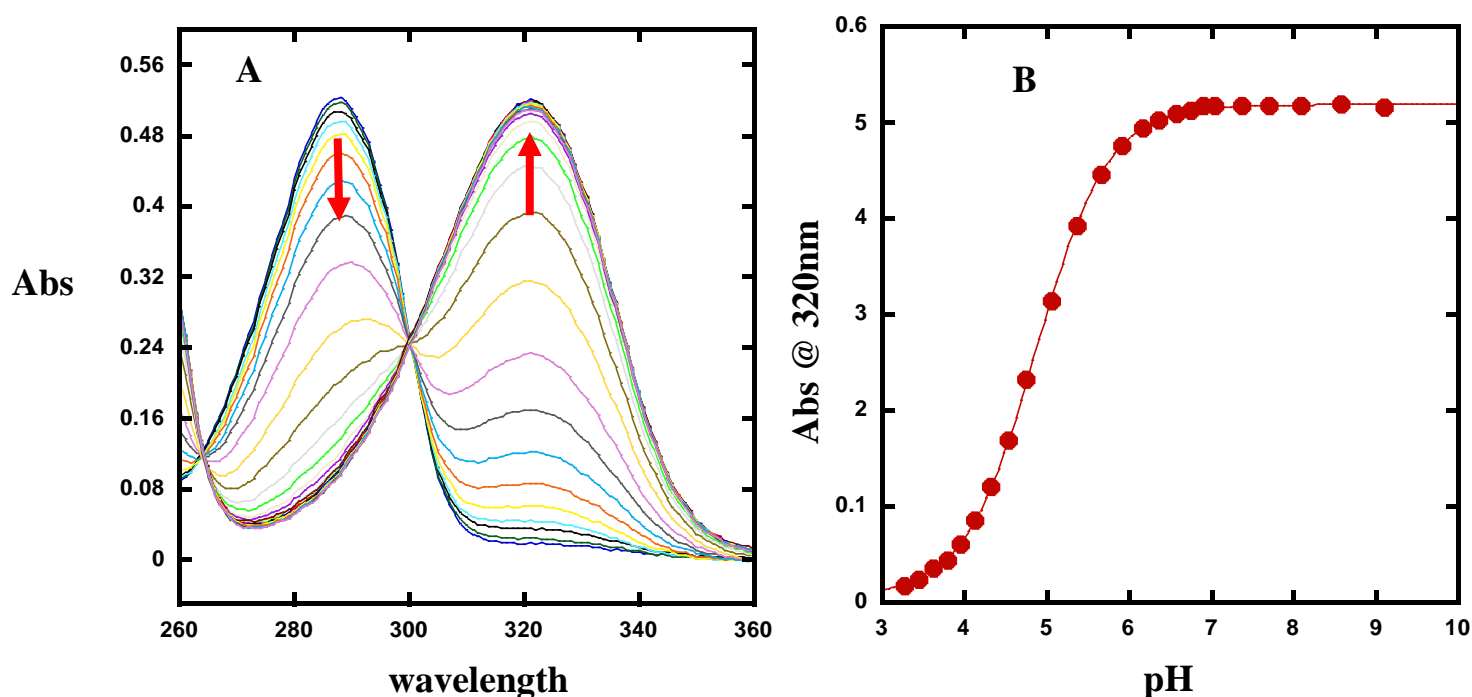
Figure 57: A: UV titration of 15; **B**: dependence of absorbance on pH 1 M NaCl; 40 ± 0.2 °C; $pK_a = 4.87 \pm 0.005$; $R^2 = 0.999$.

4.4.5 LFER of substituted pyridyl phenyl sulfate diester

A Brønsted plot (**Figure 58A**) for **35-37** yields $\beta_{lg} = -0.78 \pm 0.07$ which is in good agreement with that reported by Hengge and Younker.[99] Furthermore, the Hammett plot (**Figure 58B**) shows good correlation with $\rho = 1.7 \pm 0.1$. The values of β and ρ indicate there is negative charge developed on the oxygen atom of the leaving group in the transition state. Moreover, the linear correlation of Brønsted and Hammett could indicate there is a single mechanism for the reaction. The hydrolysis of sulfonate esters with the range of pK_a of the same leaving group **13-15** also gave close values $\beta_{lg} = -0.66$ and $\rho = 1.62$ and leads to the conclusion that the reaction occurs via single a transition state.[72]
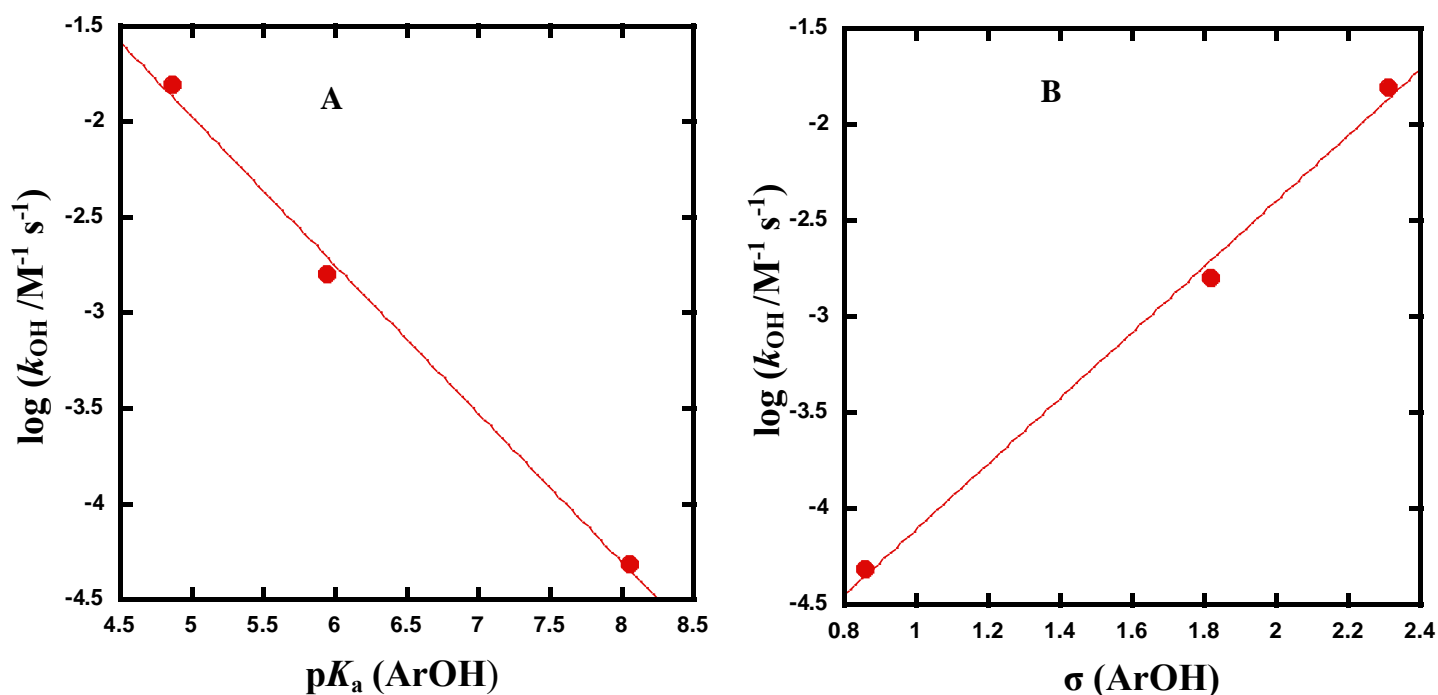
Figure 58: A: Brønsted correlation for the alkaline hydrolysis of substituted pyridyl phenyl sulfate diester compounds **35-37** giving $\beta_{lg} = -0.78 \pm 0.05$, $R^2 = 0.995$. **B**: Hammett correlation for the same data giving $\rho = 1.7 \pm 0.1$, $R^2 = 0.996$.

4.4.6 Comparison with literature

Kinetic data of compounds **35-37** were included in the study reported by Hengge and Younker (**Figure 59B**). The Brønsted plot gave very close value of Brønsted coefficient $\beta_{lg} = -0.72 \pm 0.1$ which indicates that there is developed negative charge on the oxygen atom of the leaving group in the transition state. However, the plot is a rather scattered which can be attributed to the resonance effects of leaving groups (**34a-f**) that were chosen by Hengge and Yonker[99] (**Figure 59A**). Additionally, we can see three leaving groups have a substitution at position 2 which is not desirable due to steric effects.
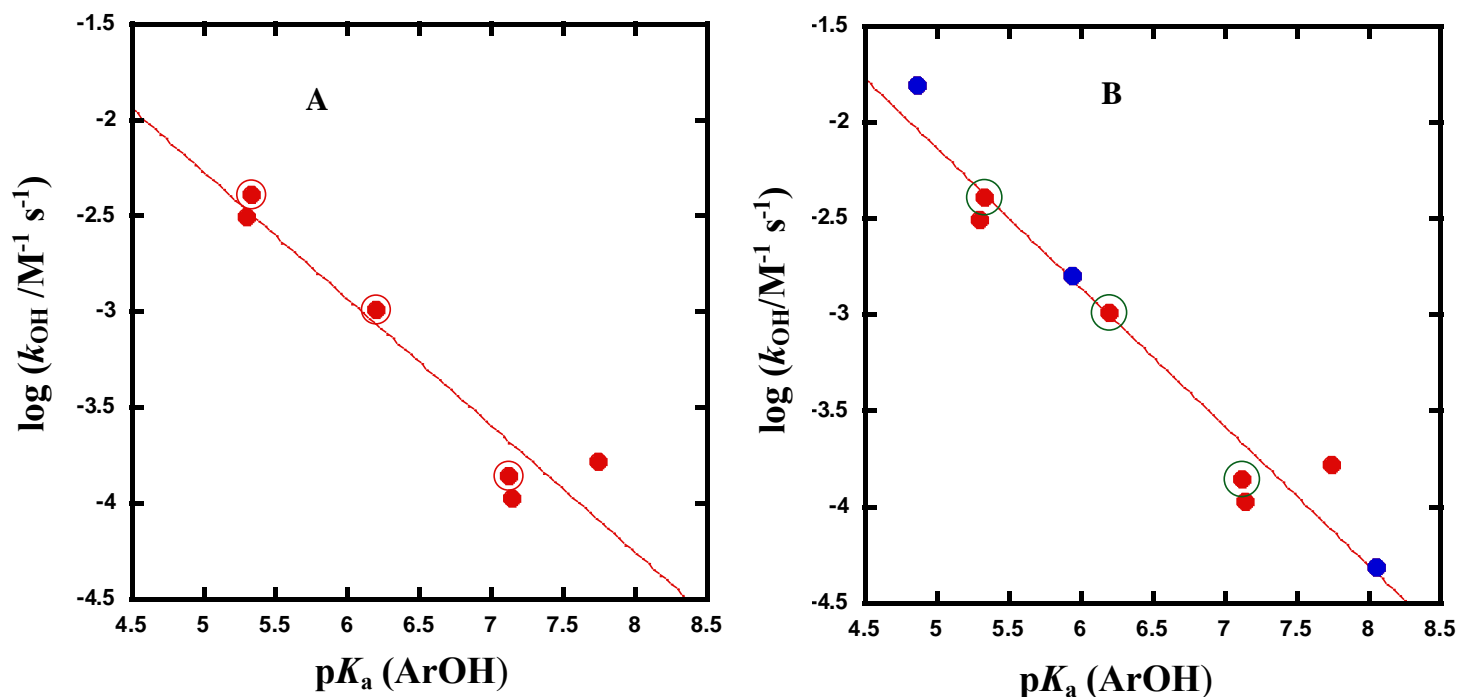
Figure 59: Brønsted plots for the alkaline hydrolysis of aryl phenyl sulfate diester at 40 ± 0.04 °C, 10% dioxane, **A**: Hengge[99] data only, the red points inside the circles correspond to the leaving group with ortho substitution, $\beta_{lg} = -0.7 \pm 0.1$, $R^2 = 0.92$. **B**: The same data after including pyridyl compounds **28-30** (blue points), the red line is the linear least squares fit all data, giving $\beta_{lg} = -0.72 \pm 0.1$, $R^2 = 0.95$.

Furthermore, Hammett plots were plotted with σ and σ⁻ as shown in **Figure 60A** and **B.** Some of the σ and σ⁻ values are not available in the literature, especially for leaving groups at ortho substituents and for those that have more than one substituent. Therefore, the σ⁻ values of **34a-f** were calculated by the subtracting the pK_a of the leaving group from the pK_a value of phenol then dividing this value by 2.2 (which is the slope (ρ) of phenol pK_a when plotted against sigma). Sigma values were calculated for leaving groups that have 4-nitro as 0.46 smaller, since the difference between σ and σ⁻ for 4-NO₂ is 0.46.
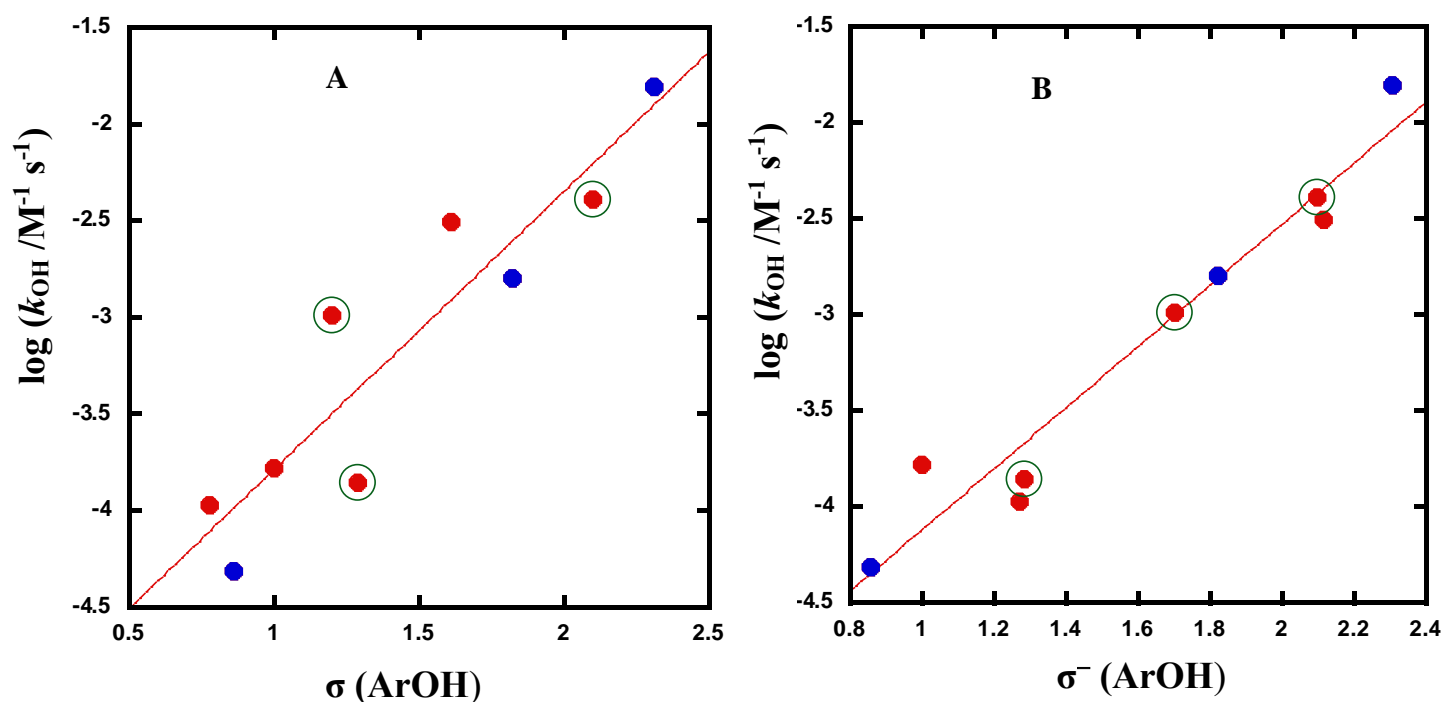
Figure 60: Hammett plots for the alkaline hydrolysis of aryl phenyl sulfate diesters at 40 °C, 10% dioxane, red points are Hengge data, the red points inside the circles correspond to the leaving group with ortho substitution, blue points correspond to compounds **35-37**. **A**: $\rho =1.44 \pm 0.23$, $R^2 = 0.85$. **B**: $\rho =1.59 \pm 0.14$, $R^2 = 0.95$.

As can be seen from **Figure 60A** and **B**, the plot with σ^- gave a better correlation than σ. The plot of σ^- is similar to the Brønsted plot for the same data (**Figure 59B**) because σ^- is similar to pK_a. The Hammett plot (**Figure 60A**) with sigma values gave very scattered correlations. This may be because the Hammett plot with the leaving groups that has substitution in ortho substituted are used in this plot. The data for sulfate diesters contrast with the results for the sulfonate esters (chapter two), which gave better correlations in the Hammett plot rather than Brønsted plot. For sulfate diesters, a better correlation with Brønsted than Hammett plot are obtained. This is may be attributed to the effect of changing C-S in the non-leaving group of sulfonate to the C-O in the sulfate diester. However, the results here are similar to phosphate diester (chapter 3) which also gave slightly better correlation with σ^- than σ. This was also

observed for the alkaline hydrolysis of a series of phenyl diphenyl phosphinates.[90]

4.4.7 Reactivity of bis-pyridyl sulfate diesters

The study was extended by investigating the effects of the non-leaving group on the reactivity by synthesising bis-pyridyl sulfate diesters compound **39**. **39** was synthesised as shown in **Scheme 14**. Distilled sulfuryl chloride was added slowly to a solution of 3-hydroxy pyridine and triethylamine in THF.
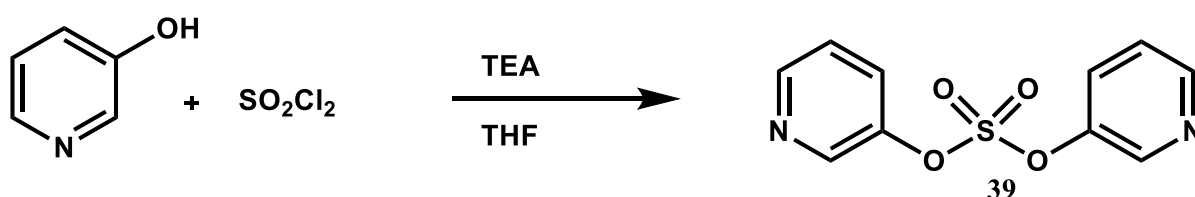
Scheme 14: Synthesis of bis-pyridyl sulfate diester **39**.

4.4.8 Alkaline hydrolysis of bis-pyridyl sulfate diester

The hydrolysis of bis-pyridyl sulfate diester **39** was followed by UV-visible spectrometry at 40 ± 0.04 °C, 10% dioxane and 1 M NaCl. The reaction was first order in sodium hydroxide.
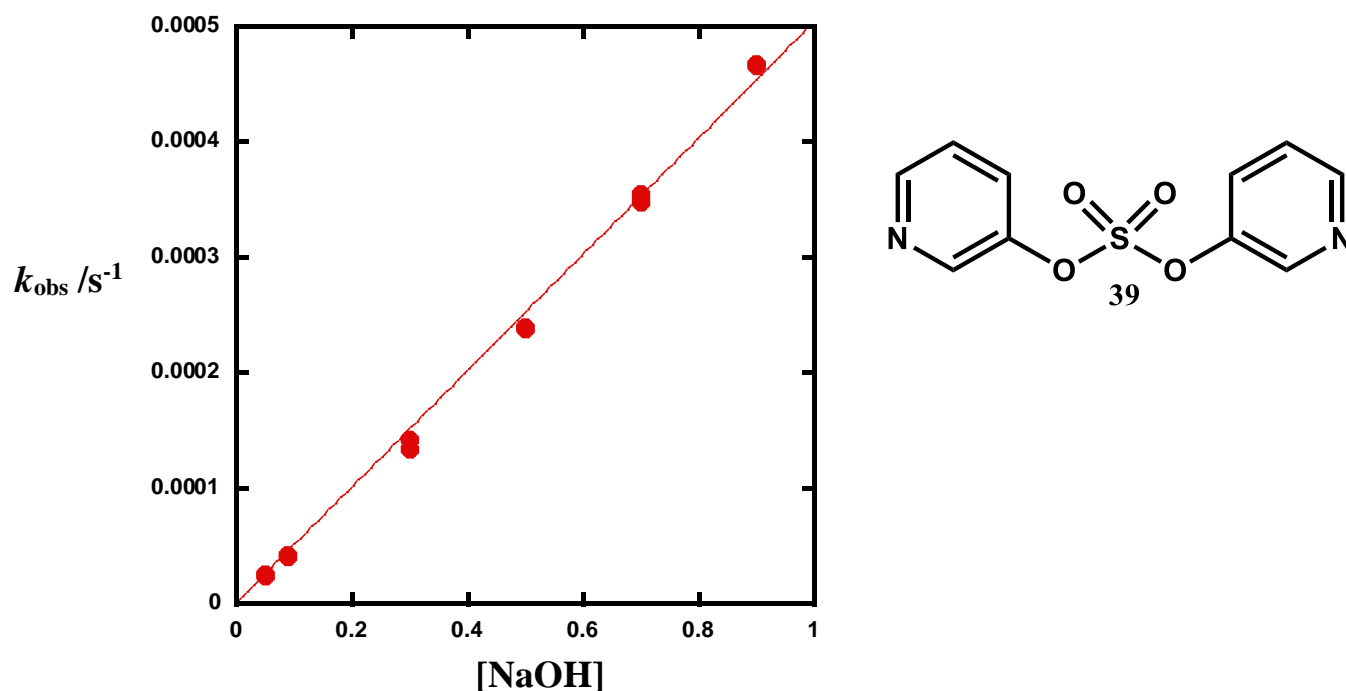
Figure 61: Alkaline hydrolysis of bis pyridyl phenyl sulfate; 1 M NaCl, 40 ± 0.04 °C; $k_{OH} = (2.52 \pm 0.06) \times 10^{-4}\,M^{-1}\,s^{-1}$; $R^2 = 0.996$.

The second order rate constant was determined to be $k_{OH} = (2.52 \pm 0.06) \times 10^{-4}\,M^{-1}\,s^{-1}$ (**Figure 61**). As **39** has two leaving groups, the rate constant is statistically adjusted. When compound **39** is compared with **35**, it can be seen that the reactivity is 5.3 fold higher.
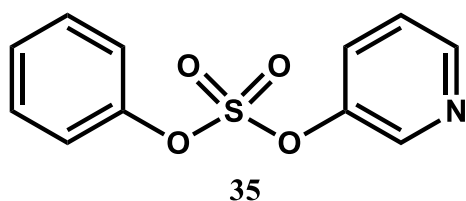
$k_{OH} = (4.80 \pm 0.04) \times 10^{-5}\,M^{-1}\,s^{-1}$
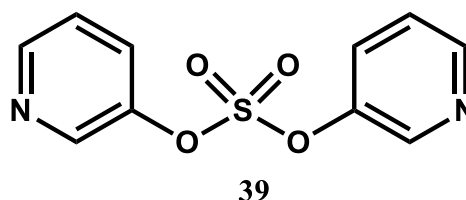
$k_{OH} = (2.52 \pm 0.06) \times 10^{-4}\,M^{-1}\,s^{-1}$

This small difference in reactivity appears to be due to the effect of the non-leaving group. For compound **35** the non-leaving group is poorer compared to compound **39**. The pyridyl in compound **39** possibly increases the electrophilicity of sulfur and that leads to this small increase in the rate of reaction. Kirby *et al.*[102] investigated the sensitivity of the rates of spontaneous hydrolysis of a series of phosphate triester **40-42** toward changing of the non-leaving group. They found the rate of reaction is affected by the electronic nature of the non-leaving group and its sensitivity depends on the nucleophile strength. They concluded β_{NLG} from the spontaneous hydrolysis reaction (β_{NLG} = -0.6) is more sensitive to the non-leaving group than the reaction with strong nucleophiles such as hydroxide which gave β_{NLG} = -0.15.

R =
a: 4-ClC$_6$H$_4$O
b: 2-pyridyl
c: 4-NO$_2$C$_6$H$_4$O

R=R'
a: (EtO)$_2$
b: (O(CH$_2$)$_3$O)$_2$
c: (CF$_3$CH$_2$)$_2$
d: (2-pyridyl)2
e: (4-SO$_3$C$_6$H$_4$O)$_2$
f: (4-NO$_4$C$_6$H$_5$)$_2$

X:
a: SO$_3$
b: H
c: Cl
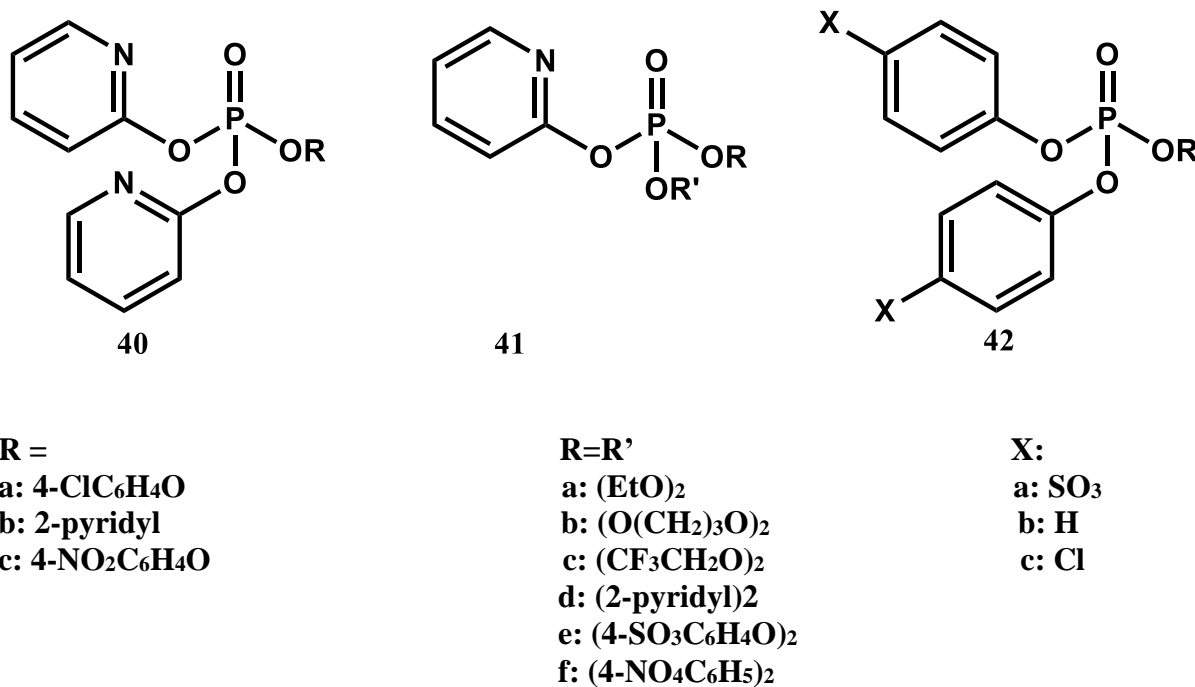
Figure 62: Phosphate triesters reported by Kirby *et al.*[103]

On the other hand, Um and co-workers[75] studied the effect of a non-leaving group of 2,4-dinitrophenyl substituted benzene sulfonate **43a-f** reactions with ethoxide at 25 °C in ethanol.

X=
a: 4-MeO
b: 4-Me
c: H
d: 4-Cl
e: 3-NO$_2$
f: 4-NO$_2$
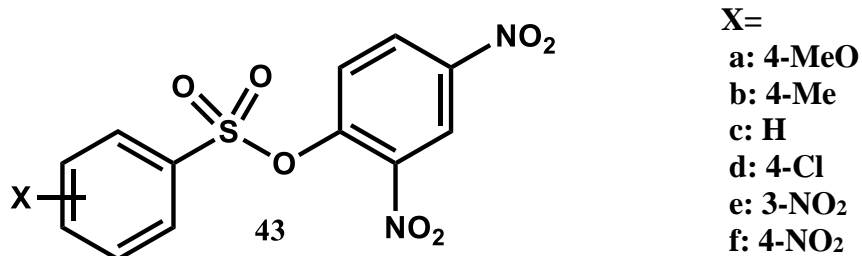
Figure 63: 2,4-dinitrophenyl substituted benzene sulfonates reported by Um and co-workers.[75]

The authors found that the electronic nature of group X affected the rate of reaction. For example, varying the non-leaving group from 4-MeO to 3-NO$_2$ changed the rate of reaction from 0.62 M^{-1} s^{-1} to 505 M^{-1} s^{-1}. In other words, changing the moiety from electron donating to electron withdrawing can increase the rate of the reaction. The Hammett plot (**Figure 64**) for this series of sulfonate dieters gave ρ = 2.88. This high value of ρ indicates that there is a developed negative charge on the sulfonyl group in the transition state. If the data for **35** and **39** are included in the Hammett plot (**Figure 61**) it can be seen that the slope is less steep. This might be due to the solvent effect since the data that was reported used ethanol and the hydrolysis of **35** and **39** were carried out in 10% dioxane in water. In addition, the pK_a of the non-leaving group of compound **43** is lower compared with the pKa of the non-leaving group of compounds **35** and **39**. Further, the slope of these points has not been calculated since they are just two points where every plot needs at least four points to be confident about the slope. Therefore, more data are needed to reach a conclusion.
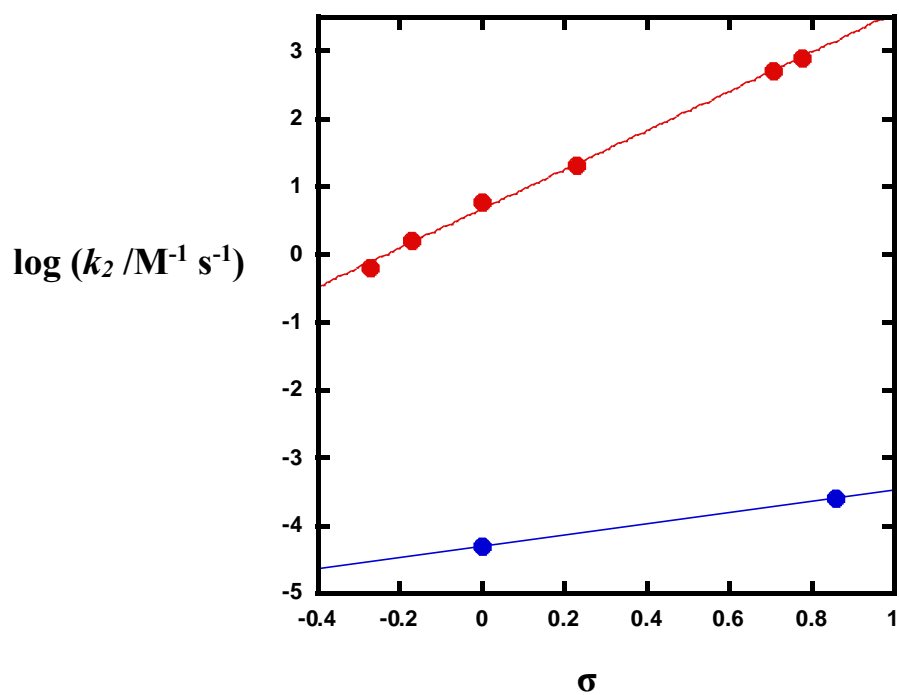
Figure 64: Hammett plot of hydrolysis of sulfonate esters **43a-f** (red points) in ethanol at 25 °C, $\rho = 2.88 \pm 0.07$, $R^2 = 0.997$; blue points are data for compounds **35** and **39** studied at 40 ± 0.1 °C, 10% dioxane.

4.5 Conclusions

Four novel compounds of pyridyl phenyl sulfate diesters and derivatives have been successfully synthesised and kinetic data determined. Brønsted and Hammett plots show good correlations and they demonstrated a better correlation compared to the literature. Inclusion of the data of compounds **35-37** in the study of Younker and Hengge[99] gave similar values of Brønsted coefficient. A Hammett plot with σ^- gave a similar correlation to the Brønsted plot and it is better than Hammett plot with σ. Based on the values of Brønsted β_{lg} = -0.72 and Hammett value ρ = 1.44 and 1.55 with σ and σ^- respectively, there is negative charge developed on the oxygen atom of the leaving group in the transition state, and there is a single mechanism which is likely to be as follows.
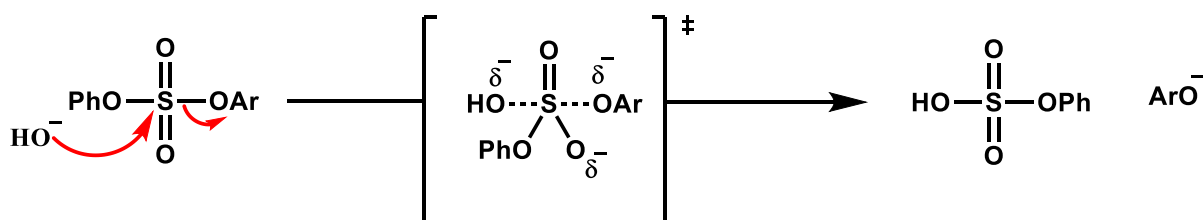
Scheme 15: Alkaline hydrolysis of aryl phenyl sulfate diester.

Furthermore, the effect of the non-leaving group on the reactivity was studied. Changing the non-leaving group from phenyl to 3-hydroxy pyridyl changed the reactivity and it increased by 5.3 fold. Similar observations are found for the effect of non-leaving groups for the hydrolysis of sulfonate esters[75] and phosphate triesters.[102] However, the effect of the non-leaving group on the reaction of sulfonate monoester and phosphate triesters is greater than with sulfate diesters.

Chapter five: Phosphate triesters

5.1 Introduction: Phosphate triesters

Phosphate esters have wide biological importance, especially mono and diesters. However, phosphate triesters do not seem to have roles in any biological activity in the biosphere.[104] Phosphate triesters do play crucial rules in the agricultural industry.[105] They form part of the key structure of pesticides and insecticides and are also found in chemical warfare agents.[106,107]

Due to their toxicity, phosphate triesters need to be destroyed safely. A common phosphate triester that has been used as a pesticide is aporaxon **49** which can inhibit human acetylcholinesterase.[108] Thus it would be interesting to understand the mechanism of degradation of these toxic compounds.[109] Enzymes which do this can hydrolyse these species and convert them into a more friendly species to the environment. Phosphotriesterase is a common enzyme that can be used to hydrolyse phosphate triesters. Also, it is found that the promiscuity enzyme of PMH can catalyse phosphate triester cleavage.[41] In this study the (PMH) enzyme was tested with diethyl 4-nitrophenyl phosphate **49** and the k_{cat}/K_M was measured to be $1.6 \times 10^{-2}\,M^{-1}s^{-1}$. The pH profile demonstrated a different shape when compared to the reaction of other species such as sulfonate, sulfate and phosphate mono and diesters. This is attributed to the position of the substrate in the active site of the PMH enzyme which may be different from other species.

Phosphate triesters have been utilized to study phosphate diester reactivity.[110] Compound **45** was designed as a model to study the properties of neutral phosphate diester **18** (chapter 3) since it is impossible to study the neutral diester reacting with hydroxide ion directly. At high pH, the deprotonated species is formed and therefore the methyl group in the phosphate triester can act as a surrogate for protonation of the phosphate diester. The second order rate constant for alkaline hydrolysis was measured to be $1 \times 10^{-6}\,M^{-1}\,s^{-1}$ and neutralizing the phosphoryl group enhances the rate of reaction by about 10^9 compared with the corresponding phosphate diester.
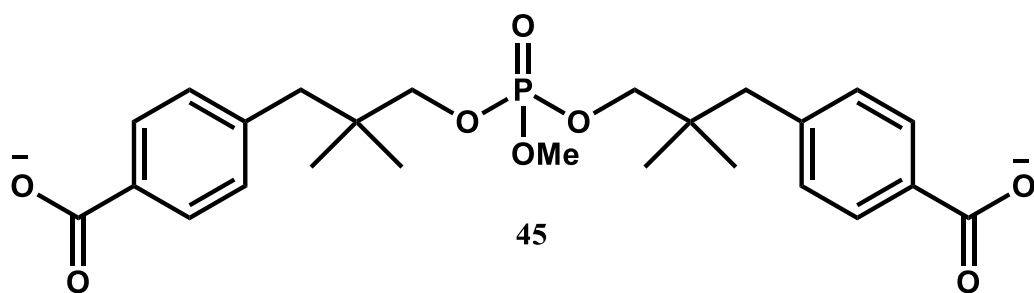
Figure 65: Phosphate triester reported by Schroeder *et al.*[79]

Cyclic phosphate esters have been utilized in prodrug strategies[111-113] as the polarity of the phosphate bond increases the solubility of the lipophilic drugs in an aqueous solution.[112] In addition cyclic phosphate esters are used in drug delivrey[114], especially as cyclic phosphate monoester have been shown to act as antiviral and in anti-cancer drugs. However, there have been challenges in delivering this medicine to the liver and subsequent diffusion through the cell since the phosphate monoester is charged. Phosphate cyclic triesters were used to tackle this problem since they are not charged. For example compound **46d** was used as an antiviral drug and it was converted to the cyclic phosphate triester in order to diffuse into the cell.[111] The first step in the mechanism of cyclic phosphate triester hydrolyses of **46a** is oxidation to convert it into **46b**. Ring opening will then occur to yield **46c**, which in turn will hydrolyse to phosphate monoester **46d** and can then be delivered to the liver as shown in **Scheme 16**.
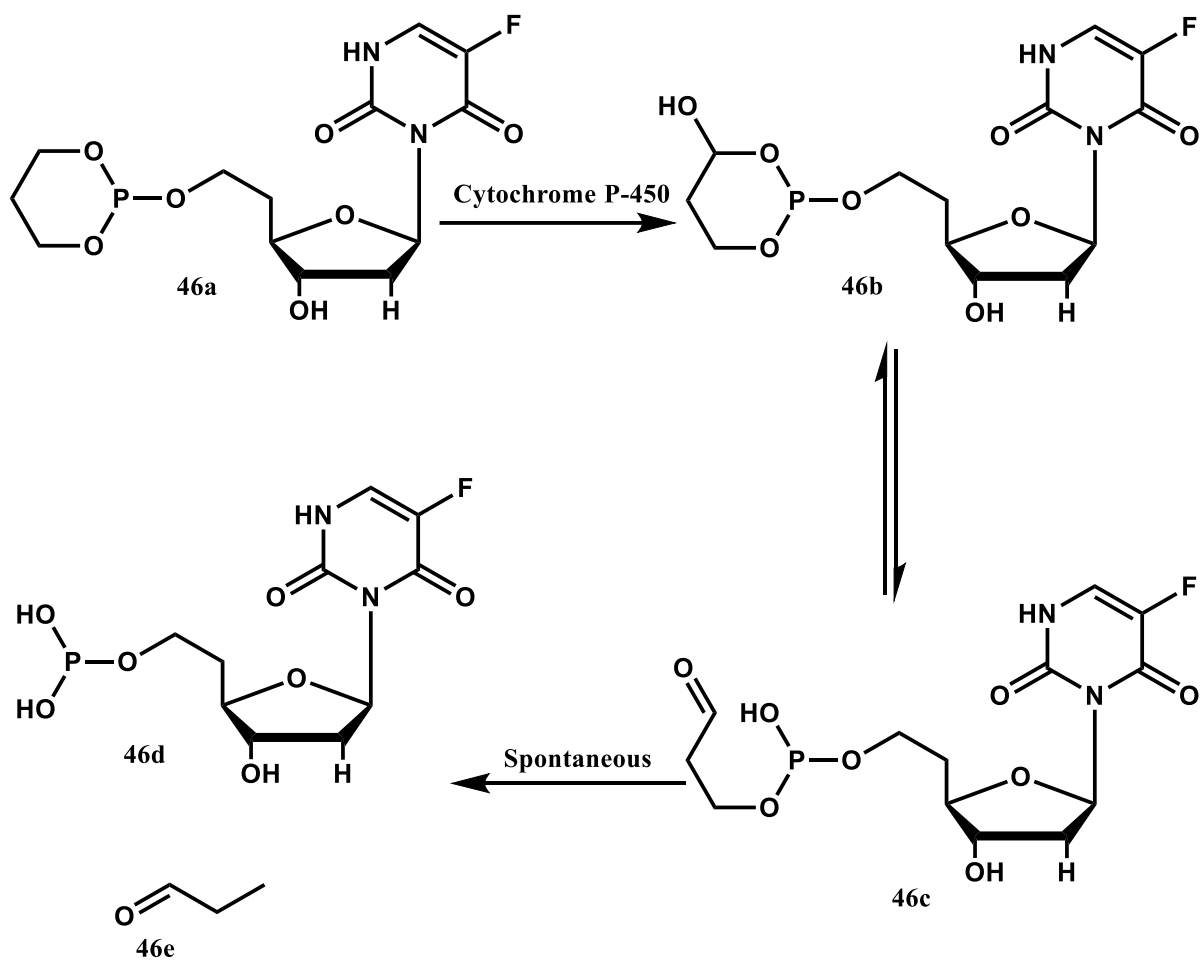
Scheme 16: Proposed mechanism to deliver cyclic phosphate monoester **46d** into the cell.[115]

5.2 Mechanism of phosphate ester hydrolysis

There are three distinct mechanisms for the hydrolysis of phosphate esters[109,116-118]: associative, dissociative or concerted mechanisms, which vary in importance depending on the type of system[1] as shown in **Figure 66**. For phosphate monoester, the reaction proceeds through a dissociative mechanism when there is no bond formation to the nucleophile and new complete bond fission to the leaving group with a tricoordinate intermediate.[5,109,118-120] The reaction of phosphate diester occurs by a concerted mechanism with a synchronous transition state which is in the middle of an associative and dissociative mechanism.[13,27,89,109,117,121,122] While for phosphate triester, the mechanism is suggested to proceed via an associative mechanism where there is no bond cleavage to the leaving group and full bond formation to the nucleophile. This step includes the formation of a phosphorane intermediate. On the other hand, the mechanism of phosphate triester with 4-nitrophenol as the leaving group was found to react by a concerted mechanism.[106,123,124]
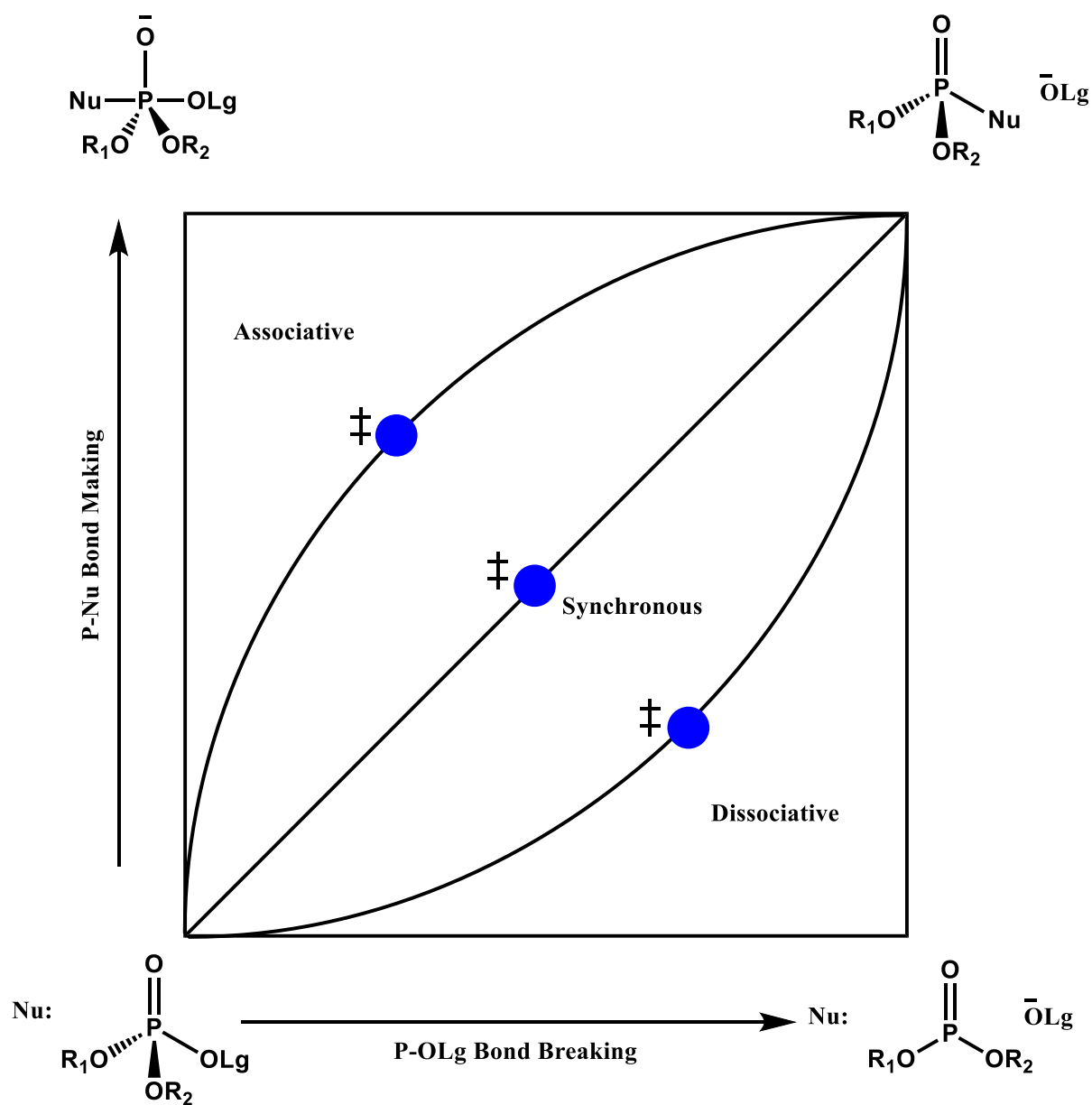
Figure 66: Possible mechanisms for hydrolysis of phosphate esters[43], Phosphate monoester: $R_1 = R_2 = H$; phosphate diester; $R_1 = $ Alkyl or aryl, $R_2 = H$; phosphate triester: $R_1 = R_2 = $ Aryl or alkyl.

5.3 Previous studies

Khan and Kirby[10] studied the reactivity of a series of cyclic substituted phenyl phosphate triesters **47a-g** with different types of nucleophile such as water, amines, and oxyanions. The authors found the reactivity of these compounds is sensitive to the nucleophile and to the pK_a of the leaving group. Additionally, the reaction in water was found to be unexpectedly slow. However, the reactivity toward hydroxide ion was extremely high.

X=
a: 2,4-(NO₂)₂
b: 4-Acetyl
c: 4-Cl
d: 4-NO₂
e: 2-NO₂
f: 3-NO₂
g: H
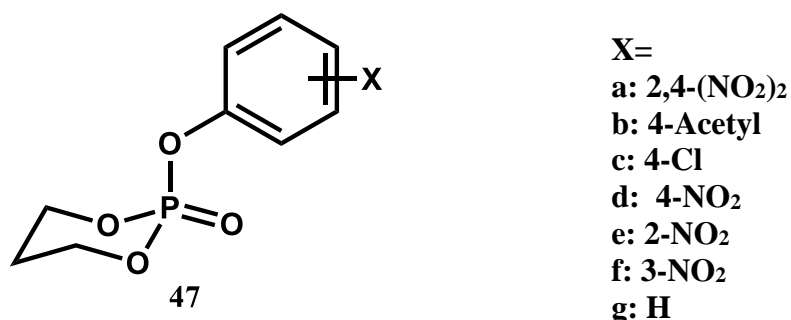
Figure 67: Series of cyclic substituted phenyl phosphate triesters reported by Khan and Kirby.[10]

Moreover, the Brønsted plot (**Figure 68**) gave $\beta_{lg} = -0.35$ for the alkaline hydrolysis reaction and $\beta_{lg} = -0.96$ for the spontaneous hydrolysis reaction. The large magnitude of the Brønsted coefficient for the spontaneous hydrolysis compared with hydroxide catalysed reaction indicates that these compounds are less sensitive to the pK_a of the leaving group with respect to a more basic nucleophile.
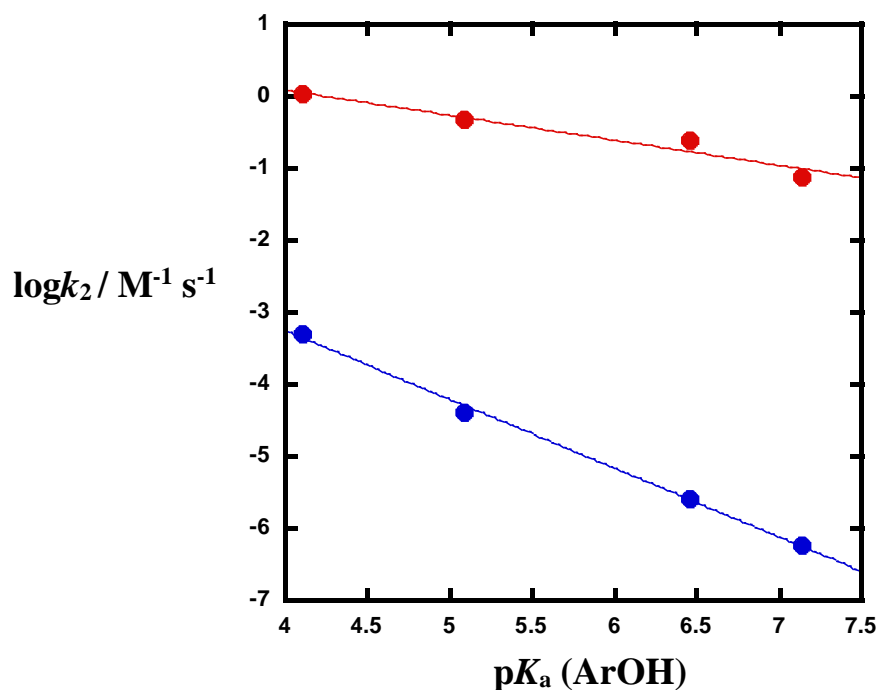
Figure 68: Brønsted plot for the hydrolysis of the cyclic substituted phosphate triester **46a-d** at 39 °C; red points are spontaneous hydrolysis reaction: β = -0.35; blue points are corresponding to alkaline hydrolysis reaction: β_{lg} = -0.96.[10]

Tarrat[125] used theoretical studies to determine the mechanism of hydrolysis for dimethyl phosphate triesters with six different substituents **48a-f**.
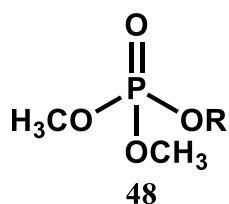
R=
a: CH₃
b: CH₂CCl₃
c: Phenyl
d: 2-NO₂ phenyl
e: 4-NO₂ phenyl
f: 2,4-(NO₂)₂ phenyl

Figure 69: The substituents of dimethyl phosphate triester studied by Tarrat.[125]

The reaction was found to occur by a stepwise mechanism when the leaving group is poor ($pK_a > 8$), but via a concerted mechanism with better leaving groups.
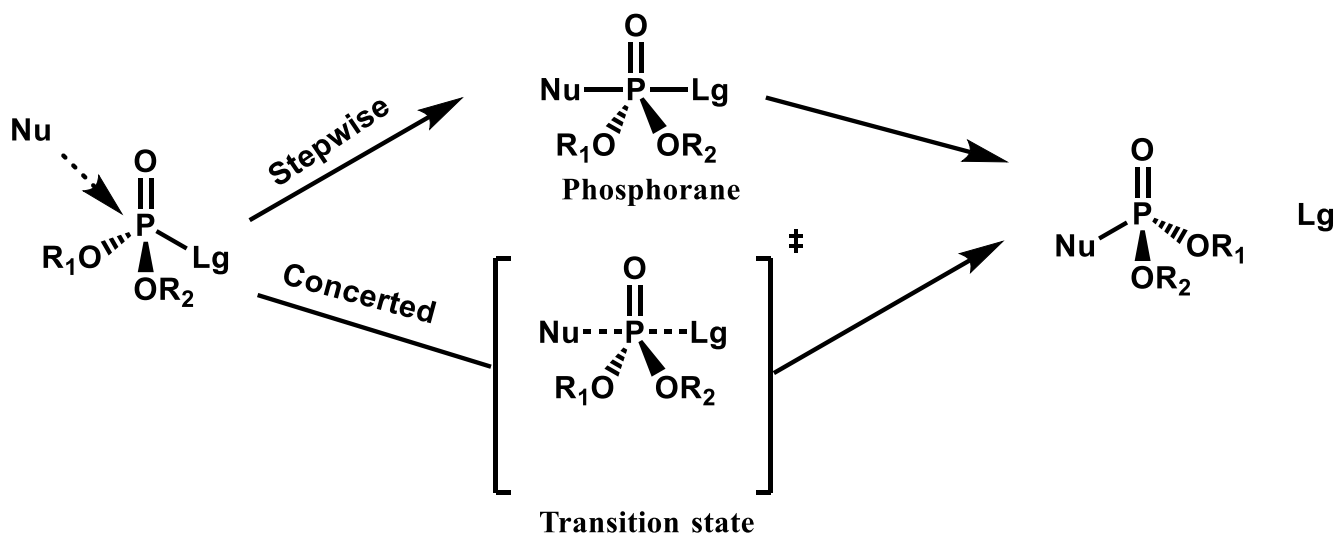
Scheme 17: Stepwise and concerted mechanisms for the alkaline hydrolysis of phosphate triesters as proposed by Tarrat.[125]

The hydroxide anion interacts with the six esters in the same way; therefore, the concerted mechanism or stepwise mechanism depends mainly on the features of the leaving group.

The mechanism of alkaline and enzymatic hydrolysis of the 4-nitrophenyl diethyl phosphate triester **49** and 4-carbamoylphenyl diethyl phosphate triester[126] **50**, were studied at 25 °C using primary and secondary kinetic isotopic effects (O^{18}) in order to investigate the transition state of the reaction and to assess whether it proceeds by an associative or dissociative mechanism.
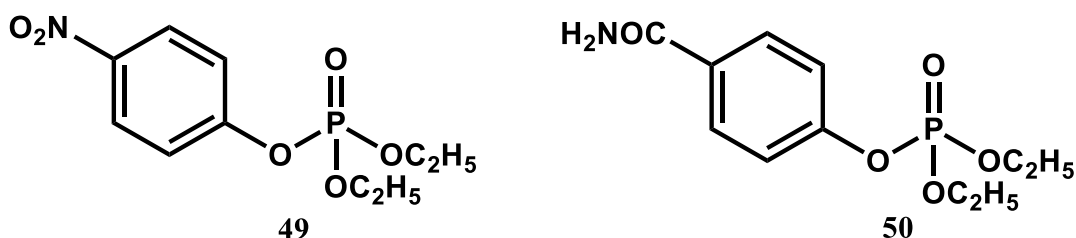
Figure 70: Phosphate triesters were reported by Caldwell *et al.*[126]

The values of the kinetic isotope effects show that there is a considerable change of bond order at the oxygen atoms of the leaving group and phosphoryl group. The reaction was suggested to occur via an associative mechanism with no evidence for a stable intermediate.

Kirby and coworkers[103] investigated the spontaneous hydrolysis of tri-2-pyridyl phosphate triester (TPP) in water at 25 °C. They suggested that general base catalysis was very efficient owing to two general bases that assist the water to attack as a nucleophile (10^8 more reactive than dialkyl phenyl phosphate triester).
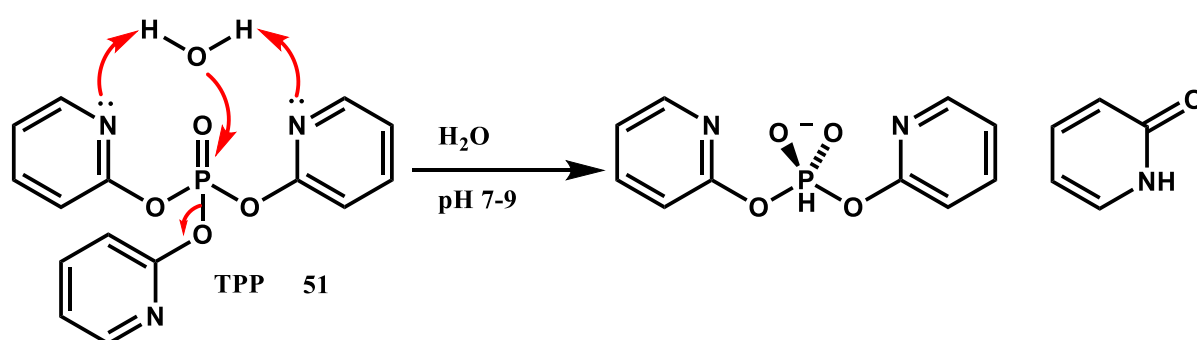
Scheme 18: Proposed mechanism of spontaneous hydrolysis of TPP.

In other words, efficient water activation is believed to be a very important feature in the enzyme active site. So, the unexpected reactivity was interpreted as being due to the effect of the nucleophile and leaving group and did not consider the effect of non-leaving groups. To further examine the unexpected reactivity of TPP, the spontaneous hydrolysis of phosphate triesters **52-54** and the reactions with selected nucleophiles were studied by Kirby and coworkers.[102] They found that the high rate of spontaneous hydrolysis was due to the electronic nature of the non-leaving group as well as the effect of leaving group and nucleophile. Moreover, they found that the spontaneous reaction was sensitive to the non-leaving group, thus depending on the value of β_{NLg}. This sensitivity decreased with increasing nucleophile strength. For example, the reaction of 2-pyridyl ester **52** with fluoride and hydroxide gave

β_{NLG} = -0.13 and -0.15 respectively. Additionally, the spontaneous hydrolysis of dialkyl aryl phosphate triester gives β_{NLG} = -0.6 and β_{LG} = -0.99 while triaryl phosphate triester gave β_{NLG} = -0.28 and β_{LG} = -0.42, which indicate the dialkyl system is more sensitive to changes in the non-leaving group and leaving group compared to the triaryl system.

R =
a: 4-ClC$_6$H$_4$O
b: 2-pyridyl
c: 4-NO$_2$C$_6$H$_4$O
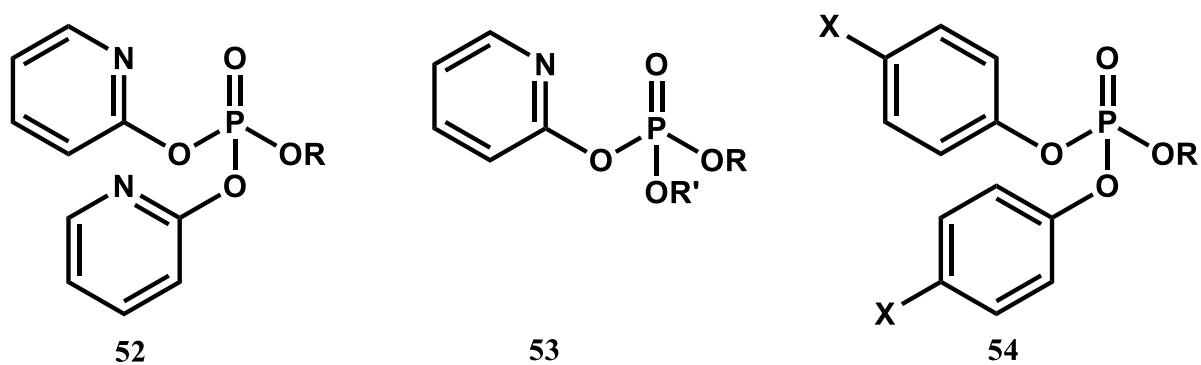
R=R'
a: (EtO)$_2$
b: (O(CH$_2$)$_3$O)$_2$
c: (CF$_3$CH$_2$O)$_2$
d: (2-pyridyl)2
e: (4-SO$_3$C$_6$H$_4$O)$_2$
f: (4-NO$_4$C$_6$H$_5$)$_2$

X:
a: SO$_3$
b: H
c: Cl

Figure 71: Phosphate triesters reported by Kirby *et al.*[103]

5.4 Aims

The aims of this chapter are to study the reactivities of cyclic phosphate triesters with different kinds of functional groups as shown in **Figure 72**.

X=
a = 4-NO$_2$
b = 3-NO$_2$
C = 3-Cl
d = H
e = 4-MeO
f = 3,4-(CH$_3$)$_2$
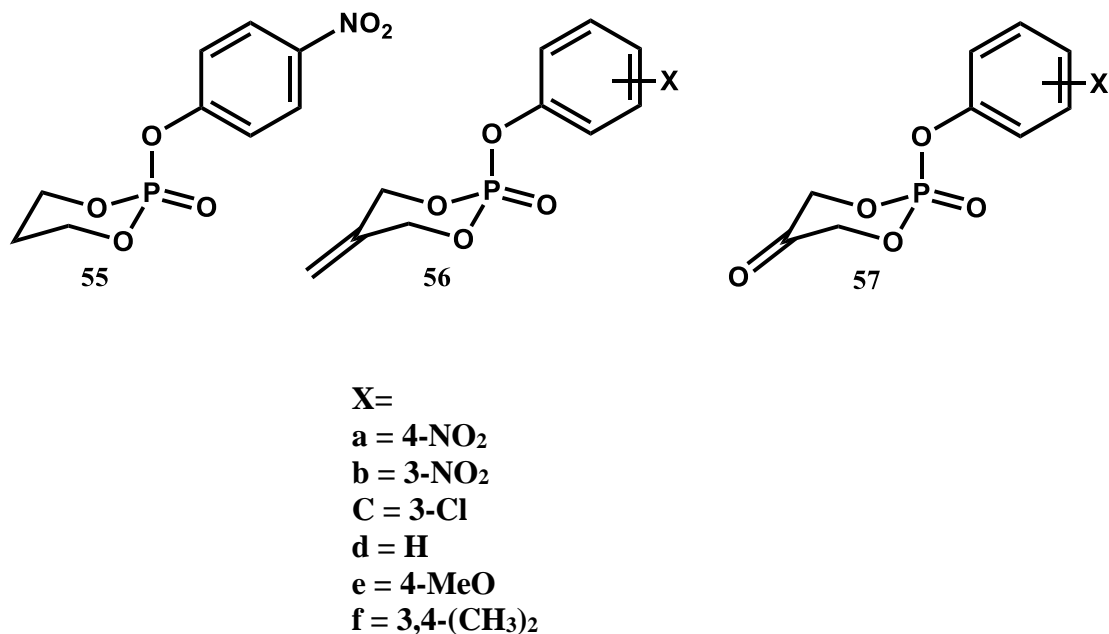
Figure 72: Series of cyclic phosphate triesters with different functional groups proposed in this study.

Compound **55** is a reference compound since it is less functionalised when compared with **56a** and **57a**. Compound **56a** was used to investigate the effect on the reactivity via introducing of sp^2 hybridization into the ring. Compound **57a** was used to examine the reactivity and effect of a carbonyl group. This addition is expected to play a significant role in giving higher reactivity when compared with **55**. Moreover, varying the pK_a range of the leaving group of **56a-f** and **57a-f** will allow for observations into the sensitivity of the reaction towards the change in leaving group. This will also allow for investigation of the transition state and enable the production of LFER in order to understand the transition state of the reaction.

5.5 Results and discussion

5.5.1 Synthesis of cyclic 4-nitrophenyl phosphate triester

Compound **55** was prepared as shown in **Scheme 19**. 1,3-propandiol with triethylamine was added to the 4-nitrophenyl dichlorophosphate to yield cyclic 4-nitrophenyl phosphate triester.
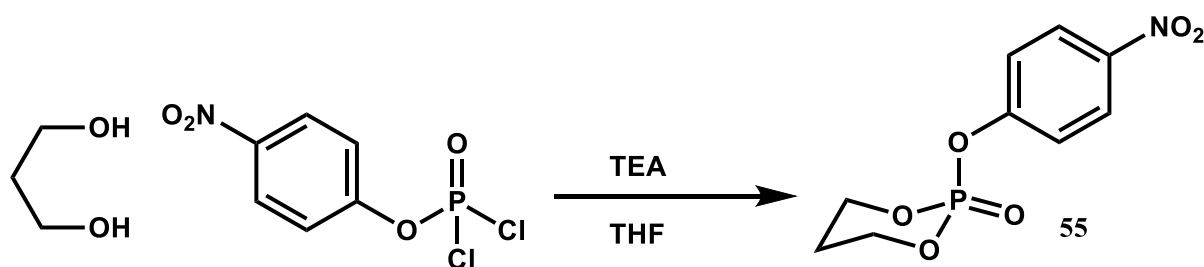
Scheme 19: Synthesis of cyclic 4-nitrophenyl phosphate triester **55**.

5.5.2 Synthesis of alkene cyclic substituted phenyl phosphate triester

The alkene cyclic substituted phenyl phosphate triesters were synthesised using two methods which are dependent on whether the aryl dichlorophosphate is commercially available or not.

First, compounds **56a** and **56d** were prepared by adding triethylamine to the mixture of 2-methylene -1,3-propandiol and the substituted phenyl dichlorophosphate in THF to produce **56a** and **56d** as shown in **Scheme 20**.
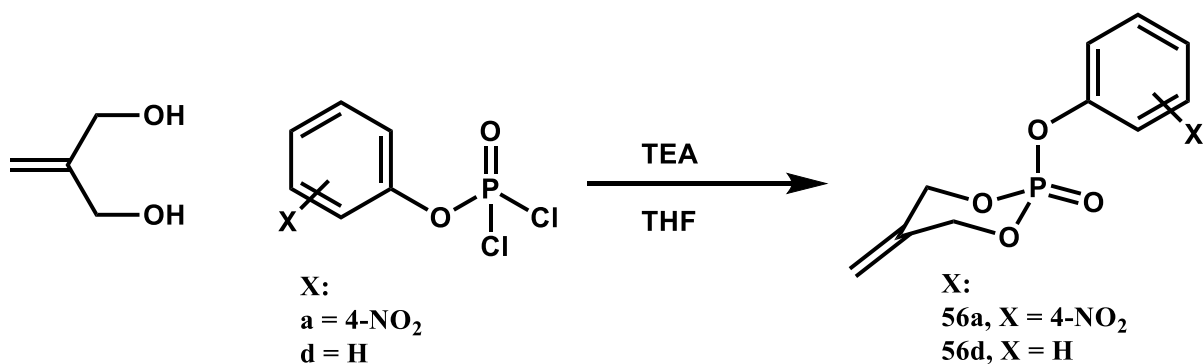
Scheme 20: Synthesis of alkene cyclic phosphate triester **56a** and **56d**.

When the aryl dichlorophosphate is not commercially available, the alkene triester were prepared as shown in **Scheme 21**. The 2-methylene 1,3-propandiol with triethylamine were added to POCl₃ to form the intermediate cyclic chloro phosphate. Adding the substituted phenol with triethylamine give the desired phosphate triester.
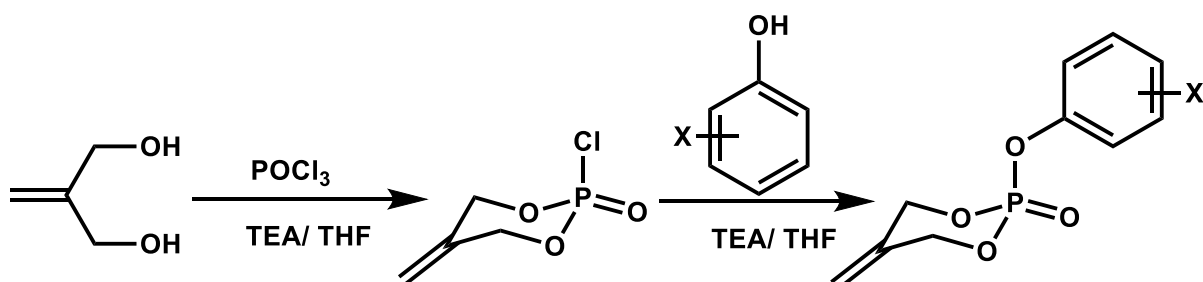
Scheme 21: Synthesis of alkene cyclic phosphate triester **56b**, **56c**, **56e** and **56f**; X= 3-NO₂, 3-Cl, 4-MeO, 3,4-(CH₃)₂ respectively.

5.5.3 Synthesis of carbonyl cyclic phosphate triester

The alkene compounds **57a-f** were converted to ketones **56a-f** by using O₃ at -78 °C as explained in **Scheme 22**. The reaction was quite efficient and took 45-60 min overall to finish the reaction.

Scheme 22: Synthesis of carbonyl cyclic substituted phenyl phosphate triester **57a-f**.

5.5.4 Synthesis of 2,2-dimethoxy cyclic 4-nitrophenyl phosphate triester

The main aim of synthesising **59** is to investigate the impact of two electron withdrawing group on the rate of reaction and to compare this with phosphate triesters which have different functional group (**55-57**). The synthesis of 2,2-dimethoxy cyclic 4-nitrophenyl phosphate triester **59** was started by synthesising the 2,2-dimethoxy propanediol (**Scheme 23**). A solution of 1,3-dihydroxy acetone dimer, trimethylorthoformate and para toluene sulfonic acid in methanol was refluxed. The reaction was then quenched with K_2CO_3 to yield 2,2 dimethoxy propanediol, which was purified either by vacuum distillation or by recrystallization, depending which gave better yield. After that, **58** with triethylamine was added to 4-nitrophenyl dichlorophosphate to yield compound **59**.
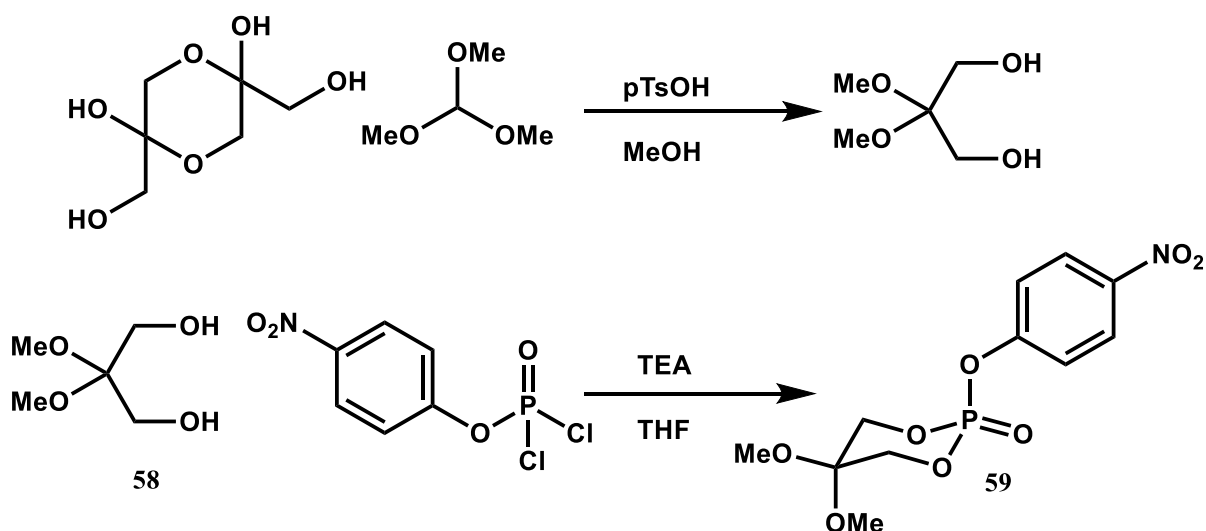
Scheme 23: Synthesis of dimethoxy cyclic 4-nitrophenyl cyclic phosphate triester **59**.

94

5.5.5 Hydration of ketone compounds and carbonyl phosphate triester

Ketone compounds exist as hydrate and ketone forms in aqueous solution. The presence of the hydrated form depends on the chemical structure. Several studies[127-129] confirm that the use of aqueous solution increases the percentage of the hydrated form. In these studies, NMR, IR and X-ray techniques were employed to determine the equilibrium state and percentage of hydrated form for DHA **60**, DHAP **61**, and cDHAP **62**. These compounds were found to have 20%, 50% and 86 % hydrate forms respectively.
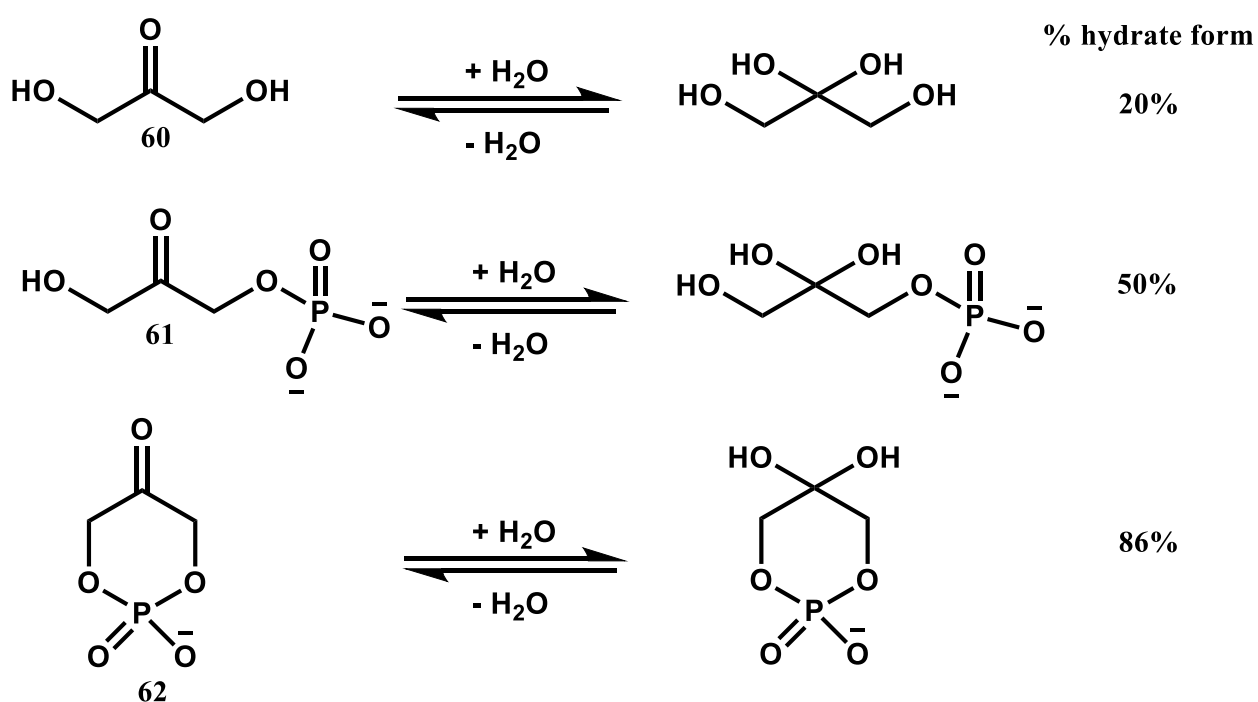
Scheme 24: The equilibrium state between a ketone and hydrated form and the percentage of hydrated form of DHA, DHAP, and cDHAP.

The same observations are found with carbonyl cyclic phosphate triesters compounds **57a-f**. **Figure 73** explain how the carbonyl compound can exist in its hydrated form even in deuterated chloroform, which contains less than 0.01% water. The ^{31}P NMR shows two ^{31}P signals, one of which is the ketone form and the other is the hydrated species. Furthermore, the carbonyl compound exists almost completely as the hydrated form in D_2O, as shown from ^1H NMR.

Moreover, mass spectra with most of the carbonyl compounds gave two molecular weights, one for the ketone and the another for the hydrate. I.R also confirms this by showing two signals at IR= 3297 cm^{-1} (OH); 1758 cm^{-1} (C=O).
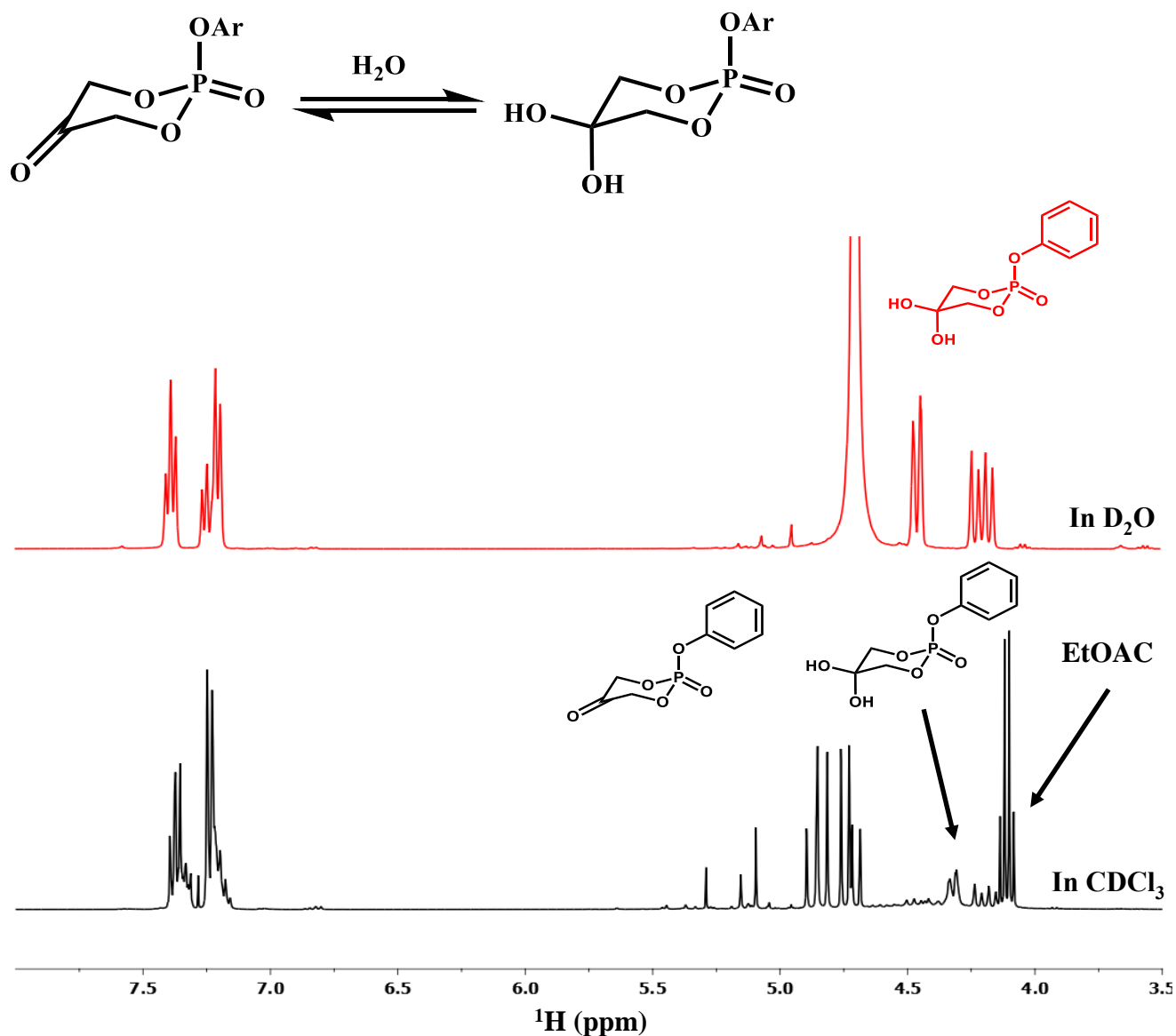
Figure 73: ^{1}H NMR for carbonyl cyclic phenyl phosphate triester and hydrated form in CDCl$_3$ and D$_2$O respectively.
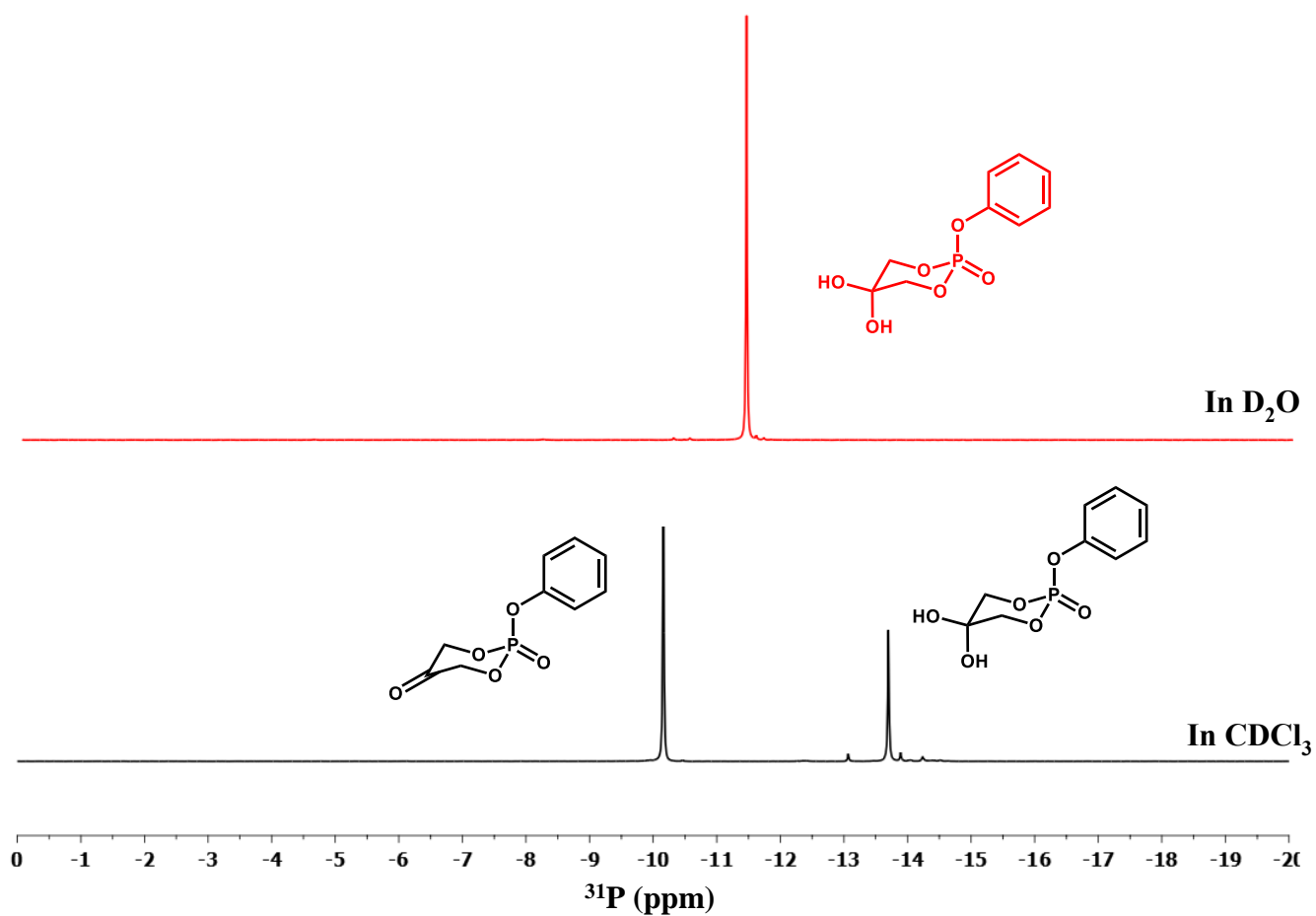
Figure 74: ^{31}P NMR for carbonyl cyclic phenyl phosphate triester and hydrated form in CDCl$_3$ and D$_2$O respectively.

Based on ^{31}P NMR the hydrated form exists 100% in D$_2$O and about 35% in CDCl$_3$. We can notice the percentage of hydrated form is surprisingly large. This percentage form in CDCl$_3$ could be due to the use of ethyl acetate during column chromatography as this can contain some water. In addition, the deuterated chloroform contains 0.01% water and this percentage could affect the formation of the hydrated species.

5.5.6 pH profile of cyclic, alkene, dimethoxy cyclic 4-nitrophenyl phosphate triesters

The pH profiles were studied for **55** (cyclic), **59** (dimethoxy), **56a** (alkene) and **57a** (carbonyl). They all have 4-nitrophenol as a leaving group. For pH above 11 NaOH was used to get the corresponding pH. For pH below 11, buffer was used and was extrapolated to zero buffer catalyst by varying the concentration of buffer at affixed pH as described later (**Figures 76-78**). HCl was used for pH between 0-2. All the pHs were measured at 25 °C after each experiment. The reactions show excellent first order or linear initial rate kinetic behaviours. For slow reactions, the initial rate measurements were conducted and they all demonstrated a linear initial rate. In general, the pH profile shows that the reaction of these compounds demonstrates acid and base catalysis as can be seen from **Figure 75**. From **Table 4**, the values of second order rate constants in basic conditions are greater than those in the acidic regions. This indicates that these compounds are more sensitive to base than to acid. In terms of reactivity of these species, the dimethoxy compound is more reactive than a cyclic compound which does not have any functional group by 22 and 45-fold in the basic and acidic regions respectively. The alkene compound that has an sp^2 carbon in the ring is slightly less reactive than dimethoxy by 1 to 3 fold and is more reactive than the reference compound by 15 and 20 times in basic and acidic regions respectively.

The carbonyl **57a** demonstrates much higher reactivity under basic conditions. The reactivity is 9×10^8, 5×10^7 and 5×10^7 fold greater than the cyclic **55**, alkene **56a**, and dimethoxy **59** respectively. The carbonyl functional group, which converts to an internal nucleophile in the presence of water is attributed to enhancing the rate of reaction.

However, in the acidic region, the **57a** (carbonyl) show insignificant reactivity compared to that of basic conditions. For example, it displays comparable reactivity to an alkene **56a** and it is 17 times more reactive than cyclic **55** and 2.8 times less reactive than a dimethoxy compound

98

59. On the other hand, the spontaneous reactions for **55**, **56a** and **59** show strong sensitivity to the structure. The dimethoxy **59** is more reactive than **55** by 70-fold and the largest impact was observed with alkene **56a** which was 167 times more reactive compared with the reference compound **55**. Kirby[102] also found the spontaneous reactions for a series of phosphate triester **53a-53c** are very sensitive to the structure. However, further research needs to be carried out in the water region. The reaction at pH 4-6 needs to be measured and must be extrapolated to zero buffer concentration, which is challenging due to strong buffer catalysis.
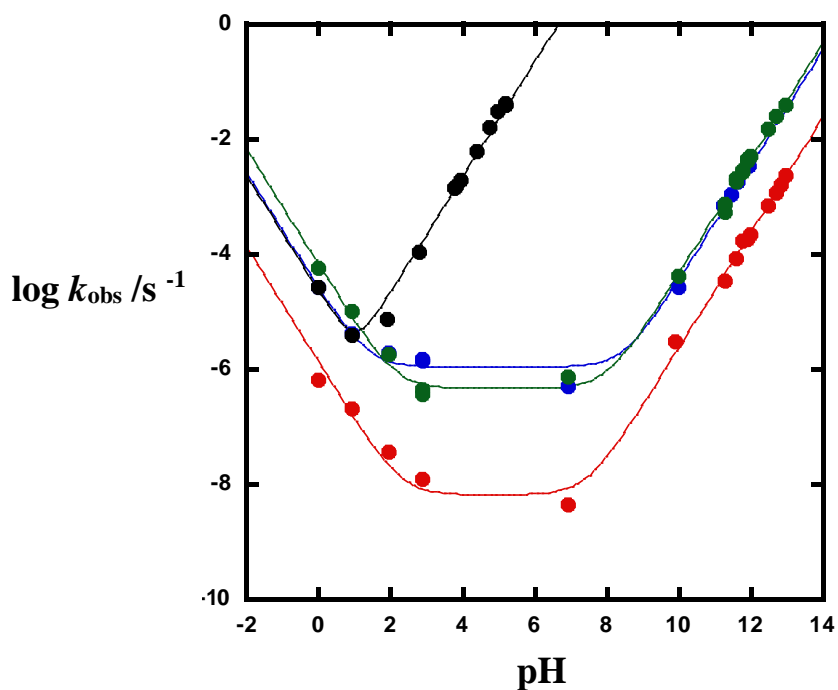
Figure 75: pH profile of cyclic, alkene and dimethoxy cyclic 4-nitro phenyl phosphate triester; 25 °C, 1 M NaCl, red points corresponding to cyclic **55**, blue alkene **56a**; green is dimethoxy **59** and black points to carbonyl **57a**.

The data for cyclic, alkene and dimethoxy compounds **55**, **56a**, and **59** were fitted to equation 11:

$\log k_{obs} = \log (k_H [H^+] + k_0 + k_{OH} [OH^-])$ **Equation 11**

The data for carbonyl **57a** were fitted to equation 12:

$\log k_{obs} = \log (k_H [H^+] + k_{OH} [OH^-])$ **Equation 12**

Substrate	k_H / $M^{-1} s^{-1}$	*Relative Rate/ k_H*	k_0 / $M^{-1} s^{-1}$	*Relative rate/ k_0*	k_{OH} / $M^{-1} s^{-1}$	*Relative rate/ k_{OH}*
Cyclic 55	(1.4 ± 0.3) $\times 10^{-6}$	1	(6 ± 2) $\times 10^{-9}$	1	0.023 ± 0.002	1
Alkene 56a	(2.6 ± 0.5) $\times 10^{-5}$	19	(1.1 ± 0.2) $\times 10^{-6}$	183	0.34 ± 0.04	15
Dimethoxy 59	(7 ± 1) $\times 10^{-5}$	50	(4.5 ± 0.8) $\times 10^{-7}$	75	0.44 ± 0.02	19
Carbonyl 57a	(2.3 ± 0.6) $\times 10^{-5}$	16	-		(2.2 ± 0.2) $\times 10^7$	9.6×10^8

Table 4: Second order rate constants for acidic, basic and water reactions for compounds **55**, **56a**, **57a** and **59**.

5.5.7 Buffer catalysis of phosphate triester

To be able to compare the reactivities of **55-57** and **59**, it was important to check the role of buffer catalysis. Thus, studies were performed by varying the concentrations of buffer at the same pH and temperature. **Figures 76-78** show the reaction of **55, 56a** and **59** is strongly buffer catalysed. Therefore, any kinetic measurements of these compounds using buffer catalyst were extrapolated to zero buffer catalyst by plotting the pseudo first order rate constants against the concentration of the buffer.

Unlike cyclic **55**, alkene **56**, dimethoxy **59**, carbonyl compounds **57c** exhibit no buffer catalysis. The buffer catalyst was tested with a member of carbonyl compounds **57c** (carbonyl 3-Cl) and it shows no buffer catalysis (**Figure 79**) because this kind of compound has an internal nucleophile in water as a result of the hydrate form of the carbonyl which prevents buffer catalyst contribution.
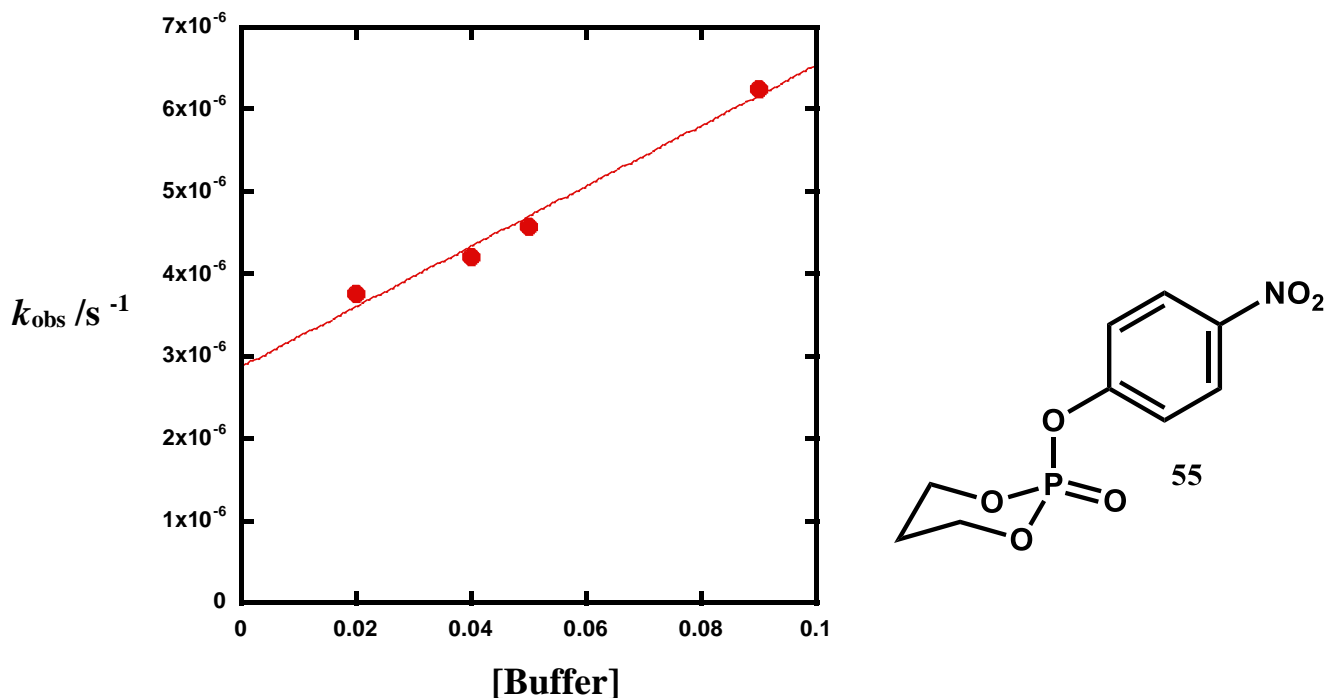
Figure 76: Buffer catalysis of cyclic 4-nitrophenyl phosphate triester **55**; pH= 9.9 ± 0.04; 25 °C, 1 M NaCl.
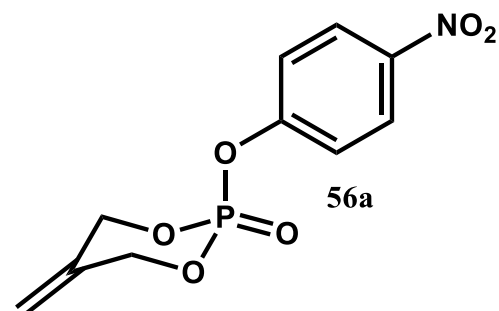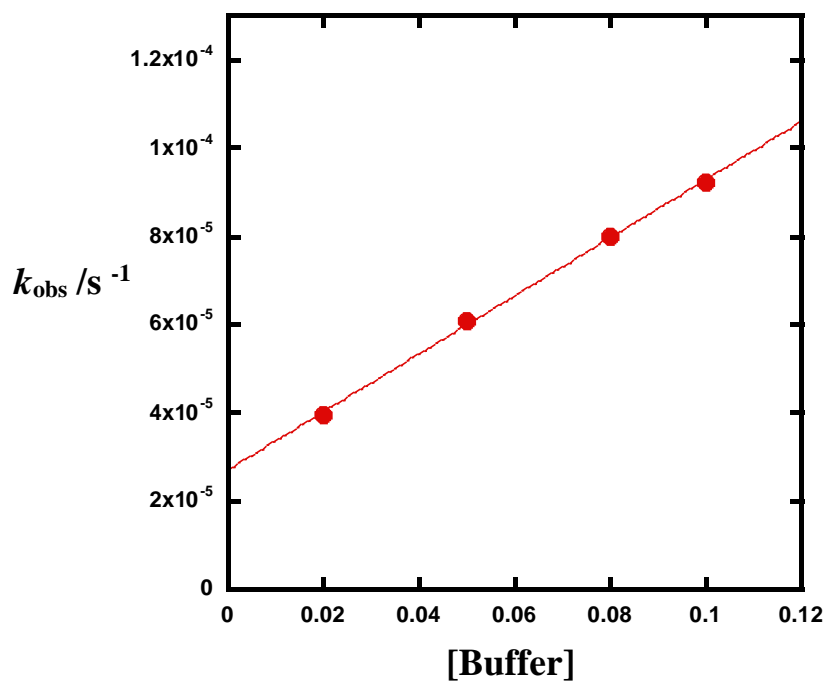
Figure 77: Buffer catalysis of alkene cyclic 4-nitrophenyl phosphate triester **56a**; pH= 9.9 ± 0.04; 25 °C, 1 M NaCl.
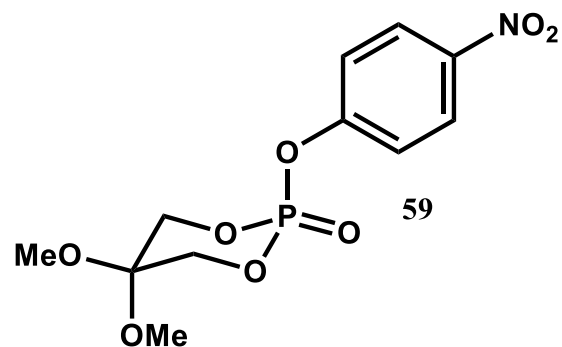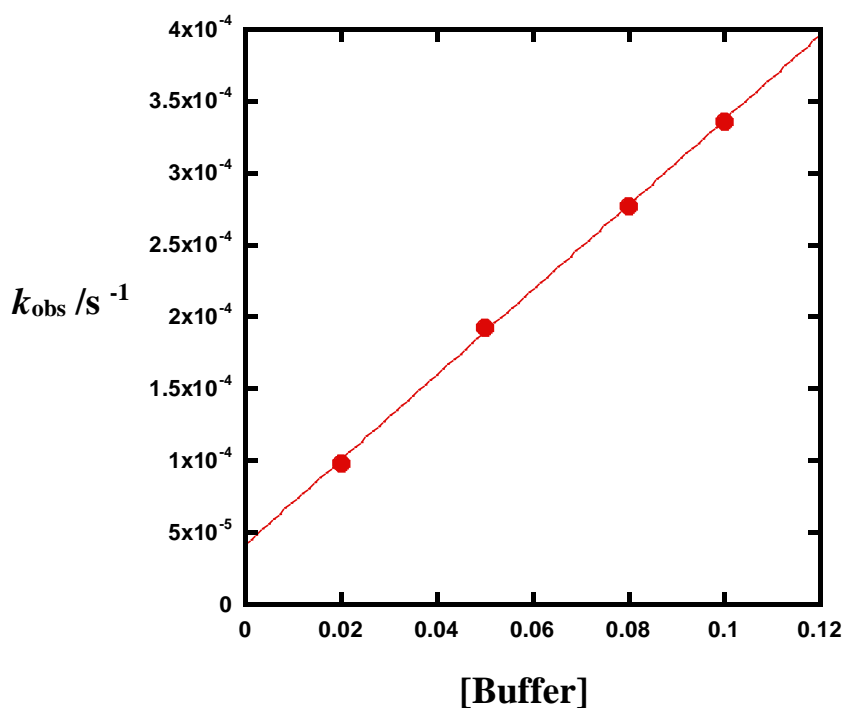
Figure 78: Buffer catalysis of dimethoxy cyclic 4-nitrophenyl phosphate triester **59**; pH= 9.9 ± 0.04; 25 °C, 1 M NaCl.

102
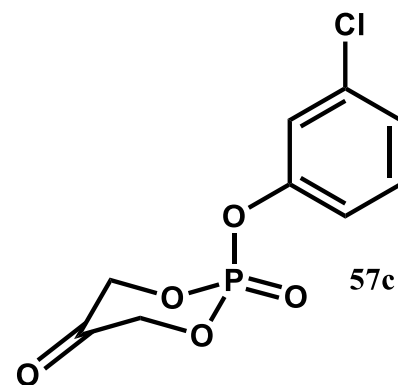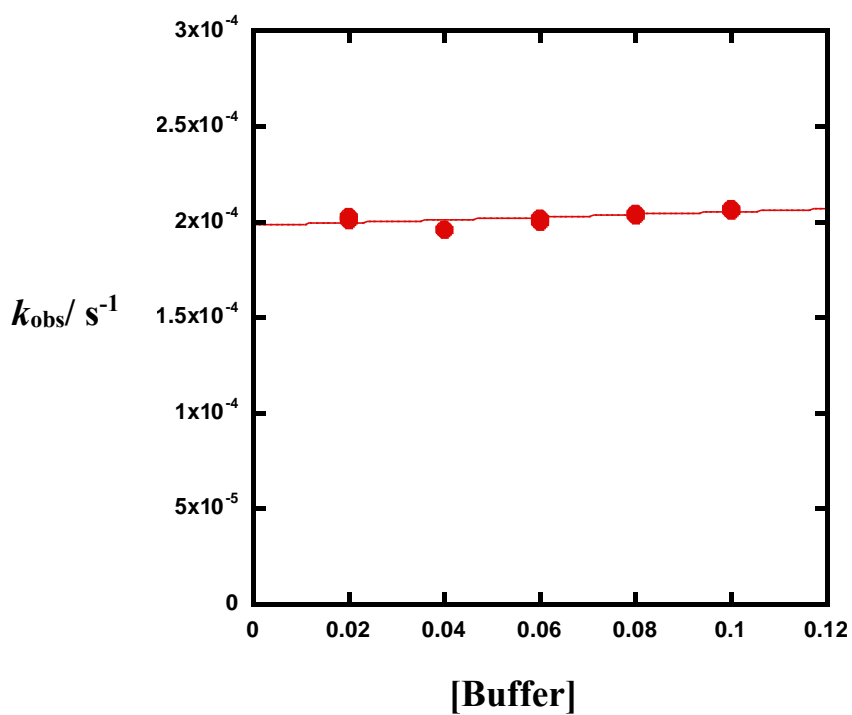
Figure 79: Buffer catalysis of carbonyl cyclic 3-chlorophenyl phosphate triester **57c** at 25 °C, (0.02-0.1) M buffer; pH= 6.1 ± 0.04, 1 M NaCl.

5.5.8 Alkaline hydrolysis of alkene cyclic substituted phenyl phosphate triesters

The alkaline hydrolysis of **56b-f** was carried out spectrophotometrically by following the absorbance of the leaving group which is a substituted phenolate ion. The reaction was maintained at 25 °C ± 0.03 and ionic strength 1 M NaCl. The concentration of sodium hydroxide was varied at least 10 times. All the reactions gave excellent first order profiles and the second order rate constants were determined by plotting k_{obs} against the concentration of NaOH as illustrated in **Figures 80-84**. As can be seen from these figures, the rate of reaction shows sensitivity to the concentration of sodium hydroxide. **Table 5** summarises the values of second order rate constants of **56a-f** with their measured pK_a.
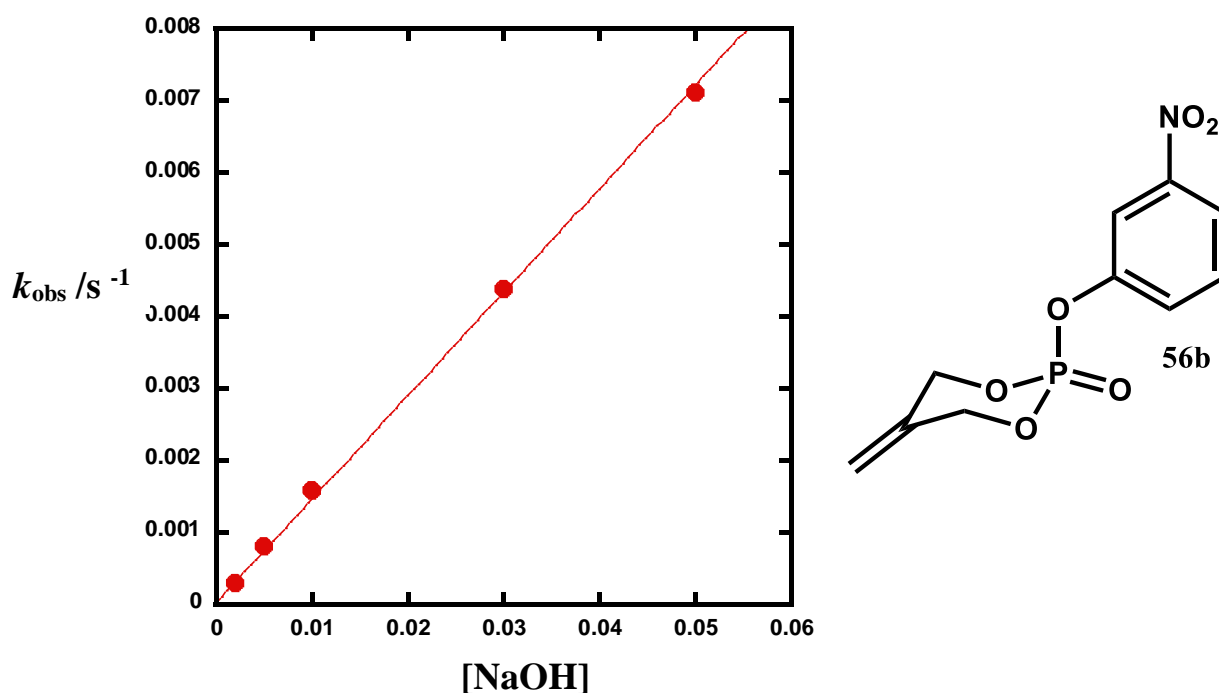
Figure 80: Alkaline hydrolysis of alkene cyclic 3-nitrophenyl phosphate triester **56b**.
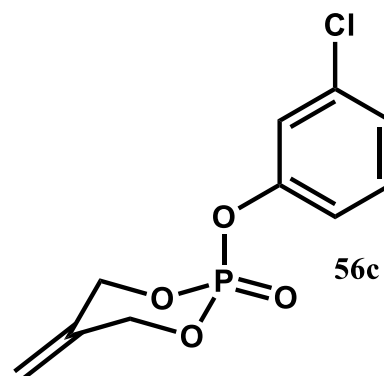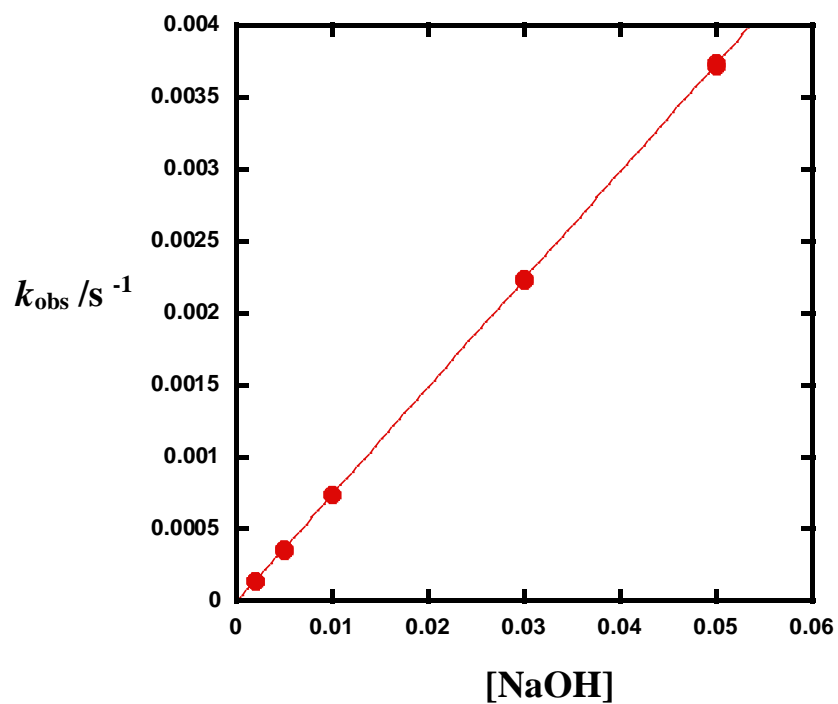
Figure 81: Alkaline hydrolysis of alkene cyclic 3-chlorophenyl phosphate triester **56c**.
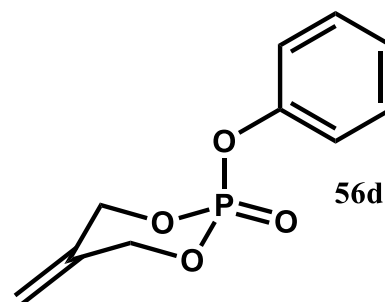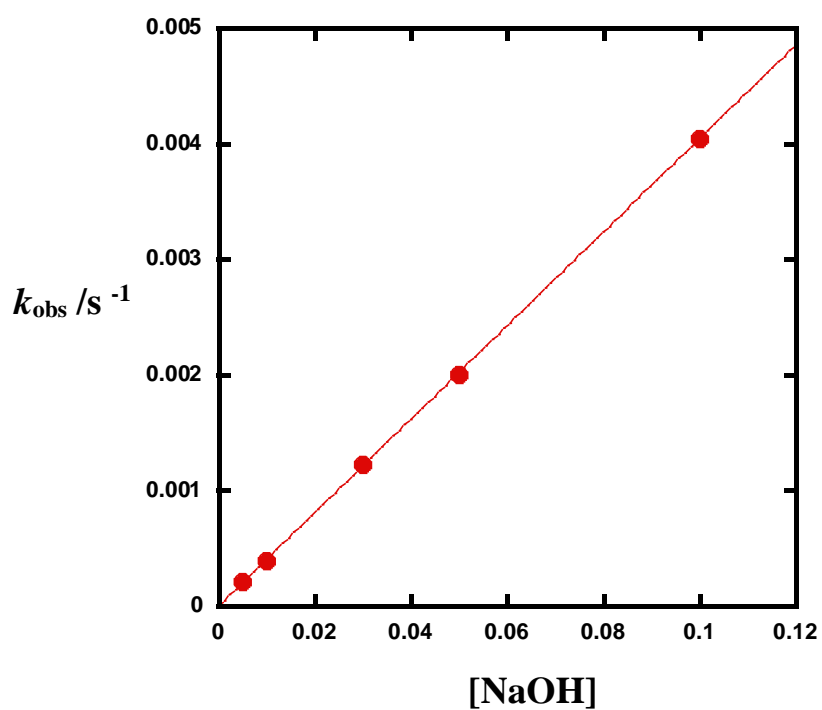
Figure 82: Alkaline hydrolysis of alkene cyclic phenyl phosphate triester **56d**.
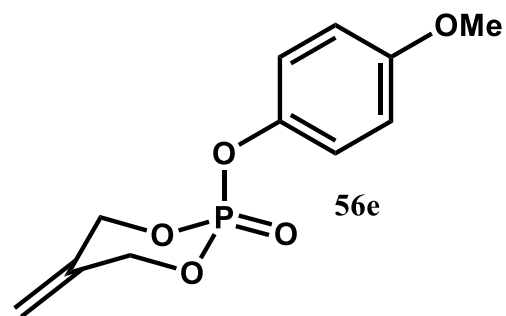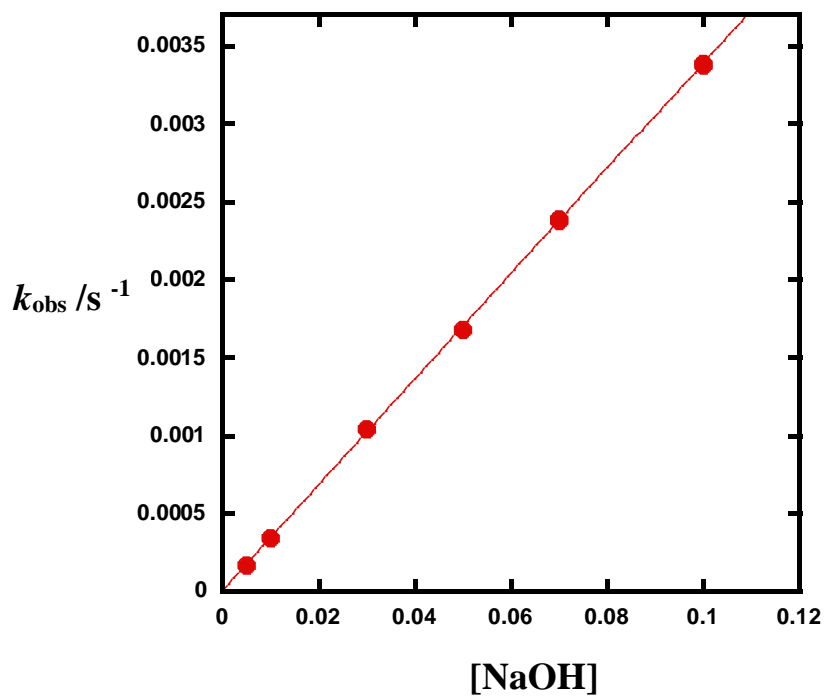
Figure 83: Alkaline hydrolysis of alkene cyclic 4-methoxyphenyl phosphate triester **56e**.
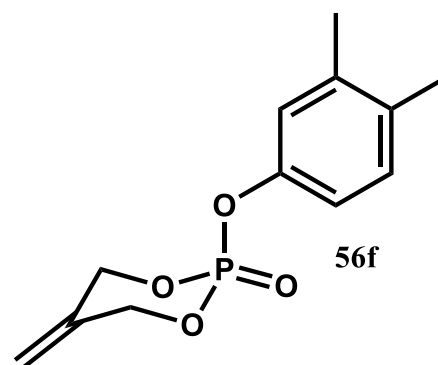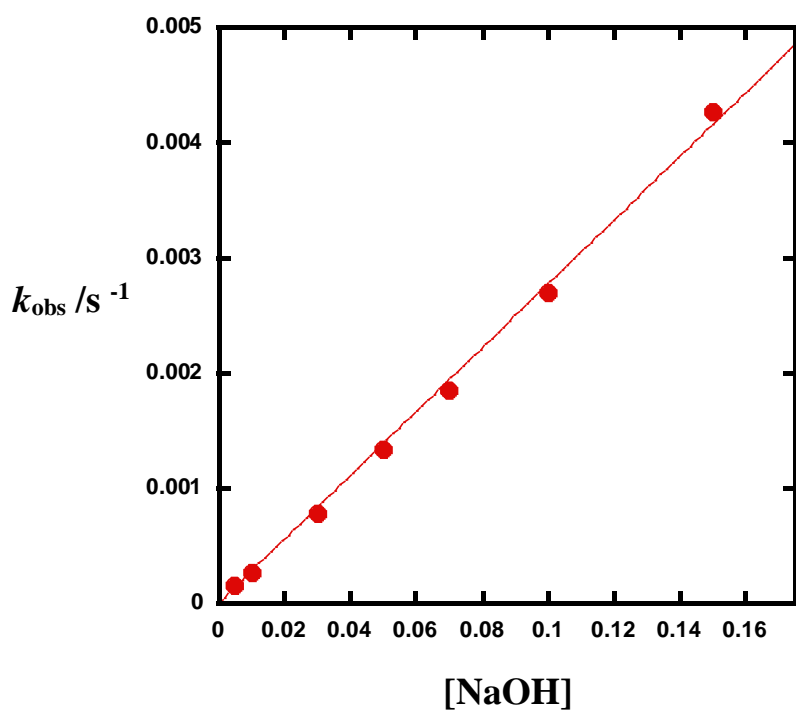
Figure 84: Alkaline hydrolysis of alkene cyclic 3,4-dimethyl phenyl phosphate triester **56f**.

106

Substrate (Alkene)	pK_a of substituted phenol	k_{OH} / M^{-1}S^{-1}
56a (4-Nitro)	6.86	$(34 \pm 4) \times 10^{-2}$
56b (3-Nitro)	8.1	$(14.4 \pm 0.2) \times 10^{-2}$
56c (3-chloro)	8.77	$(7.5 \pm 0.01) \times 10^{-2}$
56d (phenyl)	9.73	$(4 \pm 0.02) \times 10^{-2}$
56e (4-methoxy)	9.96	$(3.4 \pm 0.02) \times 10^{-2}$
56f (3,4-dimethyl)	10.1	$(2.8 \pm 0.03) \times 10^{-2}$

Table 5: Second order rate constants of alkaline hydrolysis of alkene cyclic substituted phenyl phosphate triester **56a-f** at 25 °C, 1 M NaCl.

5.5.9 Linear free energy relationship of alkene cyclic substituted phenyl phosphate triester

Plotting the logarithm of second order rate constants for the alkaline hydrolysis of alkene compounds **56a-f** against the measured pK_a of leaving group yields Brønsted coefficients of β_{lg} = -0.33 ± 0.01 as shown in **Figure 85**. The value that was obtained shows the hydroxide reaction is not very sensitive to the pK_a of the leaving the group and it is in good agreement with the study of Khan and Kirby.[10] In their study, they observed β_{lg} = -0.35 for hydroxide catalysed cleavage of compounds **47a-d**. The reactivity of the alkene compounds is more than that of the cyclic compounds as we noticed from the comparison of compound **55** and **56a**. The Brønsted values for hydroxide catalysed of both (cyclic and alkene compounds) gave very similar β_{lg} values and are much less than the β_{lg} = -0.99 which was obtained for water reactions of the cyclic compounds **47a-d**. This made for a clear conclusion; even alkene compounds show less sensitivity to the leaving groups in hydroxide reaction compared to that of the cyclic **47a-f** in water.
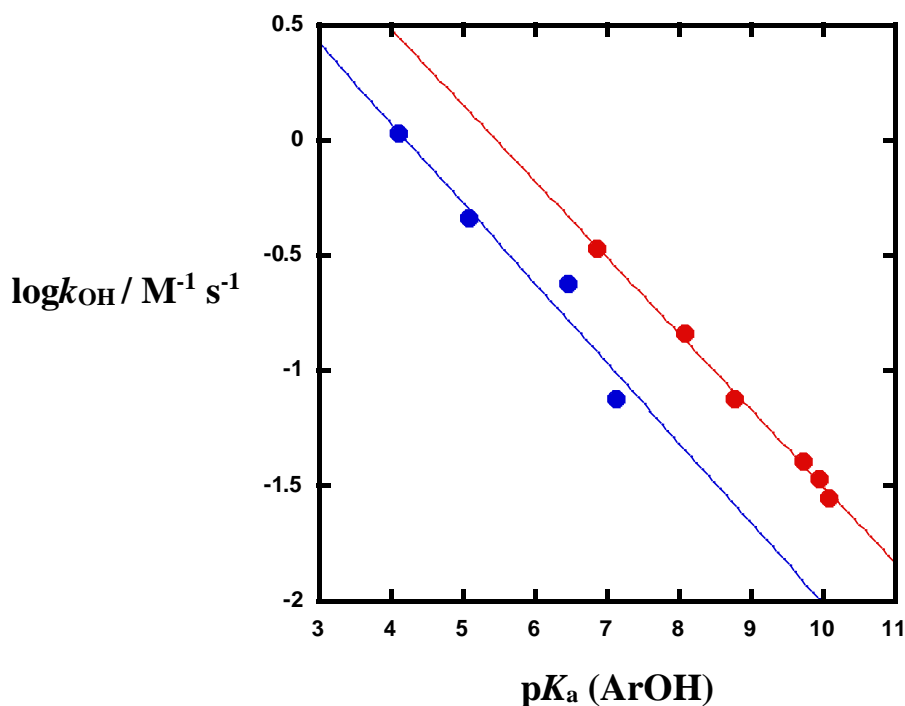
Figure 85: Brønsted plot for hydrolysis of phosphate triesters, red points (alkene cyclic **56a-f**) $\beta_{lg} = -0.33 \pm 0.01$; $R^2 = 0.996$; 25 °C; 1 M NaCl; blue points (cyclic compounds **47a-d**) reported by literature[10] $\beta_{lg} = -0.35 \pm 0.06$, $R^2 = 0.950$, 39 °C, 1 M KCl.

The Hammett plot (**Figure 85A**) was plotted with the same data and using sigma values that have been published in the literature[130], giving $\rho = 0.87 \pm 0.13$. However, the correlation is not quite linear and we can see if the 4-nitrophenol (red point inside the empty circle) was removed the plot would be improved. However, plotting the the same data with σ^- (**Figure 86B**) improved the plot and gave a good correlation which is similar to that of the Brønsted plot (**Figure 85**) for this data. This is because σ^- is smilar to pK_a, and similar observations were found with the sulfate diesters (chapter 4), which also gave better correlations with Brønsted and σ^- than σ. On the other hand, this is in contrast to sulfonate esters (chapter 2) which give good correlation with σ instead of the Bronsted plot. This can be interpreted to the effect of C-O in the sulfate diester and phosphate triester while C-S bonds in the sulfonate ester could have an effect.
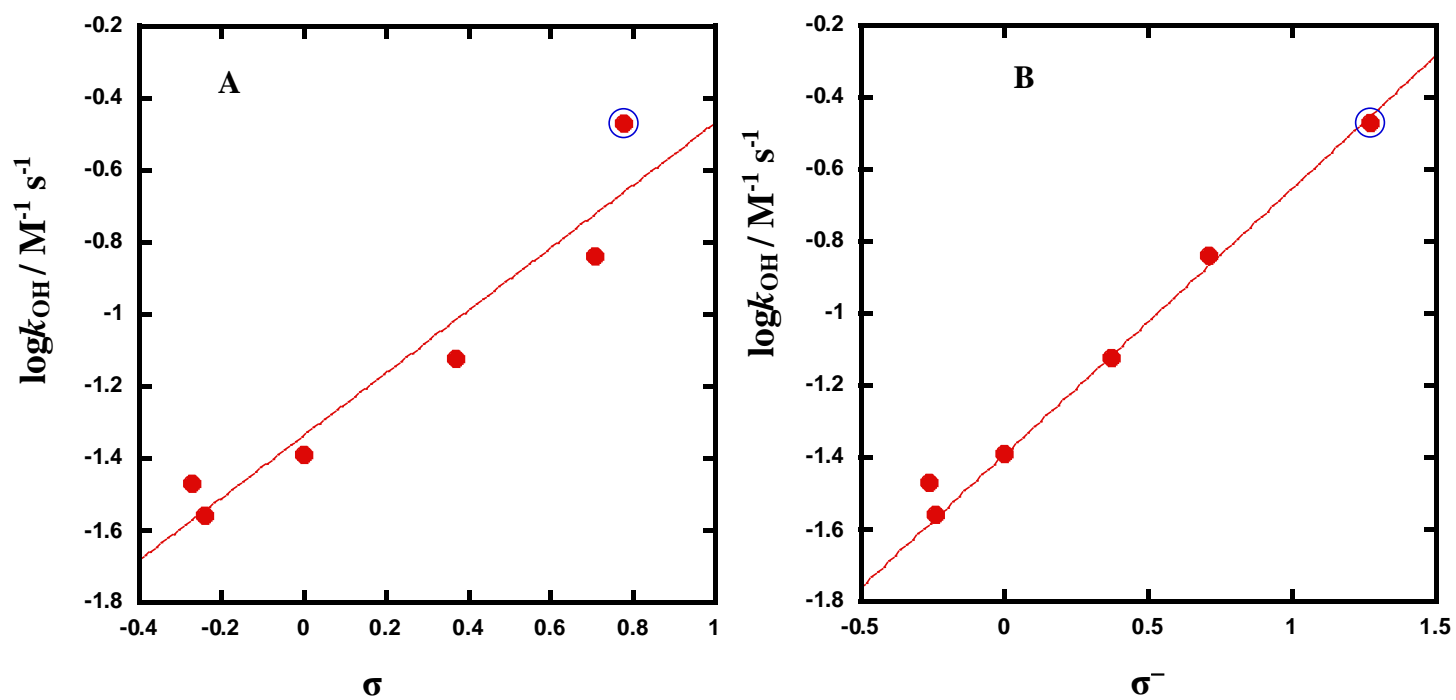
Figure 86: Hammett plot for hydrolysis of phosphate triester **56a-56f**; **A**: with sigma, $\rho = 0.87 \pm 0.13$, $R^2 = 0.913$, **B**: with sigma negative, $\rho = 0.74 \pm 0.03$, $R^2 = 0.992$.

5.5.10 pH profile of carbonyl cyclic substituted phenyl phosphate triesters

The pH rate profiles of carbonyl compounds **57a-f** were measured at 25 ± 0.03 °C and ionic strength 1 M (NaCl). The pH of the solution was maintained using different buffers from pH 4 to pH 10 and the pH of each solution was measured after each run. From **Figure 87**, the pH profile demonstrated the reaction of these compounds are base catalysed with much higher reactivity than the alkene compounds that have the corresponding leaving group. The reactions of compounds **57a-c** (4-nitro, 3-nitro, and 3-Cl) show a first order dependence on hydroxide ion. However, when poorer leaving groups were used (as can been seen for the reaction of **57d-f**, phenyl, 4-methoxy and 3,4-dimethyl), they show first order dependence on the hydroxide concentration at low pH and a second order dependence at high pH. The second order rate constants were obtained by plotting log k_{obs} against the pH of the solutions. **Table 6** summarizes all values of the rate constants of compounds **57a-f** along with their measured pK_a.
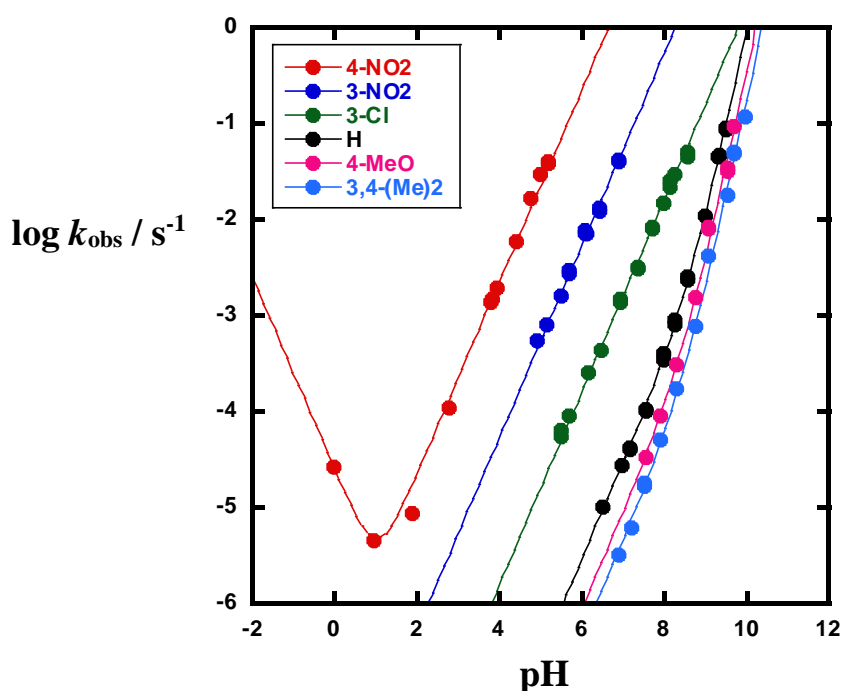
Figure 87: pH profiles of carbonyl cyclic substituted phenyl phosphate triesters **57a-57f** at 25 °C, 1 M NaCl.

The data of **57a** were fitted to equation 12, **57b-c** were fitted to equation 13 and **57d-f** to

110

equation 14.

$$\log k_{obs} = \log (k_H [H^+] + k_{OH} [^-OH]) \qquad \textbf{Equation 12}$$

$$\log k_{obs} = \log (k_{OH} [^-OH]) \qquad \textbf{Equation 13}$$

$$\log k_{obs} = \log (k_{OH} [^-OH] + k_{2OH} [^-OH]^2) \qquad \textbf{Equation 14}$$

Substrate	pK_a of substituted phenol	k_{OH} / M^{-1} s^{-1}	k_{2OH} / M^{-2} s^{-1}
57a (4-Nitro)	6.86	$(2.0 \pm .0.2) \times 10^7$	-
57b (3-Nitro)	8.1	$(5.0 \pm 0.2) \times 10^5$	-
57c (3-chloro)	8.77	$(1.53 \pm 0.04) \times 10^4$	-
57d (phenyl)	9.73	$(0.28 \pm 0.01) \times 10^3$	$(8.0 \pm 0.3) \times 10^7$
57e (4-methoxy)	9.96	$(0.09 \pm 0.01) \times 10^3$	$(3.0 \pm 0.3) \times 10^7$
57f (3,4-dimethyl)	10.1	$(0.043 \pm 0.004) \times 10^3$	$(1.6 \pm 0.1) \times 10^7$

Table 6: Rates constants of carbonyl cyclic phenyl substituted phosphate triesters **57a-f**.

5.5.11 Linear free energy relationship of carbonyl phosphate triester

A Brønsted plot was constructed for carbonyl compounds **57a-f** at 25 °C and 1 M NaCl and is shown in **Figure 88**. Thus, two values for the Brønsted coefficients and were obtained by plotting the second order rate β_{lg} = -1.8 and third order β_{lg} = -1.94 hydroxide dependent rate constants against the measured pK_a. Both plots give a high value of β_{lg}, indicating the very high sensitivity of the reaction to the pK_a of the leaving group.
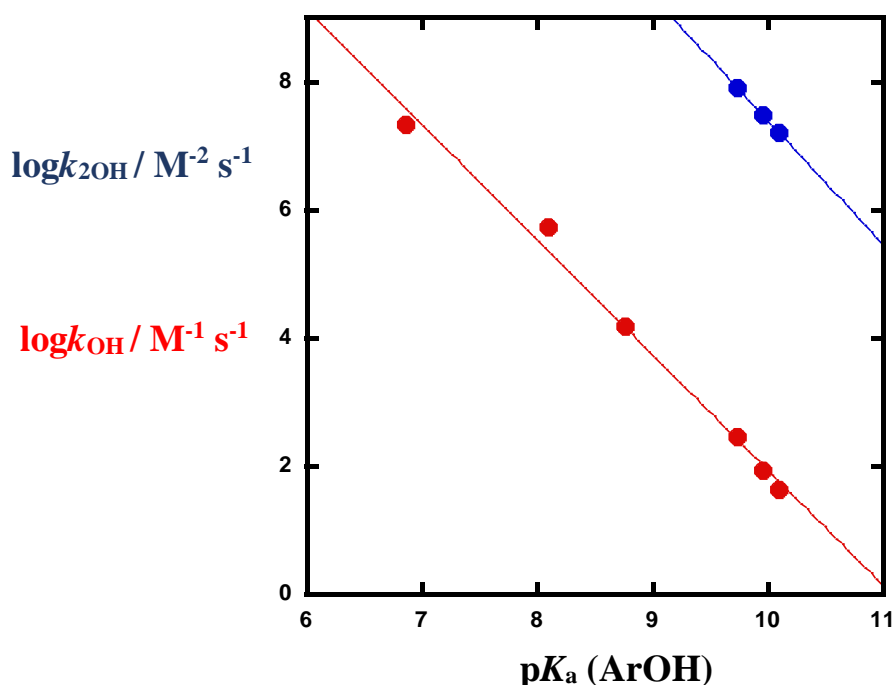
Figure 88: Brønsted plot of carbonyl cyclic substituted phenyl phosphate triester at 25 °C, I = 1; red points corresponds to the second order rate constants (**57a-f**); β_{lg} = -1.8 ± 0.08, R^2 = 0.992. Blue points correspond to the third order rate constants (**57d-f**); β_{lg} = -1.94 ± 0.06, R^2 = 0.999.

The Hammett plot shown in **Figure 89** was also constructed, giving ρ of 4.8 ± 0.6 for the second order rate constants and 2.1 ± 1.2 for the third order rate constants. The plot is more scattered compared with the Brønsted plot (**Figure 88**) of the same data. Furthermore, the same data was plotted with σ^- (**Figure 89B**) giving ρ of 3.8 ± 0.2 and 2.1 ± 1.2 which indicates a

large charge change. **Figure 89B** shows the correlation becomes better with σ⁻ compared to the same data plotted against σ and is similar to the Brønsted plot (**Figure 88**). The same observation was found with the alkene phosphate triesters with analogous leaving groups, which also gave better correlations with pK_a and σ⁻ rather than σ. However, the slopes for the carbonyl compounds are much steeper than for the alkene compounds.
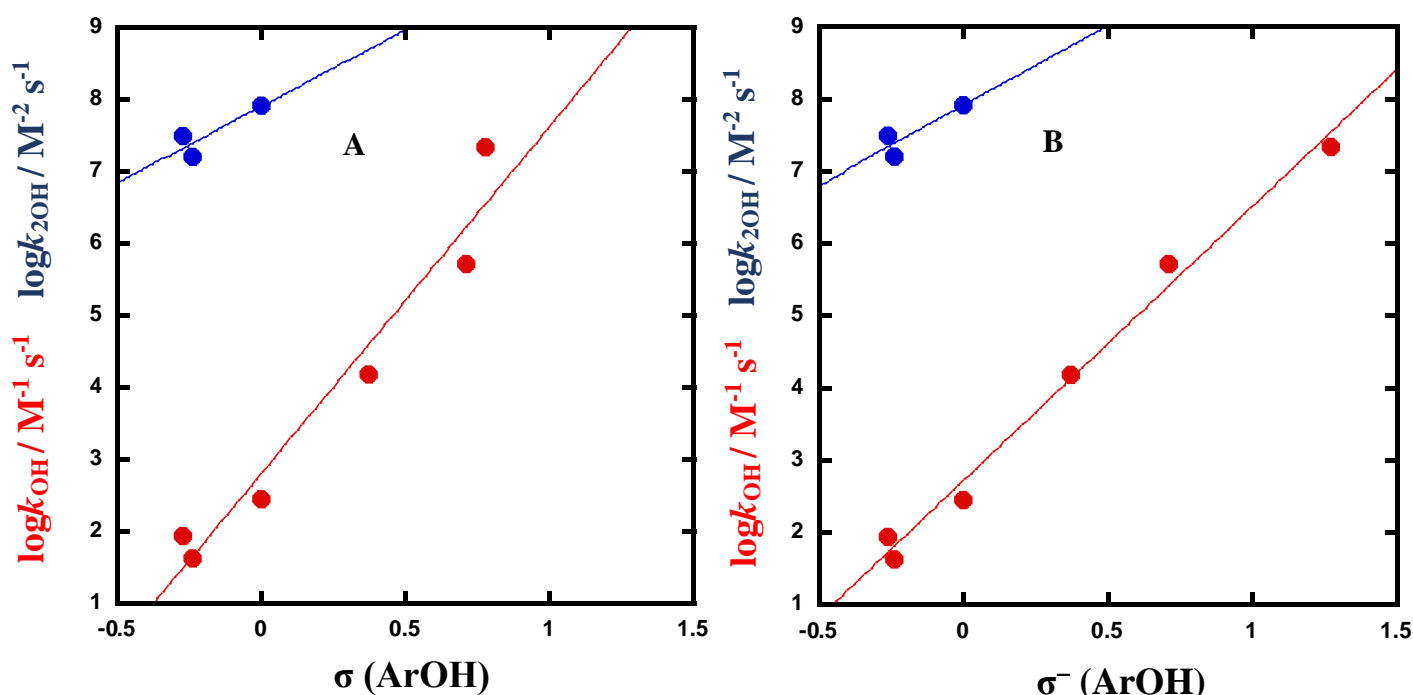
Figure 89: Hammett plot of carbonyl compound **57a-f**; **A**: with σ; $p = 4.8 \pm 0.6$, $R^2 = 0.95$ for **57a-f** and 2.1 ± 1.2, $R^2 = 0.76$ for **57d-f**, **B**: with σ⁻; $\rho = 3.8 \pm 0.2$, $R^2 = 0.990$ for **57a-f** and $\rho = 2.2 \pm 1.2$, $R^2 = 0.992$ for **57d-f**.

The carbonyl compounds show much higher sensitivity to the leaving group compared with alkene compounds which gave $\beta_{lg} = -0.3$ (**Figure 90**). This low value for β_{lg} is very similar to value obtained from the cyclic compounds that were studied by Khan and Kirby.[10] We believe the β_{lg} values of -1.8 and -1.94 are the highest values that have been obtained so far for phosphate triester hydrolysis, which could be due to the high reactivity of these species.
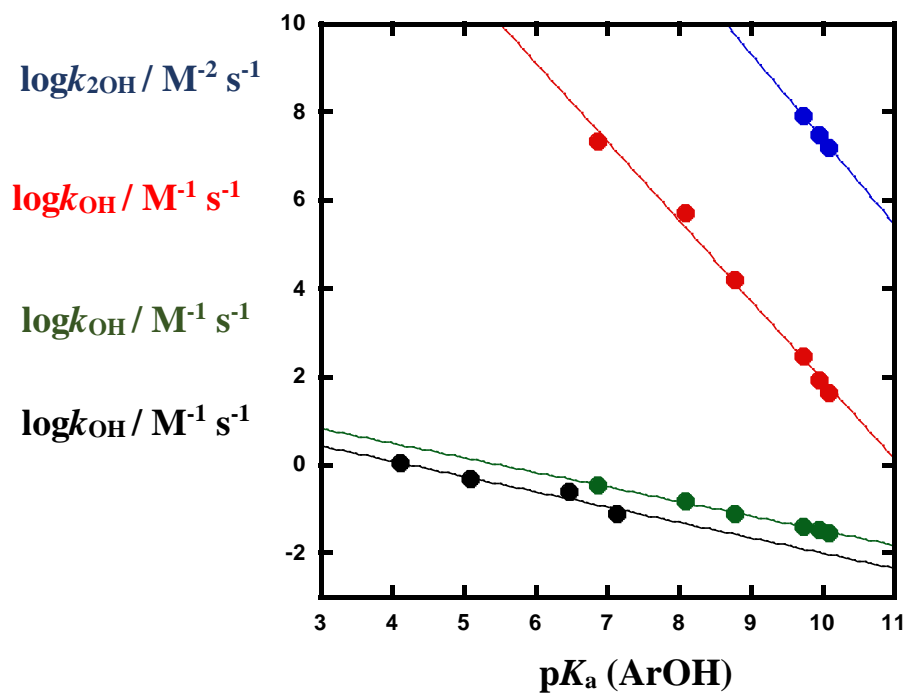
Figure 90: Brønsted plots for phosphate triesters; red points correspond to carbonyl compounds **57a-f**; $\beta_{lg} = -1.8 \pm 0.08$, $R^2 = 0.992$. Blue points correspond to carbonyl compounds **57d-f**, $\beta_{lg} = -1.94 \pm 0.06$, $R^2 = 0.999$.; green points are alkene compounds **56a-f**; $\beta_{lg} = -0.33 \pm 0.01$, $R^2 = 0.999$; Black points are cyclic compounds **47a-d** reported by Khan and Kirby $\beta_{lg} = -0.35 \pm 0.06$, $R^2 = 0.999$.

5.5.12 Product analysis of carbonyl 57d

In order to check the products after hydrolysis, phenyl phosphate triester **57d** was followed by

^{1}H and ^{31}P NMR at pH =8. The ^{1}H NMR confirms the phenol as leaving group and ^{31}PNMR

shows one peak that corresponds to cyclic phosphate as portrayed in **Figure 91** and **Figure 92**.
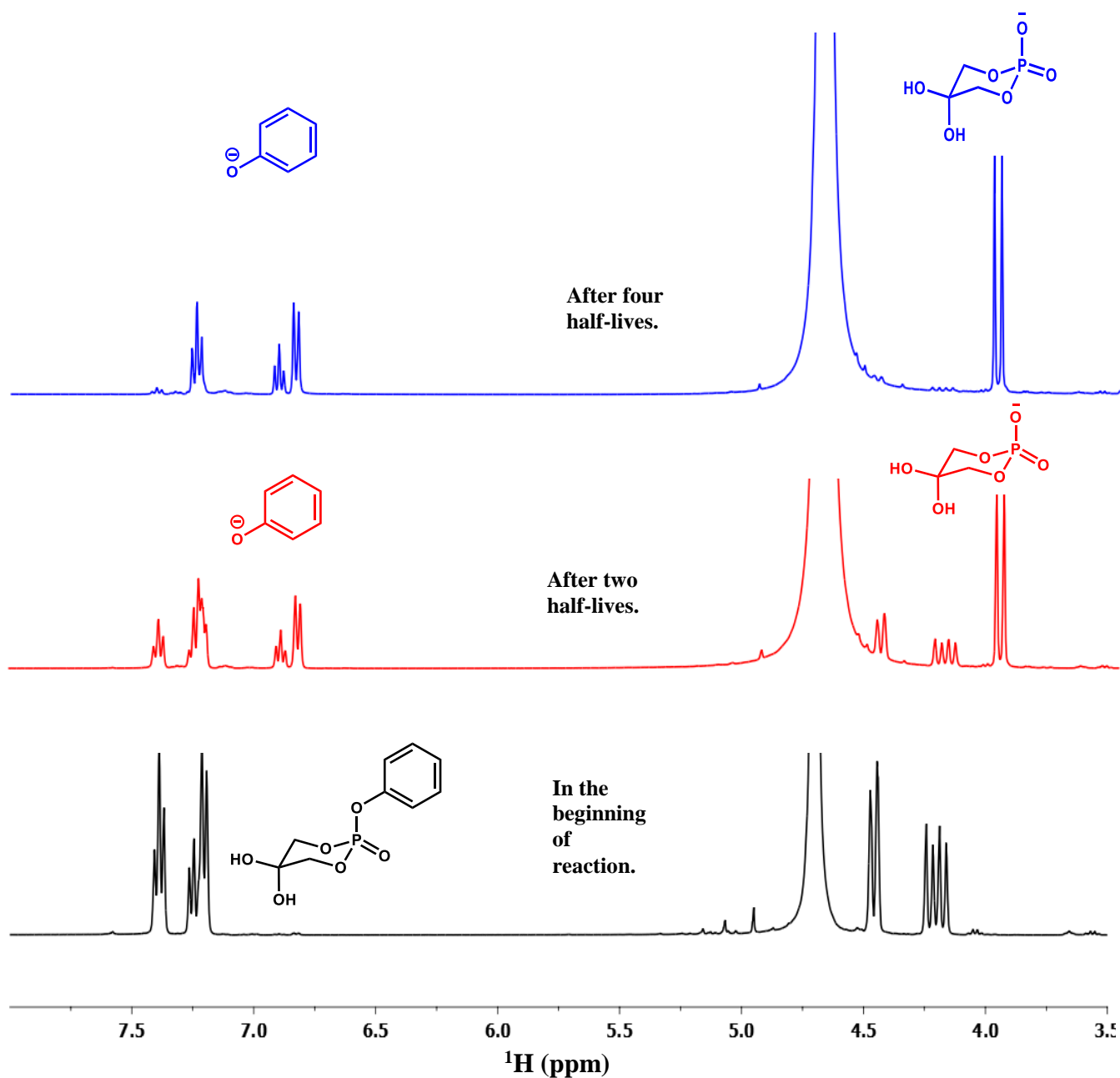
Figure 91: Following the hydrolysis of carbonyl cyclic phenyl phosphate triester **57d** using ^{1}H NMR at pH = 8 in D_2O.
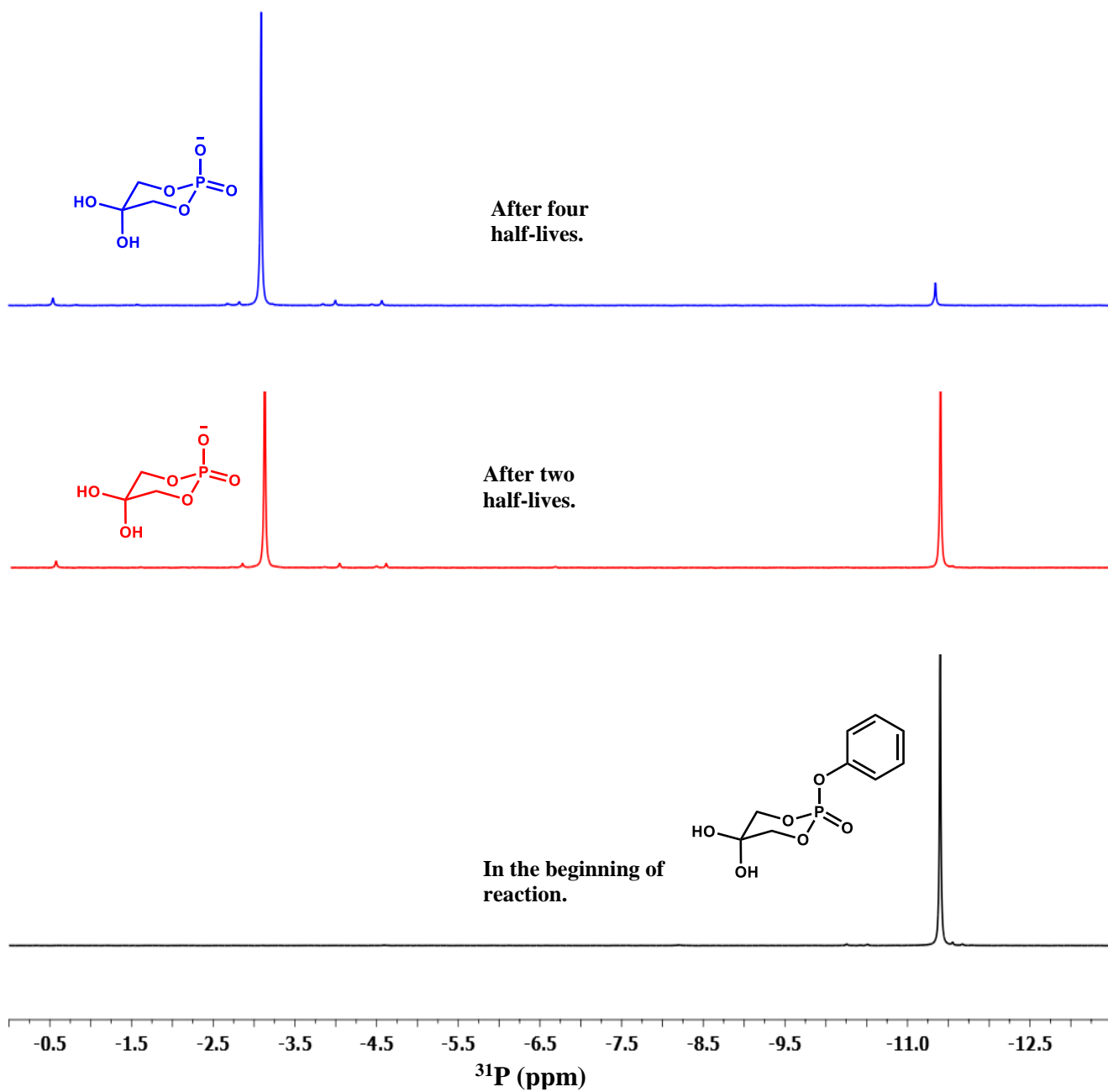
Figure 92: Following the hydrolysis of carbonyl cyclic phenyl phosphate triester **57d** using ^{31}P NMR at pH = 8 in D$_2$O.

5.5.13 Mechanism of carbonyl cyclic aryl phosphate triesters

The proposed mechanism of phosphate triester **57a-f** is shown in **Scheme 25**. The crucial step of this intramolecular reaction is converting the carbonyl group to the hydrate form in aqueous solution as shown by the NMR investigation (**Figure 91**). This hydrated form has two hydroxyl groups in different positions. An isomer **63,** where the hydroxyl group occupies an equatorial position and an isomer **64** where the hydroxyl group occupies axial position. Attack by the anion of either hydroxyl leads to an intermediate with two five-membered rings that are high energy due to strain effects.[131] The five-ring intermediate then leads to the leaving group and cyclic phosphate. These two products were detected by NMR as shown in **Scheme 25**.

It might be expected that the reaction of **63** would be faster than **64** because it is known that the nucleophile and the leaving group prefer to attack and leave from apical position.[132,133] As a consequence of this, it is worth synthesising these two isomers in order to study the reactivity and differentiate between them.
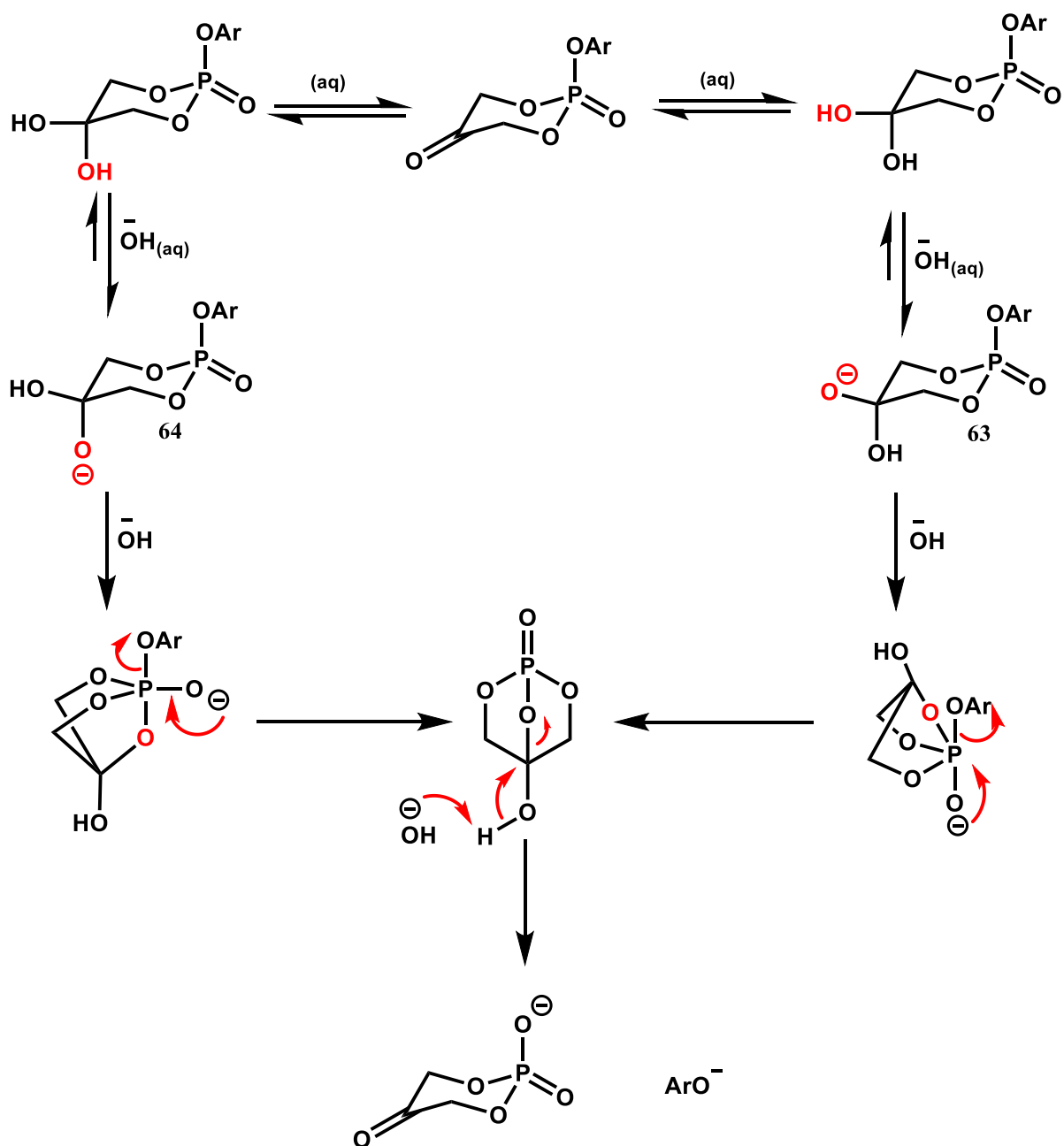
Scheme 25: The proposed mechanism of carbonyl cyclic substituted phenyl phosphate triesters **57a-f**.

5.5.14 Studying carbonyl compound with the poor leaving group

As seen from the pH profile in **Figure 87**, the carbonyl compounds with poorer leaving groups show first and second order dependence on hydroxide concentration. Therefore, to see the effect of pK_a on the reaction mechanism, **65** was synthesised as shown in **Scheme 26**. In addition, **66** was synthesised as a reference compound that does not have an internal nucleophile. The synthesis method used was different since the method of preparation of previous carbonyl compounds was not efficient and gave very low yields. The 4-nitrobenzyl alcohol and triethylamine were dissolved in THF and added slowly to a solution of POCl$_3$ in THF to yield the intermediate 4-nitrobenzyl dichlorophosphate. After this, the alkene compound was produced by the addition of alkene 1,3-propandiol with triethylamine. Ozonolysis of the alkene using O$_3$ in DCM at -78 °C followed by Me$_2$S yielded the desired compound **65**. The reference compound **66** was prepared by adding of 2,2-dimethoxy 1,3-propandiol with triethylamine to the intermediate 4-nitrobenzyl dichlorophosphate triester (**Scheme 26**).

Scheme 26: Synthesis of carbonyl **65** and dimethoxy **66**.

5.5.15 Studying reaction of carbonyl cyclic 4-nitrobenzyl phosphate triester

The hydrolysis reactions of carbonyl and dimethoxy compounds **65** and **66** were studied over the pH range 8-13 at room temperature using HPLC to monitor the reaction. The peaks for substrate and products were calibrated to an internal standard (which was 3-nitrobenzoic acid). For dimethoxy compound **66** two products appeared. The first is 4-nitrobenzyl alcohol which results from the nucleophile attacking the phosphor centre to give the leaving group and cyclic phosphate ester. The second product is due to opening the ring as shown in **Scheme 27**.
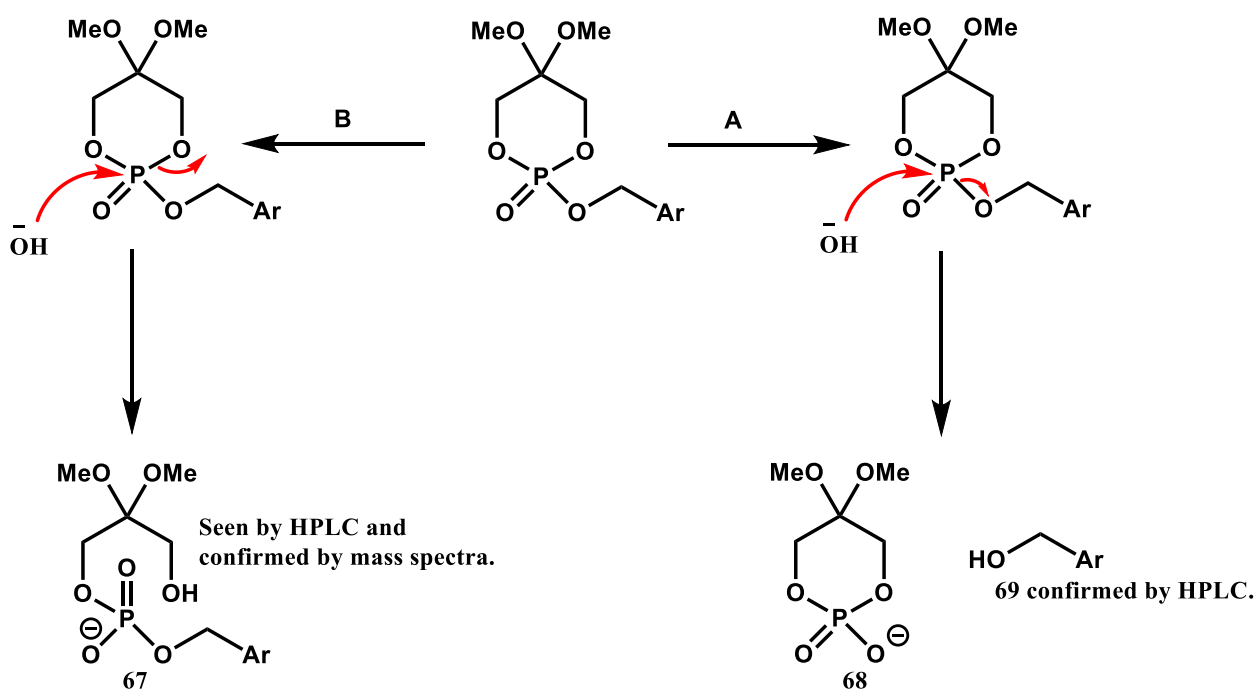
Scheme 27: Proposed mechanism hydrolysis of dimethoxy cyclic phosphate triester **66**.
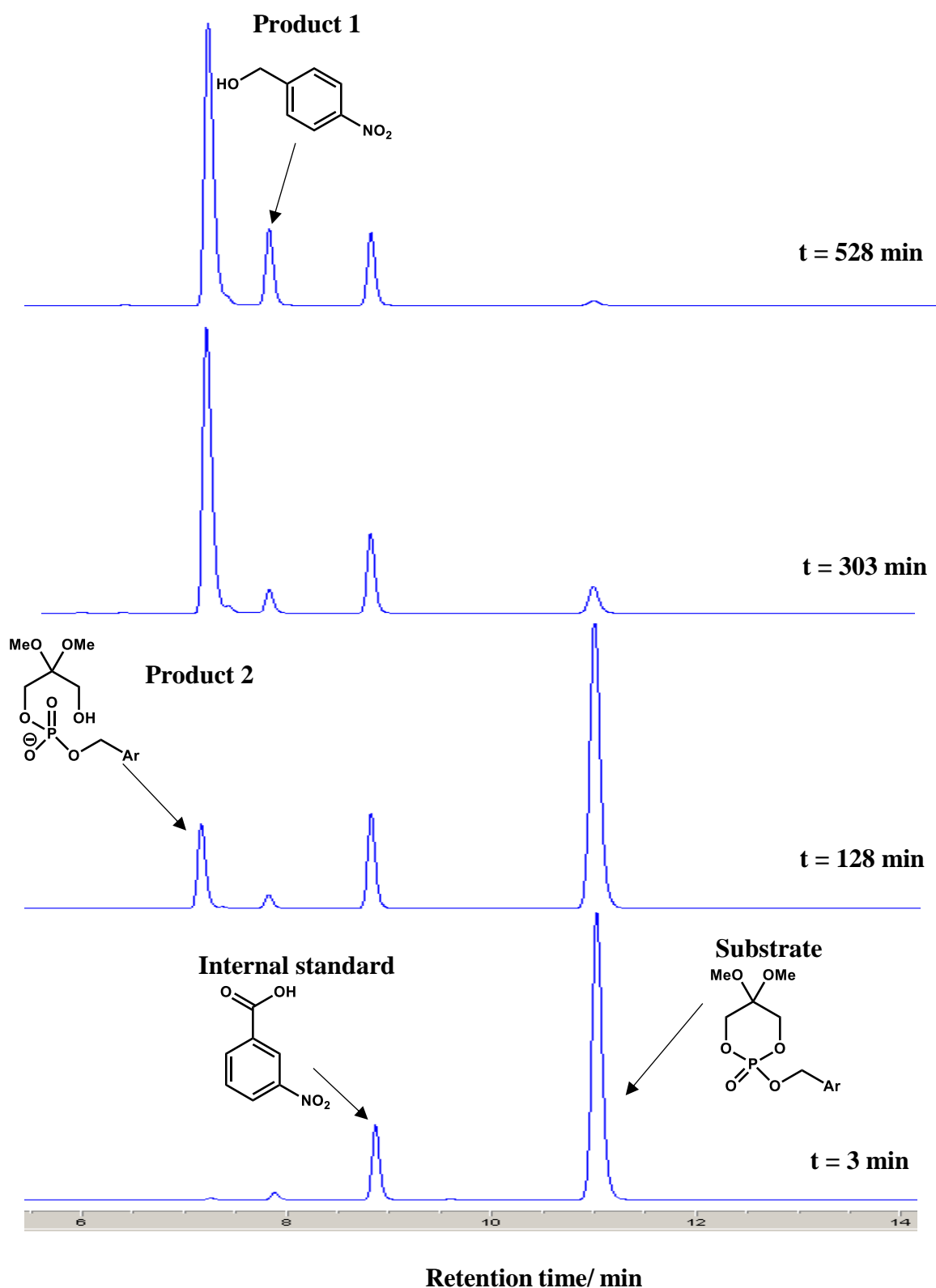
Figure 93: Following the hydrolysis of dimethoxy cyclic 4-nitrobenzyl **66** by HPLC over the time at pH = 10.4; 1 M NaCl, 25 °C.

For carbonyl compound **65**, two products also appeared in the analysis by HPLC which suggested two pathways for the reaction. **Figure 94** shows the outcome from the analysis by HPLC. The substrate appears at 7.8 min, the internal standard at 8.9 min. The first product was 4-nitrobenzyl alcohol, which appear very close to the substrate. Product 2 could be the result of an intramolecular attack by a hydroxyl group on the carbon atom in the ring. More importantly, an intermediate appeared with all the reactions that were performed at the beginning of the reaction and disappeared before the end of the reaction.
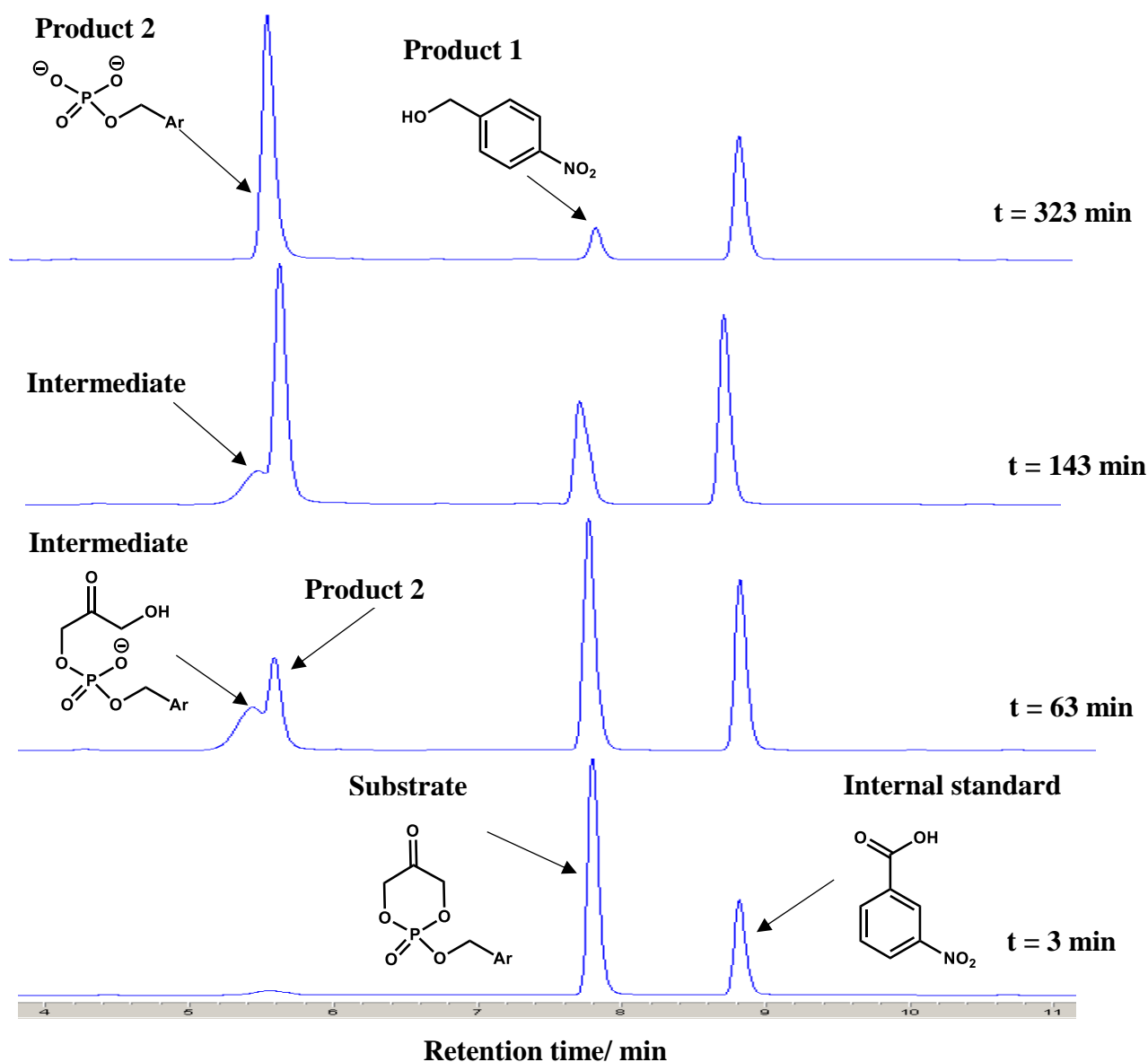
Figure 94: Following the hydrolysis of carbonyl cyclic 4-nitrobenzyl **65** by HPLC over the time at pH = 10.4; 1 M NaCl, 25 °C.

123

All the reactions followed excellent first-order behaviour. **Figure 95** show examples of how the substrate and product were followed by HPLC at pH 10.4.
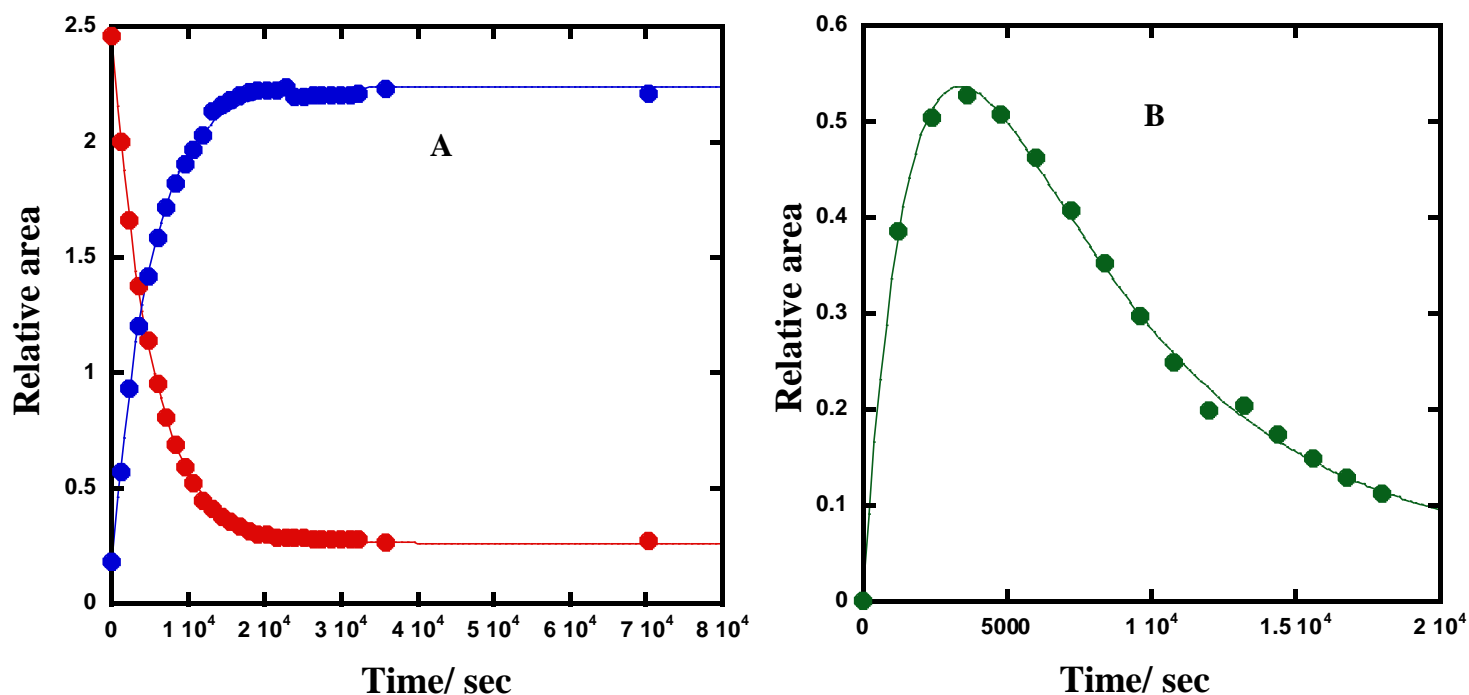
Figure 95: The hydrolysis of carbonyl cyclic 4-nitrobenzyl phosphate triester **65** at pH =10.38, 1 M NaCl.; **A**: red points correspond to substrate **65**, $k_{obs} = (1.95 \pm 0.02) \times 10^{-4}$ s^{-1}, R^2 = 0.999; blue ponts are product and intermediate, $k_{obs} = (1.96 \pm 0.04) \times 10^{-4}$ s^{-1}, R^2 = 0.999. **B**: green points is intermediate, $k_{obs \text{ (appearance)}} = (5.2 \pm 0.6) \times 10^{-4}$ s^{-1} and $k_{obs \text{ (disappearance)}} = (2 \pm 0.3) \times 10^{-4}$ s^{-1}.

The data in plot **95A** were fitted to equation 15 and the data in plot **95B** were fitted to equation 16.

$$A_0 + \Delta A \, (1-\exp^{-kt}) \qquad \qquad \textbf{Equation 15}$$

$$A_0 + \Delta A_1 \, (1-\exp^{-k_a t}) + \Delta A_2 \, (1-\exp^{-k_d t}) \quad \textbf{Equation 16}$$

5.5.16 pH profile of carbonyl and dimethoxy cyclic 4-nitrobenzyl phosphate triester

The pH profiles of **56** and **66** cyclic were studied at 25 °C and 1 M NaCl. The pH between 8 to 11 was adjusted by using (CHES and CAPS). Above pH 11, sodium hydroxide was used and the pH was measured after each run. As can be seen in **Figure 96**, both compound **65** and **66** show base promoted reactions. However, **65** also show a plateau at pH 10 which could correspond to pK_a for ionisation of a functional group in its structure. On the other hand, **66** does not show this behavior, and its reactivity was lower than **65** by 40 fold between pH 8-12. However, its reactivity is 2 fold higher above pH 12.
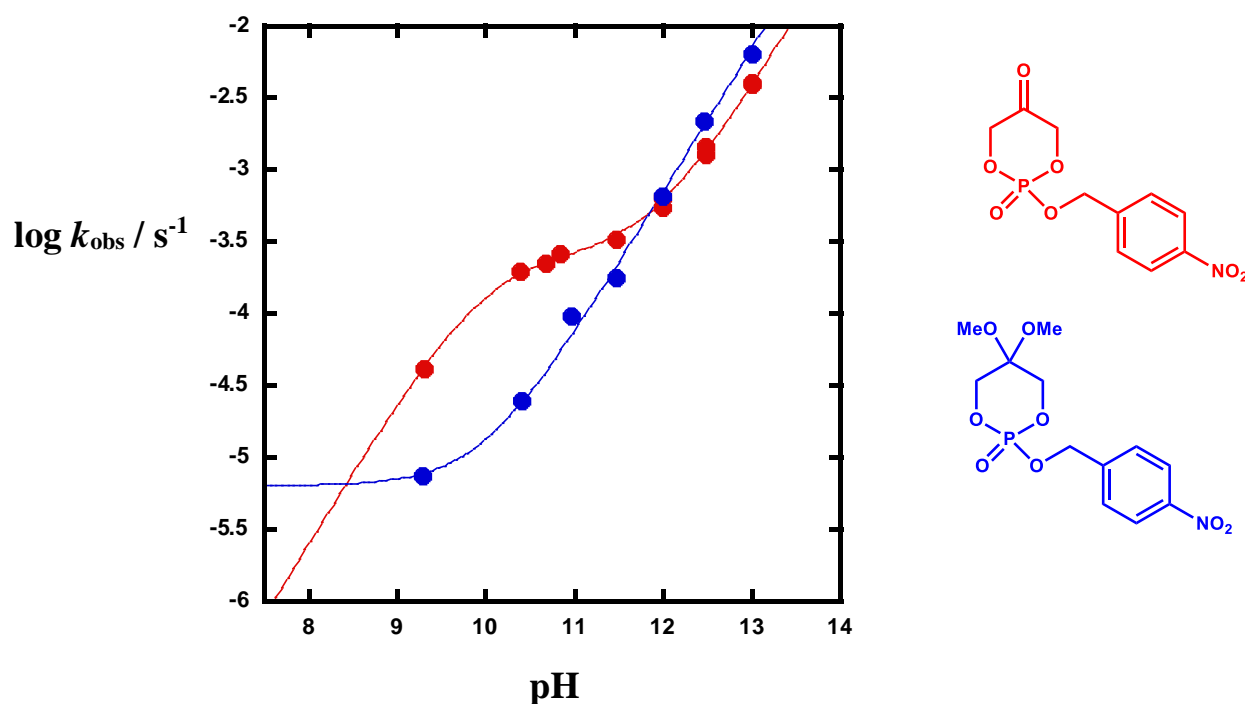
Figure 96: pH profile of carbonyl and dimethoxy cyclic 4-nitrobenzyl phosphate triester, 1M NaCl; red points are carbonyl **65** and blue points are dimethoxy **66**, R^2 for carbonyl = 0.995 and 0.992 for dimethoxy. The data of carbonyl **65** were fitted to the equation 17 and the date of dimethoxy **66** were fitted to the equation 12.

$log k_{obs} = log ((k_H [H^+]/[H^+]K_a) + k_{OH} [^-OH])$ **Equation 17**

Also, it can be noticed compound **65** did not show a second order dependence on hydroxide as

we observed with poor aryloxy leaving groups **57d-f**. The second order rate constants k_0 and k_{OH} of compound **65** and **66** were identified as shown in **Table 7**. Furthermore, the rate constants for each product from partitioning k_{obs} according to the product ratios against the pH is shown in **Figure 97**. The pH profiles show very similar shapes to the original pH profiles of carbonyl **65** and dimethoxy **66** in **Figure 96**. From **Figure 97A** the rate of reaction that give the second product (opening the ring) is greater than for the first product (4-nitrobenzyl). The difference decreases at high pH and become similar to the rate constant of dimethoxy compound **66** (**Figure 97B**). All the rate constants of products ratio are summarised in **Table 7**.
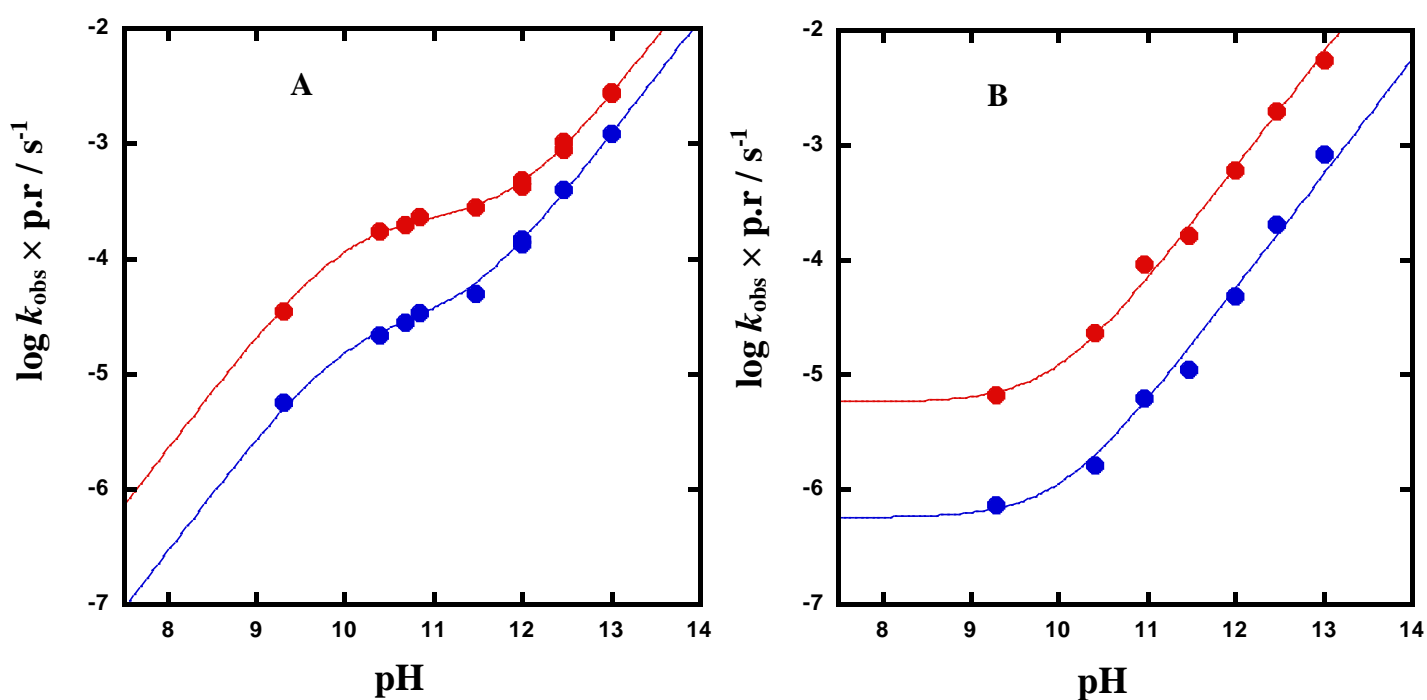
Figure 97: pH profiles for products ratio of carbonyl **65** and dimethoxy **66**; **A**: carbonyl **65**, blue points are first products (4-nitrobenzyl + cyclic phosphate), red points are second products (intermediate + phosphate monoester), **B**: dimethoxy **66**, blue points are first products (4-nitrobenzyl + cyclic phosphate ester), red points are second products.

Substrate	k_0 / M^{-1} s^{-1} pH = 8-12	k_{OH} / M^{-1} s^{-1} above 12	k_0 / M^{-1} s^{-1} 1st product	k_0 / M^{-1} s^{-1} 2nd product	k_{OH} / M^{-1} s^{-1} 1st product	k_{OH} / M^{-1} s^{-1} 2nd product
65 (carbonyl)	$(2.5 \pm 0.1) \times 10^{-4}$	$(3.6 \pm 0.1) \times 10^{-2}$	$(2.8 \pm 0.2) \times 10^{-5}$	$(2.2 \pm 0.1) \times 10^{-4}$	$(1.2 \pm 0.05) \times 10^{-2}$	$(2.4 \pm 0.1) \times 10^{-2}$
66 (dimethoxy)	$(6.3 \pm 0.6) \times 10^{-6}$	$(6.9 \pm 0.6) \times 10^{-2}$	$(5.6 \pm 2) \times 10^{-7}$	$(5.7 \pm 1.3) \times 10^{-6}$	$(5.5 \pm 0.1) \times 10^{-3}$	$(6.3 \pm 0.1) \times 10^{-2}$

Table 7: Rate constants for the hydrolysis of **65** and **66** and products ratio.

Additionally, the shape of the pH profile of carbonyl **65** is similar to that for dihydroxyacetone phosphate (DHAP) **61** reported by Richard.[134] In this study, the reaction of DHAP was observed to be base catalysed above pH 10 and pH independent reaction between 6-10. The mechanism of DHAP cleavage was proposed to proceed through an enediolate intermediate[134] (**Scheme 28**).
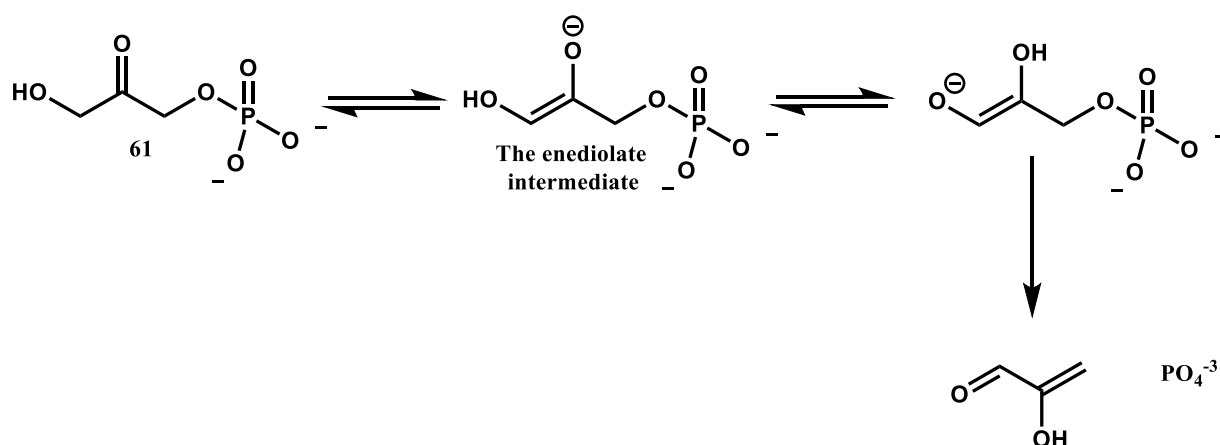
Scheme 28: The mechanism of the hydrolysis of DHAP reported by Richard.[134]

5.5.17 Product analysis of carbonyl cyclic 4-nitrobenzyl phosphate triester

The hydrolysis of compound **65** was followed by ^{31}P and ^{1}H NMR at pH 10 and 25 °C as illustrated in **Figures 98-100**. The ^{1}H NMR and ^{31}P NMR spectrums show the disappearance of substrate and appearance of new compounds. The NMR results supported HPLC results by showing the intermediate and confirm the presence of leaving group 4-nitrobenzyl alcohol and 4-nitrobenzyl phosphate monoester as proposed in the mechanism. However, the structure of intermediate still needs further investigation to be characterised completely.
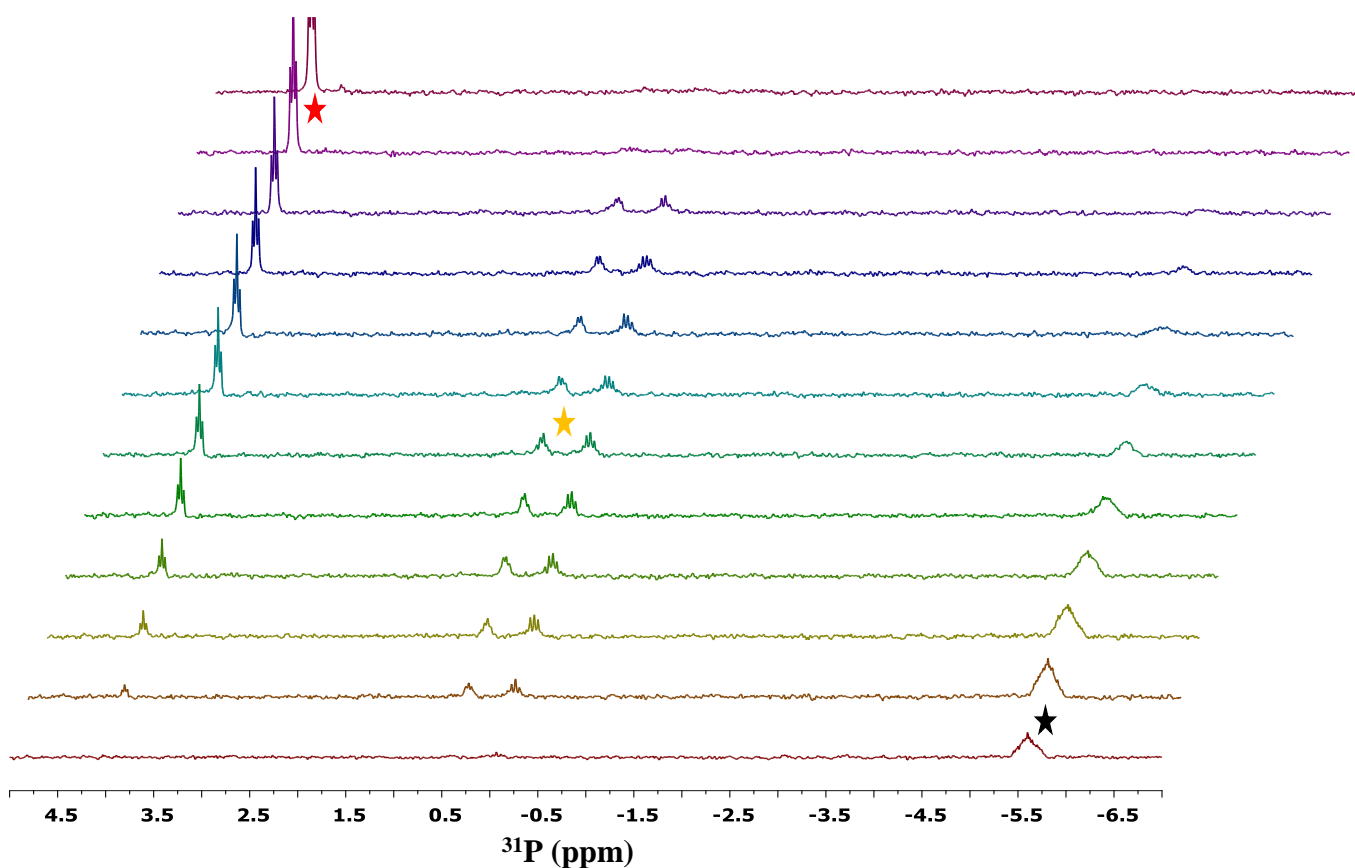
Figure 98: Coupled ^{31}P NMR for hydrolysis of compound **65** at 25 °C and pH = 10; black star is substrate, yellow start is intermediate, and red star is phosphate monoester.
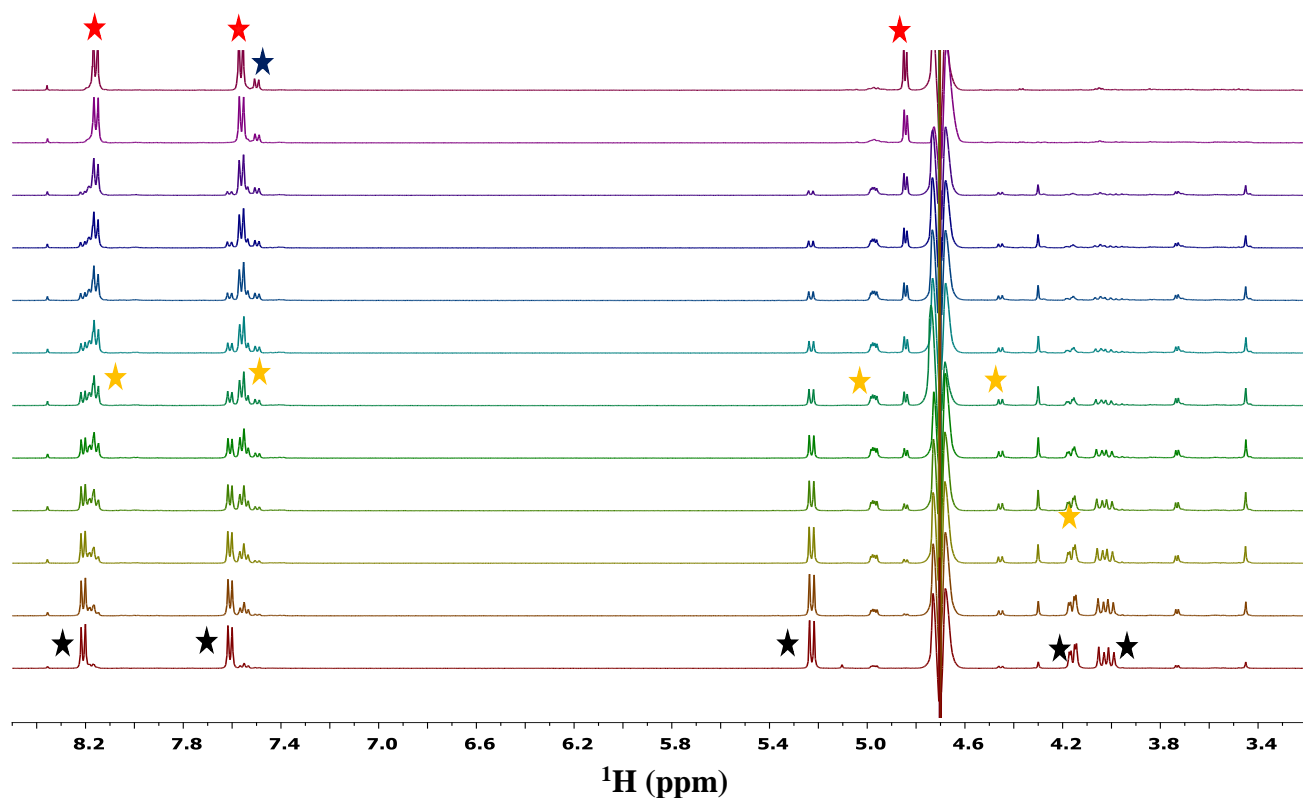
Figure 99: ^{1}H NMR for hydrolysis of compound **65** at 25°C and pH =10; black star is substrate **65**, yellow start is intermediate, green star is 4-nitrobenzyl and red star is phosphate monoester.
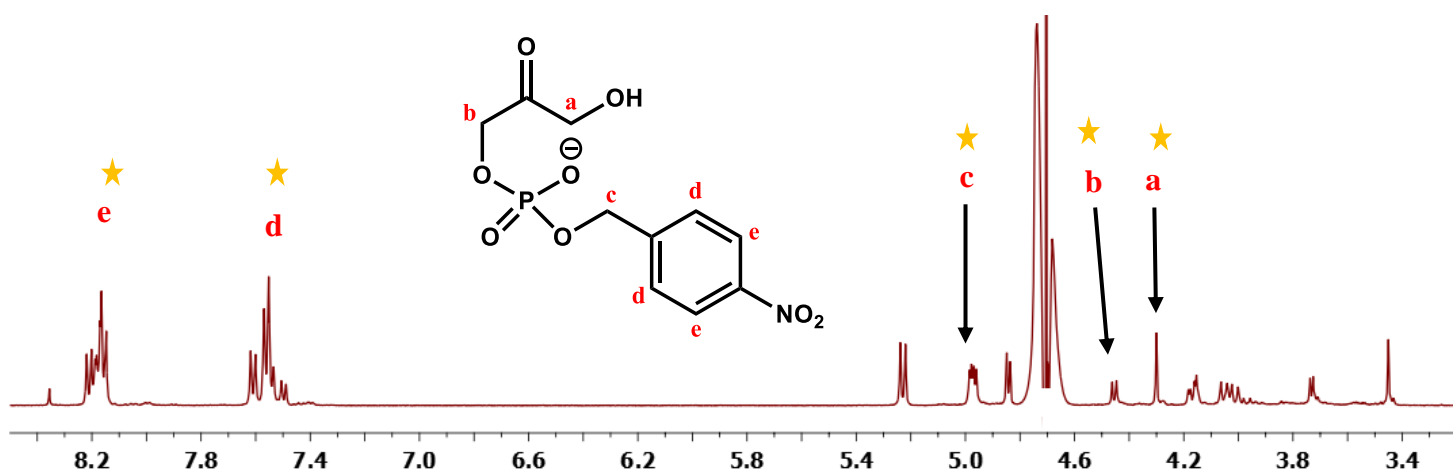
Figure 100: ^{1}H NMR of the intermediate **71**.

5.5.18 Mechanism of carbonyl cyclic 4-nitrobenzyl phosphate triester

The proposed mechanism of **65** was explained through two pathways as can been seen in **Scheme 29** based on the HPLC and NMR data. After converting **65** into the hydrated form the reaction has two pathways. Mechanism **A** which is similar to the mechanism of compounds with good leaving groups. This mechanism proceeds by intramolecular reaction at the phosphorus centre and yields the cyclic phosphate **69** and the leaving group **70** (4-nitrobenzyl alcohol) which was observed by HPLC. Mechanism **B** involves the hydroxyl group attacking the carbon atom in the ring to form an epoxide intermediate. We believe that the epoxide compound has high energy and cannot be detected but leads to the relative stable intermediate which was detected by HPLC. This intermediate **71** will hydrolyse to the phosphate monoester **72** (final product). However, despite seeing the intermediate by HPLC, we still not completely confident in characterising the chemical structure.
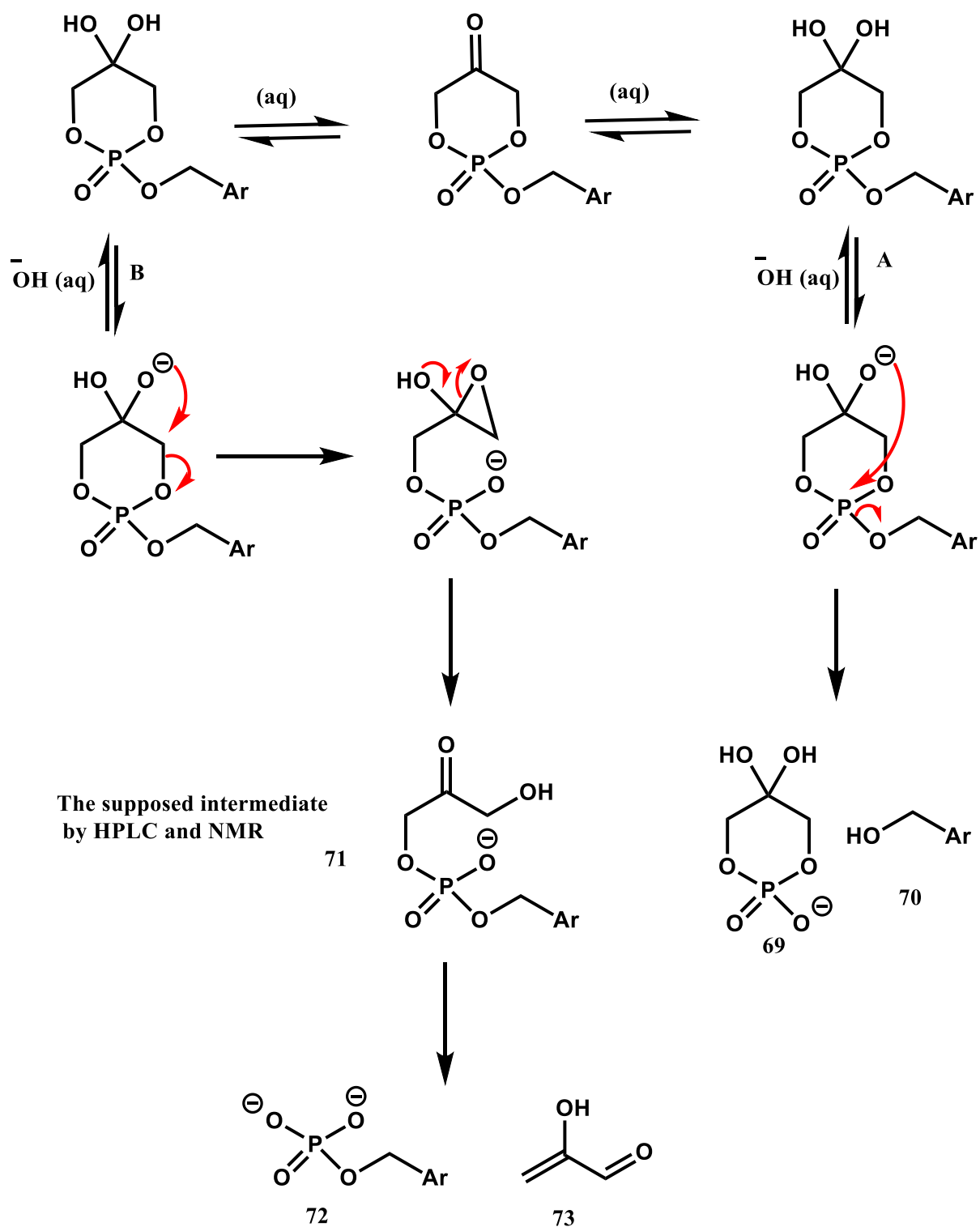
Scheme 29: Proposed mechanism of carbonyl cyclic 4-nitrobenzyl phosphate triester **65**.

5.5.19 Carbonyl cyclic ethyl cyclic phosphate triester

The aim of synthesising carbonyl compound **75** is to test whether the hydrolysis still gives two products like **65**. In other words, does the reaction with an even poorer leaving group proceed by two mechanism or not? Compound **75** was synthesised as explained in **Scheme 30**. The methylene-1,3-propandiol was added to ethyl dichlorophophate to yield alkene intermediate **74**. Then **74** was converted to carbonyl **75** by ozonolysis.
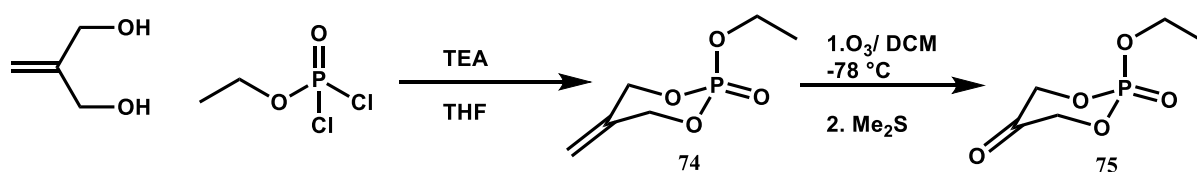
Scheme 30: Synthesis of carbonyl cyclic ethyl phosphate triester **75**.

5.5.20 Studying hydrolysis of carbonyl cyclic ethyl phosphate triester

75 does not have chromophore, therefore the hydrolysis was followed using ^{31}P NMR at pH 11.5 ± 0.12 by using 0.5 M disodium hydrogen phosphate as buffer and all the peaks were adjusted to an internal standard (methylphosphonic acid). High concentration of buffer solution was used to keep the pH constant. The rate of reaction was determined by following the disappearance of the substrate and the rate of reaction was determined to be $k_{obs} = (1.7 \pm 0.04) \times 10^{-4}$ s^{-1}. The initial results for hydrolysis by ^{31}P NMR (**Figure 101**) shows that there are two products. The first product has complicated signals at 0 and could be more than one product the second product which has signal at chemical shift at 4 ppm corresponds to phosphate monoester compound **76** (**Scheme 31**). Further, the signal at 0 looks small and broad but the integration at the end of reaction shows that it is equal to the signal of second product which is similar to analysis of carbonyl benzyl compound **65** at high pH. However, more research needs to be carried out to characterise the products at 0.
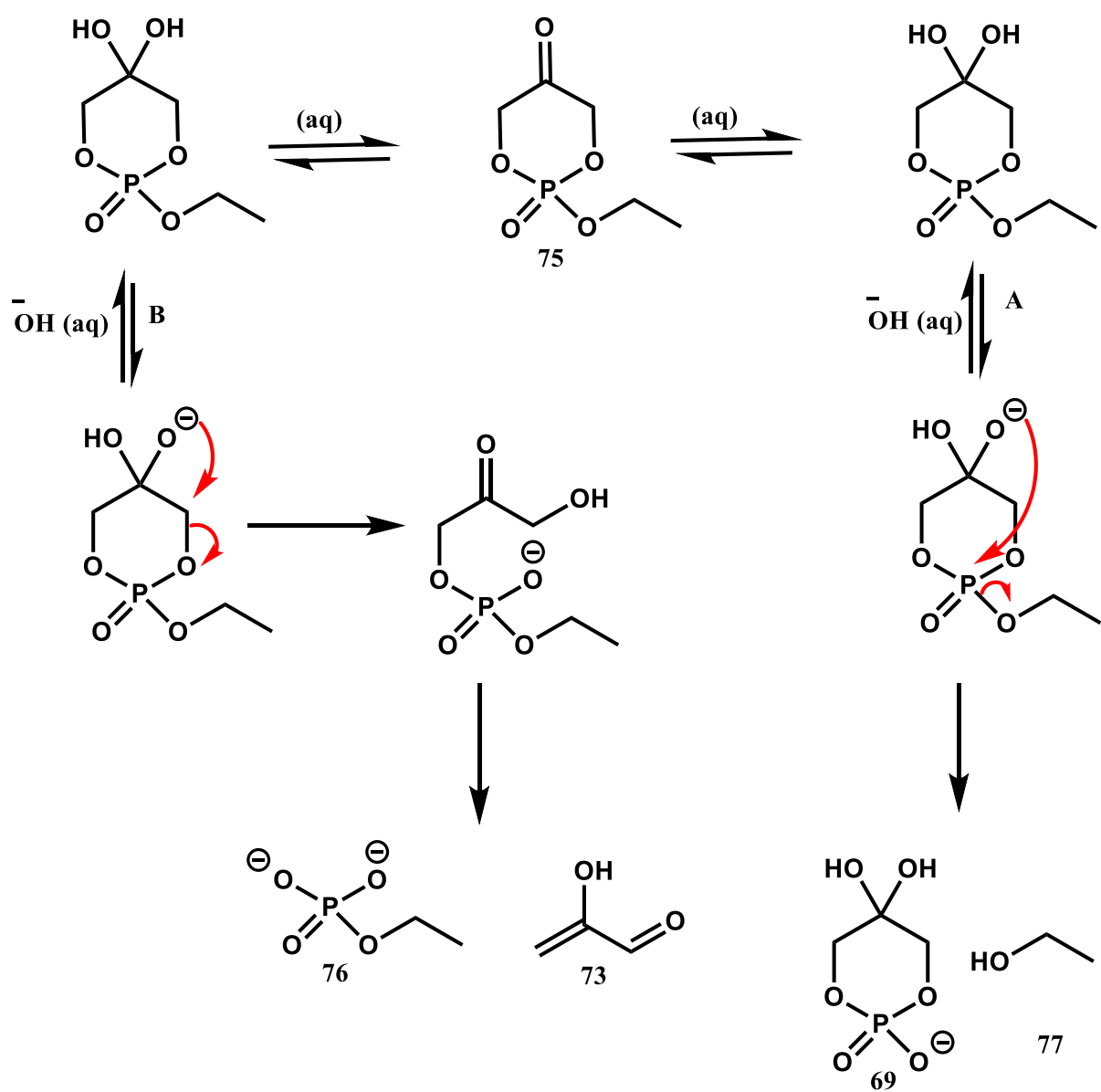
Scheme 31: The mechanism of hydrolysis of **75**.
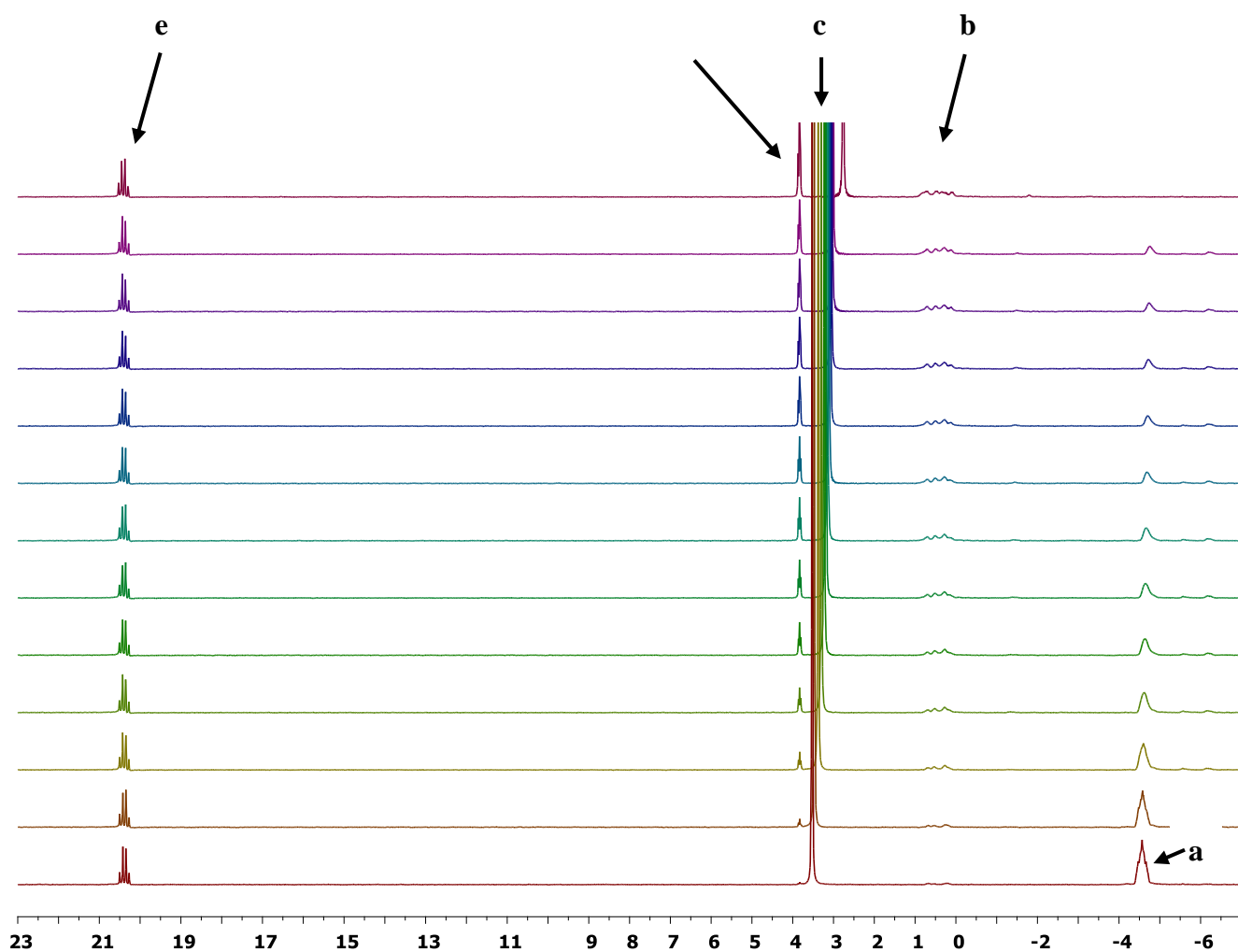
Figure 101: Coupled ^{31}P for the hydrolysis of carbonyl compound **75**; a = substrate, b = first product, c = disodium hydrogen phosphate (buffer), d = second product (phosphate monoester **76**), e = methylphosphonic acid (internal standard).

5.5.21 Study of the reactivity of hydroxyl cyclic phenyl phosphate triester

As **57** (carbonyl compound) exists in its hydrated form with two hydroxyl group in aqueous solution, therefore it would be interesting to know which hydroxyl is more reactive by studying the hydroxyl cyclic phosphate triesters **78A** and **78B** to investigate which hydroxyl is more reactive since they have different reactivity and to investigate which isomer is comparable to **57d**. The isomer that has an equatorial hydroxyl is more reactive than one which has an axial hydroxyl. To approach this question, the carbonyl can be reduced to test the reactivity of the isomeric alcohols. As can been seen from the **Scheme 32** the reduction was carried out by adding an excess of sodium borohydride in ethanol, then the reaction was protonated by acetic acid (instead of water) to reduce hydrolysis. The crude product was filtered and the solvent concentrated and dissolved in chloroform and filtered again. The product was purified by column chromatography to yield two isomers. The major peak is about 97% and the minor one 3%, based on ^{31}PNMR.
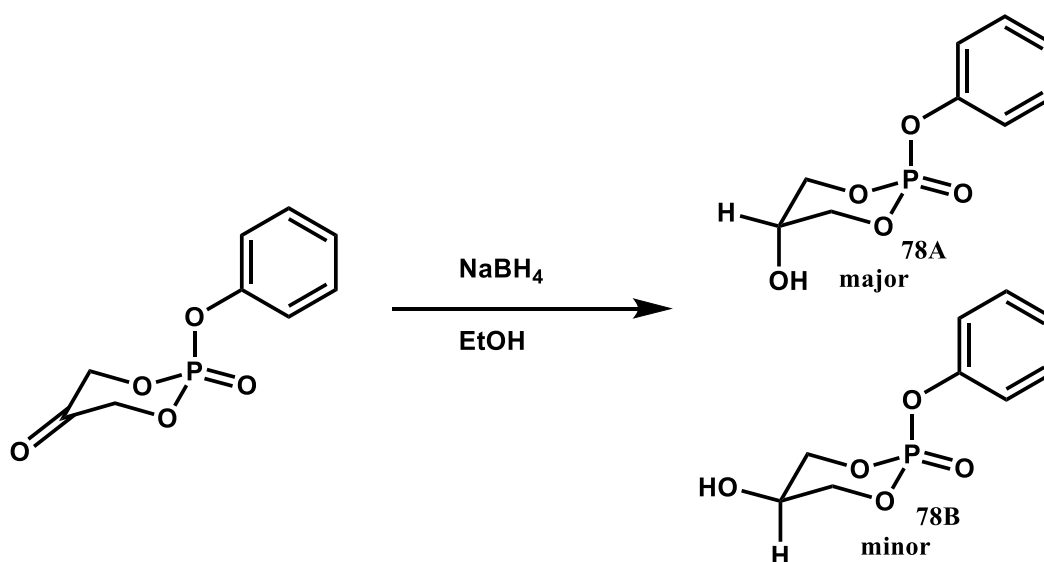
Scheme 32: Synthesis of hydroxyl cyclic phenyl phosphate triester.

5.5.22 pH profile of hydroxyl cyclic phenyl phosphate triester

The reaction of hydroxyl cyclic phenyl phosphate triester **78** was studied at 25 °C and 1 M NaCl spectrophotometrically by following the appearance of phenolate over the pH range 9.3-11.5 (**Figure 102**). The pH profile shows that the reaction is base promoted and it gave good first order behaviour with hydroxide ion. The second order rate constant was determined to be 3.72 ± 0.06 $M^{-1}s^{-1}$ by plotting the $\log k_{obs}$ against the pH. The reactivity of the minor isomer has not been measured owing to the lack of material. The reaction after hydrolysis was checked by UV and showed absorbance at 290 nm which corresponds to phenolate in basic conditions. Furthermore, the product was analysed by HPLC and gave single a peak for phenol and there was no substrate identified. If the reactivity of this hydroxyl is compared with a carbonyl compound which have the same leaving group (**Figure 102**), it can be seen the hydroxyl compound shows first order dependence. Further it can be noticed its reactivity is less than the carbonyl compound by **75** fold. On the other hand, it is found that it is 91 more reactive than the alkene compound **56d**.
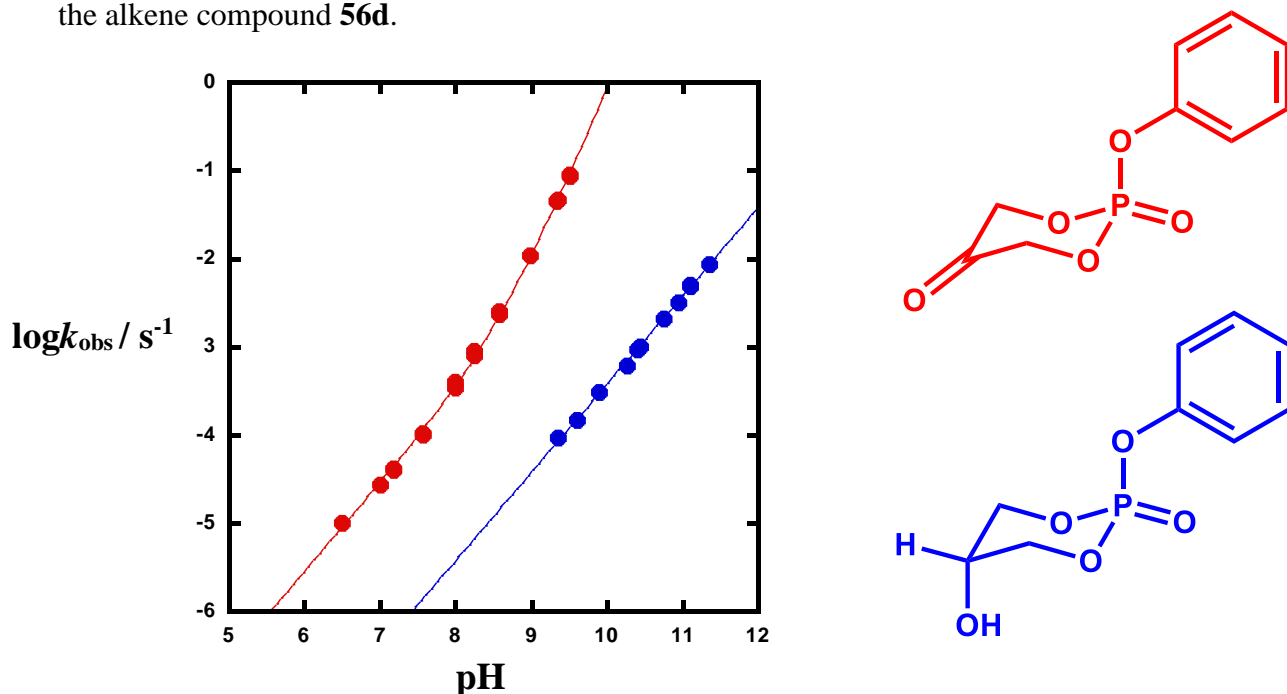
Figure 102: Comparison of pH profiles of hydroxyl (blue points) **78** and carbonyl cyclic phenyl phosphate triester (red points) **57d**. The data of compound **78** were fitted to equation 18 and **57d** were fitted to equation 19.

$$\log k_{obs} = \log (k_{OH} [\text{-}OH])$$ **Equation 18**

$$\log k_{obs} = \log (k_{OH} [\text{-}OH] + k_{2OH} [\text{-}OH]^2)$$ **Equation 19**

5.5.23 Buffer catalyst of hydroxyl cyclic phenyl phosphate triester

The presence of buffer catalysis was checked by varying the concentration of the buffer at the same pH and temperature. **Figure 103** shows that the reaction of the compound **78A** is independent of buffer concentration which suggests that the internal alkoxide plays the main role in the reaction.
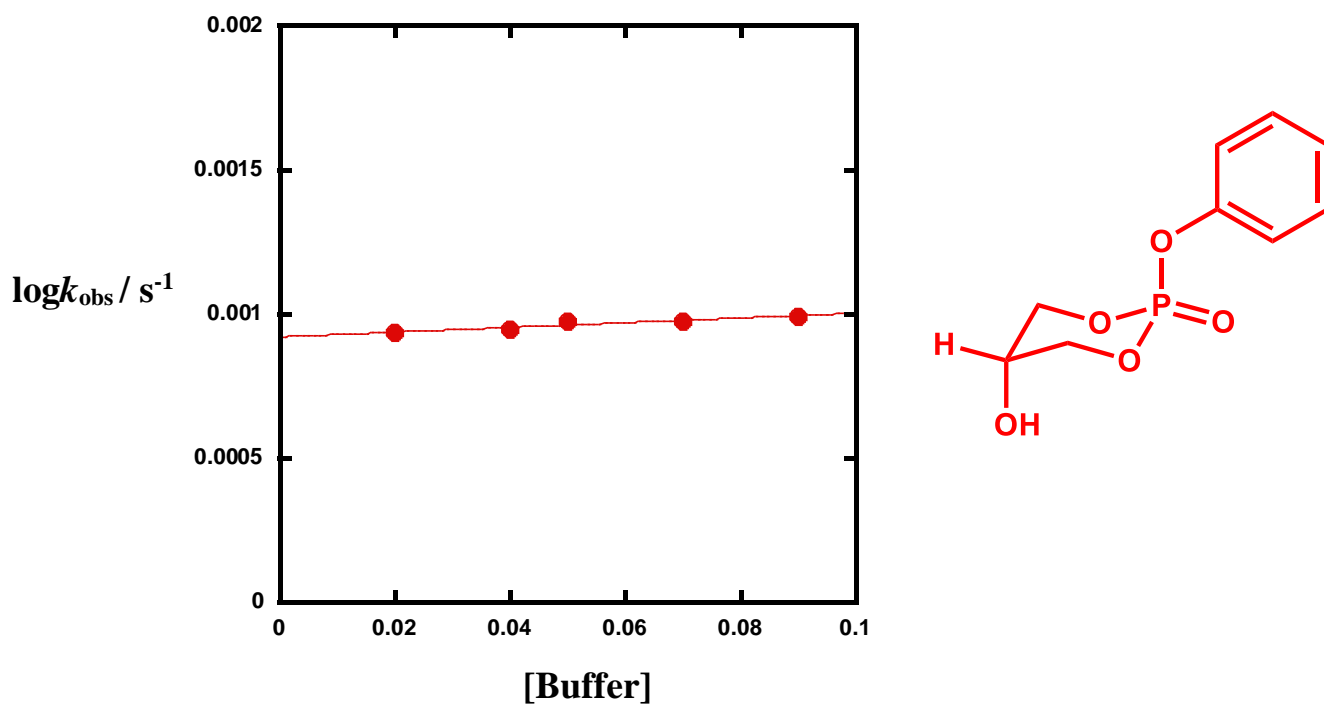
Figure 103: Buffer catalysis of hydroxyl cyclic phenyl phosphate triester **78**; 1 M NaCl, 25 °C, CAPS used as buffer.

5.5.24 Study of the reactivity of hydroxyl cyclic ethyl phosphate triester

To obtain further information about the relative reactivities of the two alcohol isomers, the hydroxyl cyclic ethyl analogous was synthesised. Compound **79A and 79B** was synthesised as described in **Scheme 33**. The reduction reaction was carried out on carbonyl compound **75** using sodium borohydride in ethanol. The reaction produced two isomers with the ratio 1:2 based on ^{31}P NMR analysis.
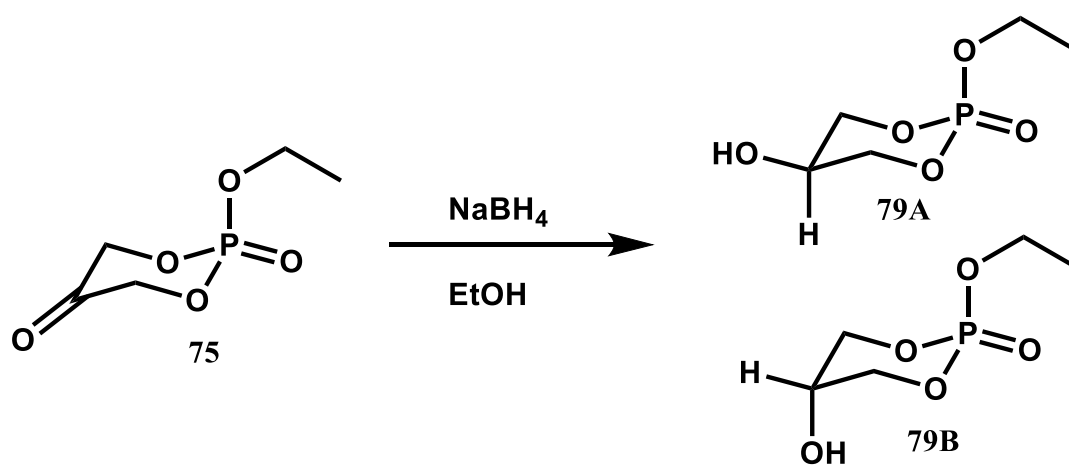
Scheme 33: Synthesis of hydroxyl ethyl cyclic phosphate triesters.

5.5.25 Attempt to separate two isomers of hydroxyl cyclic ethyl phosphate triester

An attempt was made to separate the two isomers **79A** and **79B** by protecting the hydroxyl group for each isomer by using a Boc group as shown in **Scheme 34**. The notion was that this might lead to different R_f, therefore they can be separated, then deprotection using acidic conditions (trifluoroacetic acid). The protection reaction was successful but still gave very close R_f after the protection. As a consequence, the separation of two isomers was not successful.
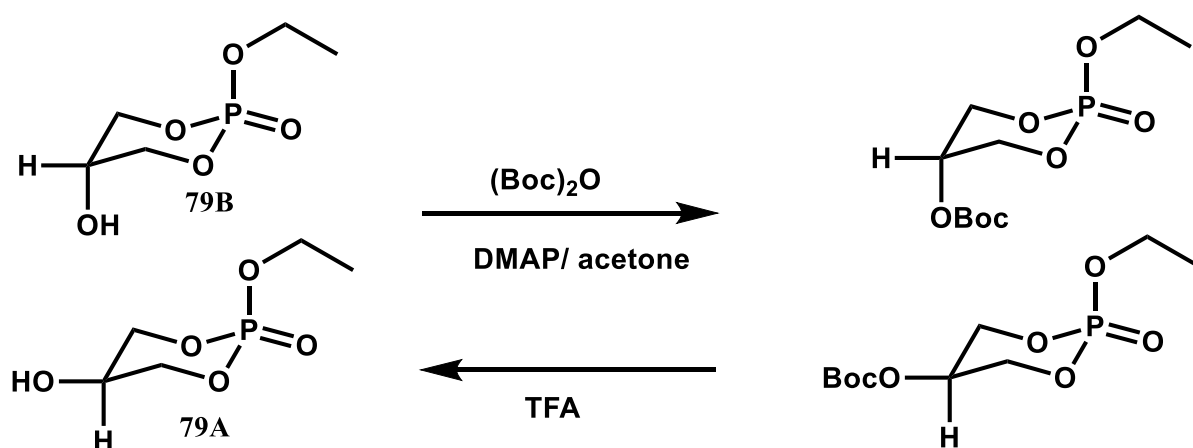
Scheme 34: Protection and deprotection of **79A** and **79B**.

5.5.26 NMR kinetic study of hydroxyl cyclic ethyl phosphate triester

As the separation of two isomers was not successful, the decision was made to study these two isomers as they are after deprotection by TFA. The hydrolysis of **79A** and **79B** was followed using kinetic ^{31}P NMR at pH 11.5 ± 0.09 by using 0.5 M disodium hydrogen phosphate as buffer and all the peaks were adjusted to an internal standard (methylphosphonic acid) to allowed for direct comparison with the hydrolysis of carbonyl analogue compound **75**. The initial results show that the reactivity of major peak which assumed the equatorial hydroxyl is more reactive than the minor peak (axial hydroxyl). Further, the products of the reaction look similar to carbonyl compound, two main signals at 0 and 4 as shown in **Figure 104**.

139
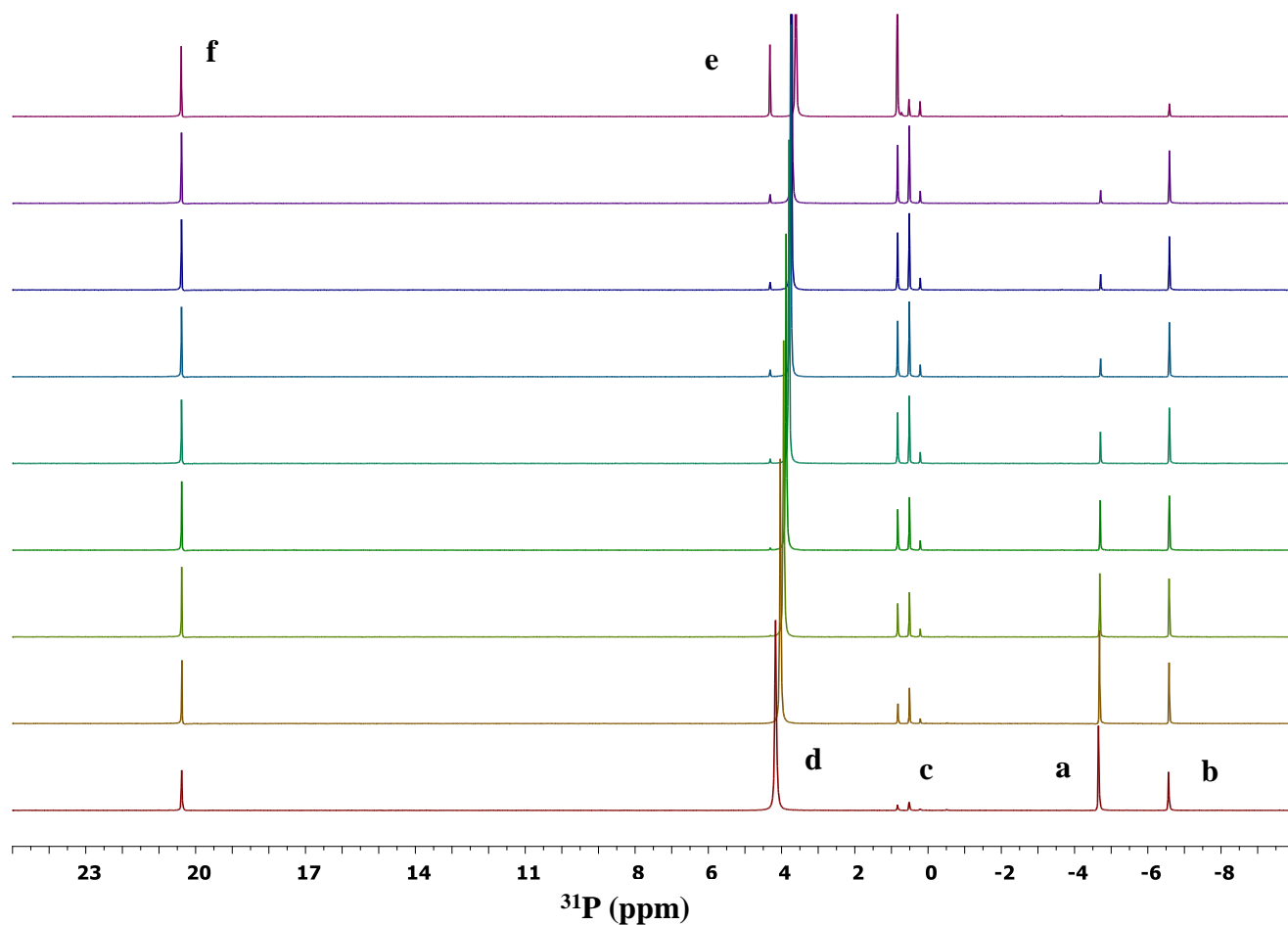
Figure 104: Decoupled ^{31}P for the hydrolysis of hydroxyl compound **79A** and **79B**; a= substrate **79A** (major peak), b = substrate **79B** (minor peak), c = first product, d = buffer, e = second product (phosphate monoester), f = methylphosphonic acid (internal standard).

In addition, the rate constants of **79A** and **79B** were measured at pH 11.5 to be $k_{obs} = (9.8 \pm 0.3) \times 10^{-5}$ s^{-1}, $k_{obs} = (5.1 \pm 0.4) \times 10^{-6}$ s^{-1}, $R^2 = 0.993$ for **79A** and **79B** respectively.
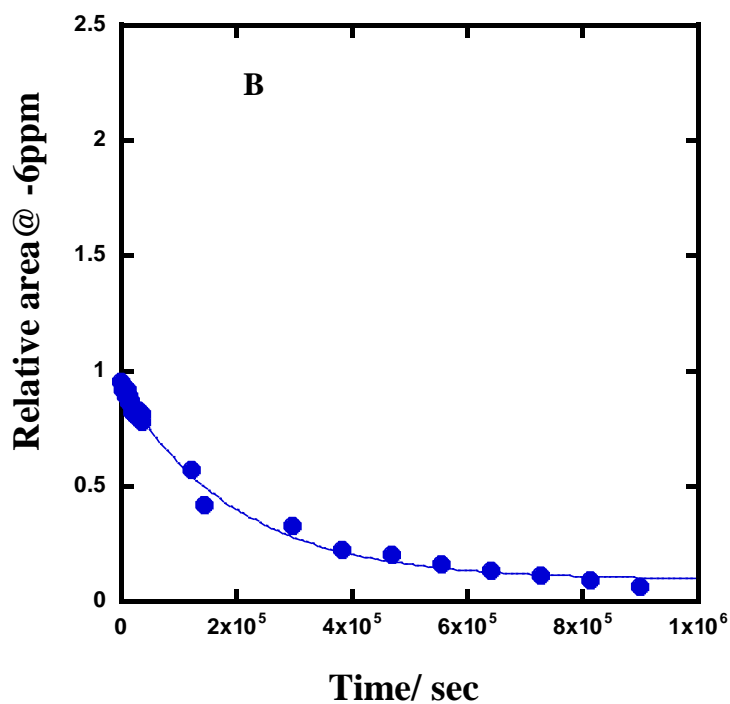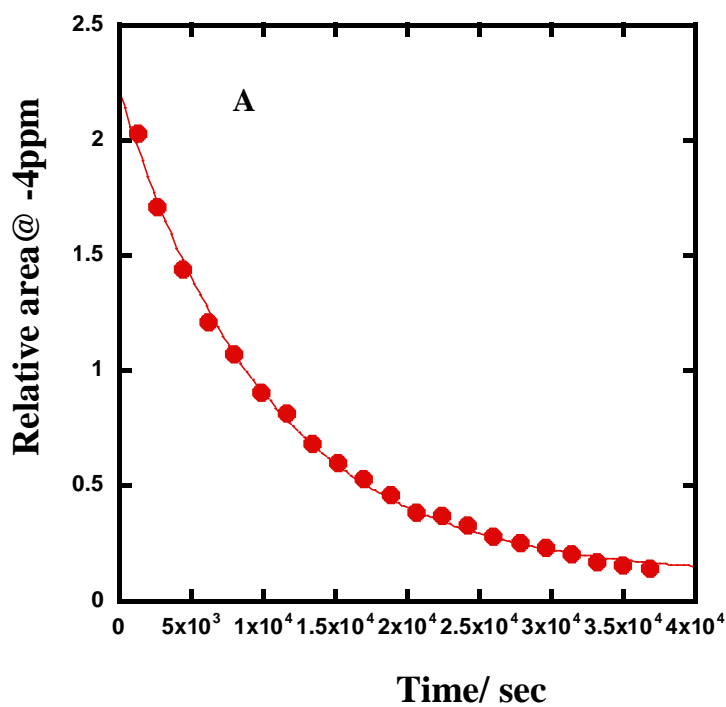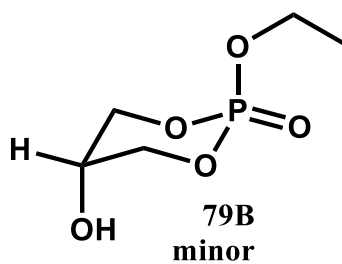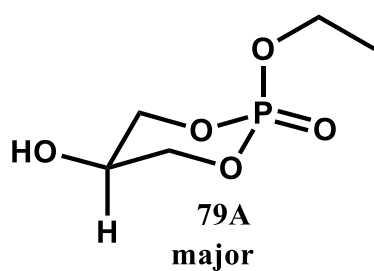
Figure 105: Alkaline hydrolysis of hydroxyl compound in pH $=11.5 \pm 0.09$; **A**: **79A** (major peak) $k_{obs} = (9.8 \pm 0.3) \times 10^{-5}$ s^{-1}, R^2 = 0.998, **B**: **79B** (minor isomer) $k_{obs} = (5.1 \pm 0.4) \times 10^{-6}$ s^{-1}, R^2 = 0.993.

From the reactivity measurements, the major isomer **79A** is more reactive than the minor isomer by 19 fold. Furthermore, the reactivity of **79A** is close to carbonyl analogue compound **75** and the difference is only 1.7 fold.

The difference of reactivity between two closely related isomers also was determined by Jones et al.[135] The authors synthesised two isomers **80A** and **80B** separately and confirm their geometry by X-ray analysis. The position of hydroxyl group in **80A** was in axial whereas it is in equatorial for **80B**.
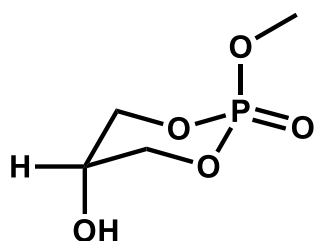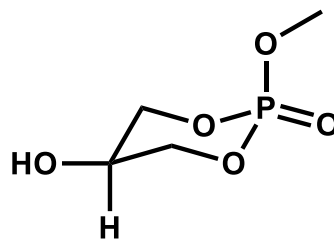
80A   **80B**

Further, in order to check which isomer is most reactive, the reactions were studied with 0.2 M HCl and they found that the half-lives were 5 h and 2 h for **80A** and **80B**. Moreover, the reactions were studied at pH =12 and the half-life of **80A** was 4h and for **80B** was 1h. Thus, the isomer which has the hydroxyl in an equatorial position was more reactive than the one in axial position. However, the mechanism and the products were not reported.

142

5.6 Conclusions

In order to study the effect of functional groups on the cleavage of cyclic of phosphate triesters, novel phosphate cyclic triesters were synthesised successfully. The six-member ring was deivatised with various functional groups such as sp^2 hybridization (alkene group), electronegative groups (dimethoxy), carbonyl and hydroxyl functional groups. The pH profiles of these compounds were studied and they all demonstrated that the reaction is base and acid promoted. However, the rates of the base promoted reactions were much greater than for acid. Comparing the reactivity of these functional groups, the electronegativite groups (two methoxy groups) enhance the reactivities and make it more reactive than the cyclic compound **55** (a reference compound which does not have a fuctional group in the ring) by 22 and 45 fold in basic and acidic conditions respectively. The alkene cyclic **56a** is only slightly less reactive than dimethoxy **59** by 1-3 fold, so the sp^2 hybridization in alkene **56a** gives a similar enhancement to the dimethoxy compound. The water reaction shows more sensitivity to the structure because the difference in reactivity was increased. The dimethoxy **59** and alkene **56a** were greater than the reference compound by 70 and 167 fold respectively.

On the other hand, introducing a carbonyl group into the ring enormously increased the reactivity. For instance, the reactivity of carbonyl **57a** is greater by 10^8 and 10^7 fold compared to the cyclic, alkene and dimethoxy compounds respectively. The enormous reactivity of carbonyl **57a** is attributed to an internal nucleophile that is formed in an aqueous solution. The pH profile of **57a** also shows acid and base catalysis but the reaction in acid is low compared with the base reaction and is comparable to alkene **56a** in the acidic region.

The compounds that form an internal nucleophile, such as carbonyl compounds **57a-f**, demonstrated zero buffer catalysis, while the others with no internal nucleophile such as cyclic **55**, dimethoxy **59**, and alkene **56a** show strong buffer catalysis. Brønsted plots show that the

143

alkenes **56a-f** show a low sensitivity to pK_a of the leaving group with β_{lg} = -0.33, while the carbonyl compounds **57a-f** show a very high sensitivity to the pK_a of the leaving group with large values of β_{lg} = -1.8 and -1.9 for **57a-f** and **57d-f** respectively. In addition, Hammett plots demonstrated better correlation with σ^- than σ with ρ = 0.74 to 0.87 for alkene compounds **56a-f** and ρ = 3.8 to 4.8 for carbonyl compounds **57a-f**.

The reactions of carbonyl compounds **57a-f** were first order in hydroxide with the good leaving groups and both first and second order in hydroxide with the poor leaving groups **57d-f** (phenyl, 4-methoxy, 3,4-dimethyl). However, this behavior was not observed with poorer leaving groups such as 4-nitrobenzyl alcohol **65,** which shows a first order dependence with a kinetic pK_a of 10 for ionised dihydroxyl. The mechanism of carbonyl phosphate triester cleavage was proposed to proceed by different pathways depending on the pK_a of leaving the group. The mechanism of carbonyls **57a-f** with leaving group range (6.85-10.2) shows one pathway. However, with the poor leaving group **65** and **75** which have pK_a range 13.6-16 show two pathways: one where the internal hydroxyl group attacks the carbon atom of the ring and forms an intermediate **71**, and another pathway, when the nucleophile attacks the phosphorus centre and yields the leaving group and the phosphate.

The hydroxyl phosphate triesters **78** and **79A-B** were studied and two compounds (phenyl and ethyl) were synthesised successfully. The hydroxyl phenyl show the major isomer (axial) with 97% abundance based on ^{31}P NMR, while the hydroxyl ethyl **79A-B** gave two isomers with ratio of 2:1 (equatorial to axial). By ^{31}P NMR, one isomer is more reactive than the other by 19 fold. In addition, the reactivity of the most reactive hydroxyl isomer is similar to the carbonyl analogue.

144

5.7 Future work

The water reactions of compounds **55**, **56a** and **59** show sensitivity to the structure. Therefore, it would be interesting to compare the reactivity of these species between pH 4-6. These measurements at this range of pH need more effort since the reactions are strongly buffer catalysed and very slow.

The carbonyl phosphate triesters with poor leaving groups **65** and **75** show interesting results by giving two mechanistic pathways as confirmed by HPLC and NMR data. One of the proposed pathways proceeds via an intermediate. So, the intermediate should be separated and characterized to be more confident about the proposed mechanism. Further, carbonyl ethyl **75** was studied by ^{31}PNMR but it would be useful if a model phosphate triester was designed with ethyl as leaving group and contain an aromatic group such as compound **81,** in order to follow the changes by HPLC and characterise all the products confidently.
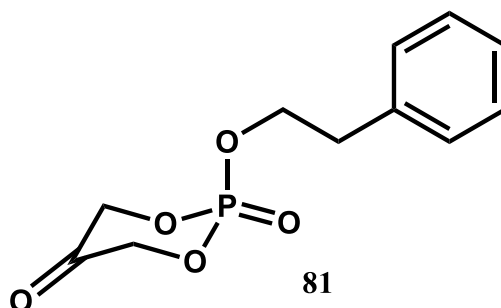
Figure 106: Proposed model of carbonyl phosphate triester.

The hydroxyl compound **79** show two isomers with ethyl group with different reactivity, but these two isomers did not separate from each other since the compound **79** gave very close R_f value. Thus, the following models **82A-B** and **83A-B** could help to separate the two isomers and investigate which isomer is more reactive by studying the reactivity by HPLC. In addition, to check if they still behave like the carbonyl phosphate triester in terms of mechanism since

the corresponding carbonyl of **81** has already been studied by kinetic NMR but the products

need to be characterised confidently.
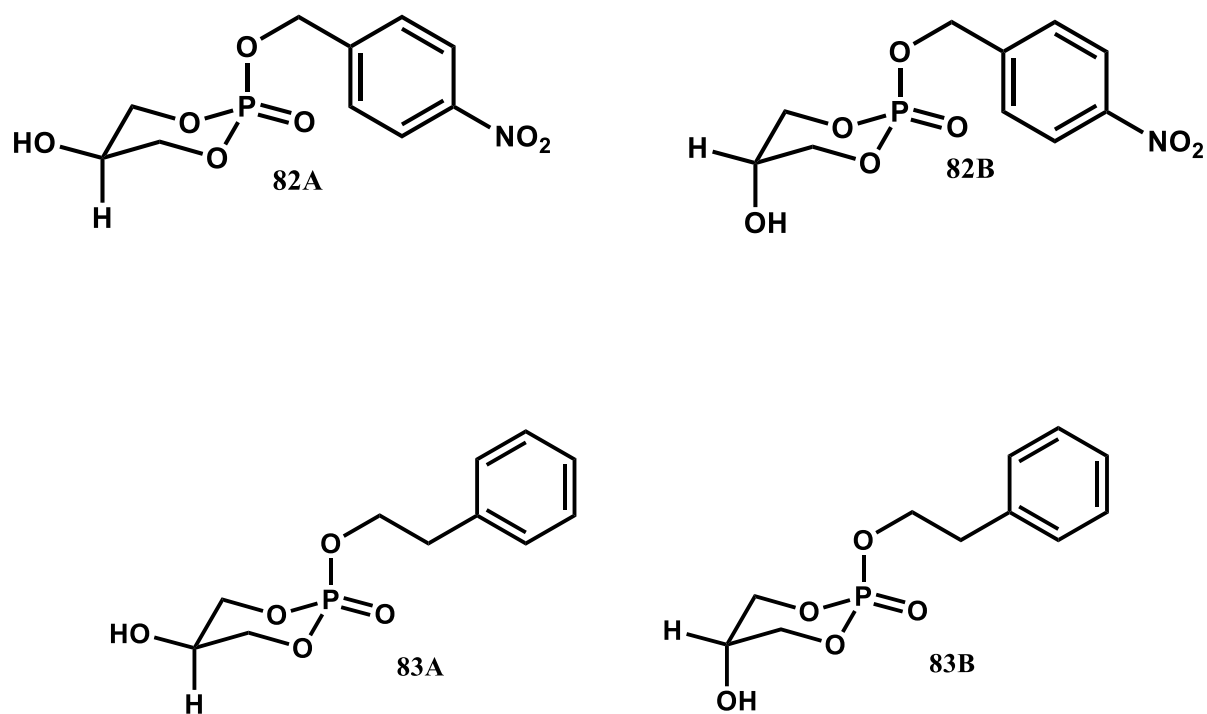
Figure 107: Proposed model compounds of hydroxyl phosphate triester.

Chapter six: Remarks conclusions

6.1 Remarks conclusions

The aims of this work were to study the reactivities of sulfonate esters, sulfates and phosphate diesters with pyridyl leaving groups and their derivatives. Furthermore, the reactivities of cyclic phosphate triesters with different functional groups were also investigated. LFERs were used to evaluate the transition state of the reaction. Therefore, the approach of this study was to use novel compounds of sulfonate, sulfate and phosphate diesters with the pyridyl leaving groups and their derivatives. Cyclic phosphate triesters with different functional groups were also synthesised successfully.

Sulfonate esters and their pyridyl derivative gave excellent correlations with Brønsted and Hammett plots. The pyridyl leaving groups play important roles in order to get conclusive answers about the mechanism of the sulfonate esters. LFER yielded a value of β_{lg} = -0.67 and ρ = 1.61 which indicate the reaction could occur by a single step concerted mechanism. A computational study supports the experimental results.[72]

Phosphate pyridyl diesters correlate quite well with previous data[15] and gave β_{lg}= -0.74 and ρ = 1.66 which indicates that there is a negative charge developed on the oxygen atom of the leaving group in the transition state.

Sulfate diesters with the pyridyl leaving groups gave good correlation with both classes of LFER. However, including our data (compounds **35-37**) with the literature values gave a slightly scattered plot with β_{lg} = -0.72 and ρ = 1.59 which demonstrated the reaction is sensitive to the pK_a of the leaving group. We believe the scattered correlation is due to using substituents in the ortho positions. Moreover, Hammett plots were studied with σ and σ⁻ and the correlation with σ⁻ was better than σ, giving similar results to the Brønsted plot. Therefore, the overall conclusion is that the pyridyl leaving groups can be better than the classic leaving groups such as 4-nitrophenol as we noticed for the sulfonate esters. Furthermore, these leaving groups could

be complementary, as has been observed, in conjunction with the phosphate and sulfate diesters.

The cyclic phosphate triesters with different functional groups show interesting results. For instance, the carbonyl cyclic phosphate triesters **57a** show enormous reactivity, up to 10^8 fold greater compared to cyclic compound **55**. This is because the carbonyl compound was found to exist as a hydrated form in the aqueous solutions. This is an important step to make an internal nucleophile and increase the reactivity, and plays a further significant role in the intramolecular nucleophile catalyst.

In order to compare the reactivity between different functional groups for cyclic phosphate triesters, the buffer catalyst was studied. In general, the phosphate triesters with an internal nucleophile reacted independently of buffer, while the others with no internal nucleophile such as dimethoxy, alkene and cyclic phosphate triester show strong buffer catalysis. Further, the effect of varying the leaving group on the reaction was investigated. The Brønsted plots gave $\beta_{lg} = -0.33$ and $\beta_{lg} = -1.8$ for alkene and carbonyl respectively. From these values, the alkene compounds were less sensitive to the leaving group whereas the carbonyl compounds showed unusual β_{lg} which indicates very high sensitivity to the leaving group and highly developed negative charge on the oxygen atom of the leaving group.

The mechanism of carbonyl phosphate triester cleavage, in general, is an intramolecular nucleophile mechanism since it has an internal nucleophile. It was found, however, that the mechanistic pathways can be affected by the pK_a of the leaving group. For instance, the compounds which have a pK_a range 6.85-10.2 show a single pathway mechanism with the nucleophile attack on a phosphorus atom. Also, the mechanisms with the poorer leaving groups, such as 4-nitrobenzyl and ethyl alcohol occur via a two pathway. One of the mechanistic pathways takes place by opening the ring, while the other pathway is similar to the

149

other leaving groups. The reaction becomes more complicated with poorer leaving groups and further research needs to be carried out to obtain conclusive answers.

In order to investigate the enormous reactivity of carbonyl cyclic phosphate triesters, hydroxyl phosphate triesters need to be synthesised with two isomers. The synthesis of hydroxyl cyclic phosphate triesters show sensitivity to the structure. For instance, one isomer **78B** prepared with phenyl as leaving group was less reactive than the carbonyl analogue by 75 fold. We believe this is representative of the isomer with hydroxyl in the axial position since it has low reactivity compared with the carbonyl compound. On the other hand, two isomers **79A** and **79B** were synthesised with ethyl as leaving group with ratio 2:1 equatorial to axial positions. These two isomers show different reactivity with one isomer being more reactive than the other by 19 fold. Furthermore, the most reactive isomer (equatorial position) gave a rate constant close to the analogue carbonyl compound. However, separation of these two isomers is needed to obtain a clear answer about the reactivity and exact mechanism of the reaction.

Chapter seven: Experimental part

7.1 General material and instruments

Moisture sensitive reactions were carried out using dry solvents and under a nitrogen atmosphere. Starting materials and reagents were commercial available from Fluorochem, Fisher Scientific, Sigma Aldrich, Acros Organics and were used without further purification, unless otherwise stated. All other chemicals were synthesised as described in chapter seven. Dry solvents were obtained from a Grubb solvents purification system. The ^{1}H NMR, ^{13}C NMR, ^{31}P NMR spectra were acquired using A Bruker AV1-400 spectrometer; ^{1}H NMR were running at 400 MHZ, ^{13}C NMR at 101 MHZ and ^{31}P at 162 MHZ. All kinetic solutions were made up with twice distilled deionised water and Analar grade reagents. UV spectra were recorded on Cary 1 Bio spectrophotometer, Cary 3 spectrophotometer and Cary 300 Bio spectrophotometer. All HPLC experiments were performed using 150 mm $\times$ 4.60 mm column in a HP 1100 Series HPLC.

7.2 Synthesis of sulfonate esters

7.2.1 Synthesis of pyridyl benzene sulfonate

10
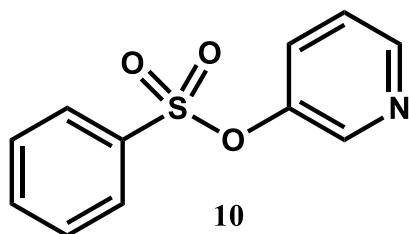
Pyridyl benzene sulfonate was synthesised according to a modified published procedure.[136] Benzylsulfonyl chloride (2.56 mL, 20 mmol) and 3-hydroxy pyridine (1.90 g, 20 mmol) were stirred in THF (50 ml) at room temperature, and triethylamine (3.35 ml, 24 mmol) and pyridine (1.93 ml, 24 mmol) were added dropwise. The reaction was stirred at room temperature for 16h, the precipitate was filtered off, and the solvent was removed *in vacuo*. The residue was dissolved in DCM (20 mL), washed with water (10 mL) and then sodium bicarbonate solution (10 mL). The solution was dried over sodium sulfate before removing the solvent and purifying the crude product by column chromatography on silica (67% petroleum ether:33% ethyl acetate) to yield 3.54 g of **10** (74%) as a colorless solid: mp 46-47 °C; ^{1}H NMR (400 MHz, CDCl$_3$) δ 8.52 (dd, J = 4.7, 1.4 Hz, 1H), 8.18 (d, J = 2.7 Hz, 1H), 7.88 – 7.81 (m, 2H), 7.76 – 7.67 (m, 1H), 7.63 – 7.52 (m, 2H), 7.47 (ddd, J = 8.4, 2.7, 1.4 Hz, 1H), 7.35 – 7.26 (m, 1H); ^{13}C NMR (100Hz, CDCl$_3$) δ$_C$ 148.3 (C-O), 146.4, 144.0, 134.7 (C-S), 130.2, 129.4, 128.5, 124.7; ESI-MS positive ion mode *m/z* 236 (MH$^+$, 100%); HRMS (TOF mode) calculated for C$_{11}$H$_{10}$NO$_3$S, 236.0381, found 236.0370.

7.2.2 Synthesis of *N*-oxide pyridine benzene sulfonate

11
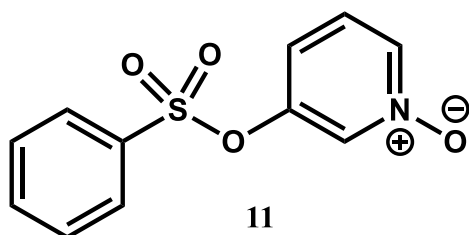
Th*e N*-oxide pyridine benzene sulfonate was prepared by following the modified procedure of Shaw.[137] Pyridyl benzene-sulfonate **10** (0.5 g, 2.1 mmol) and 3-chloroperbenzoic acid (0.55 g, 3.2 mmol) were dissolved in chloroform (50 mL) and stirred at room temperature for 24 h. The white precipitate was filtered off and the solvent was removed *in vacuo*. The crude product was purified by column chromatography on silica (95% ethyl acetate : 5% methanol) to yield 0.24 g of **11** (45%) as a white solid: mp 97-98 °C; ^{1}H NMR (400 MHz, CDCl$_3$) δ 8.13 (d, J = 6.4 Hz, 1H), 7.89 (dd, J = 7.2, 5.9 Hz, 3H), 7.77 (t, J = 7.5 Hz, 1H), 7.62 (t, J = 7.9 Hz, 2H), 7.31 – 7.21 (m, 1H), 7.13 (dd, J = 8.6, 1.1 Hz, 1H); ^{13}C NMR (100Hz, CD$_3$OD) δ$_C$ 148.2 (C-O), 138.1, 135.3, 134.6, 134.0 (C-S), 129.6, 128.4, 126.6, 122.9; ESI-MS positive ion mode *m/z* 252 (MH$^+$, 100%); HRMS (TOF mode) calculated for C$_{11}$H$_{10}$NO$_4$S, 252.0331, found 252.0331.

7.2.3 Synthesis of *N*-methyl pyridinium benzene sulfonate iodide

12
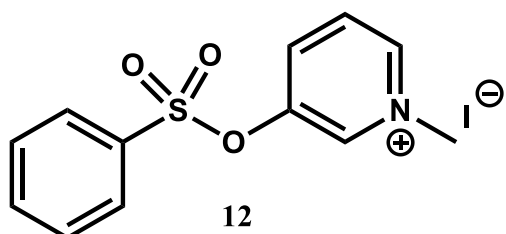
N-methyl pyridinium benzene sulfonate iodide **12** was synthesised according to a modified published procedure.[136] Pyridyl benzenesulfonate **10** (0.5 g, 2.1 mmol) and methyl iodide (1.32 mL, 21mmol) in acetone (20 mL) were refluxed for 16 h. The solvent was removed *in vacuo*, and the residue was dissolved in the minimum volume of methanol. The product was purified by the dropwise addition of diethyl ether to precipitate the product. Filtration and washing with diethyl ether to yield 0.2 g of **12** (25%) as a yellow solid: mp 144.8-145 °C; ^{1}H NMR (400 MHz, D$_2$O) δ 8.74 (s, 1H), 8.68 (d, J = 6.1 Hz, 1H), 8.09 (d, J = 8.7 Hz, 1H), 7.90 (dd, J = 8.7, 6.2 Hz, 1H), 7.85 – 7.71 (m, 3H), 7.57 (t, J = 8.0 Hz, 2H), 4.24 (s, 3H); ^{13}C NMR (100Hz, CD$_3$OD) δ$_C$ 148.3 (C-O), 144.7, 141.0, 139.0, 135.7, 133.5 (C-S), 130.0, 128.8, 128.6, 48.3; ESI-MS positive ion mode *m/z* 250 (M$^+$- I$^-$, 100%); HRMS (TOF mode) calculated for C$_{12}$H$_{12}$NO$_3$S, 250.0538, found 250.0527.

7.3 Synthesis of phosphate dieters

7.3.1 Synthesis of dimethyl pyridyl phosphate triester
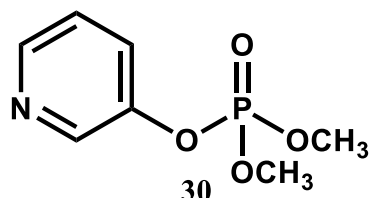
The dimethyl pyridyl phosphate triester **30** was synthesised according to the published procedure of Padovani *et al.*[82] 3-Hydroxy pyridine (0.35 g, 3.7 mmol) and dry imidazole (0.25 g, 3.7 mmol) were dissolved in dry DCM (20 mL) under nitrogen in an ice bath (0-5˚C). The solution was stirred for five minutes then dimethyl chlorophosphate (0.4 mL, 3.7 mmol) was added dropwise which formed a cloudy solution after completing the addition. The ice bath was removed and stirring continued overnight at room temperature. Next day, the white precipitate which had appeared was filtered off and washed with DCM (10 mL). The filtrate was concentrated *in vacuo* and the product purified by silica chromatography (95% EtOAC: 5% MeOH) with $R_f = 0.51$ to yield (0.13 g, 17%) of **30** as a pale-yellow oil. ^{1}H NMR (400 MHz, CDCl$_3$) δ 8.53 (d, *J* = 2.5 Hz, 1H), 8.46 (d, *J* = 4.7 Hz, 1H), 7.68 – 7.53 (m, 1H), 7.28 (dd, *J* = 8.4, 4.7 Hz, 1H), 3.90 (d, *J* = 11.4 Hz, 6H). ^{31}P NMR (162 MHz, CDCl$_3$) δ -3.97. ^{13}C NMR (101 MHz, CDCl$_3$) δ 147.6 (C-O), 146.4 (C-N), 142.1, 127.3, 124.0, 55.2.

7.3.2 Synthesis of *N*-methyl pyridinium phosphate diester[82]

29
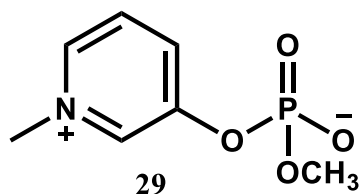
Dimethyl pyridyl phosphate triester **30** (0.12 g, 0.59 mmol) was dissolved in dry acetone (5 mL) and refluxed overnight to give a precipitate. Filtration and washing with dry acetone (5 mL) to yield (0.024 g, 24%) of **29** as a white solid. ^{1}H NMR (400 MHz, D$_2$O) δ 8.63 (s, 1H), 8.50 (d, J = 6.0 Hz, 1H), 8.25 (d, J = 8.0 Hz, 1H), 7.93 (dd, J = 8.5, 6.2 Hz, 1H), 4.31 (s, 3H), 3.64 (d, J = 11.8 Hz, 3H). ^{31}P NMR (162 MHz, D$_2$O) δ -3.82. ^{13}C NMR (101 MHz, D$_2$O) δ 151.7 (C-O), 140.5 (C-N), 138.0, 136.2, 128.6, 53.8, 48.3. ESI-MS-positive ion mode m/z (MH+); HRMS (TOF mode) calculated for C$_7$H$_{10}$NO$_4$P 204.0420; found 204.0422.

7.3.3 Synthesis of dimethyl *N*-oxide pyridyl phosphate[82]

31
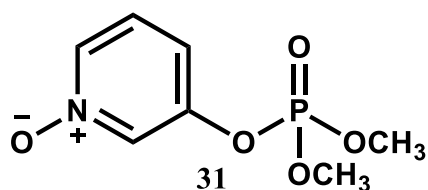
A mixture of 3-hydroxy *N*-oxide pyridine (0.41g, 3.7 mmol) and imidazole (0.26 g, 3.82 mmol) was dissolved in dry CH$_3$CN (15 mL) under nitrogen at 0-5 ˚C. Dimethyl chloro phosphate (0.4 mL, 3.7 mmol) in CH$_3$CN (5mL) was added dropwise. The reaction was stirred overnight at

157

room temperature to form a precipitate. The precipitate was filtered off and washed with CH$_3$CN (10ml). The solvent was removed to yield a clear oil (0.29 g, 36%) which was used as a crude product for the next step without further purification. ^{1}H NMR (400 MHz, D$_2$O) δ 7.87 (t, *J* = 1.9 Hz, 1H), 7.82 (d, *J* = 6.3 Hz, 1H), 7.34 (dd, *J* = 8.7, 6.3 Hz, 1H), 7.20 (dd, *J* = 8.7, 1.9 Hz, 1H), 3.43 (d, *J* = 10.7 Hz, 6H). ^{31}P NMR (162 MHz, D$_2$O) δ -3.89.

7.3.4 Synthesis of methyl *N*-oxide pyridyl phosphate[82]

28
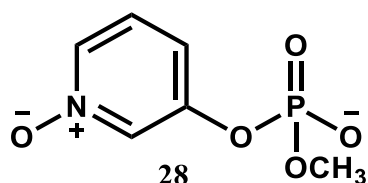
The crude product of dimethyl *N*-oxide pyridine (0.29 g,1.32 mmol) **31** was dissolved in dry acetone (10 mL) with lithium chloride (0.056 g, 1.32 mmol). The solution was stirred overnight at room temperature to yield a white precipitate which was washed with dry acetone (5mL) to remove any remaining starting material. The product was isolated after filtration as a white solid (0.11g, 39%) of **28**. ^{1}H NMR (400 MHz, D$_2$O) δ 8.20 (s, 1H), 8.09 (d, *J* = 6.0 Hz, 1H), 7.63 – 7.46 (m, 2H), 3.63 (d, *J* = 11.8 Hz, 3H). ^{31}P NMR (162 MHz, D$_2$O) δ -3.58. ^{13}C NMR (101 MHz, D$_2$O) δ 151.1 (C-O), 135.0, 132.6, 127.2, 124.4, 53.9. ESI-MS-positive ion mode m/z (MH+); HRMS (TOF mode) C$_6$H$_8$NO$_5$P 206.02129; found 206.02136.

7.4 Synthesis of sulfate diesters

7.4.1 Synthesis of phenyl chlorosulfonate[138]

38
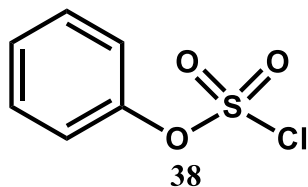
The phenyl chlorosulfonate **38** was synthesised according to the published procedure.[138] A dry round bottom flask was charged with phenol (3.16 g, 33.6 mmol) and pyridine (206 mL, 33.6 mmol) dissolved in dry diethyl ether (40 mL). The solution was stirred for 10 min at -78 °C to equilibrate at the desired temperature. A dry separate round bottom flask was charged with SO_2Cl_2 (2.8 ml,33.6 mmol) in dry diethyl ether (20 mL) at -78 °C. The solution of SO_2Cl_2 was transferred slowly via cannula to the solution of phenol and pyridine over 20 min at -78 °C. (Note: it was preferable to use a large magnetic bar since pyridinium salt was formed, and periodic manual shaking was needed to support the stirring). The stirring continued for 2 h at -78 °C, then the dry ice bath was removed and the stirring continued overnight at room temperature. After 16 h, a white precipitate was formed which was filtrated off through celite and washed with diethyl ether (50 mL). The filtrate was concentrated and the crude product purified immediately via silica chromatography (100% pet.ether) with R_f = 0.36 to yield (4.66 g, 72%) of **38** as a colorless oil. ^{1}H NMR (400 MHz, CDCl$_3$) δ 7.62 – 7.35 (m, 5H). ^{13}C NMR (101 MHz, CDCl$_3$) δ 150.2, 130.3, 128.9, 121.7. EI-MS (m/z) [M+]: Found 191.9648, Calculated for $C_6H_5ClO_3S$ 191.9642.

7.4.2 Synthesis of pyridyl phenyl sulfate

35
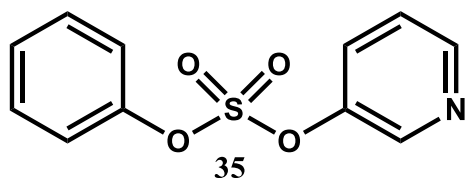
The pyridyl phenyl sulfate diester **35** was synthesised according to a published paper.[99] 3-Hdroxy pyridine (0.5 g, 5.3 mmol) with triethyl amine (0.7 mL, 0.5 g,5 mmol) were dissolved in dry THF (20 mL) under nitrogen in ice bath (0-5°C). The solution was stirred for 10min, then a solution of phenyl chlorosulfonate (1 g, 5.2 mmol) in dry THF (5 mL) was added to the solution of 3-hydroxy pyridine dropwise over 30 min. After completing the addition, the reaction was stirred overnight at room temperature. The next day, the solvent was evaporated and the crude product was purified by silica chromatography (20% ethyl acetate, 80% petroleum ether) with $R_f = 0.26$ to yield (0.6 g, 45%) of **35** as a yellow oil. ^{1}H NMR (400 MHz, CDCl$_3$) δ 8.67 – 8.59 (m, 2H), 7.75 – 7.68 (m, 1H), 7.55 – 7.23 (m, 6H). ^{13}C NMR (101 MHz, CDCl$_3$) δ 150.6 (C-O), 148.8, 147.1, 143.0, 130.6, 128.8, 128.0, 124.5, 121.0. ESI-MS positive ion mode *m/z* (MH$^+$, 100%); HRMS (TOF mode) calculated for C$_{11}$H$_9$NO$_4$S 252.0325, found 252.0324.

7.4.3 Synthesis of *N*-oxide pyridyl phenyl sulfate diester

36
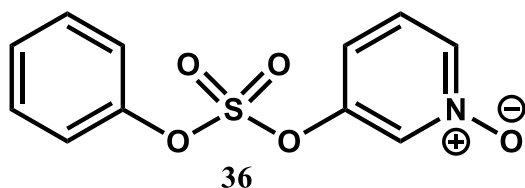
The *N*-oxide pyridyl phenyl sulfate diester **36** was prepared according to a modified published procedure.[139] 3-Chloroperbenzoic acid (0.19 g, 1.1 mmol) was dissolved in dry CHCl$_3$ (7mL) then was added dropwise to a solution of pyridyl phenyl sulfate diester **35** (0.24 g, 0.96 mmol) in dry CHCl$_3$ (8 mL) in an ice bath. After the addition was finished, the ice bath was removed and the solution stirred at room temperature. The reaction was followed by TLC and after 48 h white precipitate appeared. The reaction was quenched with K$_2$CO$_3$ 4 equivalent (0.58g, 4.2 mmol) and stirred for 10 min. The white precipitate was filtered off and the filtrate concentrated *in vacuo* and the crude product was recrystallized with cold diethyl ether to yield (0.23 g, 90%) of **36** as a white solid. ^{1}H NMR (400 MHz, CDCl$_3$) δ 8.21 (ddd, *J* = 9.7, 5.7, 1.5 Hz, 2H), 7.58 – 7.23 (m, 7H). ^{13}C NMR (101 MHz, CDCl$_3$) δ 150.1 (C-O), 148.6 (C-O), 138.5, 133.9, 130.4, 128.3, 126.0, 120.9, 118.7. ESI-MS positive ion mode *m/z* (MH$^+$, 100%); HRMS (TOF mode) calculated for C$_{11}$H$_9$NO$_5$S 268.0274) found 268.0277.

7.4.4 Synthesis of *N*-methyl pyridyl phenyl sulfate

37
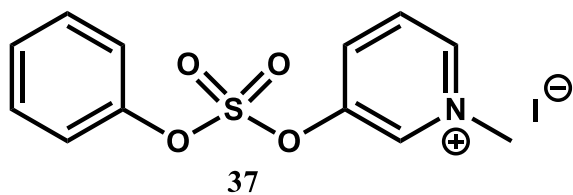
The *N*-methyl pyridyl phenyl sulfate **37** was synthesised following the published procedure.[136] Iodomethane (0.74 mL, 11.9 mmol) was added carefully to a solution of pyridyl phenyl sulfate diester (0.3 g, 1.2 mmol) in dry acetone (10 mL). The mixture was stirred at room temperature overnight to form a clear yellow solution. After 16 h, the solvent was removed *in vacuo* and the crude product was washed with diethyl ether (3×10 mL). The product was purified by column chromatography using 10% Methanol in DCM with $R_f = 0.4$ to yield (0.17g, 36%) of **37** as a yellow solid. ^{1}H NMR (400 MHz, CDCl$_3$) δ 9.46 (d, *J* = 5.9 Hz, 1H), 9.20 (s, 1H), 8.38 (ddd, *J* = 14.8, 8.8, 3.9 Hz, 2H), 7.59 – 7.39 (m, 5H), 4.74 (s, 3H). ^{13}C NMR (101 MHz, CDCl$_3$) δ 149.9 (C-O), 148.5, 145.2, 139.3, 137.6, 130.8, 129.8, 128.8, 121.3, 50.5. ESI-MS positive ion mode *m/z* (M$^+$- I$^-$, 100%); HRMS (TOF mode) calculated for C$_{12}$H$_{12}$NO$_4$S 266.0482 found 266.0486.

7.4.5 Synthesis of bis (pyridyl) sulfate diester
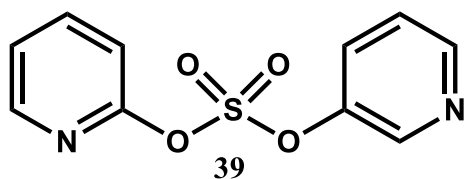
Bis (pyridyl) sulfate diester **39** was prepared according to a modified published procedure.[140] Distilled sulfuryl chloride (0.4 mL, 0.7g, 5 mmol) in dry THF (5 mL) was added dropwise to a solution of 3-hydroxy pyridine (1 g, 10 mmol) and trimethylamine (1.4 mL, 10 mmol) in dry THF (20 mL) at 0-5 °C using an ice bath. The solution was stirred for 10 min then left to stir at room temperature overnight. A brown precipitate formed, which was filtered off and washed with dry THF (10 mL). The filtrate was concentrated under vacuum and the residue purified by silica chromatography (95% DCM, 5% MeOH) with R_f = 0.42 to yield (0.34 g, 13%) of **39** as a yellow solid: mp 106-108 °C; ^{1}H NMR (400 MHz, CDCl$_3$) δ 8.68 – 8.62 (m, 4H), 7.73 (ddd, J = 8.5, 2.8, 1.4 Hz, 2H), 7.48 – 7.41 (m, 2H). ^{13}C NMR (101 MHz, CDCl$_3$) δ 149.1 (C-O), 147.2, 142.7, 128.7, 124.7. ESI-MS positive ion mode m/z (MH$^+$, 100%); HRMS (TOF mode) calculated for C$_{10}$H$_9$N$_2$O$_4$S 253.0283, found 253.0289.

7.4.6 Synthesis of 3-hydroxy *N*-oxide pyridine

14
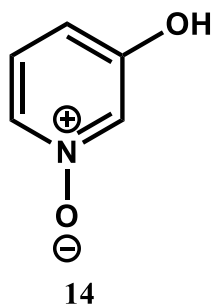
3-Hydroxy pyridine (3 g, 31.5 mmol) was dissolved in THF (30 mL) and the mixture was stirred for 10 min to allow for complete solubility. Then, 3-chloroperbenzoic acid (7.8 g, 45.2 mmol) in THF (30 mL) was added to the first solution. The reaction was stirred overnight. After 14 h, white precipitate appeared, which was filtered off and washed with THF (3 ×10 mL) to remove any remaining of starting material. The crude product was recrystallized from ethanol to yield (3.4 g, 96%) of **14** as a white solid: mp 200-203 °C; ^{1}H NMR (400 MHz, DMSO) δ 10.75 (s, 1H), 7.78 (d, *J* = 11.5 Hz, 2H), 7.35 – 7.06 (m, 1H), 6.85 (d, *J* = 8.3 Hz, 1H). ^{13}C NMR (101 MHz, DMSO) δ 156.6 (C-O), 131.1, 128.1, 126.7, 114.4. ESI-MS positive ion mode *m/z* (MH$^+$, 100%); HRMS (TOF mode) calculated for $C_5H_5NO_2$, 112.0393, found 112.0396.

7.5 Synthesis of *N*-methyl pyridinium 3-hydroxy
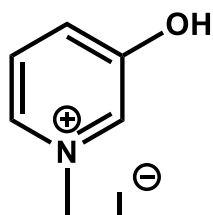
15

Methyl iodide (2.5 mL, 40.2 mmol) was added carefully to a solution of 3-hydroxy pyridine (2 g, 21 mmol) in acetone (50 mL). The reaction was refluxed for 16 h at 40 ºC. The next day, the yellow viscous precipitate which formed was filtered off and washed with THF (10 mL). The precipitate was recrystallized by dissolving in a minimum amount of methanol and precipitated out by diethyl ether to yield (4.2 g, 84%) of **15** as a yellow solid. Note: it is preferable to keep the compound immediately after purification in a dark container since it is sensitive to light. mp 103-107 °C; ^{1}H NMR (400 MHz, DMSO) δ 8.44 (d, $J = 5.2$ Hz, 2H), 8.01 – 7.78 (m, 2H), 4.30 (s, 3H). ^{13}C NMR (101 MHz, DMSO) δ 157.6 (C-O), 136.2, 134.2, 131.4, 128.7, 48.5. ESI-MS positive ion mode *m/z* (M$^+$- I$^-$, 100%); HRMS (TOF mode) calculated for C$_6$H$_8$NO, 110.0600, found 110.0604.

7.6 Synthesis of alkene cyclic phosphate triester

7.6.1 Alkene cyclic 4-nitrophenyl phosphate triester
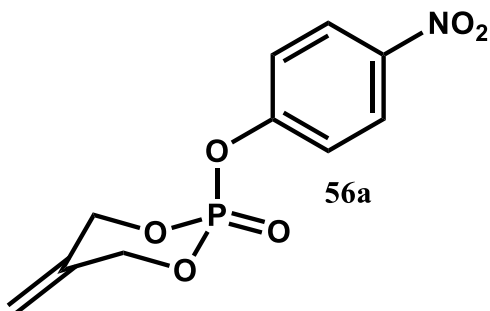
4-Nitrophenyl dichlorophosphate (0.64 g, 2.5 mmol) and 2-methylene-1,3-propandiol (0.22 g, 2.5 mmol) were dissolved in dry THF (20 mL) under nitrogen in an ice bath. The solution was allowed to stir for 10 min to cool down, then triethylamine (0.7 mL, 5 mmol) was added dropwise to the solution. The ice bath was removed and the mixture was stirred at room temperature for 16 h. A white precipitate appeared which was filtered off and the filtrate was concentrated under the vacuum. Then the crude product was dissolved in diethyl ether (20 mL) and washed with brine (10 mL). The organic layer was dried over Na_2SO_4, and the solvent was evaporated. The crude product was purified by silica chromatography using 1:1 (petroleum ether: EtOAc with R_f = 0.44 to yield 0.41 g, (61%) of **56a** as a pale yellow solid: mp 131-134 °C; ^{1}H NMR (400 MHz, CDCl$_3$) δ 8.33 (d, J = 9.2 Hz, 2H), 7.40 (d, J = 9.2 Hz, 2H), 5.39 (s, 2H), 5.04 (dd, J = 12.9, 4.5 Hz, 2H), 4.86 (dd, J = 18.9, 12.9 Hz, 2H). ^{31}P NMR (162 MHz, CDCl$_3$) δ -13.74. ^{13}C NMR (101 MHz, CDCl$_3$) δ 155.1 (C-O), 147.8, 144.8, 127.3, 123.7, 120.3, 118.6, 72.3. ESI-MS positive ion mode m/z (MH[+], 100%); HRMS (TOF mode) calculated for $C_{10}H_{10}NO_6P$, 272.0319, found 272.0317.

7.6.2 Alkene cyclic 3-nitrophenyl phosphate triester
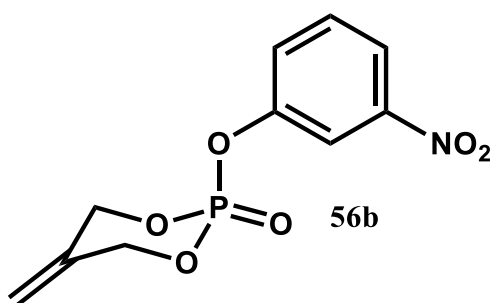
2-Methylene-1,3- propanediol (0.22 g, .2.5 mmol) and phosphoryl chloride (0.38 g, 2.5 mmol) were dissolved in dry THF (10 mL) under nitrogen at 0 °C. The reaction was stirred for 10 min then triethylamine (0.7 mL, 5 mmol) was added slowly and the solution stirred for 30 min at the same temperature. After 30 min, a mixture of 3-nitrophenol (0.35 g, 2.5 mmol) with triethylamine (0.35 mL, 2.5 mmol) in dry THF (10mL) was added slowly to the solution. The solution was stirred at room temperature for16 h. The white precipitate which formed was filtered off and the solvent was removed in *vacuo*. The remaining residue was dissolved in diethyl ether (20 mL) and washed with brine (10 mL). The organic layer was dried over Na_2SO_4 and the solvent was removed. The crude product was purified by silica chromatography using 1:1 petroleum ether: EtOAc with R_f = 0.3 to yield 0.4g, (59%) of **56b** as a pale yellow solid: mp 93-96 °C; ^{1}H NMR (400 MHz, CDCl$_3$) δ 8.09 (m, 2H), 7.74 – 7.64 (m, 1H), 7.57 (t, *J* = 8.5 Hz, 1H), 5.40 (s, 2H), 5.02 (dd, *J* = 12.7, 4.4 Hz, 2H), 4.89 (dd, *J* = 18.7, 12.7 Hz, 2H). ^{31}P NMR (162 MHz, CDCl$_3$) δ -13.23. ^{13}C NMR (101 MHz, CDCl$_3$) δ 150.8 (C-O), 149.0, 134.1, 130.7, 126.2, 120.1, 118.3, 115.3, 72.2. ESI-MS positive ion mode *m/z* 272 (MH$^+$, 100%); HRMS (TOF mode) calculated for $C_{10}H_{10}NO_6P$, 272.0319, found 272.0318.

7.6.3 Alkene cyclic 3-chlorophenyl phosphate triester
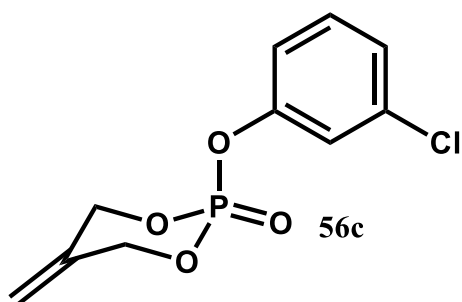
2-Methylene-1,3- propanediol (0.22 g, .2.5 mmol) and phosphorus oxychloride (0.38 g, 2.5 mmol) were dissolved in dry THF (10 mL) under nitrogen at 0 °C. The reaction was stirred for 10 min then triethylamine (0.7 mL, 5 mmol) was added slowly and the solution stirred for 30 min at the same temperature. After 30 min, a mixture of 3-chlorophenol (0.33 g, 2.5 mmol) with triethylamine (0.35 mL, 2.5 mmol) in dry THF (10 mL) was added slowly to the solution. The solution was stirred at room temperature overnight. After 16 h, the white precipitate which formed was filtered off and the solvent removed in *vacuo*. The remaining residue was dissolved in diethyl ether (20 mL) and washed with brine (10 mL). The organic layer was dried over Na$_2$SO$_4$ and the solvent was removed. The crude product was purified over silica chromatography using 1:1 petroleum ether: EtOAc with R$_f$ = 0.5 to yield 0.42 g, (65%) of **56c** as a yellow oil. ^{1}H NMR (400 MHz, CDCl$_3$) δ 7.26 (m, 2H), 7.16 (m, 2H), 5.32 (s, 2H), 4.94 (dd, J = 13.1, 4.5 Hz, 2H), 4.78 (dd, J = 19.1, 13.1 Hz, 2H). ^{31}P NMR (162 MHz, CDCl$_3$) δ - 13.22. ^{13}C NMR (101 MHz, CDCl$_3$) δ 150.8 (C-O), 135.1, 136.3, 130.7, 125.5, 120.3, 118.62, 118.8, 72.1. ESI-MS positive ion mode *m/z* (MH$^+$, 100%); HRMS (TOF mode) calculated for C$_{10}$H$_{10}$ClO$_4$P, 261.0078, found 260.0076.

7.6.4 Alkene cyclic phenyl phosphate triester
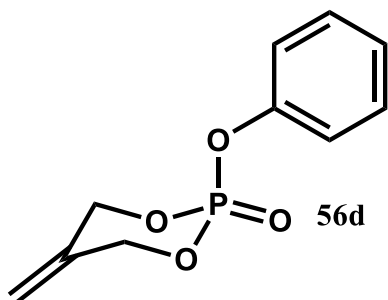
Phenyl dichlorophosphate (0.64 g, 2.5 mmol) with 2-methylene-1,3-propandiol (0.22 g, 2.5 mmol) in dry THF (20 mL) under nitrogen in ice bath. The solution was allowed to stirr for 10 min to cool down, then triethylamine (0.7 mL, 5 mmol) was added dropwise to the solution. The ice bath was removed and the mixture was stirred at room temperature for 16 h. The next day, a white precipitate appeared which was filtered off and the filtrate was concenatrated in *vacuo*. Then the crude product was dissolved in diethyl ether (30 mL) and washed with brine (20 mL) and then water (20 mL). The organic layer was dried over Na_2SO_4 and the solvent was evaporated. The crude product was purified by silica chromatography using (40% petroleum ether: 60% EtOAc with R_f = 0.33 to yield 0.39g, (69%) of **56d** as a white solid: mp 51-54 °C; ^{1}H NMR (400 MHz, CDCl$_3$) δ 7.43 – 7.31 (m, 2H), 7.30 – 7.15 (m, 3H), 5.32 (s, 2H), 4.97 (dd, J = 12.7, 5.0 Hz, 2H), 4.79 (dd, J = 19.0, 12.7 Hz, 2H). ^{31}P NMR (162 MHz, CDCl$_3$) δ -12.85. ^{13}C NMR (101 MHz, CDCl$_3$) δ 150.4 (C-O), 134.7, 129.8, 125.1, 119.6, 117.6, 71.9. ESI-MS positive ion mode *m/z* (MH[+], 100%); HRMS (TOF mode) calculated for $C_{10}H_{11}O_4P$, 227.0468, found 227.0457.

169

7.6.5 Alkene cyclic 4-methoxyphenyl phosphate triester
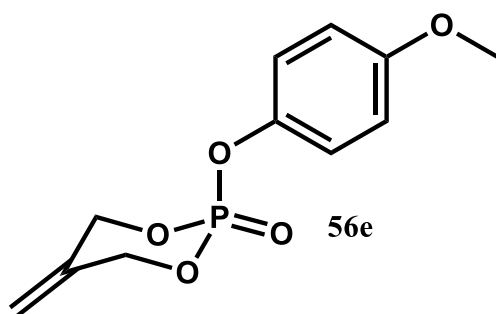
2-Methylene-1,3- propanediol (0.22 g, 2.5 mmol) and phosphoryl chloride (0.38 g, 2.5 mmol) were dissolved in dry THF (10 mL) under nitrogen at 0 °C. The reaction was stirred for 10 min then triethylamine (0.7 mL, 5 mmol) was added slowly and stirred for 30 min at the same temperature. After 30 min, a mixture of 4-methoxyphenol (0.32 g, 2.57 mmol) with triethylamine (0.35 mL, 2.5 mmol) in dry THF (10 mL) was added slowly to the solution. The solution was stirred at room temperature overnight. After 16 h, the white precipitate was filtered off and the solvent removed under vacuum. The remaining residue was dissolved in diethyl ether (20 mL) and washed with brine (10 mL) then water (10 mL). The organic layer was dried over Na$_2$SO$_4$ and the solvent was removed. The crude product was purified over silica chromatography using 60% petroleum ether and 40% EtOAc with R$_f$ = 0.2 to yield 0.27 g, (42%) of **56e** as a white solid. ^{1}H NMR (400 MHz, CDCl$_3$) δ 7.19 (d, J = 9.6 Hz, 2H), 6.87 (d, J = 9.6 Hz, 2H), 5.32 (s, 2H), 4.96 (dd, J = 13.2, 5.0 Hz, 2H), 4.80 (dd, J = 18.6, 13.2 Hz, 2H), 3.80 (s, OCH$_3$). ^{31}P NMR (162 MHz, CDCl$_3$) δ -12.27. ^{13}C NMR (101 MHz, CDCl$_3$) δ 156.8 (C-O), 144.0, 134.8, 120.7, 117.4, 114.8, 71.7, 55.7. ESI-MS positive ion mode m/z (MH$^+$, 100%); HRMS (TOF mode) calculated for C$_{11}$H$_{13}$O$_5$P, 257.0573, found 257.0572.

7.6.6 Alkene-3,4-dimethylphenyl phosphate triester
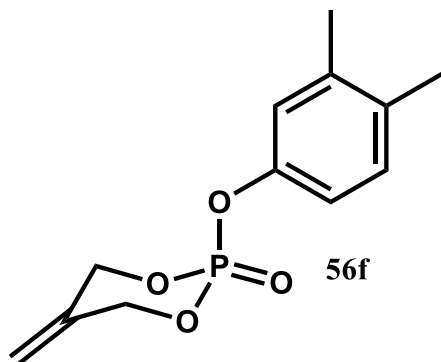
Phosphoryl chloride (0.39 g, 2.5 mmol) was dissolved in dry THF (10 mL) under nitrogen and stirred at 0-5 °C for 10 min. Then, 3,4-dimethylphenol (0.3 g, 2.5 mmol) with triethylamine (0.35 mL, 2.5 mmol) in dry THF (10 mL) were added dropwise to the solution. The mixture was stirred for another 30 min at 0 ºC. After that, 2-methylene-1,3-propandiol (0.22 g, 2.5 mmol) with triethylamine (0.7 mL, 5 mmol) were added slowly to the solution. After the addition was completed, the reaction was stirred at room temperature overnight. The next day, the solvent was evaporated and the remaining residue was dissolved in diethyl ether (30 mL) and washed with brine (20 mL) then water (20 mL). The organic layer was dried over Na_2SO_4 and the solvent was evaporated *in vacuo*. The crude product was purified by column chromatography using (60% petroleum ether: 40% EthOAc) with $R_f = 0.3$ to yield 0.48 g, (75%) of **56f** as a white milky solid. ^1H NMR (400 MHz, CDCl$_3$) δ 7.17 – 7.03 (m, 2H), 6.98 (dd, $J = 8.2$, 2.4 Hz, 1H), 5.31 (s, 2H), 4.96 (dd, $J = 13.1$, 4.5 Hz, 2H), 4.77 (dd, $J = 19.1$, 13.1 Hz, 2H), 2.27 (s, CH$_3$), 2.24 (s, CH$_3$). ^{31}P NMR (162 MHz, CDCl$_3$) δ -12.59. ^{13}C NMR (101 MHz, CDCl$_3$) δ 148.3 (C-O), 138.4, 134.8, 133.5, 130.4, 120.5, 117.4, 116.6, 71.8, 19.9, 19.1. ESI-MS positive ion mode *m/z* (MH$^+$, 100%); HRMS (TOF mode) calculated for C$_{12}$H$_{15}$O$_4$P, 255.0781, found 255.0786.

7.6.7 Alkene cyclic ethyl phosphate triester

74
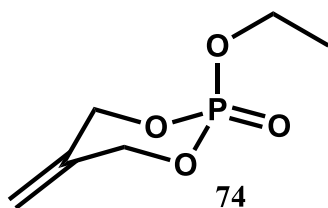
Ethyl dichlorophosphate (0.81 g, 5 mmol) was dissolved in dry THF (5 mL) under nitrogen in an ice bath and the solution was allowed to stir for 10 min to cool down. Then, 2-methylene 1,3-propandiol (0.44 g, 5 mmol) with triethylamine (1.4 mL, 10 mmol) in dry THF (5 mL) were added slowly. After the addition was complete, the solution was stirred at room temperature overnight. A white precipitate was noticed which was removed by filtration and the filtrate concentrated *in vacuo*. The crude product was purified by silica chromatography using 30% EtOAc in DCM with R_f = 0.5 to yield 0.5 g, (56%) of **74** as a colorless oil. ^{1}H NMR (400 MHz, CDCl$_3$) δ 5.22 (s, 2H), 4.84 – 4.63 (m, 4H), 4.24 – 4.11 (m, 2H), 1.35 (t, *J* = 7.1 Hz, 3H). ^{31}P NMR (162 MHz, CDCl$_3$) δ -6.40. ^{13}C NMR (101 MHz, CDCl$_3$) δ 135.3, 116.6, 71.1, 64.5, 16.1. ESI-MS positive ion mode *m/z* (MH$^+$, 100%); HRMS (TOF mode) calculated for C$_6$H$_{11}$O$_4$P, 179.0468, found 179.0465.

172

7.7 Dimethoxy cyclic 4-nitrophenyl phosphate triester
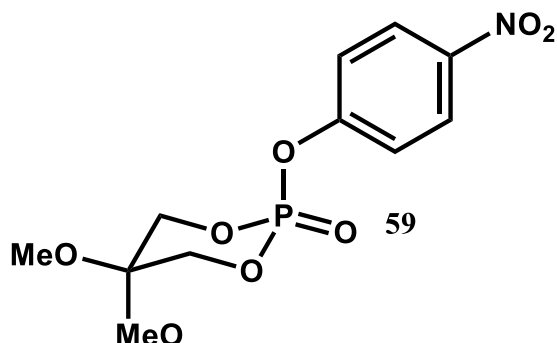
2,2-Dimethoxy -1,3-proandiol (0.35 g, 2.6 mmol) and 4-nitrophenyl dichlorophosphate (0.64 g, 2.5 mmol) were dissolved in dry THF (25 mL) under nitrogen. The solution was stirred for 10 min at 0 °C then triethylamine (0.7 mL, 5 mmol) was added dropwise to the solution. The ice bath was removed, the mixture was stirred at room temperature and the reaction was followed by TLC. After 6 h, a white precipitate appeared which was filtered off and the filtrate was concentrated in *vacuo*. Then the crude product was dissolved in diethyl ether (20 mL) and washed with brine (20 mL). The organic layer was dried over Na_2SO_4 and the solvent was evaporated. The crude product was purified by silica chromatography using (40% petroleum ether: 60% EtOAc with R_f = 0.45 to yield 0.43 g, (52%) of **59** a pale yellow solid: mp 115-118 °C; ^{1}H NMR (400 MHz, $CDCl_3$) δ 8.27 (d, *J* = 9.3 Hz, 2H), 7.44 (d, *J* = 9.3 Hz, 2H), 4.45 (dd, *J* = 21.3, 11.4 Hz, 2H), 4.31 (dd, *J* = 11.4, 4.0 Hz, 2H), 3.40 (s, 3H), 3.31 (s, 3H). ^{31}P NMR (162 MHz, $CDCl_3$) δ -13.98. ^{13}C NMR (101 MHz, $CDCl_3$) δ 155.7 (C-O), 145.3, 125.9, 120.3, 93.5, 70.2, 49.2. ESI-MS positive ion mode *m/z* (MH^+, 100%); HRMS (TOF mode) calculated for $C_{11}H_{14}NO_8P$, 320.053, found 320.0529.

173

7.8 Cyclic 4-nitrophenyl phosphate triester
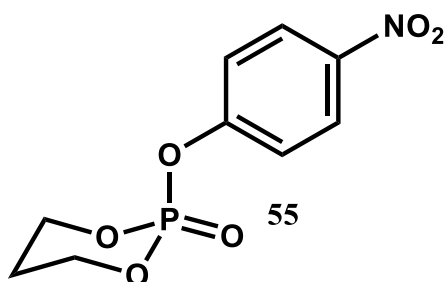

4-Nitrophenyl dichlorophosphate (0.64 g, 2.5 mmol) and 1,3-proandiol (0.19 g, 2.5 mmol) were dissolved in dry THF (10 mL) under nitrogen in an ice bath. The solution was stirred for 10 min at 0 °C then triethylamine (0.7 mL, 5 mmol) was added dropwise. The ice bath was removed, the mixture was stirred at room temperature and the reaction was followed by TLC. After 6 h, a white precipitate appeared which was filtered and the filtrate was concertad *in vacuo*. The crude product was dissolved in diethyl ether (30 mL) and washed with brine (20 ml) then water (20 ml). The organic layer was dried over Na_2SO_4 and the solvent was evaporated under the vacuum. The crude product was purified by silica chromatography using (40% petroleum ether: 60% EtOAc) with R_f = 0.2 to yield 0.39 g, (60%) of **55** as a yellow solid: mp 95-97 °C; ^{1}H NMR (400 MHz, CDCl$_3$) δ 8.25 (d, *J* = 8.7 Hz, 2H), 7.43 (d, *J* = 8.7 Hz, 2H), 4.73 – 4.39 (m, 4H), 2.54 – 2.37 (m, 1H), 1.89 (ddd, *J* = 15.1, 5.0, 2.5 Hz, 1H). ^{31}P NMR (162 MHz, CDCl$_3$) δ -14.47. ^{13}C NMR (101 MHz, CDCl$_3$) δ 155.2 (C-O), 145.7, 125.8, 120.3, 69.9, 25.8. ESI-MS positive ion mode *m/z* (MH$^+$, 100%); HRMS (TOF mode) calculated for $C_9H_{10}NO_6P$, 260.0319, found 260.0320.

7.9 Alkene cyclic 4-nitrobenzyl phosphate triester
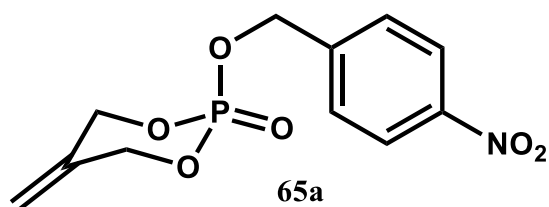
Phosphoryl chloride (0.77 g, 5 mmol) was dissolved in dry THF (10 mL) under nitrogen and stirred at 0-5 °C for 10 min. Then, 4-nitrobenzyl alcohol (0.77 g, 5 mmol) with triethylamine (0.7 mL, 5 mmol) in dry THF (10 mL) were added dropwise to the solution. The mixture was stirred for another 30 min at 0 ºC. After that, 2-methylene-1,3-propandiol (0.44 g, 5 mmol) with triethylamine (1.4 mL, 10 mmol) were added slowly to the solution. After the addition was completed, the reaction was stirred at room overnight. The next day, the solvent was evaporated and the remaining residue was dissolved in diethyl ether (30 mL) and washed with brine (20 mL). The organic layer was dried over Na_2SO_4 and the solvent was evaporated under the vacuum. The crude product was purified by column chromatography using (20% petroleum ether: 80% EtOAc) with R_f = 0.3 to yield 0.58 g, (45%) of **65a** as a yellow solid: mp 91-94 °C; ^{1}H NMR (400 MHz, CDCl$_3$) δ 8.26 (d, J = 8.8 Hz, 2H), 7.60 (d, J = 8.8 Hz, 2H), 5.31 – 5.24 (m, 4H), 4.79 (dd, J = 18.0, 10.1 Hz, 4H). ^{31}P NMR (162 MHz, CDCl$_3$) δ -6.24. [3]C NMR (101 MHz, CDCl$_3$) δ 148.0, 142.9, 135.0, 128.2, 124.0, 117.0, 71.4, 67.7. ESI-MS positive ion mode m/z (MH[+], 100%); HRMS (TOF mode) calculated for $C_{11}H_{12}NO_6P$, 286.0475, found 286.0479.

7.10 2,2-Dimethoxy-1,3- propanediol

58
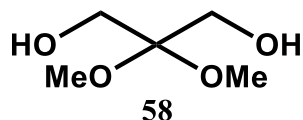
2,2-Dimethoxy-1,3- propanediol was synthesised according to modified published papers.[141-143] Dihydroxy acetone dimer (15.6 g, 86 mmol) was dissolved in methanol (190 mL) and was stirred for 10 min for complete solubility. Trimethyl orthoformate (19 mL) with p-toluene sulfonic acid (100 mg) were added to the solution. The solution was stirred at room temperature for 24 h. The next day, the solution was quenched with Na_2CO_3 (300 mg) and stirred for 12 h. After that, a brown solution with precipitate appeared which was filtered and the solvent was concentrated *in vacuo*. The remaining residue was dissolved in chloroform (100 mL) and filtered off again. The filtrate was concentrated in *vacuo* and the crude product was purified in two ways first by recrystallization from diethyl ether to give (7.4 g, 63%) a colorless semi solid. The second method was by vacuum distillation (10 bar) which desired fraction was distilled at 150-160 °C to yield 5 g, (42%) of **58** as a colorless semi solid. ^{1}H NMR (400 MHz, CDCl$_3$) δ 3.66 (s, 4H), 3.28 (s, 6H). ^{13}C NMR (101 MHz, CDCl$_3$) δ 100.3, 60.9, 48.6. ESI-MS positive ion mode *m/z* (M+Na$^+$, 100%); HRMS (TOF mode) calculated for $C_5H_{12}O_4$, 159.0628, found 159.0632.

7.11 Synthesis of carbonyl phosphate triesters

7.11.1 Carbonyl cyclic 4-nitrophenyl phosphate triester
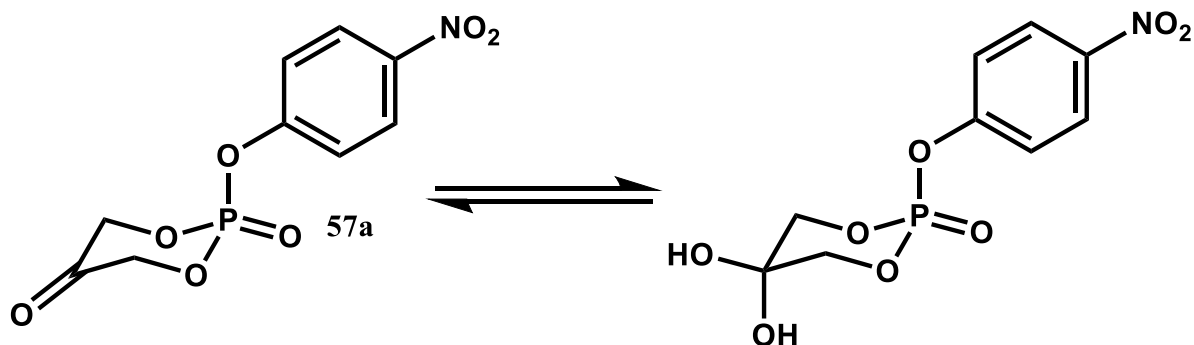
In a dry round flask, alkene cyclic 4-nitrophenyl phosphate triester **56a** (0.2 g, 0.74 mmol) was dissolved in dry DCM (15 mL). The solution was allowed to cool down to -78 °C for 10 min then the O_3 stream was allowed to bubble through the solution until the colour changed to blue (average time 45 min). After that, the O_3 line was switched off and the solution under nitrogen was quenched with dimethyl sulfide (3 equivalents) and stirred for 15 min at room temperature. After 15 min, the solution was concentrated using nitrogen stream as dimethyl sulfide has a strong smell. The crude product was purified by silica chromatography using 30% ethyl acetate in DCM with R_f = 0.25 to yield 0.17 g, (82%) of **57a** as a yellow semisolid. ^{1}H NMR (400 MHz, CDCl$_3$) δ 8.30 (d, J = 9.1 Hz, 2H), 7.45 (d, J = 9.1 Hz, 2H), 5.04 – 4.75 (m, 4H). ^{31}P NMR (162 MHz, CDCl$_3$) δ -10.47 for carbonyl, -14.57 for hydrated. For carbonyl one ^{13}C NMR (101 MHz, CDCl$_3$) δ 198.5 (C=O), 154.5 (C-O), 145.3, 126.0, 120.4, 72.3, 94.8. IR= 3297(OH); 1758(C=O). ESI-MS positive ion mode (MH$^+$, 100%); HRMS (TOF mode) calculated for C$_9$H$_8$NO$_7$P, 274.0111, found 274.0117 for (carbonyl form), ESI-MS positive ion mode m/z (MH$^+$) 292 (hydrated form).

7.11.2 Carbonyl cyclic 3-nitrophenyl phosphate triester
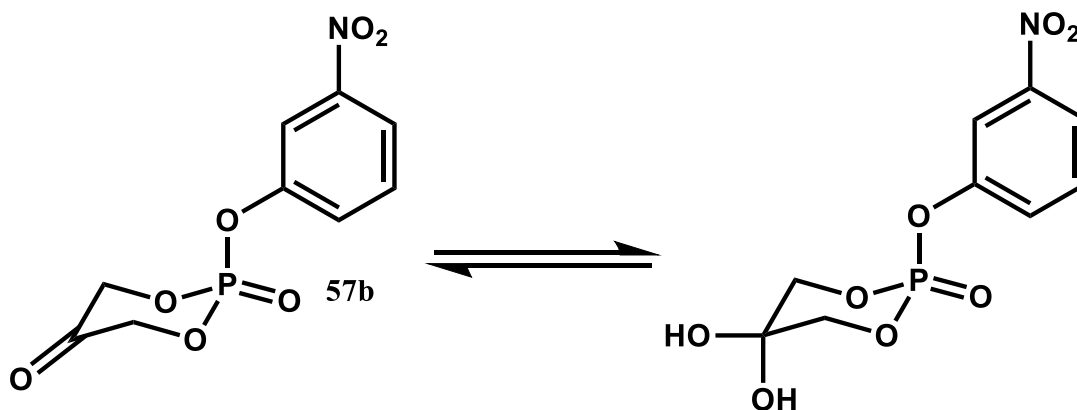
In a dry round flask, alkene cyclic 3-nitrophenyl phosphate triester **56b** (0.23 g, 0.85 mmol) was dissolved in dry DCM (20 mL). The solution was allowed to cool down to -78 °C for 10 min then the O_3 stream was allowed to bubble through the solution until the colour changed to blue (average time 45 min). After that, the O_3 line was switched off and the solution under nitrogen was quenched with dimethyl sulfide (3 equivalents) and stirred for 15 min at room temperature. After 15 min, the solution was concentrated using nitrogen stream. The crude product was purified by silica chromatography using 30% ethyl acetate in DCM with $R_f = 0.25$ to yield 0.18 g, (78%) of **57b** as a yellow viscous oil. ^{1}H NMR (400 MHz, CDCl$_3$) δ 8.10 (m, 2H), 7.72 − 7.51 (m, 2H), 5.04 − 4.74 (m, 4H). ^{31}P NMR (162 MHz, DMSO) δ -11.00 (carbonyl), -14.02 (hydrated). ^{13}C NMR (101 MHz, CDCl$_3$) δ 198.6 (C=O), 150.25, 149.1, 130.8, 126.2, 120.8, 120.3, 72.3. ESI-MS positive ion mode (MH$^+$, 100%); HRMS (TOF mode) calculated for C$_9$H$_8$NO$_7$P, 274.0111, found 274.0117 for (carbonyl form), ESI-MS positive ion mode *m/z* (MH$^+$) 292 (hydrated form).

7.11.3 Carbonyl cyclic 3-chlorophenyl phosphate triester

In a dry round flask, alkene cyclic 3-chlorophenyl phosphate triester **56c** (0.2 g, 0.77 mmol) was dissolved in dry DCM (20 mL). The solution was allowed to cool down to -78 °C for 10 min then the O_3 stream was left to bubble through the solution until the colour changed to blue as average time 45 min. After that, the O_3 line was switched off and the solution under nitrogen was quenched with dimethyl sulfide (3 equivalent) and stirred for 15 min at room temperature. After 15 min, the solution was concentrated using nitrogen stream. The crude product was purified by silica chromatography using 30% DCM in ethyl acetate with R_f = 0.37 to yield 0.15g, (75%) of **57c** as a viscous oil. ^{1}H NMR (400 MHz, CDCl$_3$) δ 7.29 (t, J = 8.0 Hz, 2H), 7.17 (d, J = 9.3 Hz, 2H), 4.95 – 4.72 (m, 4H). ^{31}P NMR (162 MHz, CDCl$_3$) δ -10.16 (carbonyl), -13.70 (hydrated). ^{13}C NMR (101 MHz, CDCl$_3$) δ 199.03 (C=O), 151.0, 135.3, 130.8, 126.1, 120.4, 118.1, 72.2. ESI-MS positive ion mode *m/z* (MH$^+$, 100%); HRMS (TOF mode) calculated for C$_9$H$_9$ClO$_5$P, 262.9876, found 262.9870.

7.11.4 Carbonyl cyclic phenyl phosphate triester
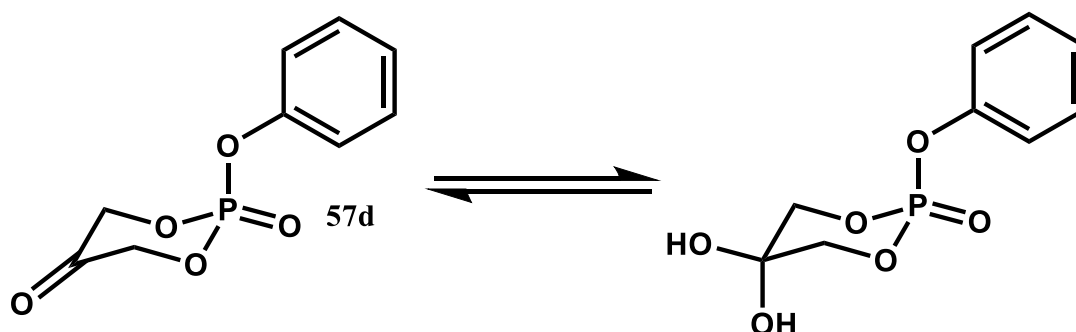
In a dry round flask, alkene cyclic phenyl phosphate triester **56d** (0.23 g, 1 mmol) was dissolved in dry DCM (15 mL). The solution was allowed to cool down to -78 °C for 10 min then the O_3 stream was allowed to bubble through the solution until the colour changed to blue as average time 60 min. After that, the O_3 line was switched off and the solution under nitrogen was quenched with dimethyl sulfide (3 equivalent) and stirred for 15 min at room temperature. After 15 min, the solution was concentrated using nitrogen stream as dimethyl sulfide has a strong smile. The crude product was purified by silica chromatography using 30% ethyl acetate in DCM with R_f = 0.25 to yield 0.2 g, (86%) of **57d** as a white semisolid. ^{1}H NMR (400 MHz, CDCl$_3$) δ 7.46 – 7.30 (m, 2H), 7.27 – 7.14 (m, 3H), 4.91 – 4.67 (m, 4H). ^{31}P NMR (162 MHz, CDCl$_3$) δ -10.05 (carbonyl), -13.42 (hydrated). ^{13}C NMR (101 MHz, CDCl$_3$) δ 199.4 (C=O), 150.0, 132.7, 127.3, 122.0, 72.2. IR= 3297(OH); 1758(C=O). ESI-MS positive ion mode (MH$^+$, 100%); HRMS (TOF mode) calculated for C$_9$H$_9$O$_5$P, 229.0260, found 229.0261 for (carbonyl form), ESI-MS positive ion mode *m/z* (MH$^+$): 247 (hydrated form).

7.11.5 Carbonyl cyclic 4-methoxyphenyl phosphate triester
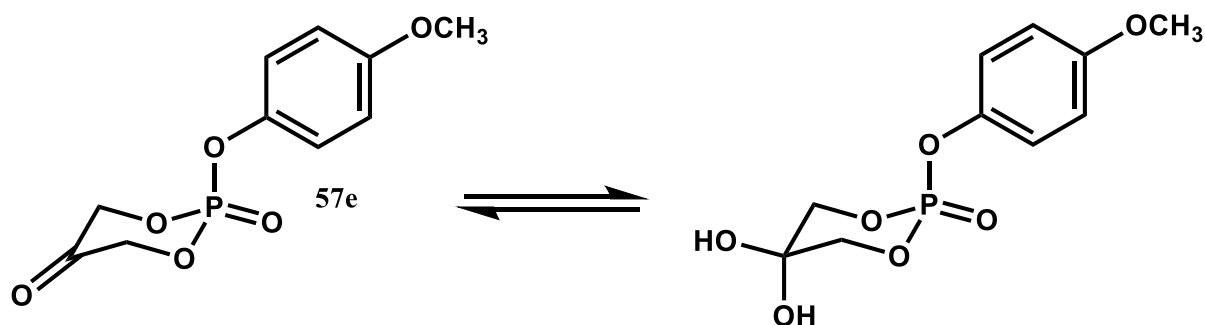
In a dry round flask, alkene cyclic 4-methoxyphenyl phosphate triester **56e** (0.17 g, 0.66 mmol) was dissolved in dry DCM (20 mL). The solution was allowed to cool down to -78 °C for 10 min then the O_3 stream was allowed to bubble through the solution until the colour changed to blue (an average time 60 min). After that, the O_3 line was switched off and the solution under nitrogen was quenched with dimethyl sulfide (0.14 mL, 2 mmol) and stirred for 15 min at room temperature. After 15 min, the solution was concentrated using a nitrogen stream. The crude product was purified by silica chromatography using 30% DCM in ethyl acetate with $R_f = 0.35$ to yield 0.12 g, (70%) of **57e** a colorless semisolid. ^{1}H NMR (400 MHz, DMSO) δ 7.31 (d, *J* = 9.7 Hz, 2H), 7.01 (d, *J* = 9.7 Hz, 2H), 4.38 – 4.18 (m, 4H), 3.75 (s, OCH₃). ^{31}P NMR (162 MHz, CDCl₃) δ -9.55 (for carbonyl), -14.14 (for hydrated). ^{13}C NMR (101 MHz, CDCl₃) δ 199.6 (C=O), 157.4, 143.5, 120.7, 114.9, 71.9, 55.7. ESI-MS positive ion mode *m/z* (MH⁺, 100%); HRMS (TOF mode) calculated for $C_{10}H_{11}O_6P$, 259.0366, found 259.0368. +ESI (M+H) 277 for hydrated one.

7.11.6 Carbonyl cyclic 3,4-dimethylphenyl phosphate triester
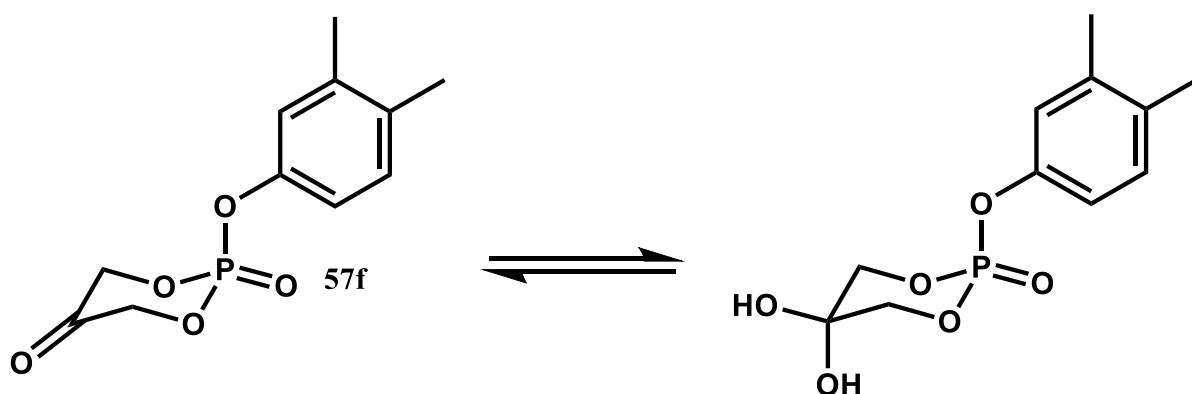
In a dry round flask, alkene cyclic 3,4-dimethylphenyl phosphate triester **57f** (0.4 g, 1.57 mmol) was dissolved in dry DCM (15 mL). The solution was allowed to cool down to -78 °C for 10 min then the O_3 stream was allowed to bubble through the solution until the colour changed to blue (average time 60 min). After that, the O_3 line was switched off and the solution under nitrogen was quenched with dimethyl sulfide (0.36 mL, 5 mmol) and stirred for 15 min at room temperature. After 15 min, the solution was concentrated using nitrogen stream as dimethyl sulfide. The crude product was purified by silica chromatography using 30% DCM in ethyl acetate with R_f = 0.4 to yield 0.2 g, (86%) of **57f** a a pale-yellow semisolid. ^{1}H NMR (400 MHz, CDCl$_3$) δ 7.11 (d, J = 8.4 Hz, 1H), 7.02 (d, J = 2.4, Hz, 1H), 6.97 (dd, J = 8.4, 2.4 Hz, 1H), 4.93 – 4.61 (m, 4H), 2.34 (s, CH$_3$), 2.25 (s, CH$_3$). ^{31}P NMR (162 MHz, CDCl$_3$) δ -9.82 (carbonyl), -14.20 (hydrated one). ^{13}C NMR (101 MHz, CDCl$_3$) δ 199.6 (C=O), 147.8, 134.2, 130.8, 120.5, 116.7, 72.1, 19.9, 19.1. ESI-MS positive ion mode m/z (MH$^+$, 100%); HRMS (TOF mode) calculated for C$_{11}$H$_{13}$O$_5$P, 257.0573, found 257.0579. +ESI (M+H): 275 for hydrated one.

7.11.7 Carbonyl cyclic ethyl phosphate
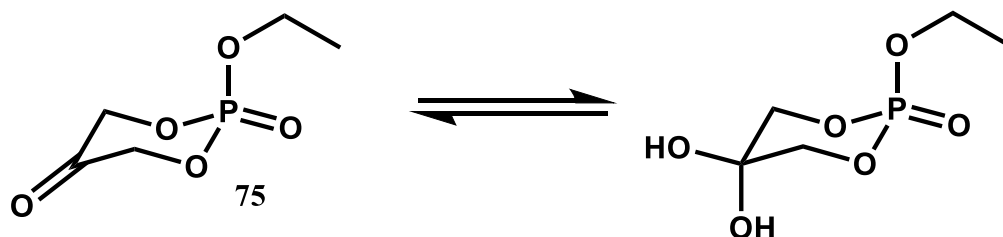
In a dry round flask, alkene cyclic ethyl phosphate triester **74** (0.2 g, 1.23 mmol) was dissolved in dry DCM (20 mL). The solution was allowed to cool down to -78 °C for 10 min then the O_3 stream was left to bubble through the solution until the colour changed to blue with an average time 45 min. After that, the O_3 line was switched off and the solution under nitrogen was quenched with dimethyl sulfide (0.26 mL, 3.66 mmol) and stirred for 15 min at room temperature. After 15 min, the solution was concentrated using nitrogen stream as dimethyl sulfide has a strong smell. The crude product was purified by silica chromatography using 100% ethyl acetate with R_f = 0.32 to yield 0.2 g, (99%) of **75** as a colorless oil. ^{1}H NMR (400 MHz, D_2O) δ 4.28 (dd, J = 10.8, 4.3 Hz, 2H), 4.23 – 4.04 (m, 4H), 1.29 (t, J = 7.1 Hz, 3H). ^{31}P NMR (162 MHz, $CDCl_3$) δ -3.39 (carbonyl), -7.27 (hydrated). ^{13}C NMR (101 MHz, D_2O) δ 87.3, 73.3, 65.7, 15.2. IR= 3297(OH); 1758(C=O). ESI-MS positive ion mode *m/z* (MH[+], 100%); HRMS (TOF mode) calculated for $C_5H_9O_5P$, 181.0260, found 181.062 (carbonyl form). ESI-MS positive ion mode *m/z* (MH[+], 100%); HRMS (TOF mode) calculated for $C_5H_{11}O_5P$, 199.0366, found 199.0364 (hydrated form).
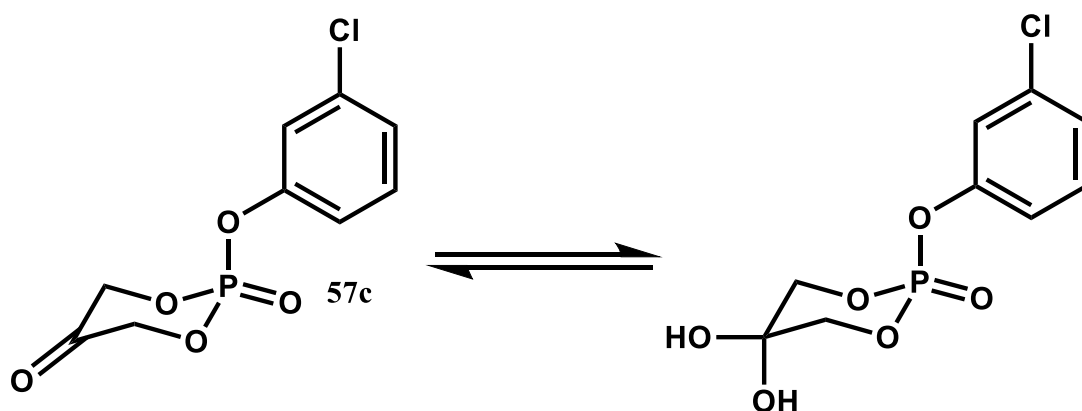
7.11.8 Carbonyl cyclic 4-nitrobenzyl phosphate triester
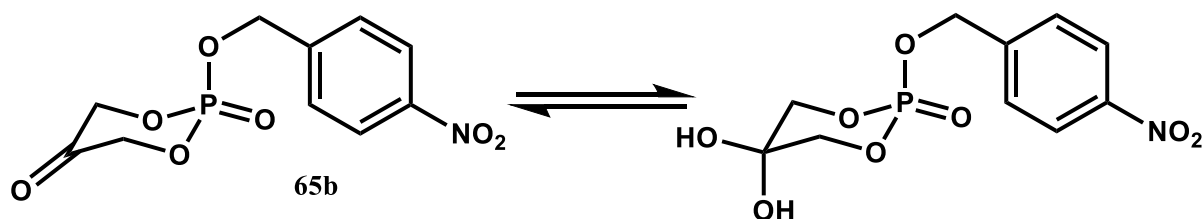
In a dry round flask, alkene cyclic 4-nitrobenzyl phosphate triester (0.5 g, 1.75 mmol) was dissolved in dry DCM (20 mL). The solution was allowed to cool down to -78 °C for 10 min then the O_3 stream was left to bubble through the solution until the colour changed to blue as average time 45 min. After that, the O_3 line was switched off and the solution under nitrogen was quenched with dimethyl sulfide (0.39 mL, 5.3 mmol) and stirred for 15 min at room temperature. After 15 min, the solution was concentrated by using nitrogen stream as dimethyl sulfide has a strong smell. The crude product was purified by silica chromatography using 20% DCM in ethyl acetate with R_f = 0.2 to yield 0.39 g, (77%) of **65b** as a yellow semisolid. ^{1}H NMR (400 MHz, CDCl₃) δ 8.27 (d, J = 8.7 Hz, 2H), 7.60 (d, J = 8.7 Hz, 2H), 5.35 (d, J = 9.5 Hz, 2H), 4.88 – 4.61 (m, 4H). ^{31}P NMR (162 MHz, CDCl₃) δ -3.05 (carbonyl), -7.53 (hydrated). ^{13}C NMR (101 MHz, CDCl₃) δ 199.7 (C=O), 148.17, 142.1, 128.3, 124.1, 71.7, 69.1. ESI-MS positive ion mode m/z (MH⁺, 100%); HRMS (TOF mode) calculated for $C_{10}H_{10}NO_7P$, 288.0268, found 288.0275 (carbonyl form), MS+ESI(M+H): 306.0374 (For hydrated one).

7.12 Dimethoxy cyclic 4-nitrobenzyl phosphate triester
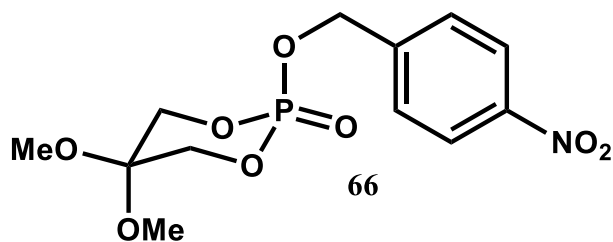
Phosphoryl chloride (0.77 g, 5 mmol) was dissolved in dry THF (15 mL) under nitrogen and stirred at 0-5 °C for 5 min. Then, 4-nitrobenzyl alcohol (0.77 g, 5 mmol) with triethylamine (0.7 mL, 5 mmol) were added dropwise to the solution. The mixture was stirred for another 15 min at the same temperature. After that, 2,2-dimethoxy 1,3 propanediol (0.71 g, 5.2 mmol) with triethylamine (1.4 mL, 10 mmol) were added slowly to the solution. After the addition was completed, the reaction was stirred at room temperature for 16 h. The next day, the solvent was evaporated *in vacuo* and the remaining residue was dissolved in chloroform (30 mL) and washed with brine (20 mL). The organic layer was dried over Na_2SO_4 and the solvent was evaporated under the vacuum. The crude product was purified by column chromatography using (60% petroleum ether: 40% EtOAc) with $R_f = 0.13$ to yield 0.5 g, (30%) of **66** as a yellow solid: mp 111-115 °C; ^1H NMR (400 MHz, CDCl$_3$) δ 8.25 (d, $J = 8.7$ Hz, 2H), 7.58 (d, $J = 8.7$ Hz, 2H), 5.23 (d, $J = 8.7$ Hz, 2H), 4.33 (dd, $J = 18.2, 11.3$ Hz, 2H), 4.16 (dd, $J = 11.3, 6.6$ Hz, 2H), 3.34 (s, 3H) 3.28 (s, 3H). ^{31}P NMR (162 MHz, CDCl$_3$) δ -6.60. ^{13}C NMR (101 MHz, CDCl$_3$) δ 147.98, 142.6, 128.2, 123.9, 93.2, 69.5, 67.8, 49.1. ESI-MS positive ion mode *m/z* (MH$^+$, 100%); HRMS (TOF mode) calculated for $C_{12}H_{16}NO_8P$, 334.0686, found 334.0686.

7.13 Hydroxyl cyclic phenyl phosphate triester
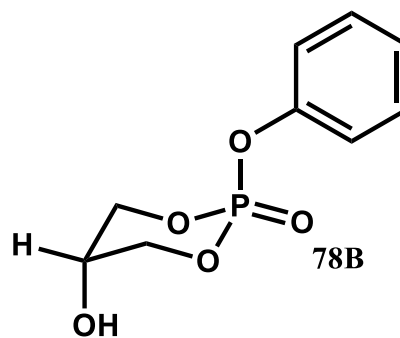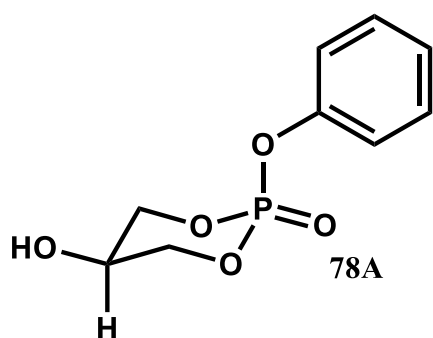
Carbonyl cyclic phenyl phosphate triester **57d** (0.34 g, 8.8 mmol) was dissolved in ethanol (10 mL) at 0-5°C using an ice bath, then sodium borohydride (0.41 g, 10.84 mmol) was added carefully. After that, the solution was stirred at room temperature and the reaction was followed by TLC. After 3 h, the reaction was quenched with acetic acid (0.8 mL) and stirred for 5 min. The precipitate was filtered off and the filtrate was concentrated in *vacuo*. The residue was dissolved in CHCl$_3$ (20 mL) and filtrated again, and the solvent was removed. The crude product was purified over silica using 1:1 pet.ether: EtOAc with R$_f$ = 0.2 to yield 0.21 g, (41%) of **78A** and **78B** as a white solid. ^{1}H NMR (400 MHz, CDCl$_3$) δ 7.42 – 7.35 (m, 2H), 7.27 – 7.20 (m, 3H), 4.41 (ddd, J = 20.0, 10.5, 3.9 Hz, 2H), 4.28 – 4.06 (m, 3H). ^{31}P NMR (162 MHz, CDCl$_3$) δ -12.42 (major isomer), -12.69 (minor isomer). ^{13}C NMR (101 MHz, CDCl$_3$) δ 150.1 (C-O), 130.0, 125.6, 119.6, 72.0, 61.5. ESI-MS positive ion mode *m/z* (MH$^+$, 100%); HRMS (TOF mode) calculated for C$_9$H$_{11}$O$_5$P, 231.0417, found 231.0419.

7.14 Hydroxyl cyclic ethyl phosphate triester
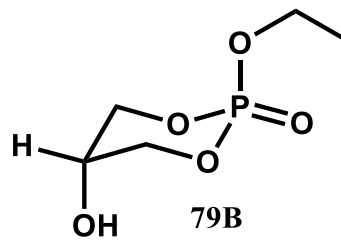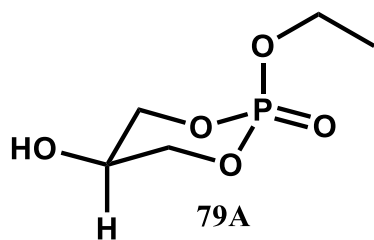
Carbonyl cyclic ethyl phosphate triester **75** (0.5 g, 2.7 mmol) was dissolved in ethanol (10 mL) in an ice bath. Sodium borohydride (0.41 g, 10.84 mmol) was added carefully. After that, the solution was stirred at room temperature and followed by TLC. After 4 h, the reaction was quenched with acetic acid (1 mL) and stirred for 5 min. The precipitate was filtered off and the filtrate was concentrated *in vacuo*. The residue was dissolved in CHCl$_3$ (30 mL) and filtrate again, and the solvent was removed. The crude product was purified over silica using 5% methanol in DCM with R$_f$ = 0.37 to give 0.34 g, (67%) of **79A** and **79B** as a colorless oil. ^{1}H NMR (400 MHz, CDCl$_3$) δ 4.57 – 4.32 (m, 2H), 4.25 – 4.02 (m, 4H), 3.86 (d, *J* = 1.9 Hz, 1H), 1.44 – 1.28 (m, 3H). ^{31}P NMR (162 MHz, CDCl$_3$) δ -6.34 (Major), -8.22 (Minor). ^{13}C NMR (101 MHz, CDCl$_3$) δ 71.7, 64.6, 61.9, 16.1. ESI-MS positive ion mode *m/z* (MH$^+$, 100%); HRMS (TOF mode) calculated for C$_5$H$_{11}$O$_5$P, 183.0000, found 183.0000.

7.14.1 Synthesis of Boc cyclic ethyl phosphate triester
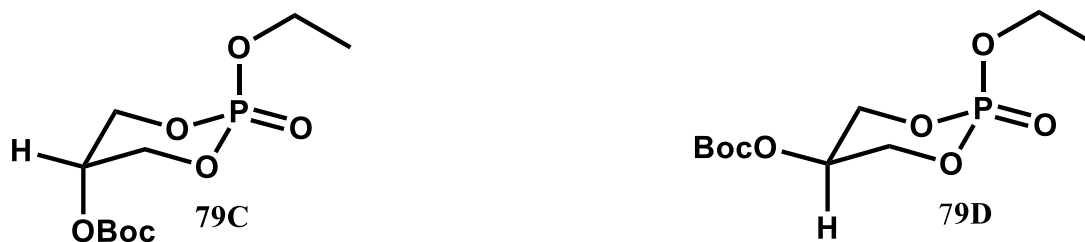
The hydroxyl cyclic ethyl phosphate triester (0.08 g, 0.44 mmol) and (Boc)$_2$O (Di-*tert*-butyl dicarbonate) (0.12 g, 0.55 mmol) were dissolved in acetone (7 mL) and stirred at room temperature for 5 min. Then, DAMP (0.07 g, 0.55 mmol) was added to the solution and the reaction continued to stir overnight. The next day, the solvent was evaporated and the crude product was purified by silica chromatography using 2% MeOH in DCM with R$_f$ = 0.3 to yield 0.1 g, (77%) of **79C** and **79D** as a colorless oil. ^{1}H NMR (400 MHz, CDCl$_3$) δ 4.88 – 4.77 (m, 1H), 4.71 – 4.59 (m, 2H), 4.43 – 4.30 (m, 2H), 4.29 – 4.18 (m, 2H), 1.51 (s, 9H), 1.38 (t, *J* = 7.1 Hz, 3H). ^{31}P NMR (162 MHz, CDCl$_3$) δ -5.95, -9.23.

188

7.15 Kinetic experiments of sulfonate compounds

Compounds **10-12** were studied using UV-vis spectroscopy to measure the rates of the reaction at 50 ± 0.1 °C in a solution of KOH and ionic strength 0.5 M KCl. Compound **10**, was monitored using wavelength 300 nm, (0.1-0.01) M KOH; compound **11** at 320 nm, (0.04-0.07) M KOH; compound **12** at 320 nm, (0.02-0.08) M KOH. The reactions were initiated by adding 5-15 µl of 0.05 M stock solution which was dissolved in DMSO or dioxane to 3 ml of KOH solution which had been equilibrated for 8-10 min at 50 ± 0.1°C.

The rate constant was calculated for 0.1 M KOH to allow us to compare these data with results of a previously reported study.[55] The pK_a values of compounds **13-15** were taken from the literature. Compound **15** has the pK_a 4.96[144] while for compound **13** and **14** is 8.42[144] and 6.45 respectively. The Hammett sigma values were taken from the literature: 3-hydroxy pyridine σ = 0.67[145], *N*-oxide 3-hydroxy pyridine σ = 1.59[146], *N*-methyl pyridinium 3-hydroxy σ = 2.31[145] and others sigma values were taken from the literature.[130]

7.16 Kinetic measurements of substituted pyridyl phenyl sulfate diester

The kinetics of substituted pyridyl phenyl sulfate diester was measured spectrophotometrically in 10% dioxane at 40 °C and the ionic strength maintained to 1 M NaCl. Compound **35** which was dissolved in dioxane was monitored using a wavelength of 300 nm, (0.05-0.8) M NaOH. Compound **36** in dioxane at 320 nm, (0.05-0.7) M NaOH. Compound **37** in D.W at 320 nm, (0.02-0.5) M NaOH. The compounds **35-37** was initiated by adding (10 -30) µL of a stock solution 0.01 M to 3 mL of NaOH which equilibrated at 40 °C for 10 min.

The pK_a values of leaving the group (3-hydroxy, 3-hydroxy-*N*-oxide, 3-hydroxy-*N*-methyl) pyridine **13-15** were measured under the same conditions of kinetic experiments 40°C, 1 M NaCl, 10% dioxane. Buffer solutions 5 mM of (acetic acid, MES, MOPS, EPPS, CHES, CAPS) used over the pH range 3-11. The pH was measured after each addition of aliquots of 1 M

NaOH and the UV scan was taken after each measurement.

7.17 The kinetic measurements of phosphate diesters

The hydrolysis of methyl phosphate diesters was implemented at 42 ˚C, (0.05-0.9) M NaOH and ionic strength was adjusted to 1 M using NaCl. The absorbance of the product *N*-oxide **28** and *N*-methyl pyridyl **29** was followed at 320 nm. The solution equilibrated for 10 min at 42 ± 0.2 °C before initiating the reaction by adding the substrate (dissolved in dioxane or water) to achieve a final concentration of 100 µM. For slow rate reactions, the rate was measured using an initial rate and varying the concentration of substrate 10 fold (100-1000) µM.

7.18 pK_a measurements of pyridyl leaving groups at 40 ºC

The pK_a measurements of the leaving groups (*N*-methyl pyridyl and *N*-oxide pyridyl) were performed by using UV probe and pH meter to take the full scan at each pH at the same time at 42 ± 0.2 °C and 1 M NaCl, 50-100 µM substrate.

The buffer that was used in titration was 5 mM of HCl, acetic acid, MOPS, EPPS, CHES, CAPS. The full scan for the substrate was taken after each addition of an aliquot of the base (1 M NaOH) and pH was measured. Then the pK_a value was obtained by plotting the absorbance that gives λ max which was at 320 nm for compound **14** and **15** against the pH and, the data were fitted to the following equation:

$$\text{Abs} = \text{Abs}_A - \left(\frac{K_a}{K_a + [H^+]}\right) + \text{Abs}_{HA}\left(\frac{[H^+]}{K_a + [H^+]}\right) \qquad \textbf{Equation 20}$$

7.19 Hydrolysis of phosphate triesters (cyclic, alkene, dimethoxy)

The hydrolysis of **55-59** was studied using UV-vis spectroscopy to measure the rates of reaction at 25 °C and adjusted to 1 M NaCl ionic strength. The measurements were performed between pH = 0-13 for **55**, **56a** and **59**. The pHs of the solutions 4-11 were maintained using various buffer solutions (MOPS, MES, EPPS, HEPES, CAPS) with 0.05 M as a final buffer concentration. When the pH was above 11, sodium hydroxide was used and for pH 0-3 hydrochloric acid was used to get the required pH. The reactions were monitored at 400 nm for neutral to basic conditions and 320 nm in acidic regions.

For compounds **56b-f**, sodium hydroxide solutions were used for the alkaline hydrolysis reactions. Compound **56b** (3-nitro) was monitored using wavelength 390 nm (0.002-0.05) M NaOH, compound **56c** (3-Cl) at 290 nm (0.002-0.05) M NaOH, compound **56d** (phenyl) at 285 nm (0.005-0.1) M NaOH, compound **56e** (4-methoxy) at 305 nm, and **56f** (3,4-dimethyl) at 295 nm (0.03-0.15) M NaOH. All the substrates were dissolved in DMSO with a concentration of (0.02-0.05) M as a stock solution. The reactions were initiated by adding 5-15 µL of the substrate to 3 mL of either buffer or sodium hydroxide solution to get (50-150) µM of the substrate. For slow reactions, an initial rate method was used and 10 times high concentration of the substrate was added (500 µM) as an average.

7.20 pK_a measurements of phenols at 25 °C

Brønsted plots rely on pK_a values and these pK_a values can be affected by the conditions of experiments such as temperature, solvent, and ionic strength. Thus, the pK_a values of all corresponding phenols were measured at 25 ± 0.1°C and 1 M NaCl.

The pK_a measurements were carried out by UV-vis titrations. UV scans were taken for the substrate over a range of 240-500 nm after an addition of a certain amount of sodium hydroxide and the pH was measured simultaneously. Then, the absorbance at wavelength when a large change is observed was taken and plotted against the measured pH to get pK_a after fitting to the equation 18. As can be seen from the **Figures 108-113**, all the plots gave good isosbestic points. The measured pK_as were close to the pK_as in the published literature.
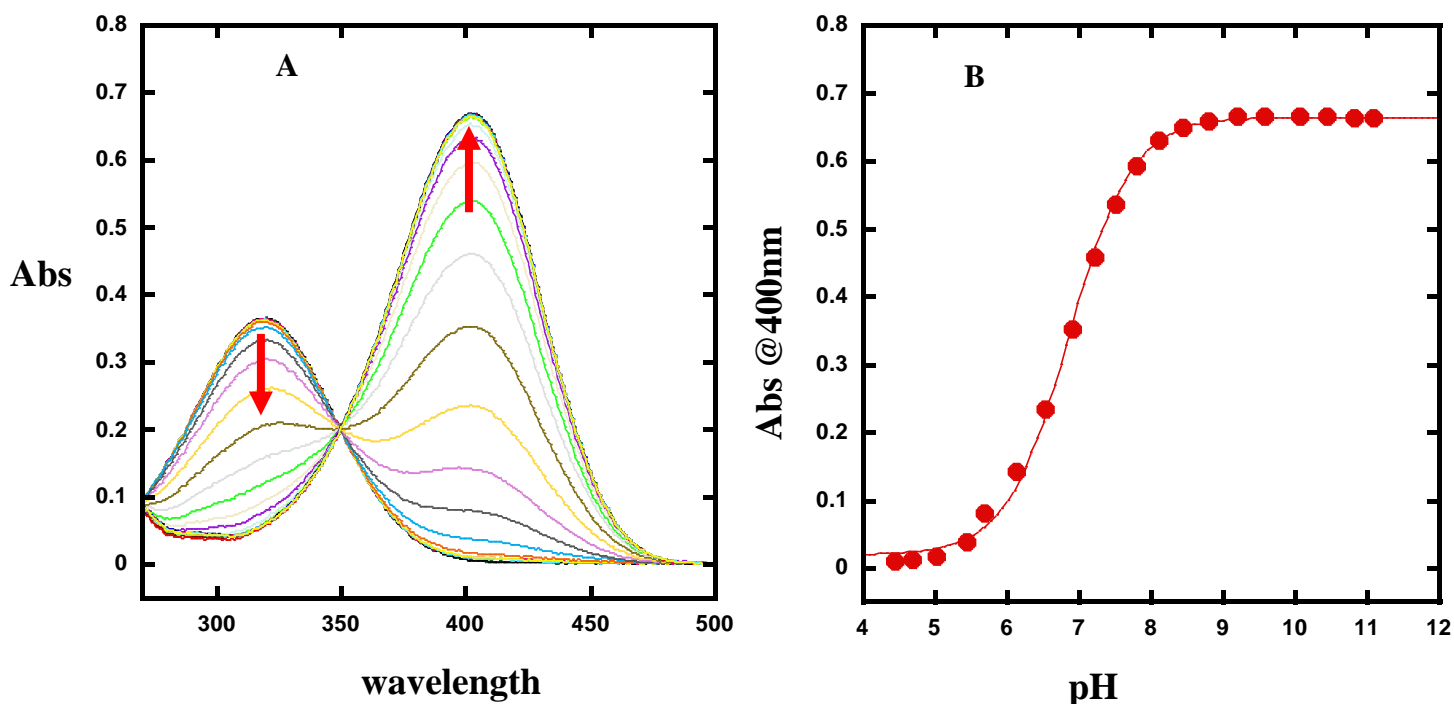
Figure 108: A: UV titration of 4-nitrophenol, **B**: dependence of absorbance on pH, 1 M NaCl, 25 °C; pK_a = 6.86 $\pm$ 0.02; R^2 = 0.998.
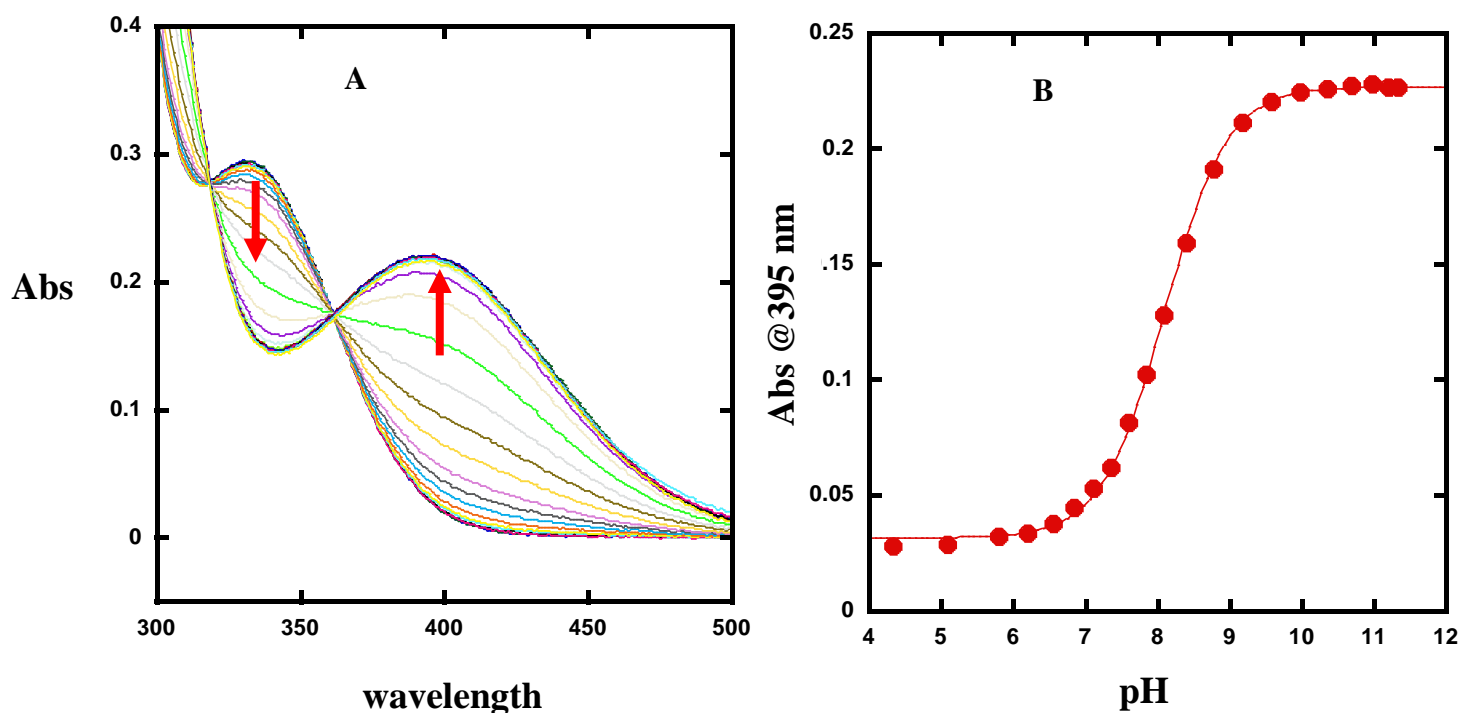
Figure 109: A: UV titration of 3-nitrophenol, **B**: dependence of absorbance on pH, 1 M NaCl, 25 °C; pK_a = 8.1 ± 0.01; R^2 = 0.999.
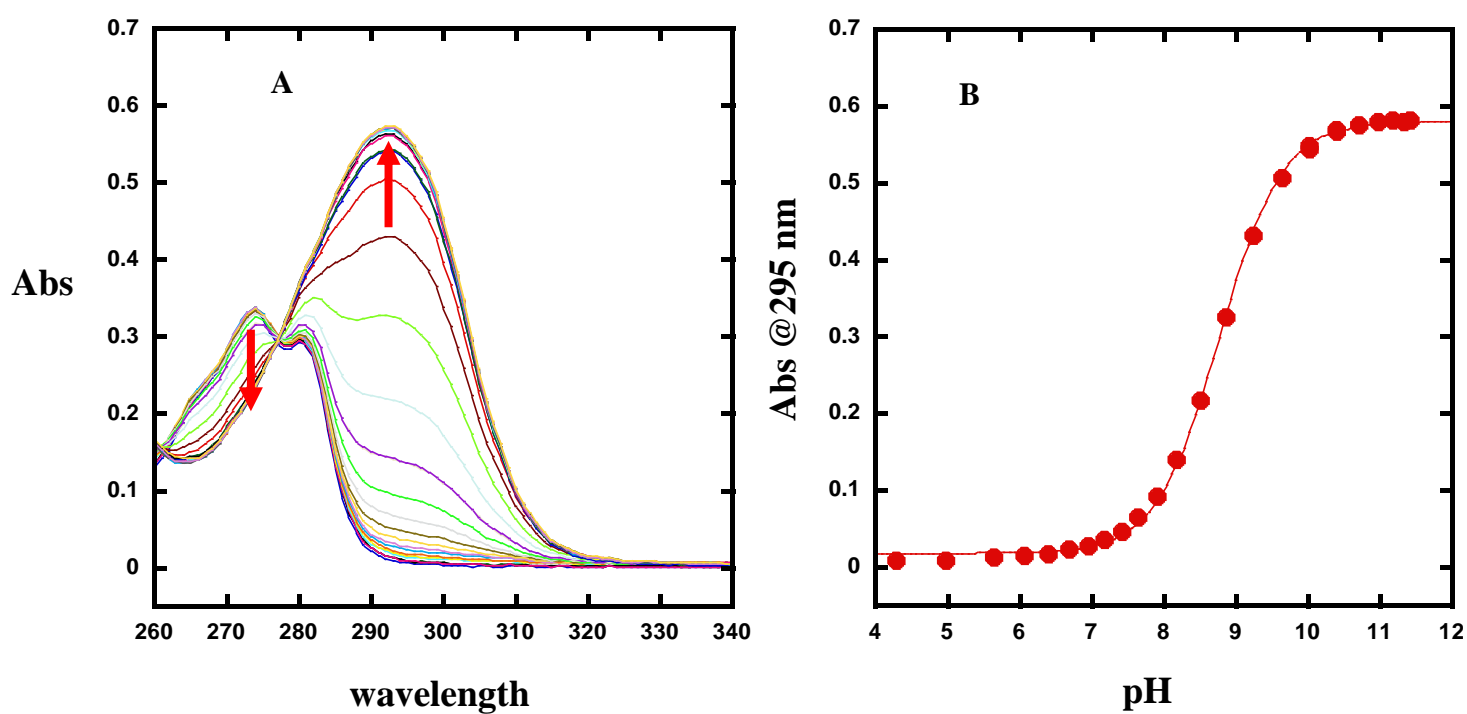
Figure 110: A: UV titration of 3-chlorophenol, **B**: dependence of absorbance on pH, 1 M NaCl, 25 °C, pK_a = 8.77 ± 0.01; R^2 = 0.999.
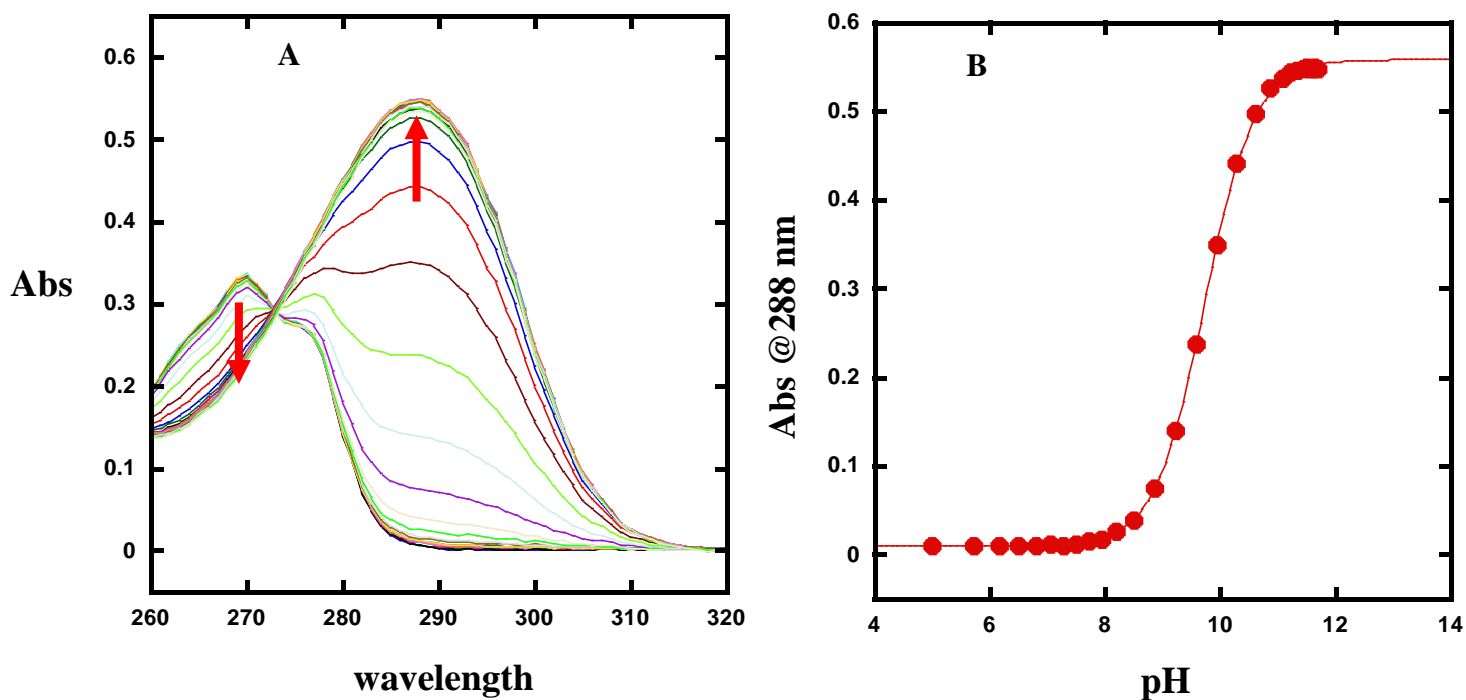
Figure 111: A: UV titration of phenol, **B**: dependence of absorbance on pH, 1 M NaCl, 25 °C; $pK_a = 9.73 \pm 0.005$; $R^2 = 0.999$.
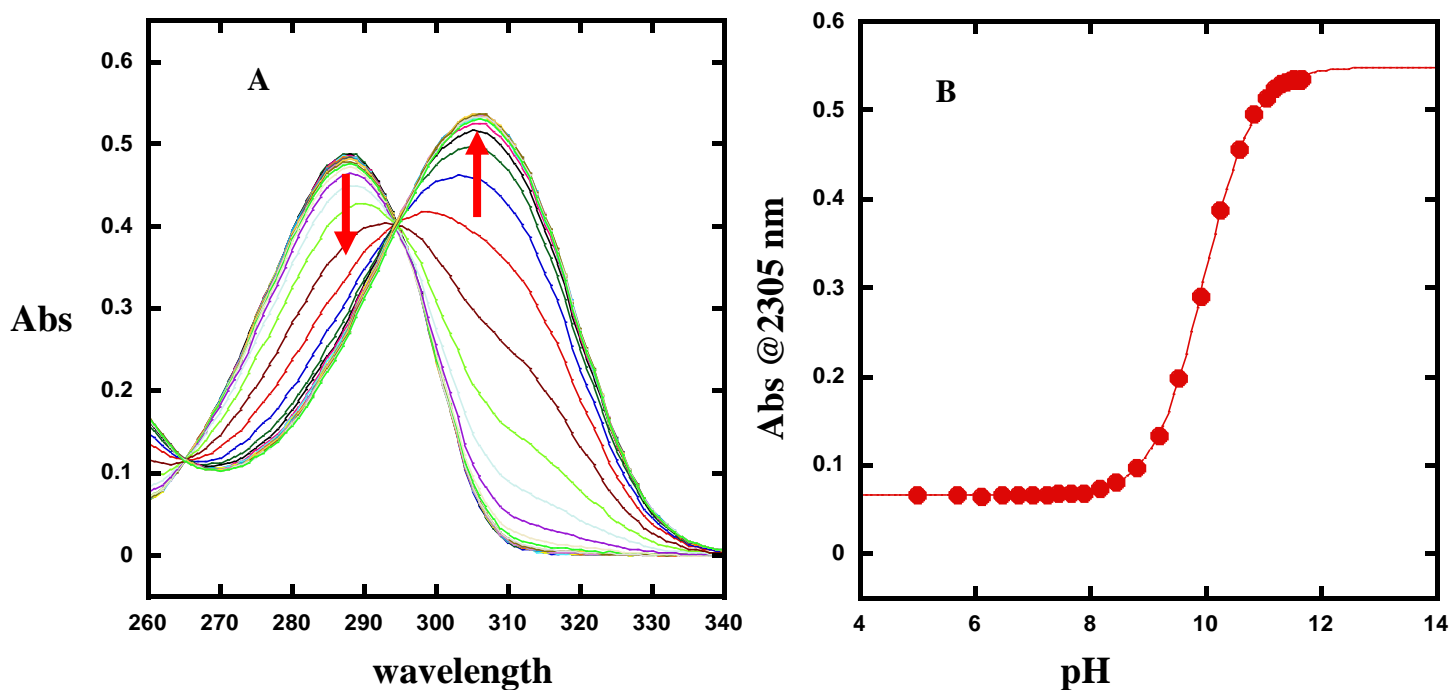
Figure 112: A: UV titration of 4-methoxyphenol, **B**: dependence of absorbance on pH, 1 M NaCl, 25 °C; $pK_a = 9.97 \pm 0.005$; $R^2 = 0.999$.

194
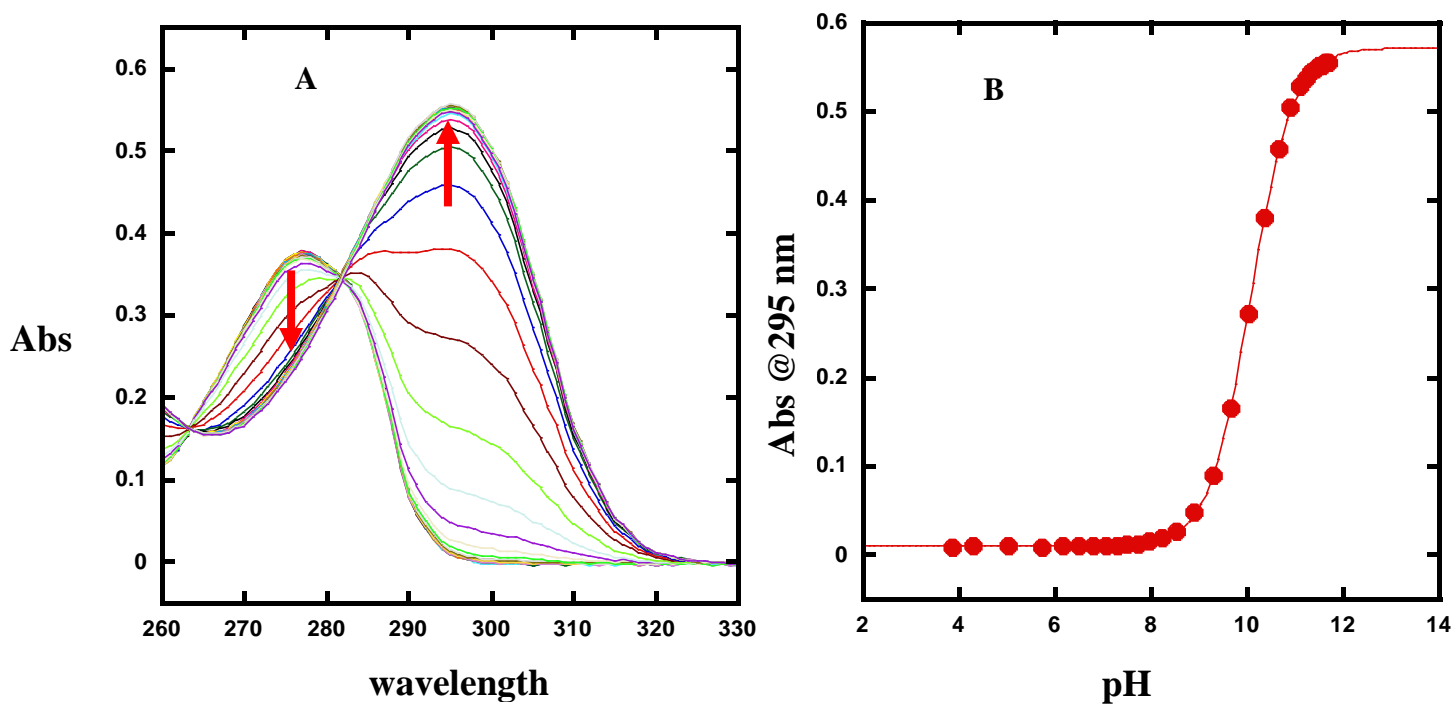
Figure 113: A: UV titration of 3,4-dimethylphenol, **B**: dependence of absorbance on pH, 1 M NaCl, 25 °C; pK_a = 10.1 ± 0.01; R^2= 0.999.

The data of pK_a measurements (**Figures 108B-113B**) were fitted to equation 21:

$$\text{Abs} = \text{Abs}_A - \left(\frac{K_a}{K_a+[H^+]} \right) + \text{Abs}_{HA} \left(\frac{[H^+]}{K_a+[H^+]} \right) \qquad \textbf{Equation 21}$$

7.21 Hydrolysis of carbonyl cyclic substituted phenyl phosphate triesters

The kinetic measurements of carbonyl compounds (**57a-f**) were carried out using UV-vis spectroscopy at 25 °C and 1 M NaCl. A pH ranges 4-10 was obtained by adding a base to the various buffer solutions (HCl, acetate, MOPS, MES, EPPS, HEPES, CHES and CAPS) with 0.05 M as a buffer concentration. Compound **57a** (4-nitro) was monitored using wavelength at 320 nm, pH (0-5.2); compound **57b** (3-nitro) at 330 nm, pH (4.9-7), compound **57c** (3-chloro) at 275 nm, pH (5.5-8.6); compound **57d** (phenyl) at 270 nm, pH (6.5-9.35); compound **57e** (4-methoxy) at 288 nm, pH (7.5-9.72); compound **57f** (3,4-dimethyl) at 280 nm, pH (7.2-9.9).

All the substrates were dissolved in DMSO with concentration (0.02-0.05) M as a stock solution. The reaction was initiated by adding 5-15 µL of the substrate to 3 mL of buffer to yield (50-150) µM of the substrate.
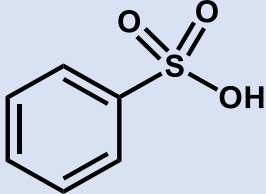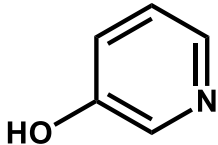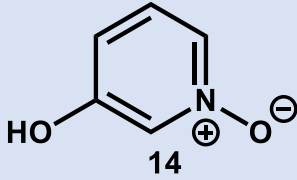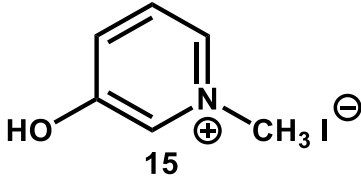
7.22 Product analyses for the hydrolyses of sulfonate esters

The products for the hydrolysis of pyridyl sulfonate ester and its derivatives (**10-12**) were analysed using 150 mm × 4.60 mm column in a HP 1100 Series HPLC, after complete hydrolysis. These compounds were mointered at 260 nm, the wavelength that detects the leaving groups and phenyl sulfonate. The injection volume was 30 µL and the solvent system was 0.1% TFA in distilled water with acetonitrile as illustrated in **Table 8**. The concentration of substrate was 2 mM in 0.05 M KOH and 1 M NaCl. The high concentration of substrate was used since compound (**16**) has a low extinction coefficient.

Time/min	CH$_3$CN %	0.1% TFA in D.W %	Flow rate mL/min
0	5	95	1
7	40	60	1
10	40	60	1
14	50	50	1
16	40	60	1
18	5	95	1
20	5	95	1

Table 8: Solvent system used in HPLC analysis to check the hydrolysis products of aryl benzene sulfonate esters **10-12**.

The products after hydrolysis were phenyl sulfonate **16** and leaving group compounds **13**, **14** and **15** respectively. The leaving groups (**13-15**) and compound **16** were injected separately and gave the same retention times which confirms their identities (**Table 9**).

Sulfonate esters	Product structure	R.t/min
10-12	 **16**	3.0
10	 **13**	2.4
11	 **14**	2.3
12	 **15**	2.0
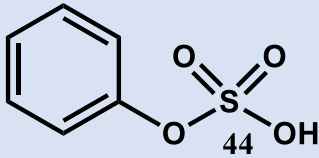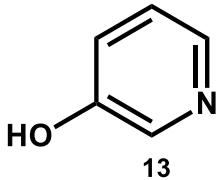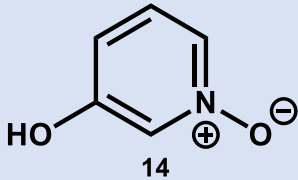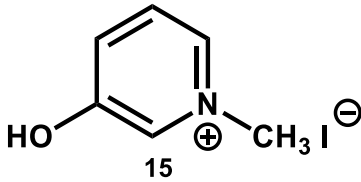
Table 9: The retention time and compound structure after hydrolysis of aryl benzene sulfonate esters **10-12**.

7.23 Product analysis for the hydrolysis of sulfate diesters

The products for the hydrolysis of substituted pyridyl phenyl sulfate diester were analysed by UV-vis and HPLC (using 150 mm × 4.60 mm column). UV scans were taken for the products after complete hydrolysis and they gave absorbance at wavelengths 300 nm, 320 nm and 320 nm which are corresponding to leaving groups of 3-hydoxy pyridine, 3-hydroxy pyridine *N*-oxide and 3-hydroxy *N*-methyl pyridinium respectively. Furthermore, the products of **35-37** after hydrolysis were injected in HPLC. The solvent system was 0.1% TFA in water with CH$_3$CN (**Table 10**) and the compounds monitored at 260 nm. The concentration of substrate was 2 mM in 0.2 M NaOH and adjusted with 1 M NaCl. The analysis from HPLC confirm the presence of the leaving group and phenyl sulfate monoester as shown in **Table 11**.

Time/min	CH$_3$CN %	0.1% TFA in D.W %	Flow rate mL/min
0	10	90	1
7	30	70	1
10	40	60	1
16	50	50	1
23	10	90	1
25	10	90	1

Table 10: The Solvent system used in HPLC analysis to check the hydrolysis products of substituted pyridyl phenyl sulfate diesters. **35-37**.

Sulfate diester	Product structure	R.t/min
35-37	**44**	3.8
35	**13**	2.7
36	**14**	1.9
37	**15**	1.8
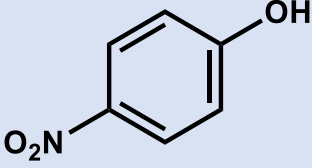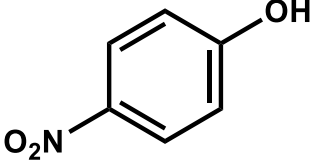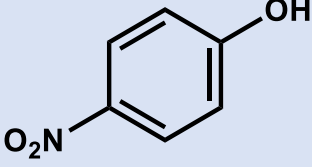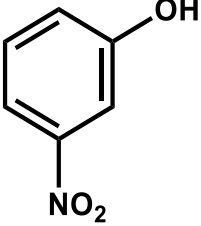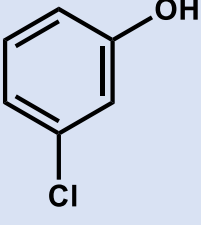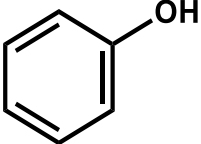
Table 11: The retention time and compounds structure after hydrolysis of substituted pyridyl sulfate diester **35-37**.
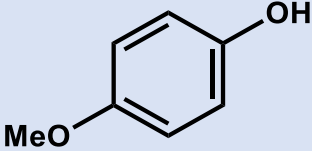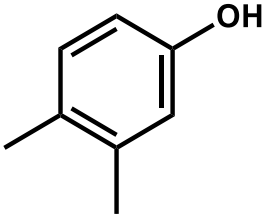
7.24 Product analysis for the hydrolysis of phosphate triesters

The products of **55**, **56a-f** and **59** after hydrolysis were analyzed by HPLC (using 150 mm ×
4.60 mm column in a HP 1100 Series HPLC). The concentrations of substrates were (50-150)
μ M and monitored using wavelength at 270 nm. The 30 μL of the solution was injected into
HPLC by the automated sampler, and loaded into column which used the solvent system as
described in **Table 12**. The analysis of products were corresponds to phenols as illustrated in
Table 13.

Time/min	CH₃CN %	0.1% TFA in D.W %	Flow rate mL/min
0	10	90	1
7	30	70	1
10	40	60	1
14	50	50	1
16	40	60	1
18	5	95	1
20	5	95	1

Table 12 : Solvent system that used in HPLC to check the product of hydrolysis **55**, **56a-f** and
59.

201

Substrate	Product structure	R.t/ min
Cyclic 55	O_2N—C6H4—OH	9.56
Dimethoxy 59	O_2N—C6H4—OH	9.56
Alkene -4- nitro 56a	O_2N—C6H4—OH	9.68
Alkene -3- nitro 56b	C6H4(OH)(NO_2)	9.74
Alkene -3- chloro 56c	C6H4(OH)(Cl)	11.78
Alkene Phenyl 56d	C6H5—OH	7.1

Alkene -4- methoxy 56e		6.89
Alkene-3,4-dimethyl 56f		11.6

Table 13: Structure and retention time of substrate and products of phosphate triesters.
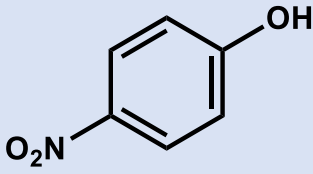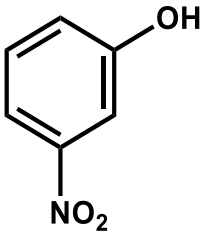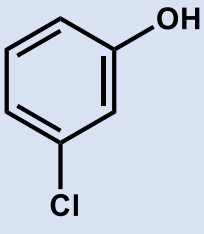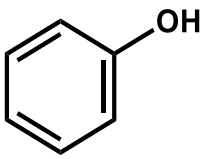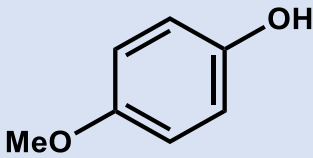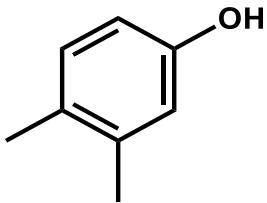
7.25 Product analysis of carbonyl cyclic phosphate triester

The products of carbonyl compounds **57a-f** after hydrolysis were analyzed by HPLC (using 150 mm × 4.60 mm column in a HP 1100 Series HPLC). The concentrations of substrates were (50-150) µM and monitored using wavelength at 270 nm. The 30 µL of the solution was injected into HPLC by the automated sampler, and loaded into column which used the solvent system as described in **Table 14**. The analysis of products were corresponds to phenols as illustrated in **Table 15**. Comparison the products of **57a-f** with the products of carbonyl and dimethoxy 4-nitrobenzyl **65** and **66** confirm that the pK_a of the leaving group has an impact on the mechanism of the reaction since the reaction of **65** and **66** gave alcohol and new product as has been described.

Time/min	CH$_3$CN %	0.1% TFA in D.W %	Flow rate mL/min
0	10	90	1
7	30	70	1
10	40	60	1
14	50	50	1
16	40	60	1
18	5	95	1
20	5	95	1

Table 14: Solvent system used in HPLC to check the product of hydrolysis carbonyl **57a-f**.

Substrate	Product structure	R.t/ min
Carbonyl -4-nitro 57a		9.76
Carbonyl -3-nitro 57b		9.77
Carbonyl -3-chloro 57c		11.77
Carbonyl -Phenyl 57d		7.15
Carbonyl -4-methoxy 57e		6.86
Carbonyl -3,4-dimethyl 57f		11.62
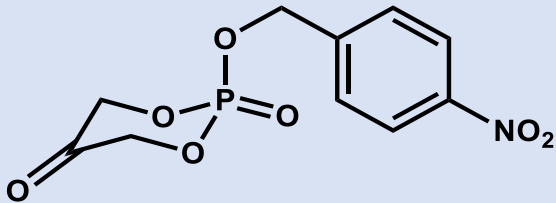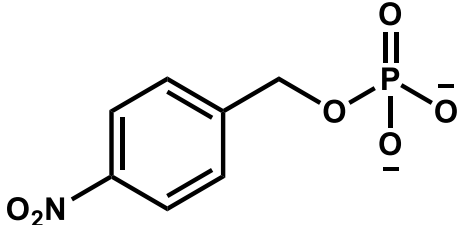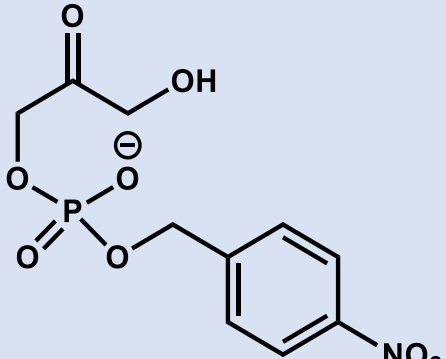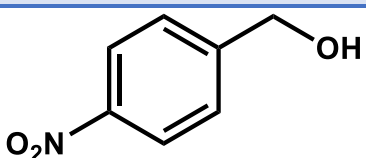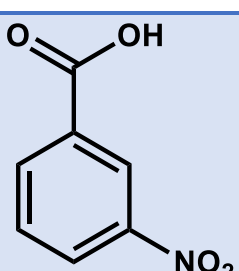
Table 15: Structure and retention time of products for carbonyl compounds **57a-f**.

7.26 Studying the hydrolysis of carbonyl and dimethoxy cyclic 4-nitrobenzyl phosphate triester by HPLC
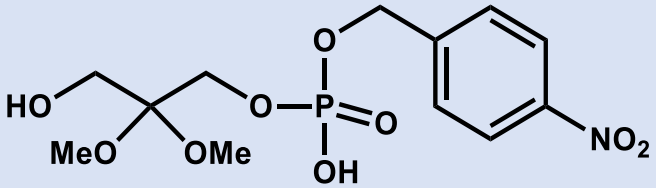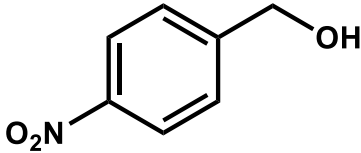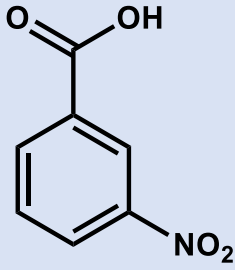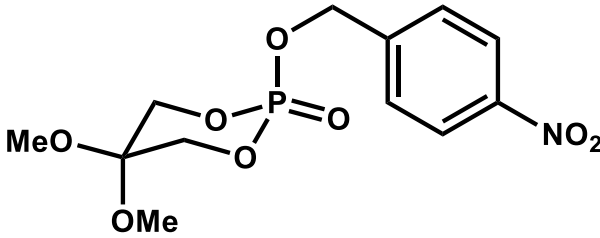
Stock solution 0.01 M of compounds **65** (carbonyl) and **66** (dimethoxy) and 3-nitrobenzoic acid as an internal standard. The reaction was monitored at 270 nm by following the appearance the products and disappearance of the substrate. The rate of reactions was measured over the pH range (8-13) using buffer solutions of (EPPS, CHES, and CAPS) and sodium hydroxide at 25 °C and 1M NaCl. The reaction was initiated by adding 25 µL of internal standard and 125 µL to 5 ml of buffer or sodium hydroxide solutions to yield 50 µM and 250 µM respectively. The aliquits (30 µL) was taken regularly by an automated sampler of the HPLC and loaded into column (using 150 mm × 4.60 mm column in a HP 1100 Series HPLC). The solvent system and retention time of compounds **65** and **66** are displayed in the **Table 17**. For fast reactions at pH 11-13, the reaction was quenched with MOPS buffer and the same process was repeated to measure the rate of reactions.

Time/min	CH$_3$CN %	0.1% TFA in D.W %	Flow rate mL/min
0	5	95	1
7	40	60	1
10	40	60	1
14	90	10	
16	40	60	1
18	5	95	1
20	5	95	1

Table 16: The Solvent system used in HPLC analysis to study the hydrolysis of compounds **65** and **66**.

Compound	Compound structure	R.t/min
Substrate 65		7.90
Product 2		5.60
Intermediate		5.40
Product 1		7.80
Internal standard		8.90

Table 17: Structure and retention times of substrate and products and internal standard for hydrolysis of **65** by HPLC.

Compound	Compound structure	R.t/Min
Product 2		7.10
Product 1		7.90
Internal standard		8.90
Substrate 66		11.10

Table 18: Structure and retention time of substrate and products and internal standard for hydrolysis of **66** by HPLC.

References

(1) Cleland, W. W.; Hengge, A. C. Enzymatic mechanisms of phosphate and sulfate transfer. *Chem. Rev. (Washington, DC, U. S.)* **2006**, *106*, 3252-3278.

(2) Lassila, J. K.; Zalatan, J. G.; Herschlag, D. Biological phosphoryl-transfer reactions: Understanding mechanism and catalysis. *Annu. Rev. Biochem.* **2011**, *80*, 669-702.

(3) Ball, L. T.; Lloyd-Jones, G. C.; Russell, C. A. Gold-Catalyzed Oxidative Coupling of Arylsilanes and Arenes: Origin of Selectivity and Improved Precatalyst. *J. Am. Chem. Soc.* **2014**, *136*, 254-264.

(4) Rosta, E.; Kamerlin, S. C. L.; Warshel, A. On the Interpretation of the Observed Linear Free Energy Relationship in Phosphate Hydrolysis: A Thorough Computational Study of Phosphate Diester Hydrolysis in Solution. *Biochemistry* **2008**, *47*, 3725-3735.

(5) Westheimer, F. H. Monomeric metaphosphates. *Chem. Rev.* **1981**, *81*, 313-326.

(6) Wolfenden, R.; Yuan, Y. Monoalkyl sulfates as alkylating agents in water, alkylsulfate rate enhancements, and the "energy-rich" nature of sulfate half-esters. *Proc. Natl. Acad. Sci. U. S. A.* **2007**, *104*, 83-86.

(7) Greig, I. R. The analysis of enzymic free energy relationships using kinetic and computational models. *Chem. Soc. Rev.* **2010**, *39*, 2272-2301.

(8) Zalatan, J. G.; Catrina, I.; Mitchell, R.; Grzyska, P. K.; O'Brien, P. J.; Herschlag, D.; Hengge, A. C. Kinetic Isotope Effects for Alkaline Phosphatase Reactions: Implications for the Role of Active-Site Metal Ions in Catalysis. *J. Am. Chem. Soc.* **2007**, *129*, 9789-9798.

(9) Hoff, R. H.; Larsen, P.; Hengge, A. C. Isotope Effects and Medium Effects on Sulfuryl Transfer Reactions. *J. Am. Chem. Soc.* **2001**, *123*, 9338-9344.

(10) Khan, S. A.; Kirby, A. J. Reactivity of phosphate esters. Multiple structure-reactivity correlations for the reactions of triesters with nucleophiles. *J. Chem. Soc. B* **1970**, 1172-1182.

(11) Lad, C.; Williams, N. H.; Wolfenden, R. The rate of hydrolysis of phosphomonoester dianions and the exceptional catalytic proficiencies of protein and inositol phosphatases. *Proc. Natl. Acad. Sci. U. S. A.* **2003**, *100*, 5607-5610.

(12) Herschlag, D.; Jencks, W. P. Pyrophosphate formation for acetyl phosphate and orthophosphate anions in concentrated aqueous salt solutions does not provide evidence for a metaphosphate intermediate. *J. Am. Chem. Soc.* **1986**, *108*, 7938-7946.

(13)   Kamerlin, S. C. L. Theoretical Comparison of p-Nitrophenyl Phosphate and Sulfate Hydrolysis in Aqueous Solution: Implications for Enzyme-Catalyzed Sulfuryl Transfer. *J. Org. Chem.* **2011**, *76*, 9228-9238.

(14)   Kamerlin, S. C. L.; Wilkie, J. The role of metal ions in phosphate ester hydrolysis. *Org. Biomol. Chem.* **2007**, *5*, 2098-2108.

(15)   Zalatan, J. G.; Herschlag, D. Alkaline Phosphatase Mono- and Diesterase Reactions: Comparative Transition State Analysis. *J. Am. Chem. Soc.* **2006**, *128*, 1293-1303.

(16)   Hammett, L. P.: *Physical Organic Chemistry; Reaction Rates, Equilibria, and Mechanisms (McGraw-Hill Series in Advanced Chemistry). 2nd ed*; McGraw-Hill, 1970.

(17)   Jaffe, H. H. A re.ovrddot.examination of the Hammett equation. *Chem. Rev. (Washington, DC, U. S.)* **1953**, *53*, 191-261.

(18)   Clayden, J.; Greeves, N.; Warren, S.; Wothers, P.: *Organic Chemistry*; Oxford University Press, 2000.

(19)   Hine, J. Polar effects on rates and equilibriums. *J. Am. Chem. Soc.* **1959**, *81*, 1126-1129.

(20)   Hine, J. Polar effects on rates and equilibriums. III. *J. Am. Chem. Soc.* **1960**, *82*, 4877-4880.

(21)   Bronsted, J. N. Acid and basic catalysis. *Chem. Rev. (Washington, DC, U. S.)* **1928**, *5*, 231-338.

(22)   Hammett, L. P. Effect of structure upon the reactions of organic compounds. Benzene derivatives. *J. Am. Chem. Soc.* **1937**, *59*, 96-103.

(23)   Williams, A.: *Free Energy Relationships in Organic and Bio-Organic Chemistry*; Royal Society of Chemistry, 2003.

(24)   Page, M.; Williams, A.: *Organic and Bio-Organic Mechanisms*; Longman, 1997.

(25)   Admiraal, S. J.; Herschlag, D. Mapping the transition state for ATP hydrolysis: implications for enzymic catalysis. *Chem. Biol.* **1995**, *2*, 729-739.

(26)   Williams, N. H.; Cheung, W.; Chin, J. Reactivity of Phosphate Diesters Doubly Coordinated to a Dinuclear Cobalt(III) Complex: Dependence of the Reactivity on the Basicity of the Leaving Group. *J. Am. Chem. Soc.* **1998**, *120*, 8079-8087.

(27)   Kirby, A. J.; Younas, M. Reactivity of phosphate esters. Diester hydrolysis. *J. Chem. Soc. B* **1970**, 510-513.

(28) Hammett, L. P. Some relations between reaction rates and equilibrium constants. *Chem. Rev.* **1935**, *17*, 125-136.

(29) Sykes, P.: *A Guidebook to Mechanism in Organic Chemistry. 6th Ed*; Longman, 1986.

(30) Clayden, J.; Greeves, N.; Warren, S.: *Organic chemistry*; Oxford university press: Oxford, 2012.

(31) Yukawa, Y.; Tsuno, Y. Resonance effect in Hammett relation. III. The modified Hammett relation for electrophilic reactions. *Bull. Chem. Soc. Jpn.* **1959**, *32*, 971-981.

(32) Um, I.-H.; Han, J.-Y.; Hwang, S.-J. Analysis of linear free-energy relationships combined with activation parameters assigns a concerted mechanism to alkaline hydrolysis of X-substituted phenyl diphenylphosphinates. *Chem. - Eur. J.* **2008**, *14*, 7324-7330.

(33) Nakata, K.; Fujio, M.; Nishimoto, K.; Tsuno, Y. Theoretical study of substituent effects on the gas-phase stabilities of phenoxide anions. *J. Phys. Org. Chem.* **2013**, *26*, 115-123.

(34) Feng, G.; Tanifum, E. A.; Adams, H.; Hengge, A. C.; Williams, N. H. Mechanism and Transition State Structure of Aryl Methylphosphonate Esters Doubly Coordinated to a Dinuclear Cobalt(III) Center. *J. Am. Chem. Soc.* **2009**, *131*, 12771-12779.

(35) Blandamer, M. J.; Burgess, J.; Robertson, R. E.; Scott, J. M. W. Dependence of equilibrium and rate constants on temperature and pressure. *Chem. Rev.* **1982**, *82*, 259-286.

(36) O'Brien, P. J.; Herschlag, D. Catalytic promiscuity and the evolution of new enzymatic activities. *Chem. Biol.* **1999**, *6*, R91-R105.

(37) Olguin, L. F.; Askew, S. E.; O'Donoghue, A. C.; Hollfelder, F. Efficient Catalytic Promiscuity in an Enzyme Superfamily: An Arylsulfatase Shows a Rate Acceleration of 1013 for Phosphate Monoester Hydrolysis. *J. Am. Chem. Soc.* **2008**, *130*, 16547-16555.

(38) Jensen, R. A. Enzyme recruitment in evolution of new function. *Annu. Rev. Microbiol.* **1976**, *30*, 409-425.

(39) Babtie, A.; Tokuriki, N.; Hollfelder, F. What makes an enzyme promiscuous? *Curr. Opin. Chem. Biol.* **2010**, *14*, 200-207.

(40) Pabis, A.; Kamerlin, S. C. L. Promiscuity and electrostatic flexibility in the alkaline phosphatase superfamily. *Curr. Opin. Struct. Biol.* **2016**, *37*, 14-21.

(41) van Loo, B.; Jonas, S.; Babtie, A. C.; Benjdia, A.; Berteau, O.; Hyvonen, M.; Hollfelder, F. An efficient, multiply promiscuous hydrolase in the alkaline phosphatase superfamily. *Proc. Natl. Acad. Sci. U. S. A.* **2010**, *107*, 2740-2745, S2740/2741-S2740/2713.

(42)   Pabis, A.; Duarte, F.; Kamerlin, S. C. L. Promiscuity in the Enzymatic Catalysis of Phosphate and Sulfate Transfer. *Biochemistry* **2016**, *55*, 3061-3081.

(43)   Mohamed, M. F.; Hollfelder, F. Efficient, crosswise catalytic promiscuity among enzymes that catalyze phosphoryl transfer. *Biochim. Biophys. Acta, Proteins Proteomics* **2013**, *1834*, 417-424.

(44)   Duarte, F.; Amrein, B. A.; Kamerlin, S. C. L. Modeling catalytic promiscuity in the alkaline phosphatase superfamily. *Phys. Chem. Chem. Phys.* **2013**, *15*, 11160-11177.

(45)   Williams, N. H.; Takasaki, B.; Wall, M.; Chin, J. Structure and Nuclease Activity of Simple Dinuclear Metal Complexes: Quantitative Dissection of the Role of Metal Ions. *Acc. Chem. Res.* **1999**, *32*, 485-493.

(46)   Khersonsky, O.; Roodveldt, C.; Tawfik, D. S. Enzyme promiscuity: evolutionary and mechanistic aspects. *Curr. Opin. Chem. Biol.* **2006**, *10*, 498-508.

(47)   Aharoni, A.; Gaidukov, L.; Khersonsky, O.; McQ, G. S.; Roodveldt, C.; Tawfik, D. S. The 'evolvability' of promiscuous protein functions. *Nat Genet* **2005**, *37*, 73-76.

(48)   Jensen, R. A. Enzyme recruitment in evolution of new function. *Annu. Rev. Microbiol.* **1976**, *30*, 409-425.

(49)   Hollfelder, F.; Herschlag, D. The nature of the transition state for enzyme-catalyzed phosphoryl transfer. Hydrolysis of O-aryl phosphorothioates by alkaline phosphatase. *Biochemistry* **1995**, *34*, 12255-12264.

(50)   Lassila, J. K.; Zalatan, J. G.; Herschlag, D. Biological phosphoryl-transfer reactions: Understanding mechanism and catalysis. *Annu. Rev. Biochem.* **2011**, *80*, 669-702.

(51)   Kamerlin, S. C. L.; Sharma, P. K.; Prasad, R. B.; Warshel, A. Why nature really chose phosphate. *Q. Rev. Biophys.* **2013**, *46*, 1-132.

(52)   Kamerlin, S. C. L. Theoretical Comparison of p-Nitrophenyl Phosphate and Sulfate Hydrolysis in Aqueous Solution: Implications for Enzyme-Catalyzed Sulfuryl Transfer. *J. Org. Chem.* **2011**, *76*, 9228-9238.

(53)   Edwards, D. R.; Lohman, D. C.; Wolfenden, R. Catalytic Proficiency: The Extreme Case of S-O Cleaving Sulfatases. *J. Am. Chem. Soc.* **2012**, *134*, 525-531.

(54)   McWhirter, C.; Lund, E. A.; Tanifum, E. A.; Feng, G.; Sheikh, Q. I.; Hengge, A. C.; Williams, N. H. Mechanistic Study of Protein Phosphatase-1 (PP1), A Catalytically Promiscuous Enzyme. *J. Am. Chem. Soc.* **2008**, *130*, 13673-13682.

(55) Babtie, A. C.; Lima, M. F.; Kirby, A. J.; Hollfelder, F. Kinetic and computational evidence for an intermediate in the hydrolysis of sulfonate esters. *Org. Biomol. Chem.* **2012**, *10*, 8095-8101.

(56) Wolfenden, R.; Yuan, Y. Monoalkyl sulfates as alkylating agents in water, alkylsulfate rate enhancements, and the "energy-rich" nature of sulfate half-esters. *Proc. Natl. Acad. Sci. U. S. A.* **2007**, *104*, 83-86.

(57) Kertesz, M. A. Riding the sulfur cycle - metabolism of sulfonates and sulfate esters in Gram-negative bacteria. *FEMS Microbiol. Rev.* **2000**, *24*, 135-175.

(58) Van der Ploeg, J. R.; Eichhorn, E.; Leisinger, T. Sulfonate-sulfur metabolism and its regulation in Escherichia coli. *Arch. Microbiol.* **2001**, *176*, 1-8.

(59) Oae, S.; Okuyama, T.; Editors: *Organic Sulfur Chemistry: Biochemical Aspects*; CRC, 1992.

(60) Simpkins, N. S.: *Sulfones in Organic Synthesis*; Pergamon, 1993.

(61) Page, P.; Editor: *Organosulfur Chemistry, Volume 2: Synthetic and Stereochemical Aspects*; Academic, 1998.

(62) Jonas, S.; Hollfelder, F. Mapping catalytic promiscuity in the alkaline phosphatase superfamily. *Pure Appl. Chem.* **2009**, *81*, 731-742.

(63) Khersonsky, O.; Tawfik, D. S. Enzyme promiscuity: a mechanistic and evolutionary perspective. *Annu. Rev. Biochem.* **2010**, *79*, 471-505.

(64) Pregel, M. J.; Dunn, E. J.; Buncel, E. Metal ion catalysis in nucleophilic displacement reactions at carbon, phosphorus, and sulfur centers. III. Catalysis vs. inhibition by metal ions in the reaction of p-nitrophenyl benzenesulfonate with ethoxide. *Can. J. Chem.* **1990**, *68*, 1846-1858.

(65) Pregel, M. J.; Dunn, E. J.; Buncel, E. Metal ion catalysis in nucleophilic displacement reactions at carbon, phosphorus, and sulfur centers. 4. Mechanism of the reaction of aryl benzenesulfonates with alkali-metal ethoxides: catalysis and inhibition by alkali-metal ions. *J. Am. Chem. Soc.* **1991**, *113*, 3545-3550.

(66) Um, I. H.; Lee, S. J.; Kim, J. J.; Kwon, D. S. A mechanistic study on nucleophilic substitution reactions of aryl benzenesulfonates with anionic nucleophiles. *Bull. Korean Chem. Soc.* **1994**, *15*, 473-477.

(67) D'Rozario, P.; Smyth, R. L.; Williams, A. Evidence for a single transition state in the intermolecular transfer of a sulfonyl group between oxyanion donor and acceptors. *J. Am. Chem. Soc.* **1984**, *106*, 5027-5028.

(68)   Im, L.-R.; Park, Y.-M.; Um, I.-H. A mechanistic study on alkaline hydrolysis of Y-substituted phenyl benzenesulfonates. *Bull. Korean Chem. Soc.* **2008**, *29*, 2477-2481.

(69)   Loennberg, H.; Stroemberg, R.; Williams, A. Compelling evidence for a stepwise mechanism of the alkaline cyclisation of uridine 3'-phosphate esters. *Org. Biomol. Chem.* **2004**, *2*, 2165-2167.

(70)   Zaborsky, O. R.; Kaiser, E. T. Substituent effects in the alkaline hydrolyses of aromatic 5-membered cyclic sulfonates. Hydrolyses of 5-substituted 2-hydroxy-α-toluenesulfonic acid sultones. *J. Amer. Chem. Soc.* **1970**, *92*, 860-862.

(71)   Farrar, C. R.; Williams, A. Intramolecular nucleophilic assistance in the hydrolysis of sulfonate esters: equilibrium constant for sultone formation. *J. Am. Chem. Soc.* **1977**, *99*, 1912-1915.

(72)   Duarte, F.; Geng, T.; Marloie, G.; Al Hussain, A. O.; Williams, N. H.; Kamerlin, S. C. L. The Alkaline Hydrolysis of Sulfonate Esters: Challenges in Interpreting Experimental and Theoretical Data. *J. Org. Chem.* **2014**, *79*, 2816-2828.

(73)   Williams, A. Effective charge and Leffler's index as mechanistic tools for reactions in solution. *Acc. Chem. Res.* **1984**, *17*, 425-430.

(74)   Williams, A.: *Free Energy Relationships in Organic and Bio-Organic Chemistry*; Royal Society of Chemistry, 2003.

(75)   Um, I.-H.; Kang, J.-S.; Shin, Y.-H.; Buncel, E. A Kinetic Study on Nucleophilic Displacement Reactions of Aryl Benzenesulfonates with Potassium Ethoxide: Role of K+ Ion and Reaction Mechanism Deduced from Analyses of LFERs and Activation Parameters. *J. Org. Chem.* **2013**, *78*, 490-497.

(76)   Vetter, I. R.; Wittinghofer, A. Nucleoside triphosphate-binding proteins: different scaffolds to achieve phosphoryl transfer. *Q. Rev. Biophys.* **1999**, *32*, 1-56.

(77)   Mildvan, A. S. The role of metals in enzyme-catalyzed substitutions at each of the phosphorus atoms of ATP. *Adv. Enzymol. Relat. Areas Mol. Biol.* **1979**, *49*, 103-126.

(78)   Hubscher, U.; Maga, G.; Spadari, S. Eukaryotic DNA polymerases. *Annu. Rev. Biochem.* **2002**, *71*, 133-163.

(79)   Schroeder, G. K.; Lad, C.; Wyman, P.; Williams, N. H.; Wolfenden, R. The time required for water attack at the phosphorus atom of simple phosphodiesters and of DNA. *Proc Natl Acad Sci U S A* **2006**, *103*, 4052-4055.

(80)   Younas, M.; Rahman, A.; Iqbal, M. Hydroxide ion catalyzed hydrolysis of diaryl phosphates. *J. Chem. Soc. Pak.* **1981**, *3*, 139-142.

214

(81) Jaffe, H. H. A reëxamination of the Hammett equation. *Chem. Rev. (Washington, DC, U. S.)* **1953**, *53*, 191-261.

(82) Padovani, M.; Williams, N. H.; Wyman, P. Mononuclear Co(III)-complex promoted phosphate diester hydrolysis: Dependence of reactivity on the leaving group. *J. Phys. Org. Chem.* **2004**, *17*, 472-477.

(83) Tirel, E. Y.; Williams, N. H. Enhancing phosphate diester cleavage by a zinc complex through controlling nucleophile coordination. *Chem. - Eur. J.* **2015**, *21*, 7053-7056.

(84) McWhirter, C.; Lund, E. A.; Tanifum, E. A.; Feng, G.; Sheikh, Q. I.; Hengge, A. C.; Williams, N. H. Mechanistic Study of Protein Phosphatase-1 (PP1), A Catalytically Promiscuous Enzyme. *J. Am. Chem. Soc.* **2008**, *130*, 13673-13682.

(85) Behrman, E. J.; Biallas, M. J.; Brass, H. J.; Edwards, J. O.; Isaks, M. Reactions of phosphonic acid esters with nucleophiles. I. Hydrolysis. *J. Org. Chem.* **1970**, *35*, 3063-3069.

(86) Alkherraz, A.; Kamerlin, S. C. L.; Feng, G.-Q.; Sheikh, Q. I.; Warshel, A.; Williams, N. H. Phosphate ester analogues as probes for understanding enzyme catalysed phosphoryl transfer. *Faraday Discuss.* **2010**, *145*, 281-299.

(87) Chin, J.; Banaszczyk, M.; Jubian, V.; Zou, X. Cobalt(III) complex-promoted hydrolysis of phosphate diesters: comparison in reactivity of rigid cis-diaquo(tetraaza)cobalt(III) complexes. *J. Am. Chem. Soc.* **1989**, *111*, 186-190.

(88) Liao, X.; Anjaneyulu, P. S. R.; Curley, J. F.; Hsu, M.; Boehringer, M.; Caruthers, M. H.; Piccirilli, J. A. The Tetrahymena ribozyme cleaves a 5'-methylene phosphonate monoester ~102-fold faster than a normal phosphate diester: Implications for enzyme catalysis of phosphoryl transfer reactions. *Biochemistry* **2001**, *40*, 10911-10926.

(89) Ba-Saif, S. A.; Davis, A. M.; Williams, A. Effective charge distribution for attack of phenoxide ion on aryl methyl phosphate monoanion: studies related to the action of ribonuclease. *J. Org. Chem.* **1989**, *54*, 5483-5486.

(90) Hong, H.-J.; Lee, J.; Bae, A. R.; Um, I.-H. Kinetics and reaction mechanism for alkaline hydrolysis of Y-substituted-phenyl diphenylphosphinates. *Bull. Korean Chem. Soc.* **2013**, *34*, 2001-2005.

(91) Leffler, J. E. Parameters for the description of transition states. *Science (Washington, DC, U. S.)* **1953**, *117*, 340-341.

(92) Bourne, N.; Williams, A. Effective charge on oxygen in phosphoryl (-PO32-) group transfer from an oxygen donor. *J. Org. Chem.* **1984**, *49*, 1200-1204.

(93) Kirby, A. J.; Varvoglis, G. A. Reactivity of phosphate esters. Monoester hydrolysis. *J. Am. Chem. Soc.* **1967**, *89*, 415-423.

215

(94) Hanson, S. R.; Best, M. D.; Wong, C.-H. Enzyme chemistry: Sulfatases: structure, mechanism, biological activity, inhibition, and synthetic utility. *Angew. Chem., Int. Ed.* **2004**, *43*, 5736-5763.

(95) Simpson, L. S.; Widlanski, T. S. A Comprehensive Approach to the Synthesis of Sulfate Esters. *J. Am. Chem. Soc.* **2006**, *128*, 1605-1610.

(96) Buncel, E.; Raoult, A.; Wiltshire, J. F. Bond-scission processes in sulfur compounds. VII. Alkyl-oxygen scission in the neutral and alkaline methanolysis of methyl p-nitrophenyl sulfate. *J. Amer. Chem. Soc.* **1973**, *95*, 799-802.

(97) Buncel, E.; Chuaqui, C. Reactivity-selectivity correlations. 2. Reactivity of alkyl aryl sulfates toward oxygen nucleophiles and the reactivity-selectivity principle. *J. Org. Chem.* **1980**, *45*, 2825-2830.

(98) Kaiser, E. T.; Katz, I. R.; Wulfers, T. F. Alkaline hydrolysis of pyrocatechol cyclic sulfate. Extraordinary rate acceleration. *J. Am. Chem. Soc.* **1965**, *87*, 3781-3782.

(99) Younker, J. M.; Hengge, A. C. A mechanistic study of the alkaline hydrolysis of diaryl sulfate diesters. *J Org Chem* **2004**, *69*, 9043-9048.

(100) Hopkins, A.; Day, R. A.; Williams, A. Sulfate group transfer between nitrogen and oxygen: evidence consistent with an open "exploded" transition state. *J. Am. Chem. Soc.* **1983**, *105*, 6062-6070.

(101) Guthrie, R. D.; Jencks, W. P. IUPAC recommendations for the representation of reaction mechanisms. *Acc. Chem. Res.* **1989**, *22*, 343-349.

(102) Kirby, A. J.; Medeiros, M.; Oliveira, P. S. M.; Orth, E. S.; Brandao, T. A. S.; Wanderlind, E. H.; Amer, A.; Williams, N. H.; Nome, F. Activating Water: Important Effects of Non-leaving Groups on the Hydrolysis of Phosphate Triesters. *Chem. - Eur. J.* **2011**, *17*, 14996-15004, S14996/14991-S14996/14915.

(103) Kirby, A. J.; Medeiros, M.; Oliveira, P. S. M.; Brandao, T. A. S.; Nome, F. Activating Water: Efficient Intramolecular General Base Catalysis of the Hydrolysis of a Phosphate Triester. *Chem. - Eur. J.* **2009**, *15*, 8475-8479, S8475/8471-S8475/8410.

(104) Kirby, A. J.; Nome, F. Fundamentals of phosphate transfer. *Acc. Chem. Res.* **2015**, *48*, 1806-1814.

(105) Ghanem, E.; Raushel, F. M. Detoxification of organophosphate nerve agents by bacterial phosphotriesterase. *Toxicol. Appl. Pharmacol.* **2005**, *207*, S459-S470.

(106) Zheng, F.; Zhan, C.-G.; Ornstein, R. L. Theoretical studies of reaction pathways and energy barriers for alkaline hydrolysis of phosphotriesterase substrates paraoxon and related toxic phosphofluoridate nerve agents. *J. Chem. Soc., Perkin Trans. 2* **2001**, 2355-2363.

216

(107) Munro, N. Toxicity of the organophosphate chemical warfare agents GA, GB, and VX: implications for public protection. *Environ Health Perspect* **1994**, *102*, 18-38.

(108) Raushel, F. M. Bacterial detoxification of organophosphate nerve agents. *Curr. Opin. Microbiol.* **2002**, *5*, 288-295.

(109) Xia, F.; Tian, K.; Zhu, H. Density functional calculations on alcoholysis and thiolysis of phosphate triesters: Stepwise or concerted? *Comput. Theor. Chem.* **2013**, *1017*, 60-71.

(110) Schroeder, G. K.; Lad, C.; Wyman, P.; Williams, N. H.; Wolfenden, R. The time required for water attack at the phosphorus atom of simple phosphodiesters and of DNA. *Proc. Natl. Acad. Sci. U. S. A.* **2006**, *103*, 4052-4055.

(111) Krise, J. P.; Stella, V. J. Prodrugs of phosphates, phosphonates, and phosphinates. *Adv. Drug Delivery Rev.* **1996**, *19*, 287-310.

(112) Huttunen, K. M.; Raunio, H.; Rautio, J. Prodrugs - from serendipity to rational design. *Pharmacol. Rev.* **2011**, *63*, 750-771.

(113) Sartillo-Piscil, F.; Quintero, L.; Cruz-Gregorio, S.; Espinosa-Aguirre, J.; Elinos-Baez, C. M.; Hopfl, H.; Serrano, A. Further Evidence on the Favorable Role of the Anomeric Effect on the Cleavage of HepDirect and Cyclophosphamide Prodrugs. *J. Org. Chem.* **2014**, *79*, 9647-9654.

(114) Huttunen, K. M.; Maehoenen, N.; Leppaenen, J.; Vepsaelaeinen, J.; Juvonen, R. O.; Raunio, H.; Kumpulainen, H.; Jaervinen, T.; Rautio, J. Novel Cyclic Phosphate Prodrug Approach for Cytochrome P450-activated Drugs Containing an Alcohol Functionality. *Pharm. Res.* **2007**, *24*, 679-687.

(115) Farquhar, D.; Kuttesch, N. J.; Wilkerson, M. G.; Winkler, T. Synthesis and biological evaluation of neutral derivatives of 5-fluoro-2'-deoxyuridine 5'-phosphate. *J. Med. Chem.* **1983**, *26*, 1153-1158.

(116) Florian, J.; Warshel, A. Phosphate Ester Hydrolysis in Aqueous Solution: Associative versus Dissociative Mechanisms. *J. Phys. Chem. B* **1998**, *102*, 719-734.

(117) Hengge, A. C.; Tobin, A. E.; Cleland, W. W. Studies of Transition-State Structures in Phosphoryl Transfer Reactions of Phosphodiesters of p-Nitrophenol. *J. Am. Chem. Soc.* **1995**, *117*, 5919-5926.

(118) Admiraal, S. J.; Herschlag, D. The Substrate-Assisted General Base Catalysis Model for Phosphate Monoester Hydrolysis: Evaluation Using Reactivity Comparisons. *J. Am. Chem. Soc.* **2000**, *122*, 2145-2148.

(119) Maegley, K. A.; Admiraal, S. J.; Herschlag, D. Ras-catalyzed hydrolysis of GTP: a new perspective from model studies. *Proc. Natl. Acad. Sci. U. S. A.* **1996**, *93*, 8160-8166.

217

(120) Hengge, A. C.; Cleland, W. W. Direct measurement of transition-state bond cleavage in hydrolysis of phosphate esters of p-nitrophenol. *J. Am. Chem. Soc.* **1990**, *112*, 7421-7422.

(121) Cassano, A. G.; Anderson, V. E.; Harris, M. E. Evidence for Direct Attack by Hydroxide in Phosphodiester Hydrolysis. *J. Am. Chem. Soc.* **2002**, *124*, 10964-10965.

(122) Lopez-Canut, V.; Ruiz-Pernia, J.; Tunon, I.; Ferrer, S.; Moliner, V. Theoretical Modeling on the Reaction Mechanism of p-Nitrophenylmethylphosphate Alkaline Hydrolysis and its Kinetic Isotope Effects. *J. Chem. Theory Comput.* **2009**, *5*, 439-442.

(123) Ba-Saif, S. A.; Waring, M. A.; Williams, A. Single transition state in the transfer of a neutral phosphoryl group between phenoxide ion nucleophiles in aqueous solution. *J. Am. Chem. Soc.* **1990**, *112*, 8115-8120.

(124) Ba-Saif, S. A.; Waring, M. A.; Williams, A. Dependence of transition-state structure on nucleophile in the reaction of aryl oxide anions with aryl diphenylphosphate esters. *J. Chem. Soc., Perkin Trans. 2* **1991**, 1653-1659.

(125) Tarrat, N. Alkaline hydrolysis of phosphate triesters in solution: Stepwise or concerted? A theoretical study. *J. Mol. Struct.: THEOCHEM* **2010**, *941*, 56-60.

(126) Caldwell, S. R.; Raushel, F. M.; Weiss, P. M.; Cleland, W. W. Transition-state structures for enzymic and alkaline phosphotriester hydrolysis. *Biochemistry* **1991**, *30*, 7444-7450.

(127) Davis, L. Structure of dihydroxyacetone in solution. *Bioorg. Chem.* **1973**, *2*, 197-201.

(128) Slepokura, K.; Lis, T. Dihydroxyacetone phosphate, DHAP, in the crystalline state: monomeric and dimeric forms. *Carbohydr. Res.* **2010**, *345*, 512-529.

(129) Slepokura, K. Preparation and structural characterization of cDHAP-cyclic form of dihydroxyacetone phosphate-revealing chair and skew conformations of 1,3,2-dioxaphosphorinane ring. *Carbohydr. Res.* **2013**, *368*, 96-103.

(130) Hansch, C.; Leo, A.; Taft, R. W. A survey of Hammett substituent constants and resonance and field parameters. *Chem. Rev.* **1991**, *91*, 165-195.

(131) Westheimer, F. H. Pseudo-rotation in the hydrolysis of phosphate esters. *Accounts Chem. Res.* **1968**, *1*, 70-78.

(132) Dennis, E. A.; Westheimer, F. H. The geometry of the transition state in the hydrolysis of phosphate esters. *J. Am. Chem. Soc.* **1966**, *88*, 3432-3433.

(133) Westheimer, F. H. The hydrolysis of phosphate esters. *Pure Appl. Chem.* **1977**, *49*, 1059-1067.

(134) Richard, J. P. Acid-base catalysis of the elimination and isomerization reactions of triose phosphates. *J. Am. Chem. Soc.* **1984**, *106*, 4926-4936.

(135) Jones, A. S.; Kumar, A.; Walker, R. T. Structure of two isomeric 1,3,2-dioxaphosphorinanes. *J. Org. Chem.* **1986**, *51*, 4310-4311.

(136) Hussein, F. A.; Hammo, K. A. Relation between chemical structure and biological activity of arylsulfonates of quaternary 3-hydroxypridine. *Iraqi J. Sci.* **1977**, *18*, 1-11.

(137) Shaw, E. Analogs of aspergillic acid. I. The tautomerism of the hydroxypyridine N-oxides. *J. Am. Chem. Soc.* **1949**, *71*, 67-70.

(138) DeBergh, J. R.; Niljianskul, N.; Buchwald, S. L. Synthesis of Aryl Sulfonamides via Palladium-Catalyzed Chlorosulfonylation of Arylboronic Acids. *J. Am. Chem. Soc.* **2013**, *135*, 10638-10641.

(139) Kokatla, H. P.; Thomson, P. F.; Bae, S.; Doddi, V. R.; Lakshman, M. K. Reduction of Amine N-Oxides by Diboron Reagents. *J. Org. Chem.* **2011**, *76*, 7842-7848.

(140) Kim, S.; Yi, K. Y. Di-2-pyridyl sulfite. A new useful reagent for the preparation of N-sulfinylamines, nitriles, isocyanides, and carbodiimides under mild conditions. *Tetrahedron Lett.* **1986**, *27*, 1925-1928.

(141) Slepokura, K.; Lis, T. Crystal structures of dihydroxyacetone and its derivatives. *Carbohydr. Res.* **2004**, *339*, 1995-2007.

(142) Zawaneh, P. N.; Doody, A. M.; Zelikin, A. N.; Putnam, D. Diblock copolymers based on dihydroxyacetone and ethylene glycol: synthesis, characterization, and nanoparticle formulation. *Biomacromolecules* **2006**, *7*, 3245-3251.

(143) Weiser, J. R.; Zawaneh, P. N.; Putnam, D. Poly(carbonate-ester)s of dihydroxyacetone and lactic acid as potential biomaterials. *Biomacromolecules* **2011**, *12*, 977-986.

(144) Albert, A.; Phillips, J. N. Ionization constants of heterocyclic substances. II. Hydroxy-derivatives of nitrogenous six-membered ring-compounds. *J. Chem. Soc.* **1956**, 1294-1304.

(145) Blanch, J. H. Determination of the Hammett substituent constants for the 2-, 3-, and 4-pyridyl and -pyridinium groups. *J. Chem. Soc. B* **1966**, 937-939.

(146) Jaffe, H. H. The electrical effect of the *N*-oxide group in pyridine 1-oxide. *J. Am. Chem. Soc.* **1954**, *76*, 3527-3531.

Appendix

1.1 Appendix of chapter two: Sulfonate esters

[KOH]	Compound 10 k_{obs} s^{-1}
0.01	0.000616
0.04	0.00270
0.07	0.00486
0.1	0.00656

Table 19: Hydrolysis of compound **10**; 0.5 M KCl, 50 °C.

[KOH]	Compound 11 k_{obs} s^{-1}
0.004	0.00546
0.007	0.0108
0.008	0.0127
0.008	0.0127
0.010	0.0156
0.04	0.0608
0.07	0.105
0.1	0.155

Table 20: Hydrolysis of compound **11**; 0.5 M KCl, 50 °C.

[KOH]	Compound 12 k_{obs} s^{-1}
0.002	0.0252
0.002	0.0245
0.004	0.0474
0.004	0.0449
0.006	0.0731
0.006	0.0740
0.008	0.0931
0.008	0.100

Table 21: Hydrolysis of compound **12**; 0.5 M KCl, 50 °C.

1.2 Appendix of chapter three: Phosphate diesters

Hydrolysis of phosphate diester

[NaOH]	k_{obs} s^{-1}/N-oxide phosphate diester 28
0.05	1.61×10^{-6}
0.05	1.27×10^{-6}
0.09	3.19×10^{-6}
0.3	1.27×10^{-5}
0.3	1.18×10^{-5}
0.5	2.02×10^{-5}
0.5	2.07×10^{-5}
0.7	2.77×10^{-5}
0.7	2.86×10^{-5}
0.9	3.61×10^{-5}
0.9	3.70×10^{-5}

Table 22: Alkaline hydrolysis of compound **28** (*N*-oxide); 1 M NaCl, 42 °C ± 0.04.

[NaOH]	k_{obs} s^{-1} /N-methyl phosphate diester 29
0.05	1.40×10^{-5}
0.09	2.87×10^{-5}
0.2	6.25×10^{-5}
0.3	9.22×10^{-5}
0.5	0.000167
0.5	0.000167
0.6	0.000203
0.6	0.000204
0.7	0.000239
0.7	0.000239
0.8	0.000279
0.8	0.000278
0.9	0.000322
0.9	0.000321

Table 23: Alkaline hydrolysis of compound **29** (*N*-methyl); 1 M NaCl, 42 °C ± 0.04.

pKₐ measurements of substituted pyridyl

No of addition	pH ± 0.002	Abs @320 nm
1	3.666	0.009
2	3.875	0.012
3	4.074	0.015
4	4.318	0.023
5	4.594	0.037
6	4.940	0.073
7	5.335	0.136
8	5.689	0.229
9	5.990	0.322
10	6.257	0.400
11	6.482	0.456
12	6.691	0.498
13	6.873	0.523
14	7.061	0.545
15	7.232	0.557
16	7.413	0.565
17	7.582	0.572
18	7.759	0.575
19	7.949	0.577
20	8.157	0.579
21	8.384	0.579
22	9.037	0.579
23	9.701	0.579

Table 24: pH and absorbance measurements of *N*-oxide pyridyl at 42 °C, 1 M NaCl.

No of addition	pH ± 0.002	Abs @320nm
1	3.262	0.025
2	3.441	0.033
3	3.631	0.047
4	3.800	0.064
5	3.984	0.093
6	4.180	0.131
7	4.382	0.183
8	4.593	0.250
9	4.835	0.334
10	5.114	0.433
11	5.426	0.521
12	5.692	0.575
13	5.949	0.610
14	6.162	0.631
15	6.364	0.641
16	6.552	0.648
17	6.713	0.652
18	6.865	0.656
19	7.023	0.658
20	7.394	0.658
21	7.769	0.662
22	8.195	0.657
23	8.724	0.661

Table 25: pH and absorbance measurements of *N*-methyl pyridyl at 42 °C, 1 M NaCl.

1.3 Appendix of chapter four: Sulfate diesters

[NaOH]	k_{obs} /s^{-1}/ **pyridyl sulfate 35**
0.05	1.73×10^{-6}
0.09	5.00×10^{-6}
0.3	1.40×10^{-5}
0.5	2.42×10^{-5}
0.7	3.34×10^{-5}
0.8	3.85×10^{-5}

Table 26: Alkaline hydrolysis of 3-hydroxy pyridine pheyl sulfate diester **35**; (0.05-0.8) M NaOH, 1 M NaCl.

[NaOH]	k_{obs} /s^{-1}/*N*-oxide pyridyl sulfate 36
0.02	2.83×-05
0.04	5.79×-05
0.08	0.000119
0.2	0.000295
0.2	0.000297
0.3	0.000439
0.3	0.000455
0.4	0.000622
0.5	0.000778
0.6	0.000956
0.7	0.001134

Table 27: Alkaline hydrolysis of *N*-oxide pyridine phenyl sulfate diester **36**; (0.02-0.7) M NaOH; 1 M NaCl.

[NaOH]	k_{obs} /s^{-1}/*N*-methyl pyridyl sulfate 37
0.02	0.000269
0.05	0.000767
0.05	0.000762
0.09	0.001386
0.1	0.001486
0.2	0.003043
0.3	0.00463
0.3	0.004814
0.5	0.00776

Table 28: Alkaline hydrolysis of *N*-methyl pyridine phenyl sulfate diester **37**; (0.02-0.5) M NaOH; 1 M NaCl.

[NaOH]	k_{obs} /s^{-1}/bis pyridyl sulfate diester 39
0.05	2.39 × -05
0.05	2.50 × -05
0.09	4.05 × -05
0.09	4.14 × -05
0.3	0.000133
0.3	0.000142
0.5	0.000238
0.5	0.000239
0.7	0.000355
0.7	0.000347
0.9	0.000466
0.9	0.000466

Table 29: Alkaline hydrolysis of bis pyridyl sulfate diester **39**; (0.05-0.9) M NaOH, 1 M NaCl;

No of addition	pH ± 0.003	Abs@300nm/ 13
1	3.998	0.121
2	4.235	0.130
3	4.508	0.136
4	4.837	0.151
5	5.234	0.168
6	5.629	0.180
7	5.972	0.186
8	6.281	0.190
9	6.538	0.194
10	6.782	0.197
11	6.987	0.206
12	7.185	0.211
13	7.388	0.219
14	7.576	0.233
15	7.78	0.251
16	8.018	0.280
17	8.288	0.315
18	8.568	0.357
19	8.904	0.400
20	9.228	0.426
21	9.532	0.444
22	9.857	0.452
23	10.176	0.458
24	10.448	0.462
25	10.69	0.465

Table 30: Summary of pH and absorbance for titration of 3-hydroxy pyridine **13**.

No of addition	pH ± 0.003	Abs@320nm/14
1	3.962	0.014
2	4.194	0.021
3	4.46	0.024
4	4.787	0.040
5	5.196	0.072
6	5.596	0.137
7	5.935	0.209
8	6.233	0.274
9	6.508	0.321
10	6.741	0.352
11	6.95	0.373
12	7.145	0.384
13	7.34	0.393
14	7.552	0.400
15	7.742	0.403
16	7.963	0.405
17	8.205	0.408
18	8.477	0.408
19	8.775	0.407
20	9.085	0.408
21	9.401	0.407

Table 31: Summary of pH and absorbance for titration of *N*-oxide 3-hydroxy pyridine **14**.

No of addition	pH ± 0.003	Abs@320nm/15
1	3.28	0.017
2	3.446	0.024
3	3.627	0.034
4	3.795	0.043
5	3.958	0.060
6	4.133	0.086
7	4.328	0.121
8	4.53	0.169
9	4.76	0.231
10	5.061	0.314
11	5.366	0.391
12	5.663	0.445
13	5.927	0.475
14	6.169	0.494
15	6.368	0.502
16	6.569	0.508
17	6.749	0.512
18	6.902	0.517
19	7.043	0.517
20	7.374	0.516
21	7.716	0.516
22	8.092	0.518
23	8.575	0.518
24	9.108	0.515

Table 32: Summary of pH and absorbance for titration of *N*-methyl-3-hydroxy pyridine **15**.

Calculation of pK_a of 3-hydroxy pyridine

This is what is measured:
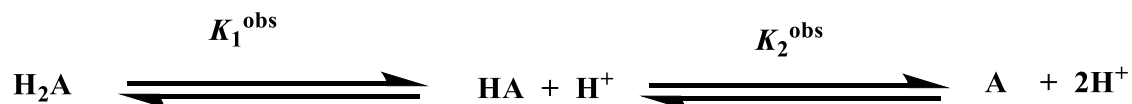
This is what is happening at a molecular scale:
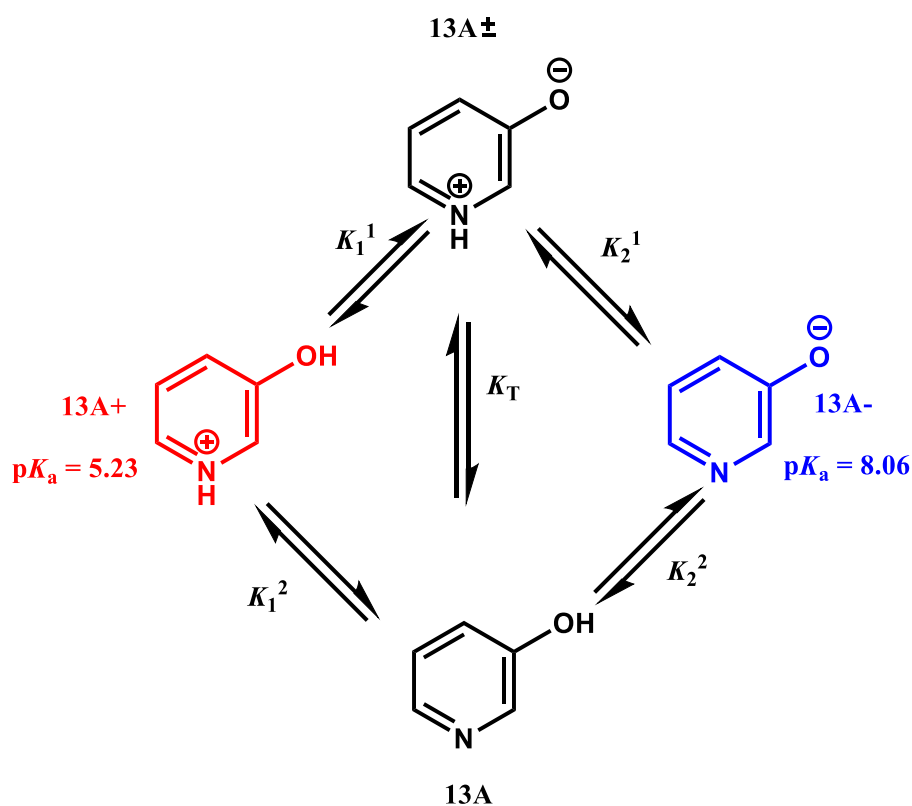
We want to know how to relate what we measure to what is happening at the molecular scale on occasion. For example, to have a value for the loss of a proton from a particular site, so that we can use the appropriate pK_a in a Brønsted plot.

Definitions:

$$K_1^1 = \frac{A^{\pm}.H^+}{A^+}$$

$$K_1^2 = \frac{A.H^+}{A^+}$$

$$K_2^1 = \frac{A^-.H^+}{A^{\pm}}$$

$$K_2^2 = \frac{A^-.H^+}{A}$$

$$K_T = \frac{A}{A^{\pm}}$$

Which means that:

$$K_T = \frac{K_1^2}{K_1^1} = \frac{K_2^1}{K_2^2}$$

We also have:

$$K_1^{obs} = \frac{(A^{\pm} + A).H^+}{A^+} = \frac{A^{\pm}.H^+}{A^+} + \frac{A.H^+}{A^+} = K_1^1 + K_1^2 = K_1^1(1 + K_T)$$

and

$$K_2^{obs} = \frac{A^-.H^+}{(A^{\pm} + A)}$$

so

233

$$\frac{1}{K_2^{obs}} = \frac{A^{\pm}}{A^-.H^+} + \frac{A}{A^-.H^+} = \frac{1}{K_2^1} + \frac{1}{K_2^2} = \frac{1}{K_2^2}\left(1 + \frac{1}{K_T}\right) = \frac{1}{K_2^2}\left(\frac{1 + K_T}{K_T}\right)$$

which means that:

$$K_1^1 = \frac{1}{(1 + K_T)} K_1^{obs}$$

$$K_1^2 = \frac{K_T}{(1 + K_T)} K_1^{obs}$$

$$K_2^1 = (1 + K_T) K_2^{obs}$$

$$K_2^2 = \frac{(1 + K_T)}{K_T} K_2^{obs}$$

So if we know what K_T is, then we can convert the observed values to the microscopic values that we need to know.

$$pK_1^1 = pK_1^{obs} + log\left[\frac{(1 + K_T)}{1}\right]$$

$$pK_1^2 = pK_1^{obs} + log\left[\frac{(1 + K_T)}{K_T}\right]$$

$$pK_2^1 = pK_2^{obs} + log\left[\frac{1}{(1 + K_T)}\right]$$

$$pK_2^2 = pK_2^{obs} + log\left[\frac{K_T}{(1 + K_T)}\right]$$

As K_T is always >0, this means that the microscopic pK_as are (always) higher than the first observed pK_a, and (always) lower than the second pK_a.

As T gets very big or small, $pK_a{}^{obs}$ matches one of the microscopic ionisations closely, and the other value is very different to the observed value (this happened when there is only a small amount of one of the tautomers).

Notice that if K_T is about 1 (which it is in this example), then the microscopic values are 0.5 times $K_1{}^{obs}$ for the first ionisation, and 2 times $K_2{}^{obs}$ for the second ionisation. This means that the microscopic pK_as are 0.30 units higher than $pK_{a1}{}^{obs}$ and 0.3 units lower than $pK_{a2}{}^{obs}$. Therefore, the first pK_a is 5.23 and the second pK_a is 8.06.

1.4 Appendix of chapter five: Phosphate triesters

[Buffer]	k_{obs} /s^{-1}/cyclic 55
0.02	3.7469×10^{-6}
0.04	4.1988×10^{-6}
0.05	4.5637×10^{-6}
0.09	6.2454×10^{-6}

Table 33: Buffer catalysis of cyclic 4-nitrophenyl phosphate triester **55**; pH= 9.9 ± 0.04, 25 °C, 1 M NaCl.

[Buffer]	k_{obs} /s^{-1}/alkene 56a
0.02	3.94×10^{-5}
0.05	6.05×10^{-5}
0.08	7.97×10^{-5}
0.1	9.21×10^{-5}

Table 34: Buffer catalysis of alkene cyclic 4-nitrophenyl phosphate triester **56a**; pH= 9.9 ± 0.04, 25 °C, 1 M NaCl.

[Buffer]	k_{obs} /s^{-1}/dimethoxy 59
0.02	9.82×10^{-5}
0.05	0.000193
0.08	0.000276
0.1	0.000336

Table 35: Buffer catalysis of dimethoxy cyclic 4-nitrophenyl phosphate triester **59**; pH= 9.9 ± 0.04, 25 °C, 1M NaCl.

[Buffer]	k_{obs} /s^{-1}/**carbonyl 57c**
0.02	0.000203
0.02	0.000201
0.04	0.000196
0.06	0.000202
0.06	0.0002
0.08	0.000203
0.08	0.000204
0.1	0.000207
0.1	0.000206

Table 36: Buffer catalysis of carbonyl 3-chloro phenyl phosphate triester **45c** at 25 °C, (0.02-0.1) M buffer, PH= 6.1 ± 0.04.

pH	k_{obs} /s^{-1}/**cyclic 55**
13	0.002248
13	0.002233
12.845	0.001552
12.698	0.001105
12.698	0.001112
12.477	0.000669
12	0.000212
11.903	0.000175
11.778	0.000169
11.6	8.25×10^{-5}

11.3	3.46×10^{-5}
6.96	4.37×10^{-9}
2.9	1.23×10^{-8}
1.95	3.72×10^{-8}
0.95	2.02×10^{-7}
0	6.51×10^{-7}

Table 37: k_{obs} values for hydrolysis of cyclic 4-nitrophenyl phosphate triester **55**.

pH	k_{obs} /s^{-1}/alkene cyclic 56a
11.95	3.35×10^{-3}
11.66	1.78×10^{-3}
11.45	1.07×10^{-3}
11.23	0.000697
10	2.68×10^{-5}
10	2.68×10^{-5}
6.95	5.07×10^{-7}
2.9	1.38×10^{-6}
2.9	1.51×10^{-6}
1.95	1.86×10^{-6}
0.95	3.97×10^{-6}
0	2.57×10^{-5}
0	2.54×10^{-5}

Table 38: k_{obs} values for hydrolysis of Alkene cyclic 4-nitrophenyl phosphate triester **56a**.

pH	k_{obs} /s^{-1}/dimethoxy cyclic 59
13	0.03941
12.698	0.024192
12.477	0.014648
12	0.004914
11.903	0.004044
11.903	0.004375
11.778	0.00288
11.778	0.00268
11.6	0.002036
11.6	0.001797
11.3	0.000724
11.3	0.000533
6.95	7.35×10^{-7}
2.9	4.30×10^{-7}
2.9	3.53×10^{-7}
1.95	1.83×10^{-6}
0.95	9.72×10^{-6}
0	5.50×10^{-5}
0	5.61×10^{-5}

Table 39: k_{obs} values for hydrolysis of dimethoxy cyclic 4-nitrophenyl phosphate triester **59**.

pH	k_{obs} /s^{-1}/carbonyl cyclic 4-nitro 57a
5.2	0.038487
5.2	0.039707
5.2	0.03822
5	0.029262
4.77	0.016194
4.4	0.005883
3.97	0.00196
3.82	0.00148
3.8	0.001372
2.8	0.000109
1.9	7.08×10^{-6}
0.95	3.76×10^{-6}
0	2.64×10^{-5}

Table 40: k_{obs} values for hydrolysis of carbonyl cyclic 4-nitrophenyl phosphate triester **57a**.

[NaOH]	k_{obs} /s^{-1}/alkene-3-nitro 56b
0.002	0.000291
0.005	0.000803
0.01	0.001576
0.01	0.001586
0.03	0.004368
0.05	0.00711

Table 41: k_{obs} values for hydrolysis of alkene **56b**.

[NaOH]	k_{obs} /s^{-1}/alkene-3-chloro 56c
0.002	0.000133
0.002	0.000139
0.005	0.000355
0.005	0.000349
0.03	0.002222
0.05	0.00373

Table 42: k_{obs} values for hydrolysis of alkene **56c**.

[NaOH]	k_{obs} /s^{-1}/alkene-phenyl 56d
0.005	0.000205
0.01	0.000391
0.03	0.001226
0.05	0.002005
0.1	0.004049

Table 43: k_{obs} values for hydrolysis of alkene **56d**.

[NaOH]	k_{obs} /s^{-1}/alkene-4-methoxy 56e
0.005	0.000161
0.01	0.000335
0.03	0.001043
0.05	0.001675
0.07	0.00239
0.07	0.002375
0.1	0.003386
0.1	0.003373

Table 44: k_{obs} values for hydrolysis of alkene 56e.

[NaOH]	k_{obs} /s^{-1}/alkene-3,4-dimethyl 56f
0.005	0.000152
0.01	0.000258
0.03	0.000782
0.05	0.001333
0.07	0.001846
0.1	0.002699
0.15	0.004265

Table 45: k_{obs} values for hydrolysis of alkene 56f.

pH	k_{obs} /s^{-1}/carbonyl 3-nitro 57b
4.91	0.000546
5.17	0.000797
5.52	0.001605
5.7	0.0029
5.7	0.002738
5.7	0.002691
6.1	0.007058
6.1	0.007562
6.1	0.007019
6.46	0.01196
6.46	0.01195
6.46	0.012942
6.9	0.040478
6.9	0.041777

Table 46: k_{obs} values for hydrolysis of carbonyl **57b**.

pH	k_{obs} /s^{-1}/carbonyl 3-chloro 57c
5.52	6.31×10^{-5}
5.52	5.43×10^{-5}
5.72	8.97×10^{-5}
6.183	0.000249
6.478	0.000426
6.939	0.00137
6.93	0.001474
7.37	0.003218
7.37	0.002997
7.725	0.007887
7.725	0.008361
7.98	0.014553
7.98	0.014553
7.98	0.01454
8.166	0.021943
8.166	0.02519
8.263	0.029767
8.263	0.028979
8.58	0.049948
8.58	0.044044

Table 47: k_{obs} values for hydrolysis of carbonyl **57c**.

pH	k_{obs} /s^{-1}/carbonyl phenyl 57d
6.5	1.01×10^{-5}
7	2.72×10^{-5}
7.18	4.10×10^{-5}
7.18	4.05×10^{-5}
7.57	0.000102
7.57	0.000101
7.99	0.000395
7.99	0.000347
8.25	0.000905
8.25	0.000791
8.58	0.002528
8.58	0.002361
8.99	0.01069
8.99	0.010832
9.35	0.046051
9.35	0.046879
9.33	0.043926
9.52	0.090368
9.52	0.086354

Table 48: k_{obs} values for hydrolysis of carbonyl **57d**.

pH	k_{obs} /s⁻¹/carbonyl 4-methoxy 57e
7.57	3.31×10^{-5}
7.91	8.87×10^{-5}
7.91	8.80×10^{-5}
8.32	3.08×10^{-4}
8.78	0.001504
9.1	0.007991
9.1	0.008117
9.57	0.032257
9.57	0.033963
9.72	0.092944
9.72	0.091495

Table 49: k_{obs} values for hydrolysis of carbonyl **57e**.

pH	k_{obs} /s^{-1}/carbonyl 3,4-dimethyl 57f
6.9	3.14×10^{-6}
7.2	6.08×10^{-6}
7.54	1.78×10^{-5}
7.54	1.62×10^{-5}
7.9	4.93×10^{-5}
8.32	0.00017
8.78	0.000771
9.1	0.004197
9.1	0.004151
9.57	0.017518
9.72	0.050263
9.72	0.048596
9.99	0.11855
9.99	0.11802

Table 50: k_{obs} values for hydrolysis of carbonyl **57f**.

pH	k_{obs} /s^{-1}/hydroxyl phenyl 78
9.35	9.33×10^{-5}
9.6	1.49×10^{-4}
9.9	3.02×10^{-4}
10.27	6.17×10^{-4}
10.4	9.18×10^{-4}
10.44	0.001001
10.75	0.002059
10.95	0.003166
10.95	0.003147
11.1	0.004817
11.1	0.005025
11.35	0.00843

Table 51: k_{obs} values for hydrolysis of hydroxyl **78**.

[Buffer]	k_{obs} /s^{-1}/hydroxyl phenyl 78
0.02	9.33×10^{-4}
0.04	9.45×10^{-4}
0.05	9.72×10^{-4}
0.07	9.73×10^{-4}
0.09	9.91×10^{-4}

Table 52: k_{obs} values for buffer catalysis of hydroxyl **78**.

pH	k_{obs} /s^{-1}/carbonyl-4-nitrobenzyl-substarte 65	k_{obs}/s^{-1}/carbonyl-4-nitrobenzyl-product 65
8.114	4.63×10^{-6}	5.31×10^{-6}
9.3	4.17×10^{-5}	3.98×10^{-5}
10.388	1.96×10^{-4}	0.00019531
10.67	2.19×10^{-4}	0.00022587
10.85	2.54×10^{-4}	0.0002682
11.477	0.00031667	0.00032847
12	0.00063519	0.00062852
12	0.00054897	0.00054897
12.477	0.0014343	0.0013967
12.477	0.0012913	0.0012458
13	0.0037261	0.0040661
13	0.0040021	0.004064

Table 53: k_{obs} values for hydrolysis of carbonyl **65**.

pH	k_{obs}/s^{-1}/dimethoxy-4-nitrobenzyl-substarte 66	k_{obs}/s^{-1}/dimethxoy-4-nitrobenzyl-product 66
7.79	2.24×10^{-6}	50784×10^{-6}
9.295	7.45×10^{-6}	7.3215×10^{-6}
10.4	2.27×10^{-5}	2.58285×10^{-5}
10.959	9.71×10^{-5}	9.55652×10^{-5}
11.477	1.75×10^{-4}	0.000173261
12	0.000658	0.000632557
12.47	0.00213	0.002191291
13	0.0061	0.006379696

Table 54: k_{obs} values for hydrolysis of carbonyl **66**.

pK_a measurements of phenols at 25 °C

No of addition	pH ± 0.004	Abs @400 nm-4-nitropheol
1	5.202	0.043868
2	5.665	0.081334
3	6.05	0.13084
4	6.387	0.24559
5	6.675	0.37544
6	6.906	0.48297
7	7.142	0.5852
8	7.359	0.65084
9	7.577	0.71508
10	7.778	0.74732
11	8.018	0.77649
12	8.293	0.80497
13	8.618	0.82298
14	8.981	0.82806
15	9.339	0.83251
16	9.651	0.82901

Table 55: pH and absorbance measurements of 4-nitrophenol at 25 °C, 1 M NaCl.

No of addition	pH ± 0.004	Abs @395 nm-3-nitrophenol
1	4.34	0.028133
2	5.098	0.028404
3	5.798	0.031922
4	6.205	0.033498
5	6.561	0.037316
6	6.837	0.044204
7	7.109	0.052465
8	7.35	0.062075
9	7.604	0.081018
10	7.84	0.10226
11	8.099	0.12788
12	8.399	0.15893
13	8.774	0.1912
14	9.181	0.21086
15	9.583	0.22041
16	9.984	0.22415
17	10.359	0.22559
18	10.691	0.22688
19	10.979	0.22754
20	11.19	0.22665
21	11.34	0.22635

Table 56: pH and absorbance measurements of 3-nitrophenol at 25 °C, 1 M NaCl.

No of addition	pH ± 0.004	Abs @295 nm-3-chlorophenol
1	4.282	0.0081992
2	4.97	0.0087852
3	5.648	0.013117
4	6.073	0.015173
5	6.412	0.017485
6	6.697	0.022977
7	6.951	0.027782
8	7.186	0.03525
9	7.419	0.046916
10	7.654	0.063964
11	7.909	0.091943
12	8.182	0.13885
13	8.182	0.13909
14	8.503	0.21659
15	8.874	0.32558
16	9.254	0.43055
17	9.646	0.50618
18	10.032	0.54417
19	10.032	0.54735
20	10.395	0.5683
21	10.395	0.56679
22	10.72	0.57537
23	10.988	0.57864
24	11.185	0.58172
25	11.325	0.58027
26	11.428	0.58132

Table 57: pH and absorbance measurements of 3-chlorophenol at 25 °C, 1 M NaCl.

No of addition	pH ± 0.004	Abs @288 nm-phenol
1	4.993	0.0094289
2	5.718	0.010181
3	6.157	0.010305
4	6.504	0.0098489
5	6.797	0.0101
6	7.047	0.011154
7	7.277	0.010538
8	7.492	0.011717
9	7.713	0.014904
10	7.944	0.017016
11	8.198	0.025433
12	8.502	0.039209
13	8.856	0.07382
14	9.226	0.13911
15	9.59	0.23696
16	9.944	0.34936
17	10.288	0.4413
18	10.6	0.49718
19	10.87	0.52562
20	11.078	0.53667
21	11.23	0.54413
22	11.343	0.54507
23	11.433	0.54751
24	11.5	0.54894
25	11.559	0.54801
26	11.609	0.54759

Table 58: pH and absorbance measurements of phenol at 25 °C, 1 M NaCl.

No of addition	pH ± 0.004	Abs @306 nm-4-methoxy phenol
1	4.999	0.065558
2	5.69	0.065088
3	6.125	0.064479
4	6.473	0.066417
5	6.76	0.064848
6	7.01	0.065968
7	7.238	0.065615
8	7.456	0.067389
9	7.672	0.067817
10	7.902	0.067699
11	8.157	0.073036
12	8.456	0.079529
13	8.809	0.095468
14	9.183	0.13221
15	9.542	0.19677
16	9.907	0.28868
17	10.265	0.38734
18	10.576	0.45533
19	10.842	0.49551
20	11.048	0.51427
21	11.195	0.52418
22	11.312	0.53006
23	11.402	0.53159
24	11.476	0.53321
25	11.536	0.5352
26	11.589	0.53385
27	11.632	0.53411
28	11.674	0.53541

Table 59: pH and absorbance measurements of 4-methoxyphenol at 25 °C, 1 M NaCl.

No of addition	pH ± 0.004	Abs @295 nm-3,4-dimethylphenol
1	3.88	0.0086134
2	4.317	0.009039
3	5.032	0.0091344
4	5.722	0.0079452
5	6.159	0.0092263
6	6.51	0.0091858
7	6.802	0.0093292
8	7.056	0.0088895
9	7.286	0.0088033
10	7.504	0.010735
11	7.724	0.012342
12	7.954	0.014375
13	8.227	0.017933
14	8.548	0.026732
15	8.915	0.047298
16	9.294	0.088783
17	9.663	0.1648
18	10.025	0.27099
19	10.358	0.37896
20	10.66	0.4571
21	10.914	0.50431
22	11.1	0.52736
23	11.244	0.53763

24	11.347	0.54413
25	11.431	0.54765
26	11.498	0.55076
27	11.555	0.55174
28	11.605	0.55324
29	11.646	0.55535
30	11.683	0.55439
31	11.718	0.55516

Table 60: pH and absorbance measurements of 3,4-dimethylphenol at 25 °C, 1 M NaCl.